SYNTHESES AND REACTIVITY OF TRANSITION METAL COMPLEXES OF MONO- AND BICYCLO- MACROCYCLIC LIGANDS

by

CHAO XU

B.Sc., Sichuan University, 1984

A DISSERTATION SUBMITTED IN PARTIAL FULFILLMENT

OF THE REQUIREMENTS FOR THE DEGREE OF

DOCTOR OF PHILOSOPHY

in the Department

of

Chemistry

ACCEPTED
FACULTY OF GRADUATE STUDIES

DEAN

DATE 91/08/21

We accept this dissertation as conforming
to the required standard

Dr. A. McAuley

Dr. G. W. Bushnell

Dr. P. Wan

Dr. J. B. Tatum

Dr. Y. L. Chow

Supervisor: Professor A. McAuley

ABSTRACT

Optically-active bis((-)-(R)-2-methyl-1,4,7-triazacyclononane) complexes of Ni(II)/(III) have been synthesized. The molar optical rotation, $[M]_D$, of the Ni(II) complex is -1.3×10^3 deg. $M^{-1}m^{-1}$, and that of the Ni(III) complex $+1.9\times10^3$ deg.$M^{-1}m^{-1}$. The Ni(II) complex is relatively stable in acidic media, and the rate of decomposition is first-order in $[H^+]$ with $k_H = (1.81 \pm 0.09)\times10^{-4}$ $M^{-1}s^{-1}$. The kinetics of the redox reaction at the nickel centre were investigated using *Marcus Cross-correlation*, and the self-exchange rate determined to be $(1.2 \pm 0.5)\times10^4$ $M^{-1}s^{-1}$.

The synthesis of a macrobicyclic ligand containing 14- and 9-membered rings is described, which involves a Cu(II)-template reaction of bis-pendant [9]aneN_2O with glyoxal to form a cyclam ring. The isolated condensation product was an amidol species formed from a series of proton-shifts of the initial Schiff-base intermediate. Insufficient hydrogenation of the amidol complex resulted in an enamine species. The crystal structures of tetra-protonated ligand perchlorate salt and its Cu(II) complex, together with the amidol and enamine reaction intermediates, were solved. The mechanisms involved in both processes are discussed. In all the Cu(II) complexes, the metal ion is in a square pyramidal geometry with the ether oxygen binding at the apical position and the metal ion

sitting above the N_4 plane towards the apical donor.

The spectroscopic and electrochemical properties of square pyramidal Cu(II) complexes of bicycloN_4X (X = O, S or N) ligands were investigated. As the apical donor was changed from O to S and N, a correlation between the d-d transition band, A_{Cu} and the oxidation potential was observed, and rationalized in terms of σ-bonding strength. In the case of N_4O, a "square-scheme" involving both electrochemical and chemical processes was observed in the cyclic-voltammetric reduction, whereas in the case where X = S or N, the reduction is of reversible character.

The macrobicycloN_4O Ni(II) complex was synthesized. The crystal structure showed a distorted octahedral geometry with an axial coordination of the ether oxygen and a perchlorate anion, and the Ni(II) ion below the N_4 plane towards the coordinated perchlorate. The substitution reactions of the $[Ni(III)(N_4O)(OH_2)]^{3+}$ complex with Cl^- and SCN^- in aqueous media were investigated. The reaction rate is dependent not only on $[H^+]$, but also the nature and concentration of both the entering ligand and the supporting electrolyte. A mechanism involving ion-pairing equilibria and deprotonation of the coordinated water is proposed.

The preparation and characterization of the ethylene-bridged highly-conjugated binuclear Ni(II) complex, $[Ni_2(1,1'$-bicyclo-3,6,10,13-tetraazatetradeca-2,13-dienyliden)$]^{4+}$, are described, and the mechanism involving radical intermediates

was proposed accounting for the dehydrogenation and dimerization processes. Both the molecular structure and chemical reactivities of the compound showed "quasi-aromatic" nature. Hydrolysis of this compound was ligand-based, whereas its oxidation was metal-based. The electrochemical reduction of the compound was a one-electron/two-step process with $E_{1/2}$ of 0.19 V and -0.03 V (*vs* $Fc^{+/0}$ in CH_3CN), respectively. The self-exchange rate of the first reduction was determined (using *Marcus Cross-correlation*) to be 5.1×10^6 $M^{-1}s^{-1}$, and that of the second 180 $M^{-1}s^{-1}$.

Examiners:

Dr. A. McAuley

Dr. G.W. Bushnell

Dr. P. Wan

Dr. J.B. Tatum

Dr. K.L. Chow

Table of Contents

LIST OF TABLES

LIST OF FIGURES

LIST OF SCHEME

LIST OF ABBREVIATIONS

Me-[9]aneN$_3$ (L1)	(-)-(R)-2-methyl-1,4,7-triazacyclononane
L2	6-hydroxy-17-oxa-1,5,8,12-tetraazabicyclo[10.5.2]-nonadec-5-ene
L3	17-oxa-1,5,8,12-tetraazabicyclo[10.5.2]-nonadec-6-ene
L4	1,1'-bicyclo-3,6,10,13-tetraazatetradeca-2,13-dienylidene
L'	N,N'-di(3-aminopropyl)-1-oxa-4,7-diazacyclononane
L"	6-oxo-17-oxa-1,5,8,12-tetraazabicyclo[10.5.2]-nonadecane
bicycloN$_4$O (N$_4$O)	17-oxa-1,5,8,12-tetraazabicyclo[10.5.2]-nonadecane
bicycloN$_5$ (N$_5$)	1,5,8,12,17-pentaazabicyclo[10.5.2]-nonadecane
bicycloN$_4$S (N$_4$S)	17-thia-1,5,8,12-tetraazabicyclo[10.5.2]-nonadecane
[9]aneN$_3$	1,4,7-triazacyclononane
[9]aneN$_2$O	1-oxa-4,7-diazacyclononanecyclam 1,4,8,11-tetraazacyclotetradecane
[16]aneN$_5$	1,4,7,10,13-pentaazacyclohexadecane
[16]aneN$_4$S	1-thia-4,7,11,13-tetraazacyclohexadecane
[16]aneN$_4$O	1-oxa-4,7,11,13-tetraazacyclohexadecane
daptacn	1,4-di-(3-aminopropyl)-1,4,7-triazacyclononane
en	1,2-diaminoethane
phen	1,10-phenanthroline
oxim	3,14-dimethyl-4,7,10,13-tetraazahexadeca-3,13-diene-2,15-dionedioximate
TCNE	tetracyanoethylene
AT	11,13-dimethyl-1,4,7,10-tetraazacyclotrideca-10,12-dieno(-)
AT'	5,7-dimethyl-1,4,8,11-

	tetraazacyclotetradeca-4,7-dieno(-)
$[NiATH]_2$	1,1'-bi(2,13-dimethyl-3,6,9,12-tetraazacyclotrideca-2,12-dienylidene)
PnAO-6H	2,2,3,9,10,10-hexamethyl-5,7-dioxa-6-hydra-1,4,8,11-tetraazacyclotetradeca-3,8,11,13-tetraene

ACKNOWLEDGEMENTS

I would like to thank my supervisor, Dr. A. McAuley, for his guidance, encouragement and help during the course of this work. I would also like to thank Dr. T. Whitcombe, Dr. S. Subramaniam, Dr. D. G. Fortier, and Dr. Savitri Chandrasekar for their assistance, and many useful and interesting discussions. The help from Ms. B. Cameron, Ms. B. Chak, and Mr. K. Coulter, is acknowledged. I thank all the staff, both technical and nontechnical, of the department of Chemistry for their assistance.

I especially thank Mrs. Kathy Beveridge for completing the X-ray crystal structures of the compounds presented in this thesis, and Dr. T. Whitcombe for his help with part of the kinetic studies in the thesis work.

Last but not least, I would particularly like to thank my wife, Yongxin, for her patience and assistance during the course of this work.

To my wife

and

my parents

Chapter 1. Introduction

1.1 Macrocyclic Complexes

1.1.1 Background

A macrocyclic ligand, according to the definition provided by Melson, is "a cyclic compound with nine or more members (including all hetero atoms) and with three or more donor (ligating) atoms".[1] The discovery and study of coordination compounds containing macrocyclic ligands date back as early as the beginning of this century; however, the early work in this field was limited to complexes of naturally occurring ligands such as porphyrins, corrins and phthalocyanines due to their relation to biologically important species (e.g. hemes, cytochromes, and chlorophyll) or their potential as dyestuffs and pigments.[2-5] Before 1960, there were only a few scattered reports of "synthetic macrocycles", most of which were often incidental to the research rather than the prime motivation for their coordination chemistry.

In the early 1960's, several groups,[6-10] working independently, synthesized a variety of coordination compounds containing synthetic macrocyclic ligands. Curtis[6] described the reaction between *trans*-bisethylenediaminenickel(II) perchlorate and acetone, and later,[7] assigned to the product the macrocyclic structure shown in Scheme 1.1. Following these reports, the generality of the above type of reaction was demonstrated, and a new series of synthetic macrocycles was developed.[11] Since then, a very large number of other synthetic

macrocycles have been prepared and this has led to a great increase in interest in all aspects of the chemistry of such systems.

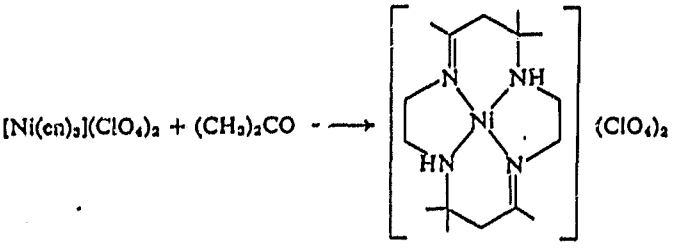

Scheme 1.1

Simultaneously, there has been enhanced interest in the role of metal ions in biological systems, and, as a result, "bioinorganic chemistry" has emerged as a new branch of chemistry,[12] in which complexes of both natural and synthetic macrocycles are involved. Thus, there has been an element of cross-fertilization between these two developing areas. As a consequence of this close relationship, a considerable amount of the research involving synthetic macrocycles has been directed towards the preparation of model compounds for natural macrocycles. Although these efforts have not always met with spectacular success, the resulting development of new macrocyclic ligand chemistry has provided a valuable background against which the natural systems can often be seen in clear perspective.

Apart from the biological significance, the development of macrocyclic complexes has opened up a wide front of

coordination chemistry, with which is associated a number of new terms such as "macrocyclic effect",[13] "template effect",[8] "effects on coordinated metal and ligand",[7] "multiple juxtapositional fixedness",[14] "cryptate effect",[15] "catenand effect",[16] "tethering effect"[17] and so on. The extension of this field has impinged on topics such as metal-ion catalysis, organic synthesis, metal-ion discrimination, and analytical methods, as well as on a number of industrial, medical and other applications.

1.1.2 Syntheses of Macrocycles

Syntheses of macrocyclic ligand compounds can be achieved in many different ways. However, procedures for cyclization may be broadly subdivided into two major categories: (a) direct synthesis and (b) template synthesis. In (a), the cyclization proceeds by a conventional organic reaction and does not depend on the directing influence of a metal ion. However, in (b), the generation of the cyclic product is influenced by the presence of a metal ion, which acts as a "template" for the cyclization reaction.

A normal priority of both direct and template procedures is to maximize yields of the required product by choosing strategies which inhibit competing linear polymerization and other reactions. Unless special circumstances are met, polymeric materials are often the major product when macrocyclic syntheses are attempted.

Direct Synthesis

A typical direct synthetic procedure involves the reaction of two reagents (in equimolar concentrations) incorporating the required fragments for the target macrocycle such that a 1:1 condensation occurs. Such reactions are frequently carried out under dilute conditions, which tend to favour cyclization by enhancing the prospect of the "half-condensed" moiety reacting with itself "head-to-tail" rather than undergoing an intermolecular condensation with another molecule in the reaction solution. Depending on the nature of the reaction, the condition required can be either very high dilution or moderate to low dilution. The high dilution procedures are often necessary in the preparation of the polyether class of macrocycles, and an apparatus for accurately controlling this experimental condition during such synthesis has been developed.[18]

A range of direct synthesis has been performed under conditions of moderate to low dilution but still led to isolation of the required cyclic product in reasonable to high yield. This type of cyclization is often applied in preparation of polyazamacrocycles. The most commonly used method under this category is the Richman and Atkins reaction.[19] In this reaction, as illustrated in Scheme 1.2, the cyclization is achieved by reacting two pre-tosylated (tosyl = *p*-toluenesulphonyl; Ts) reactants, and the desired macrocycle can then be obtained by detosylation using either

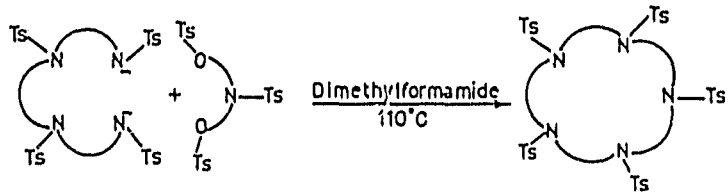

Scheme 1.2

acidification or redox methods. Reasonable yields (often considerably better than 50%) of tosylated macrocycles may be achieved in spite of the fact that such reactions are usually performed at moderate dilution. These good yields are believed to stem, in part, from the influence of the bulky tosyl groups. These groups will reduce the number of conformational degrees of freedom (such as bond rotation) in the reactants and/or intermediates. It is this reduction which is thought to facilitate cyclization relative to polymerization for these systems; in essence, the enhancement of cyclization can be considered to be largely a consequence of favourable entropic effects.

Metal-Ion Template Syntheses

Success in synthesis of macrocycles by using a metal-ion to direct the organic reactions is largely due to the **template effect.** This term was first introduced by Busch to account for the controlling influence of the metal-ion in a particular synthesis.[8] Further study of this effect has shown that the template effect may be further divided a kinetic and a thermodynamic effect. In the kinetic template effect, it is the directing influence of the metal-ion which controls the

steric course of condensation such that formation of the required cyclic product is facilitated. In the thermodynamic template effect, the metal-ion perturbs an existing equilibrium in an organic system and the required product is formed. Examples for both types of the effects have been documented.[20] However, while these effects are useful concepts, very often the role of the metal-ion in a given *in situ* reaction may be quite complicated and involve both effects.

An essential feature of template reactions is the formation of a new chelate ring. This can be achieved through reaction on either the coordinated donors or the uncoordinated atoms influenced by the donor. Some of the typical ring-closing reactions are listed in Table 1.1. It is worth mentioning that most of the reactions listed in Table 1.1 are quite sensitive to the chosen reaction conditions and are influenced by such factors as: the nature of the solvent, the pH, the order of addition of reagents, the temperature, the time of the reaction and/or the need (or otherwise) to protect the system from the atmosphere. In addition, particular reactions will be quite dependent on the nature of the metal chosen for the template reaction.

A macrocyclic ring obtained by a template reaction often requires modification by further reactions. This ligand reaction step may be performed either with the template metal-ion still intact or after removal of the metal-ion from the ring, depending on the nature of the ligand. For instance, in

the absence of a coordinated metal-ion many of the Schiff-base macrocycles are unstable and may undergo hydrolytic decomposition in acidc or basic aqueous media. In this case, the hydrogenation of the coordinated imine functicns is often required to stabilize the macrocycle before the metal-ion is discharged.

Table 1.1 Typical Ring-closing Reactions

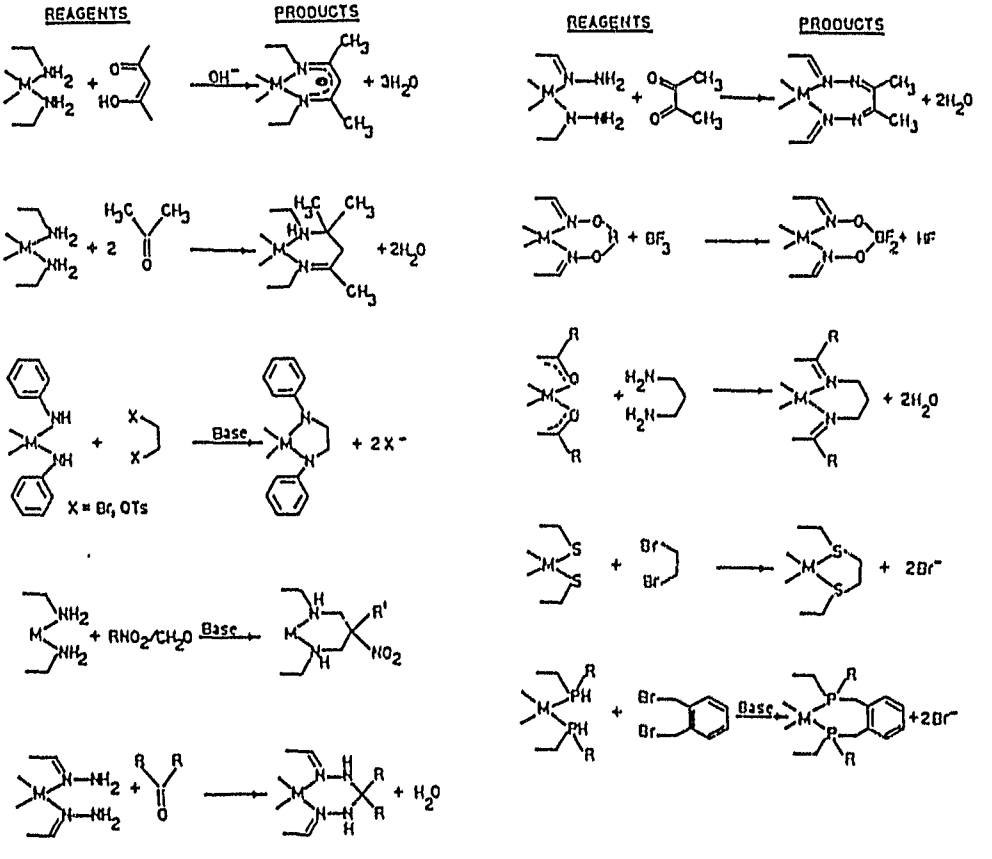

To obtain a free ligand, the coordinated metal-ion in the macrocyclic complex from the template reaction can be removed using one of following procedures:

a) Addition of excess acid to an amine-containing macrocycle to protonate the amine functional groups as they dissociate from the metal ion and thus "scavenge" the macrocyclic ligand as a N-protonated form;

b) Addition of a strongly competing ligand to a solution of the macrocyclic complex (such as CN^- to remove Ni^{2+} or S^{2-} to remove Cu^{2+});

c) Deliberately using a weak template ion so it can be removed easily later by dissolution of the complex in a coordination solvent in which the free macrocyclic ligand has poor solubility;

d) Reducing the metal ion so that the metal-ligand bond is weakened (in some cases, reduction of the metal-ion to a low oxidation state [for instance, to the M(0) state] leads to its spontaneous dissociation from macrocycles).

1.1.3 Macrocyclic Effect

The term "macrocyclic effect" was first introduced by Cabbinus and Margerum[13] in 1969 to account for the great thermodynamic stability of complexes containing macrocyclic ligands as compared with those of non-macrocyclic ligands but similar structure. An example of this is shown in Table 1.2.[21] Although it is expected that the stability of a particular

complex type increases as the number of chelate rings increases (the **chelate effect**), the additional stability of the macrocyclic copper complex was about an order of magnitude greater than expected solely from the presence of an additional chelate ring. The origins of this macrocyclic effect have been investigated on two fronts: thermodynamic and kinetic.

Table 1.2 Thermodynamics of Formation of Complexes of Cu^{2+} with Tetraamine Ligands in Water[21]

Ligand	log *K*	ΔH (kcal mol^{-1})	$T\Delta S$ (kcal mol^{-1})
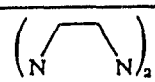 (en)	19.7	−25.2	1.7
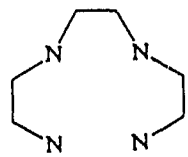 (2,2,2-tet)	20.1	−21.6	5.8
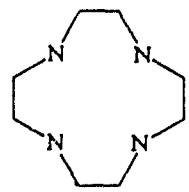 (cyclen)	24.8	−18.3	15.3

Thermodynamic Consideration

From the earliest studies, the thermodynamic origins of the macrocyclic effect, especially involving complexes of tetraaza ligands, have long been the subject of debate. For

the particular systems the additional stability was assigned

Table 1.3 Parameters Illustrating the Macrocyclic Effects for the High-spin Ni(II) Complexes of Tetraaza Macrocycles[22]

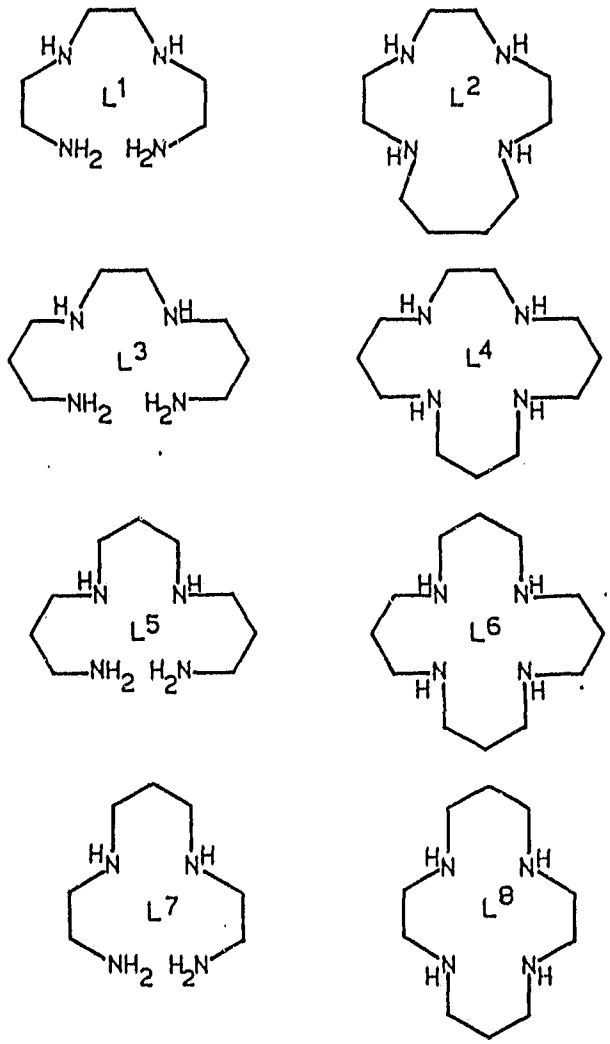

$$[NiL_{oc}]^{2+} + L_{mac}^{2+} \rightleftharpoons [NiL_{mac}]^{2+} + L_{oc}$$

where oc = open chain; mac = macrocylic.

L_{oc}/L_{mac}	$-\Delta G$ / kJ mol^{-1}	ΔH / kJ mol^{-1}	$T\Delta S$ / kJ mol^{-1}
L^1/L^2	2.43	5.1	7.4
L^3/L^4	21.05	5.3	26.4
L^5/L^6	15.69	3.5	19.2
L^7/L^8	33.67	−20.5	13.2

either wholly to entropy factors or to enthalpy factors Later, it was clear that these contradictory results were mostly due to the large uncertainty of the measurements (ΔH was derived from the temperature dependence of the respective stability constants), and were resolved by subsequent calorimetric determinations. Table 1.3 summarizes the thermodynamic parameters related to the macrocyclic effect for the high-spin Ni(II) complexes of four tetraaza macrocyclic ligands and their open-chain analogues (the open-chain derivative which yields the most stable nickel complex was used in each case). Clearly, the enthalpy and entropy terms make substantially different contributions to complex stability along the series. Depending on the system concerned, both enthalpy and entropy can play a dominant role in contributing to the effect.

Kinetic Consideration

It is widely accepted that the kinetic origin of the macrocyclic effect can be attributed to "**multiple juxtapositional fixedness**", a term which was introduced by Busch and co-workers.[14] In this view, the cyclic ligand has no "tail" from which preparation and decomplexation can begin, in contrast to linear polydentate amines where protonation is linked to progressive removal of the metal ion. As a consequence, extremely slow decomplexation rates are frequently observed in the macrocyclic complexes. In comparison with the open-chain analogues, although the rates

of complexation may sometimes be slower in the case of macrocyclic complexes, their decomplexation rates are normally decreased to an even greater extent, and it is the latter which is reflected in the enhanced thermodynamic stabilities which are characteristic of the macrocyclic effect.

Other Comments

In part, it is the phenomenon of the macrocyclic effect which stimulates the high degree of interest in the field of chemistry of macrocyclic complexes. The extension of the macrocyclic effect has led to recognition of a number of other effects (such as the cryptate effect, the catenand effect, and the tethering effect), which are involved in a vast variety of macrocycles (including bicycles and multicycles). The introduction provided here is only a brief outline of the thermodynamic and kinetic bases for understanding the macrocyclic effect. More fundamental factors involved in this effect have been discussed by Hancock and Martell[23] in terms of: a) preorganization of the ligand; b) desolvation of the donor atoms in the confined space of the macrocyclic cavity; c) intrinsic basicity effect; d) dipole-dipole repulsion in the cavity of the ligand. More recently, Busch and Stephenson[17] used a more general term "molecular organization" which attributes all the effects above to five elementary structural factors: the topological factor, the metric factor, the shape factor, the rigidity factor, and complementarity factor. However, these topics are far beyond the scope of this

introduction and will not be discussed here.

It is also worth noting that although the macrocyclic effect is widely observed in macrocyclic complexes, it does not mean that all of such complexes manifest this effect. Manifestation of the macrocyclic effect depends on a number of factors, such as the nature of the donors, the match between the metal-ion size and the cavity of cyclic ligands, the size of chelate rings, the rigidity of the structure formed, the nature of the solvent, and so on. Indeed, it is not rare to observe some macrocyclic complexes that are less stable than their open-chain counterparts.[24]

1.1.4 Other Effects Involved in Macrocyclic Complexes

Effect on the Ligand Field

Investigation of ligand field spectra, together with data from magnetic susceptibilities and electron spin resonance (esr), provide the basis for the assignment of electronic configurations of transition-metal ions. Macrocyclic ligands offer several important advantages for spectroscopic studies of transition-metal complexes. Considerable use has been made of the ability of tetradentate macrocycles to maintain a constant planar stereochemistry about a metal ion while additional noncyclic axial ligands are varied systematically. These studies of the influence of tetragonal geometries on the electronic configurations of metal ions have been greatly aided by macrocyclic ligands.[14,25-28] Such ligands normally

produce stronger ligand fields than the corresponding open-chain ligands. This increase in ligand field by coordination of the macrocyclic ligand was attributed in early studies to a constraining or constrictive effect.[26-28] More recently, however, investigation carried out by Hancock *et al*[29] has shown that the increase in the intrinsic basicity of nitrogen donors is a dominant factor in the triazamacrocyclic systems. It may be possible that both of these two factors have an effect on the increase in the ligand field, and which one of them is more important will depend on the system concerned.

Effect on the Redox Nature of the Metal Centre

The capacity of macrocyclic ligands to stabilize unusual oxidation states of a coordinated metal ion has been well-documented.[30] For example, both the high-spin and low-spin Ni(II) complexes of cyclam are oxidized more readily to Ni(III) species than are the corresponding open-chain complexes. Indeed, this capacity has been widely used in the syntheses of a variety of complexes with metal centers exhibiting less common oxidation states, which may not be stable otherwise.[30]

In general, the effect of macrocycles on the redox nature of the metal center is reflected in the change in E° of the metal concerned, and results from the specific preference of the macrocycle for the metal centre at one oxidation state over another. This may be best explained by the equations shown in eq. (1.1). The change in the redox potential of the

metal center, ΔE, is directly related to the ratio of the complexation constants of the macrocyclic ligand with the

$$\begin{array}{ccccc} & ML_{mac}^{n+} & \rightarrow & ML_{mac}^{(n+1)+} + e^- & (E^\circ_{(mac)}) \\ (K_{1(mac)}) & \| & & \| & (K_{2(mac)}) \\ & M^{n+} + L_{mac} & \rightarrow & M^{(n+1)+} + L_{mac} + e^- & (E^\circ_{(M)}) \end{array}$$

$$E^\circ_{(mac)} = E^\circ_{(M)} - (RT/nF)\log(K_{2(mac)}/K_{1(mac)}) \qquad (1.1)$$

or

$$\Delta E = E^\circ_{(mac)} - E^\circ_{(M)}$$
$$= -(RT/nF)\log(K_{2(mac)}/K_{1(mac)}) \qquad (1.2)$$

metal ion at different oxidation states, $K_{2(mac)}/K_{1(mac)}$. When the macrocyclic ligand has a higher complexation constant, $K_{2(mac)}$, with a metal at a higher oxidation state, [(n+1)+], than that, $K_{1(mac)}$, at a lower oxidation state, [n+], the redox potential on the metal centre for the [(n+1)+]/[n+] couple will be reduced, and thus the metal center at the oxidation state of [(n+1)+] is stabilized. This is often the case for Ni(III) polyazamacrocyclic complexes.[30] On the other hand, if the ligand bonds more strongly with the lower oxidation state metal ion, the redox potential will be increased, and hence, the lower oxidation state will be stabilized. This occurs frequently with the Cu(I) complexes of polythia or imine macrocyclic ligands where the d orbitals on the S donor or the *anti*-bonding π orbital of the C=N bond are able to withdraw electron density from the Cu(I) metal center through $d_M \rightarrow d_s$ or $d_M \rightarrow \pi_{imine}$ interactions, and consequently, strengthen the M-donor

bonds and increase the complexation constant, $K_{1(mac)}$. (This can also be interpreted in terms of the delocalization of the electron density at the Cu(I) center).

The structural factors influencing electrochemistry around the Ni(II) center have been investigated by Busch and co-workers[31-33] using a variety of tetraazamacrocyclic ligands. The typical results are shown in Fig. 1.1. It was demonstrated

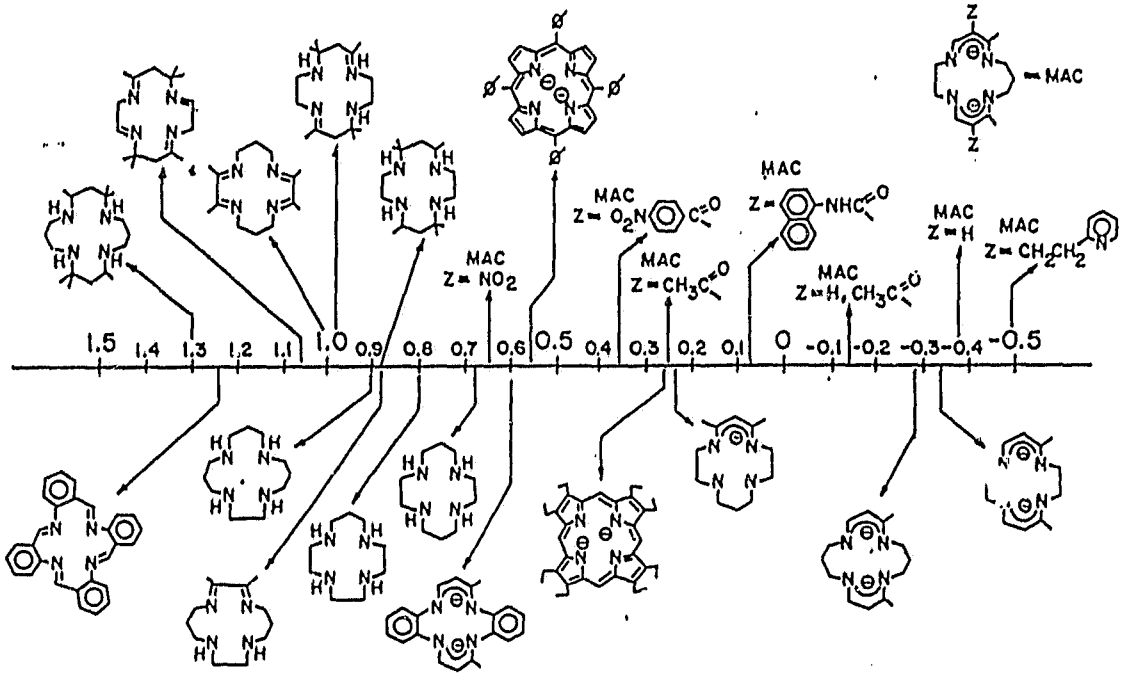

Figure 1.1 $E_{1/2}$ for the Ni^{2+}/Ni^{3+} Couple in Tetraaza Macrocyclic Complexes vs. $Ag/AgNO_3$ (0.1M) Reference Electrode (in V).[33]

that the overall redox properties of a given system are influenced by the macrocyclic ring size, the charge on the ligand, the nature of the ligand substituents and the extent

and type of ligand unsaturation, and the effects of these factors appear to be separable and additive. Later, this work was extended to the system where a different type of donor was involved.[34] In general, the structural factors which favour high oxidation states are: (i) the increase in the negative charge on the ligand, and (ii) the better match between the size of the Ni(III) ion and the cavity of the cyclic ligand. An increase in ligand unsaturation, and substitution on the chelate rings both favour the lower oxidation states. Furthermore, as the donor type changes from O, S, to N, the Ni(III) state becomes more stable.

The generality of the results above can also be extended to the Cu(II)/Cu(III) system.[35] However, because the Cu(III) ion is smaller than the Ni(III) ion, the smaller macrocycles (such as [12]aneN$_4$) are able to stabilize Cu(III) further than the large ones (such as [14]aneN$_4$),[35] while the Ni(III) ion matches the best with [14]aneN$_4$.

In some cases, the better orbital overlap between the metal and the donors, caused by conformation or rigidity of the cyclic ligand, may also make a significant contribution in stabilizing unusual oxidation states.

Effects on Coordinated Macrocyclic Ligands

Coordination of the metal ion to a macrocyclic ligand not only has an impact on the chemistry of the metal centre, but also influences the chemical reactivity of the ligand. In the course of the development of synthetic routes to macrocyclic

complexes, a variety of interesting and useful reactions of the coordinated ligands have been discovered. These reactions may not occur, or at least not as easily, without the metal-ion coordination. The remarkable resistance to total decomposition of many macrocyclic complexes has made this area of study particularly fruitful. In some cases, the ability of the cyclic ligand to stabilize unusual oxidation states such as Ni(III) or Cu(III) appears to play an important role in mediating reactions of the ligands. The nature of these reactions may vary from oxidative dehydrogenation, hydrogenation, substitution on the ligand, N-alkylations to addition reactions on the imine groups. Because of the limit in space, only the former two reactions will receive further brief discussion here.

i) Oxidative dehydrogenation:

Oxidation of metal complexes of substituted cyclam derivatives often results in the formation of C=N double bonds in the ligand.[36-40] The position of this C=N bond in the ligand structure depends largely on the nature of the metal-ion used. For Fe(II) complexes, this double bond occurs preferentially in the five-membered ring.[38-40] When Fe(II) is replaced by Ni(II), the product often has the imine group in the six-membered ring.[37] The oxidation can be performed chemically (using HNO_3, O_2, Cl_2, *etc.*) or electrochemically. A general stepwise reaction scheme has been proposed, and is shown in Scheme 1.3. The discussion on the mechanisms involved in the

scheme can be found in ref. 30.

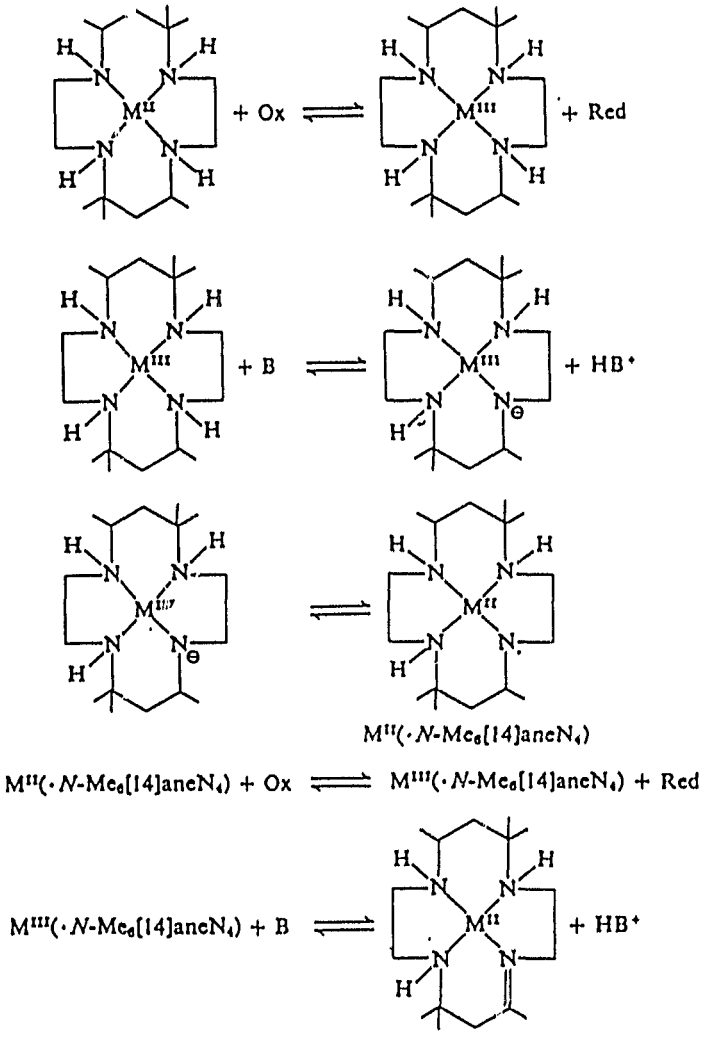

Scheme 1.3 Mechanistic Scheme of Oxidative Dehydrogenation[30]

Apart from the formation of the imine product, oxidation of the coordinated tetrazamacrocyclic ligands sometimes has other consequences, particularly when the ligand containing β-

diimine moieties are involved.[41] These compounds can be relatively easily oxidized. For example, the M(Me$_2$[14]-1,11-dienate(-)N$_4$)$^{n+}$ complex exhibits an $E_{1/2}$ of ~ 0.4 - 0.8 V *vs.* NHE, more or less independent of the nature of the metal-ion (M can be Ni(II) or Co(III)), and attributable to the one-electron oxidation of the ligand:

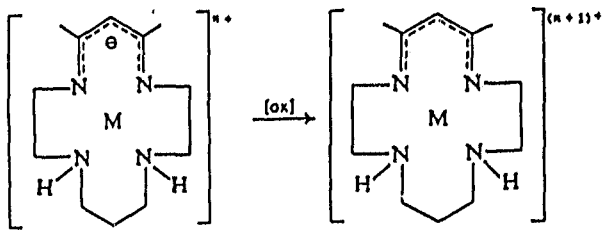

(1.8)

The oxidant in the reaction may be either external (O_2, $FeCl_3$ *etc.*) or internal (Co(III), Ni(III), *etc.*). The radical species formed may be intercepted by scavengers such as O_2 or may dimerize:

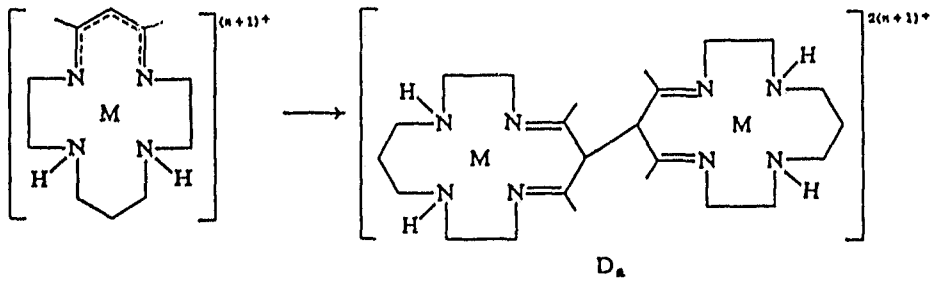

D_a

(1.9)

The dimeric-β-diimine complexes may be dehydrogenated under very mild conditions ($FeCl_3$, O_2, *etc.*) to form a second dimer:[41,42]

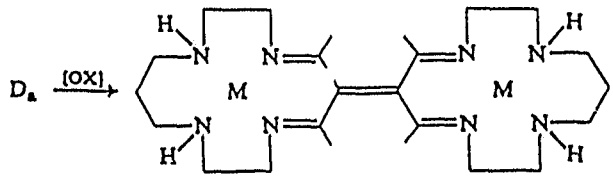

(1.10)

Dimerization of similar complexes by electrochemical oxidation

has also been reported.[43]

ii) Hydrogenation

A large number of macrocyclic complexes containing unsaturated ligands have been successfully hydrogenated. Indeed, hydrogenation of the imine groups of tetraazamacrocyclic complexes has become a common practice in the modification of the template reaction products. The reaction can be performed chemically (e.g. using $NaBH_4$ in methanol), catalytically (e.g. using H_2 in the presence of a catalyst such as Pt/C) or electrochemically.

Reduction of unsaturated tetraazamacrocyclic ligands of Ni(II) complexes has been achieved using a wide range of reductants.[11,37,44] However, the similar reactions with Cu(II) as the metal center produced only decomposed products.[11,44,45] This may be due to the ease of reducing Cu(II) to Cu(I). The Cu(I) has a d^{10} electron configuration which prefers tetrahedral geometry and has less affinity towards nitrogen donors than other "conventional" transition-metal ions. Therefore, without extra assistance, the tetraazamacrocyclic ligands are not able to hold the Cu(I) during the course of the reaction. However, if the ligands are modified, for example, by addition of another coordinating cyclic ring so that the copper ion can be trapped in the three-dimensional hole formed by the bicyclic rings, the Cu(I) may have a better chance of remaining coordinated until the reaction is completed.

1.2 Kinetic and Mechanistic Aspects of Inorganic Reactions Involving the Transition Metal Complexes

In general, inorganic reactions of the transition metal complexes may be classified in two ways:

i) substitution reactions, which involve the replacement of at least one coordinated donor by another ligand, and

ii) redox reactions, which involve electron transfer.

Occasionally, the two types of reactions may not be distinguished clearly, especially when a redox reaction occurs between the metal center and the leaving ligand, or involves the ligand transfer from one metal center to another as an "electron-carrier". Since these cases are not common, they will not be considered here, and only the "classical", or "typical", substitution and redox reactions will be discussed in the general terms of kinetics and mechanism.

1.2.1 Substitution Reactions

Mechanistically, the substitution reactions involving the transition metal complexes have been classified in three categories:[46,47]

i) the dissociation (**D**) reaction, with an intermediate of low coordination number;

ii) the association (**A**) reaction, with an intermediate of higher coordination number;

iii) the interchange (**I**) reaction, which has no intermediate but a transition state (**TS**) of higher

coordination number.

When the "intimate mechanism",[47] which relates to the activation of the reaction process, is considered the reactions can be further modified as "associative activation" reaction (**a**), and "dissociative activation" reaction (**d**). In the **a** reaction, the **TS** energy is sensitive to the nature of the entering ligand, whereas the **TS** energy of the **d** reaction is associated with the nature of the leaving group. Thus the **I** reactions may be further divided into the I_a reaction and the I_d reaction. **A** and **D** reactions obviously belong to **a** and **d** reactions, respectively, hence there is no need to make any further description of these two.

The mechanism of a substitution reaction involving transition metal complexes is largely determined by the electron configuration of the metal center,[48] though the changes in the effective charge and the size of the metal center,[49] the structure of the unreacting and the reacting ligands, and the reaction conditions sometimes may also have substantial influences.[47,51] The effect of the electron configuration on the mechanism operates mainly through the preference of this particular configuration for the particular coordination geometry over others at both the ground state and the **TS** in terms of **C**rystal **F**ield **S**tabilization **E**nergy (CFSE). For a number of years, a considerable amount of research has been focussed on the complexes of the low-spin d^6 ions and of the low spin d^8 metal ions (this is largely due to their

relative kinetic inertness which makes the kinetic measurements easy to handle).[47] For the former complexes such as those with Co^{3+} ion as the reaction center), I_d or D mechanisms are often observed. This is in part due to the full occupation of the coordination sphere in their complexes at the ground states (having six-donor octahedral coordination which gives the highest CFSE to both electron-configurations), which leaves no room for an entering ligand to come in before one of the coordinated ligands leaves or loosens. In the case of the low spin d^8 metal (such as Pt^{2+}) complexes, the mechanism often seen is A, or less frequently I_a. This is partly because of the square planar geometry these complexes usually adopt (which has the coordination sphere widely open on both sides so that an entering ligand can come in with little difficulty) and partly because of the higher CFSE the metal center gains in their five-coordinated square-pyramidal or trigonal-bipyramidal geometry **TS** in comparison to that of the three-coordinated trigonal geometry **TS**.

However, this does not mean that the mechanisms assigned above for these two kinds of complexes are always the case. Exceptions have been observed from time to time, and often relate to the specific effects (such as the charge, steric, structural rigidity effects etc.) of the ligands involved and the reaction conditions. For example, the displacement of Me_2SO from *cis*-$[Pt(R)_2(Me_2SO)_2]$ (R = Ph, 4-MeC_6H_4) by Me_2SO or bidentates (such as 2,2′-bipyridyl and 1,10-phenanthroline)

was found to be dissociative in nature (due to the steric effect).[51] Indeed, study of these effects has been, and still is, a subject of very active investigations.

Recently, there has been growing interest in the mechanism involving the metals other than those classical ones mentioned above.[53] For example, Ni(III) has a configuration of d^7. It is of interest to see how this configuration affects the mechanism of substitution reactions. Though the high effective charge on the Ni(III) center may favour a I_a process, the Jahn-Teller effect on the d_{z^2} electron, in the case of tetragonal elongation, is expected to weaken the axial bonds such that the **D** or I_d mechanism may become a common pathway for the axial substitution of the octahedral Ni(III) complexes (the electron-configurational effect).[53]

The rate of substitution reactions of transition metal complexes also depends on the electron-configuration of the metal center, as well as the effective charges at the metal center and the structure of the ligands. The effect of the electron-configuration operates normally on the basis of the amount of CFSE lost on going from the ground state to the **TS**. The more CFSE lost, the more inert the reaction. For the **D** or I_d reactions, the higher effective charge gives rise to the more inert (or slower) reaction for the same type of metal, given the same condition. Similarly, among the elements of the same group, as the metal changes from the first row to the second and to the third, the rate of substitution becomes less

inert. This can be readily understood in terms of electrostatic attraction, since the higher-charged metal ion tends to form a stronger M-donor bond and has a higher CFSE effect as well (excluding the d-d or d-π interactions). The variation in the rate of the substitution reactions from the ligands are much more complicated, and involve a number of effects: the steric effect, the chelate effect, the charge effect, the *trans* effect and so on.[47,52] Only the *trans* effect will receive further discussion here, the others being discussed in ref. 47, 52.

The kinetic *trans* effect was first recognized by Werner,[54] and later elaborated on by Chernyaev.[55] It relates to the special effects of *trans* substitutions on the lability of a leaving group, and is frequently observed in the substitution reactions of transition metal complexes, especially the square planar d^8 complexes. There have been many papers written on the theory of the *trans* effect. Notable contributions are those of Grinberg[56] involving electron-polarization theory, the π-bonding theory of Chatt et al[57,58] and Orgel,[59] and the proposal by Gray and Langford[47] based on the combination of both σ and π interactions. Basically, the simple explanation of the *trans* effect is that when a donor forms a strong bond with a metal ion (considering the σ interaction only), it draws much of the bonding p_z orbital of the metal center such that a lesser amount of the orbital electron density (which is normally equally distributed) is left on the opposite side.

Hence, the bond "*trans*" to the donor becomes weakened and made easier to be broken (this effect actually acts at the ground state, and sometimes is also called the "*trans* influence" in thermodynamic terms).

1.2.2 Redox Reactions

The redox reactions of transition metal complexes have been classified,[46] in terms of mechanism, into two classes: outer-sphere and inner-sphere reactions. In the former case, the coordination shells of the reactions remain intact, with transfer of an electron through the ligand. The inner-sphere reactions involve formation of an activated complex in which one ligand is common to both the reactants, and forms a "bridge" between them.

Outer-sphere reactions

The mechanism involved in the outer-sphere electron transfer reactions is simple and may be expressed as eq. (1.11)

$$M_1^{n+}L_1 + M_2^{m+}L_2 \overset{K_p}{\rightleftharpoons} (M_1^{n+}L_1, M_2^{m+}L_2) \xrightarrow{k_e} (M_1^{(n-1)+}L_1, M_2^{(m+1)+}L_2)$$

$$\xrightarrow{k_d} M_1^{(n-1)+}L_1 + M_2^{(m+1)+}L_2 \qquad (1.11)$$

In the first step, two reactants (oxidant and reductant) move toward each other forming an "ion-pair", or "precursor", with a pre-equilibrium constant, K_p. This is then followed by an electron transfer from one metal center to the other at the rate constant of k_e. In the last step, the ion-pair formed

after the electron transfer falls apart and gives rise to two individual products. The first two steps are usually of rate-determining. The last step often proceeds very fast, and has little influence on the overall reaction rate. However, on occasion it may be the slow step in the process.

In general, there are three factors determining the rate of electron-transfer of the outer-sphere reactions. The first is the energy required to bring the reactants close enough (the separation distance) so that the two can react (the first step in eq. 1.23); the second is a barrier to electron transfer created by the equilibrium standard differences between the reactants and the products (inner-shell reorganization energy); the third is an additional barrier that is created in the surrounding solvent by the change in charge distribution associated with the electron transfer (the outer-shell reorganization energy).

Two different theoretical approaches have been developed which incorporate all of three factors above and attempt to account for electron transfer rates quantitatively. The first, by Marcus[60] (and later modified by Hush[61]), is classical in nature, and the second is based on quantum mechanics and time dependent perturbation theory.[62-65] The theoretical aspects of electron transfer reactions in chemical[63] and biological[65] system have been discussed in a series of reviews. Again, the limitation of space makes it impossible to cover all of these aspects here, and only the classical treatment will be briefly

introduced.

Within the classical framework, the rate constant for the outer-sphere reactions which involve a net standard free energy change will relate quite closely to the magnitude of this change and the rate constants for the component exchange reactions. That is, the rate constant, k_{12}, for the process

$$M_1^{n+}L_1 + M_2^{m+}L_2 \underset{k_{21}}{\overset{k_{12}}{\rightleftharpoons}} M_1^{(n-1)+}L_1 + M_2^{(m+1)+}L_2 \quad (K_{12}=k_{12}/k_{21}) \tag{1.12}$$

can be obtained from the equilibrium constant, K_{12}, and the rate constants for the symmetrical reactions

$$M_1^{(n-1)+}L_1^* + M_1^{n+}L_1 \overset{k_{11}}{\rightarrow} M_1^{n+}L_1^* + M_1^{(n-1)+}L_1 \tag{1.13}$$

$$M_2^{(m+1)+}L_2^* + M_2^{m+}L_2 \overset{k_{22}}{\rightarrow} M_2^{m+}L_2^* + M_2^{(m+1)+}L_2 \tag{1.14}$$

using the expression

$$k_{12} = (k_{11}k_{22}K_{12}f_{12})^{1/2}W_{12} \tag{1.15}$$

where

$$\ln f_{12} = [\ln K_{12} + (w_{12} - w_{21})/RT]^2 / 4[\ln(k_{11}k_{22}/A_{11}A_{22}) + (w_{11} + w_{22})/RT]$$

$$W_{12} = \exp[-(w_{21} + w_{12} - w_{11} - w_{22})/2RT]$$

$$A_{ii} = [(4\pi N\sigma^2\upsilon_n\delta r)/1000]_{ii}$$

$$w_{ij} = Z_iZ_je^2/[D_s\sigma_{ij}(1 + \beta\sigma_{ij}I^{1/2})]$$

w_{ij} represents the work required to bring together ions i and j (charges Z_i, Z_j) to the separation distance σ_{ij} (= $r_i + r_j$), and $\beta = (8\pi Ne^2/1000D_skT)^{1/2}$. The nuclear vibration frequency which destroys the activated complex configuration is designated υ_n, δr is the thickness of the reaction layer, and

it is assumed $A_{ij} = (A_{ii}A_{jj})^{1/2}$.

Provided that $\ln f_{12} \sim 0$ and the work terms cancel, the eq. (1.15) simplifies to

$$k_{12} = (k_{11}k_{22}K_{12})^{1/2} \qquad (1.16)$$

which is valid when the driving force, K_{12}, is not too large.

The above equations are called "Marcus cross-relations". Equation (1.16) has been widely used to rationalize the rate of moderately exothermic reactions, often with considerable success.[66] At higher exothermicities it is necessary to use the full equation (1.15).

The significance of the Marcus cross-relations is that the direct relationship between k_{12} and K_{12} makes it possible to estimate the kinetic values from the "thermodynamic" results which are relatively much easier to obtain; secondly, the self-exchange rate, k_{11} or k_{22}, can be derived from the indirect means. This is particularly useful in estimating the self-exchange rates of complexes which may not be sufficiently stable after change in the oxidation state or may pose a great difficulty for a direct measurement of its self-exchange rate.

Inner-sphere reactions

The general mechanism for inner-sphere reactions can be formulated in terms of a sequence of steps:

1)	$Red_1^o + L\text{-}Ox_2 \rightarrow Red_1^o\text{-}L\text{-}Ox_2$	**bridge formation**
1′)	$Red_1^o\text{-}L + Ox_2 \rightarrow Red_1^o\text{-}L\text{-}Ox_2$	(very uncommon)
2)	$Red_1^o\text{-}L\text{-}Ox_2 \rightarrow Ox_1\text{-}L\text{-}Red_2^o$	**electron-transfer**
3)	$Ox_1\text{-}L\text{-}Red_2^o \rightarrow Ox_1\text{-}L + Red_2^o$	

or Ox_1 + L-Red_2^o **bridge breaking**

or Ox_1 + Red_2^o + L

Processes (1) and (3) are nothing more complicated than ligand substitution reactions, and only (2) involves any change in oxidation state of metal centers. Occasionally it is possible to find a two-step electron transfer process with the ligand mediation:[67]

$$Red_1^o\text{-L-}Ox_2 \rightarrow Ox_1\text{-}L^o\text{-}Ox_2 \rightarrow Ox_2\text{-L-}Red_2^o$$

In principle, any of these steps, either simply or in combination, can be rate-determining. The rate law will depend on the rate-determining step, and vary with individual cases. When (1), or (3), is the rate-determining step, the system can be treated as a substitution reaction. In the case where (2) is the rate determining step, it is often successful to apply the Marcus theory (or its modification, Marcus-Hush theory) in rationalization of the kinetic results (such as in the case of intervalence transitions in binuclear complexes containing metals in different oxidation states).[68]

1.2.3 Application of Macrocyclic Complexes in Study of the Inorganic Reactions

Owing to the remarkable resistance towards decomposition and structure distortion, macrocyclic complexes have long been used in studies of both substitution and redox reactions. In the field of substitution reactions, the most common problems in study of the complexes with a transition metal ion other

than the "classical" ones (such as Co^{3+}, and Pt^{2+}) are instabilities against decompositions and redox reactions. Using macrocycles as the coordinating ligands can often stabilize these complexes to a great extent because of the macrocyclic effect, and hence, the complexes concerned will not decompose during the course of investigation. Another advantage of macrocycles in the study of substitution reactions is that the complex can be modified such that only one specific coordination site is "active" and the rest remain intact during the period of reaction. This makes it much easier to investigate the specific effect on the ligand without interference from the reactions on the other coordination sites.

In the aspect of redox reactions, the most common application of macrocycles is to form the fully coordinated stable complexes with metals (which "normally" form labile complexes), so that there is no interference to the desired outer-sphere reaction by possible inner-sphere pathways. And also, the ability of macrocyclic ligands to stabilize the less common oxidation states makes it possible to carry out the cross-reactions from both directions (measuring k_{12} and k_{21}), which sometimes is very informative about the mechanistic details in "apparently" simple reactions.[69]

The inner-shell reorganization energy involved in the outer-sphere electron-transfer is closely associated with the changes in the M-donor bond-lengths before and after the

reaction. Recently there has been a growing interest[70] in study of the impact of this change on the self-exchange rate of metal center. The advantage of using macrocycles in this study is that the rigidity of the ligand may be closely monitored so that the variety of metal-donor bond-lengths is under control. A systematic study can, therefore, be achieved. In addition to this, a large part of macrocycle is normally made of hydrophobic organic chains, which lower the degree of complex solvation in aqueous media to some extent. Therefore, the study of complexes of this type in water solvent may reduce the effect from outer-shell reorganizations, and make it easier to rationalize the results.

Chapter 2. Experimental Methods

2.1 Syntheses:

2.1.1 Bis((-)-(R)-2-methyl-1,4,7-triazacyclononane)nickel(II) and -nickel(III)complexes:

The ligand (-)-(R)-2-methyl-1,4,7-triazacyclononane ((R)-Me-[9]aneN$_3$) was prepared initially as described in the literature.[71a] However, better yields were obtained in a two-stage deprotonation of the tosylated propanediamine and cyclization to yield the tosylated macrocycle.

The synthetic route is outlined in the reaction scheme 2.1, and detailed discussion provided in section 3.2 (*vide infra*).

(-)-(R)-2-Methyl-1,4,7-triazacyclononane, L1

The free ligand (-)-(R)-diaminopropane was prepared (90% optical purity) by using the method of Dwyer and co-workers.[71b] This compound was then bis-N-tosylated, and the tosylated product (0.1 mol, 38.2 g) in dimethylformamide (1 L) reacted with NaH (0.1 mol, 60% suspension in mineral oil) to yield the monosodium salt. After effervescence, the temperature was raised first to 70°C and then to 110°C, at which time 0.1 mol (56.7 g) of the tritosylate of bis(ethanol)amine was added dropwise with stirring. The solution was left for 1 hour at this temperature. On cooling to 70°C, a second 0.1 mol of sodium hydride was added and the temperature raised to 110°C and maintained at this level for 4 hours. On reduction in volume to 200 mL and addition to ice-cold water, the cyclic

tritosylate precipitated. This could be recrystallized from methanol (34.4 g, 50% yield): mp 198 °C (the same as reported in literature); mass spectrum *m/e* 605.

Detosylation (17.2 g) was carried out in concentrated sulfuric acid at 155 °C for 30 minutes, after which the solution was allowed to cool to room temperature. The mixture was dropped into 300 mL of ice-cold ethanol (stirring) followed by addition of 1 L of diethyl ether. Filtration and removal of the organic layer and subsequent addition of concentrated HCl (75 mL) yielded the ligand trihydrochloride (4.3 g, 59%). Neutralization with base and continuous extraction into $CHCl_3$ provided the free ligand as a yellow oil.

^{13}C nmr ($CDCL_3$): 19.71 (Me), 51.70 (C_2), 50.96 (C_3), 46.08 (C_5), 46.99 (C_6, C_8), 44.28 ppm (C_9).

Mass (*m/e*): 143.

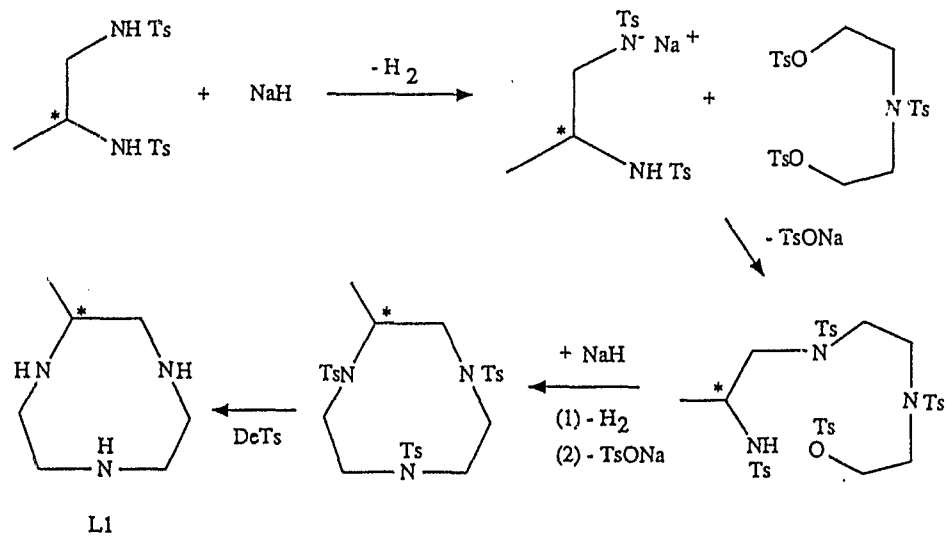

Scheme 2.1

$[Ni^{II}(L1)_2](ClO_4)_2$

A 1.01 g (4 mmol) sample of the ligand hydrochloride was dissolved in 12 mL of 1 M NaOH (0.012 mol), and the solution was warmed on a steam bath. Nickel(II)acetate (0.498 g, 2 mmol) was dissolved in 15 mL of methanol, and the mixture was added to the solution of the free ligand. The pH of solution was adjusted to 10.5. Upon warming, the solution turned pink and it was allowed to stand for 30 minutes. The pH was reduced to about 5 by using 1 M $HClO_4$ and on cooling (0 °C), purple crystals of the complex were obtained. A second crop was provided by adding saturated sodium perchlorate. In some preparations, prior to crystallization, the purple pH 5 solution was passed down a Sephadex G25 column. In this way two minor pink bands and any traces of free Ni^{2+} were removed. One trace band was eluted with water and the other with 0.45 M $NaNO_3$ following elution of the major product with nitrate (0.35 M).

Anal. for $NiC_{14}H_{34}N_6O_8Cl_2$

calc.: C, 30.90; H, 6.25; N, 15.45; Ni, 10.80.

Found: C, 30.80; H, 6.17; N, 15.17; Ni, 10.60 %.

The Ni(II) complex may be oxidized readily to nickel(III) by using aquacobalt(III) in aqueous media or NO^+ in aprotic (CH_3CN) solvents.

A convenient synthesis of the nickel(III) complex was achieved by oxidation with 3.5 M HNO_3. To $[Ni(L1)_2](ClO_4)_2$ (400 mg) was added 0.5 mL of 3.5 M nitric acid. After a few seconds

the solution turned from purple to a deep yellow-green color, and within minutes precipitation of the brownish green Ni(III) species commenced. When the solution was allowed to stand overnight at 0 °C, the yield of the nitrate salt was essentially quantitative.

2.1.2 17-Oxa-1,5,8,12-tetraaza[10.5.2]-bicyclonadecane Ligand and Its Complexes

The synthetic route to the macrocyclic ligand is outlined in reaction schemes 2.2 and 2.3, and detailed discusions of the complexes formed may be found in section 4.2 (*vide infra*).

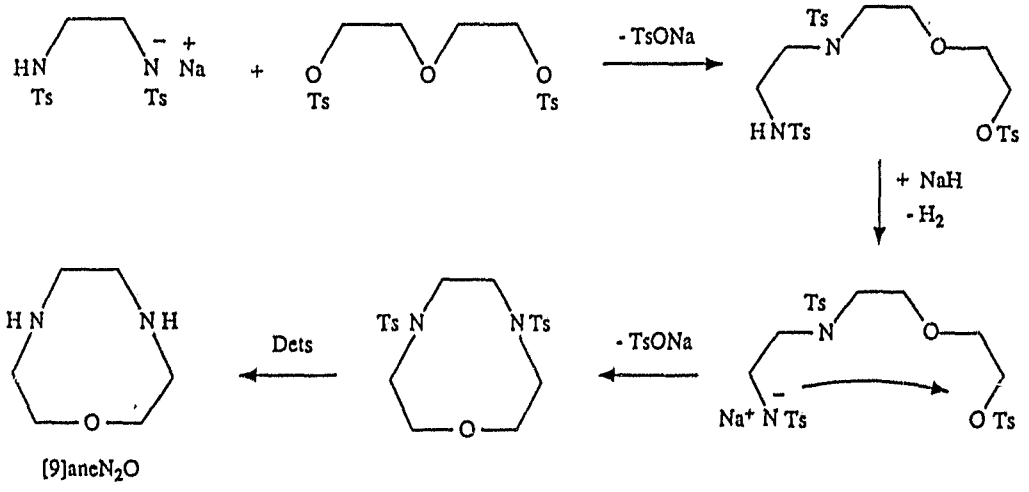

Scheme 2.2

1-Oxa-4,7-diazacyclononane, [9]aneN$_2$O

The cyclic ditosylate was prepared initially in a manner similar to that described by other workers.[72,73] An alternate route employed was to react (in 1L DMF) 0.1 mol of the mono-

sodium salt of the ditosylate of ethylenediamine with one equivalent of the ditosylate of bis-(2-hydroxyethyl)ether. The reaction mixture was maintained at 120°C overnight before cooling and one equivalent of sodium hydride was added. The solution was heated slowly to 70°C for one hour after which no effervescence was observed. The temperature was raised to 120°C for 4 hours before cooling to room temperature. After reduction of the volume to 200 mL, the solution was dropped into 3L ice cold water with vigorous stirring. Following filtration, the white ditosylate was recrystallized from methanol. Yield 13g, 30%.

The cyclic ditosylate, 10 g (0.023 mol) was dissolved in 30 mL conc. H_2SO_4 at 140°C and stirred for 5 minutes. The resulting solution was allowed to cool slowly to room temperature. Upon addition to a well-stirred solution of ice-cold ethanol, a milk-like suspension was formed which separated overnight at 0°C. The supernatant was further extracted with ether. The resulting solids were dissolved in water (30 mL), the pH adjusted to 12, and the ligand extracted with CH_2Cl_2. After removal of solvent, addition of conc. HCl (20 mL) in the ethanol solution (200 mL) yielded the dihydrochoride of [9]aneN_2O (see scheme 2.2). (4 g, 86%)

N,N'-di(2-cyanoethy)-4,7-diaza-1-oxacyclononane

To a solution of the free ligand [9]aneN_2O (1.3 g, 1 mmol) in $CHCl_3$, was added K_2CO_3 (2.0 g) and acrylonitrile (20

mL, about a 10-fold excess) and the solution was refluxed overnight. The K_2CO_3 was filtered off and the solvent removed under reduced pressure to give the desired product (2.0 g).

^1H nmr ($CDCl_3$): 3.7 (t, J = 4.5 Hz, 4H, O-CH_2); 2.8 (m, 12H, N-CH_2); 2.5 (t, J = 7 Hz, 4H, CH_2-CN).

M.S. (CI): (M+1) 237, (M+29) 265, (M+41) 277.

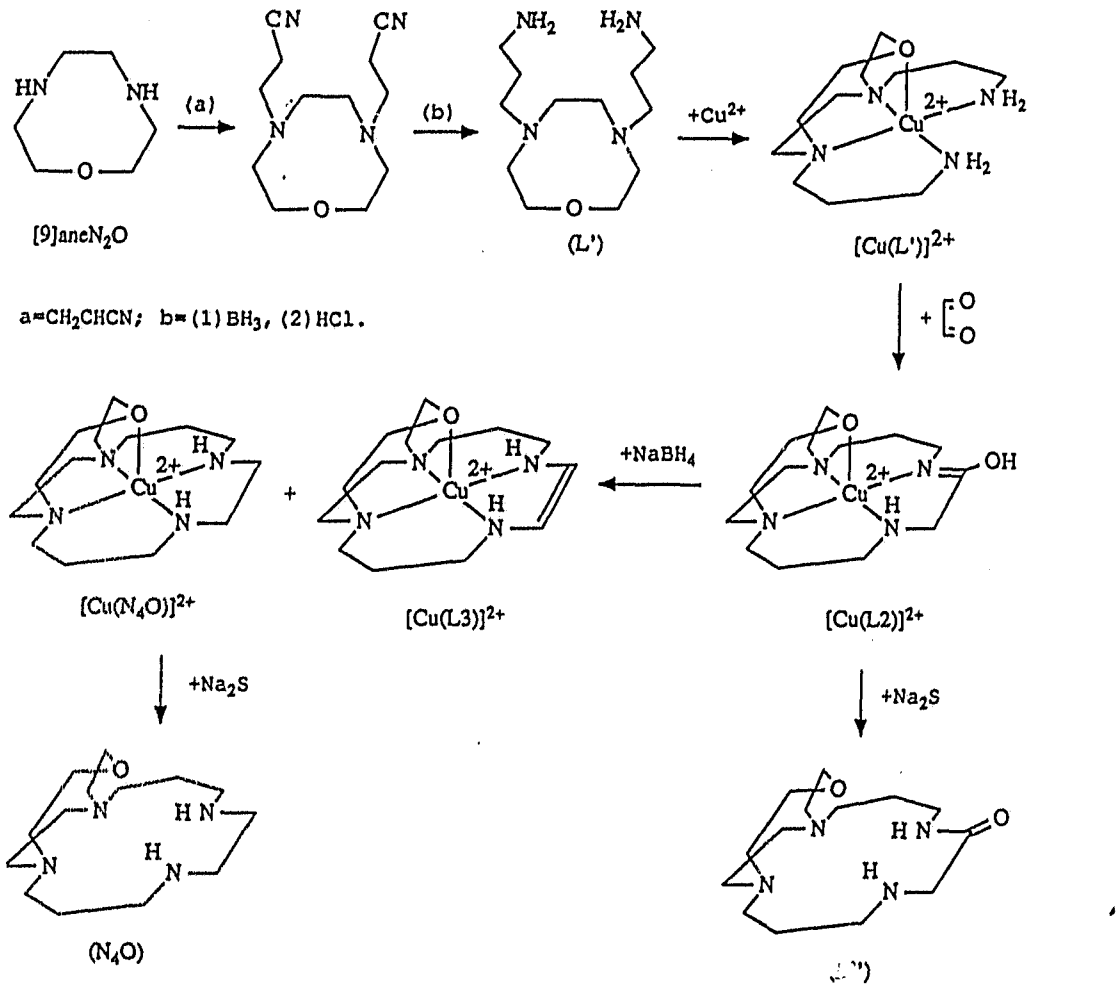

Scheme 2.3

N,N'-di(3-aminopropyl)-1-oxa-4,7-diazacyclononane, L'

The cyanoethyl derivative obtained above (2 g, 8 mmol)

was dissolved in BH_3·thf (1M in thf, 80 mL) and brought to reflux for 4 hours. Ethanol (40 mL) was added carefully to the cooled solution in order to destroy the excess BH_3. The mixture was taken to dryness under reduced pressure and subsequently dissolved in a methanolic solution of HCl (4M, 80 mL) and refluxed for 1 hour. The solvent was again removed under reduced pressure, and the resulting oil dissolved in 3M NaOH (40 mL) and extracted into CH_2Cl_2 (5x30 mL). The organic layers were combined, dried over Na_2SO_4, and taken to dryness. The resulting oil, (2.5 g) contained the desired product.

^1H nmr: 3.7 (t, J = 4.5 Hz, 4H, O-CH_2); 2.8 (m, 16H, N-CH_2); 1.6 (q, J = 8 Hz, 4H, CH_2-CH_2-CH_2); 1.4 (s, 4H, NH_2).

Mass (CI): (M+1) 245; (M+29) 273; (M+41) 285.

The ligand was purified by crystallization as the corresponding copper(II) salt.

Cu(L′)(ClO_4).H_2O

To a solution of the oil (1 g) containing L′ in water (50 mL) was added $Cu(ClO_4)_2.6H_2O$ (5.2 g, 17 mmol). The solution turned blue immediately, but was heated to 80°C for 1 hour to ensure complete complexation. Upon cooling, purplish-blue crystals were produced. The product was filtered, rinsed with ethanol, then ether and air dried. Yield 1.6g.

IR: NH_2 stretches, 3260(s), 3290(s) cm^{-1}; NH_2 scissor, 1600(s) cm^{-1}; perchlorate, 620(s), 1100(s, br) cm^{-1}.

Anal.: for $[Cu(C_{12}H_{28}N_4O)](Cl_2O_8)H_2O$

Calc.: C, 27.44; H, 5.76; N, 10.68.

Found: C, 27.59; H, 5.37; N, 10.62 %.

(6-Hydroxy-17-oxa-1,5,8,12-tetraaza-bicyclo[10.5.2]nonadec-5-ene)copper diperchlorate. [Cu(L2)$(ClO_4)_2$]

To a solution of [Cu(L')$(ClO_4)_2$] (400 mg, 0.8 mmol) in methanol/water (9/1, 600 mL) was added glyoxal (40% solution in water, 0.16 mL, 1.1 mmol) and the pH adjusted to about 4. The mixture was refluxed overnight, the color becoming slightly more purplish-blue. After the reaction mixture was taken to dryness under reduced pressure, the product was recrystallized from hot water (7 mL) acidified with conc. $HClO_4$ (1 mL). The crystals obtained, some of which were of X-ray quality, were rinsed with ethanol, ether and air dried. Yield 350 mg, 83%.

IR: NH stretches, 3260(m) cm^{-1}; -N=C-OH, 1420(m), 1670(m) cm^{-1}; perchlorate, 620(s), 631(s), 1100(s, br) cm^{-1}.

Anal.: for [Cu$(C_{14}H_{28}N_4O_2)(ClO_4)_2$]

Calc.: C, 30.67; H, 5.15; N, 10.23.

Found: C, 30.56; H, 5.06; N, 10.09 %.

6-Oxo-17-oxa-1,5,8,12-tetraazabicyclo[10,5,2]nonadecane, L"

To a solution of [Cu(L2)]$(ClO_4)_2$ (120 mg, 0.2 mmole in 10 ml H_2O), more than two fold excess of Na_2S was added. After the pH was adjusted to ~13, the bluish-purple solution was refluxed overnight until the purple color disappeared.

Thereafter, the resulting solution was filtered through a fine glass frit to remove the black CuS precipitate formed. The supernatant was saturated with Na_2CO_3 before being extracted with $CHCl_3$ (3x10 ml). The organic layers were combined, dried over Na_2SO_4 and taken to dryness under reduced pressure, leaving a colorless hydroscopic oil. Yield 36 mg (0.09 mmole, 47%).

M.S. (CI): (M+1) 285; (M+29) 313; (M+41) 325.

^1H nmr ($CDCl_3$): 1.6 (q, J = 7 Hz, 4H, C-CH_2-C); 2.1 (s, 2H, N-CH_2-CO); 2.4 - 2.8 (m, 16H, N-CH_2); 3.35 (s, 1H, C-NH-C); 3.7 (t, J = 4.5 Hz, 4H, O-CH_2); 8.5 (s, 1H, HN-CO).

(17-Oxa-1,5,8,12-tetraaza-bicyclo[10,5,2]nonadecane)copper diperchlorate, [Cu(N$_4$O)(ClO$_4$)$_2$]

To a solution of [Cu(L')(ClO_4)$_2$].H_2O (760 mg, 1.5 mmol) in methanol/water (9/1, 750 mL) was added glyoxal (40% solution in water, 0.3 mL, 2 mmol). The mixture was refluxed overnight, after which the cooled solution was treated with $NaBH_4$ (240 mg, 4.4 mmol) and further heated to reflux for 2 hours. The reaction mixture was taken to dryness under reduced pressure. The product was recrystallized from hot water (*ca.* 15 mL) acidified with conc. $HClO_4$ (1 mL). The magenta crystals were filtered, rinsed with ethanol and air dried. Yield 650mg (81%).

IR: NH stretches, 3080(s), 3140(s), 3220(s), 3285(s) cm^{-1}; perchlorate, 622(s), 634(s), 1100(s, br) cm^{-1}.

Anal.: for $[Cu(C_{14}H_{30}N_4O)(ClO_4)_2]$

Calc.: C, 31.54; H, 5.68; N, 10.52;

Found: C, 31.50; H, 5.56; N, 10.46 %.

(17-Oxa-1,5,8,12-tetraaza-bicyclo[10.5.2]nonadec-6-ene)copper diperchlorate, $[Cu(L3)(ClO_4)_2]$

A sample of the reaction mixture from $[Cu(L2)]^{2+}$ (*vide supra*) was eluted on a Sephadex column (CM C-25). When washed with 0.2M NaCl, three bands appeared. The first band eluted was confirmed as $[Cu(L2)]^{2+}$, and the second principal segment was $[Cu(N_4O)]^{2+}$. The third blue-purple band was taken to dryness and, after removal of NaCl, the material was recrystallized from water (5 mL) containing 1 mL 9M $HClO_4$. The dark blue crystals formed were filtered, washed with ethanol and air dried. On some occasions this band was not observed. However, when present, the material could also be derived by fractional crystallization from the reaction mixture since the dark blue colour was distinguishable from the magenta $[Cu(N_4O)]^{2+}$ ion.

IR: NH stretches, 3420(s), 3495(s) cm^{-1}; perchlorate, 628(s), 1100(s) cm^{-1}.

Anal. calc. for $[Cu(C_{14}H_{28}N_4O)(ClO_4)_2]$ (found): C, 31.65(31.25); H, 5.32(5.53); N, 10.56(10.32)%.

17-Oxa-1,5,8,12-tetraaza-bicyclo[10.5.2]nonadecane, N_4O

To a solution of $Cu(L2)(ClO_4)_2$ (480 mg, 0.9 mmol) in water

(100mL) was added a solution of Na_2S (2 g, 8.3 mmol, 25 mL). The mixture was refluxed overnight whereupon the reddish-blue colour of the complex had disappeared. The CuS precipitate was filtered by use of a fine glass frit and the supernatant was taken to 1/4 of the original volume under reduced pressure. Sodium hydroxide was added (*ca.* 3 g, 3 M) and the ligand was extracted into CH_2Cl_2 (5x20 mL). The organic layers were combined, dried with Na_2SO_4 and the solvent removed leaving a colourless hydroscopic oil. Yield 0.2 g (82%).

^1H nmr ($CDCl_3$): 1.6 (s, br, 4H, C-CH_2-C); 2.8 (m, 20H, N-CH_2); 3.7 (s, br, 4H, O-CH_2); 1.3 (s, 2H, NH).

^{13}C nmr ($CDCl_3$): 77.0 (C-CH_2-C); 58.9, 58.4, 54.6 (N-CH_2-C); 49.0, 47.8 (NH-CH_2).

(17-Oxa-1,5,8,12-tetraazabicyclo[10.5.2]nonadecane)nickel diperchlorate, [Ni(N$_4$O)(ClO$_4$)](ClO$_4$)

The ligand L2 was dissolved in 25 mL dry ethanol and a four-fold exess of nickel(II)acetate was added with stirring. The mixture was refluxed for 48 hours, after which the cooled solution was reduced in volume to 5 mL. Unreacted nickel acetate was centrifuged off as a very fine green precipitate leaving a clear purple supernatant to which $NaClO_4$ (4M) was added dropwise. The purple precipitate of [Ni(L2)(ClO_4)](ClO_4) formed immediately. The product was filtered, washed with ethanol and ether and air dried. Yield 320 mg (78%). X-ray quality crystals were prepared by diffusion of ether into a

nitromethane solution of the complex.

Anal.: for $NiC_{14}H_{30}N_4O_9Cl_2$

Calc.: C, 31.84; H, 5.68; N, 10.62.

Found: C, 31.43; H, 5.57; N, 10.41 %.

2.1.3 [Ni_2(1,1'-bicyclo-3,6,10,13-tetraazatetradec-2,13-dienylidene)] $(ClO_4)_4$, [Ni_2(L4)] $(ClO_4)_4$

To a yellow solution of Ni(II)cyclam (1.0 g) in 1.0 M $HClO_4$ (30 mL), which was preheated to 70°C, was added 20 drops of 30% H_2O_2/H_2O with stirring. After the solution had turned to a dark red color, it was immediately placed in an ice/water bath. After 10 minutes, a dark reddish precipitate was formed. The product was isolated with filtration and washed with ethanol, then ether and air dried. Yield 0.227 g (~ 25%).

X-ray quality crystals of Ni(II)(L4)$(ClO_4)_4$ were obtained by dissolving 300 mg of material in 1.5 mL of H_2O, followed by addition of 5 drops of conc. $HClO_4$. After 10 minutes, the precipitate formed was filtered off, and the supernatant was kept still (absolutely no disturbance) and allowed to evaporate very slowly for 10 days. This procedure was repeated until X-ray quality crystals were formed.

IR: C=N stretch, 1610(m) cm^{-1}; C=C stretch, 1410(m) cm^{-1}; ClO_4^-, 1100(s), 620(m) cm^{-1};

Ana.: for [$Ni_2C_{20}H_{36}N_8Cl_4O_{16}$]

Calc.: C, 26.57; H, 3.98; N, 12.40;

Found: C, 26.40; H, 3.82; N, 12.08 %.

2.1.4 Common Reagents:

All materials used in this thesis work were of reagent grade, unless specified otherwise.

$LiClO_4$: This was prepared by reacting $HClO_4$ with $LiCO_3$. The trace amount of sulphate ion shown to be present in the product may be removed by addition of small portion of $Ba(ClO_4)_2$. After recrystallising from water three times, a stock solution of about 3 M $LiClO_4$ was prepared by dilution with deionised water, and was standardised by hydrogen ion exchange. An aliquot (400 µl) was passed through a column containing Dowex 50W-X8 (50-100 mesh, 15x1 cm) ion-exchange resin in the H^+ form. The column was rinsed with deionised water until the eluant was neutral. This solution was then titrated against 0.100 M NaOH using phenolphthalein as an indicator.

Hexaaquocobalt(III): A glass electrolysis cell containing two compartments separated with a glass frit, was filled with 100 mL of 4 M $HClO_4$. To the anodic compartment, 0.4 g of $Co(ClO_4)_2 \cdot 6H_2O$ was added and, using platinum wire electrodes, 4 V were applied across the cell in a refrigerator and under darkness for 24 hours. The resulting deep blue Co(III) solution was stored in a freezer, where it could be kept for several months. The concentration of Co(III) was measured spectrophotometrically (ε_{605nm} = 35.3 $M^{-1}cm^{-1}$)[74] before use.

Dry Acetonitrile for Electrochemistry: Reagent grade acetonitrile was dried overnight over calcium hydride, then

distilled under an Argon atmosphere over fresh calcium hydride immediately before use.

2.2 Instrumentaton:

2.2.1 Stopped-flow:

The measurement of reaction rates can be achieved by monitoring of some observable property of reactants or products with respect to time. For rapid reactions, there are a number of techniques available. Among them the stopped-flow technique is the most commonly used. This is because it has a wide range of applicability with regard to observable reaction rates (1 *ms* < $t_{1/2}$ < 5 min.), is adaptable to variety of detection methods (such as UV-Visible, ESR, and nmr spectrometers), and requires minimum amount of reagent solution (*ca.* 10 mL). In this laboratory, the primary method of detection employed is spectroscopic using UV and visible light.

Generally speaking, the way a stopped-flow works is to stop a flowing mixture of reagents, and then monitor the concentration change of a particular species which can be either the reactants or the products. Taking a redox reaction as a example, a solution containing the reductant (A of Fig. 2.1) and a solution containing the oxidant (B) are mixed together rapidly in a eight-jet, two-stage tangential mixing chamber (C), and the resulting reacting solution flows through an observation cell (D). There is a finite time required for

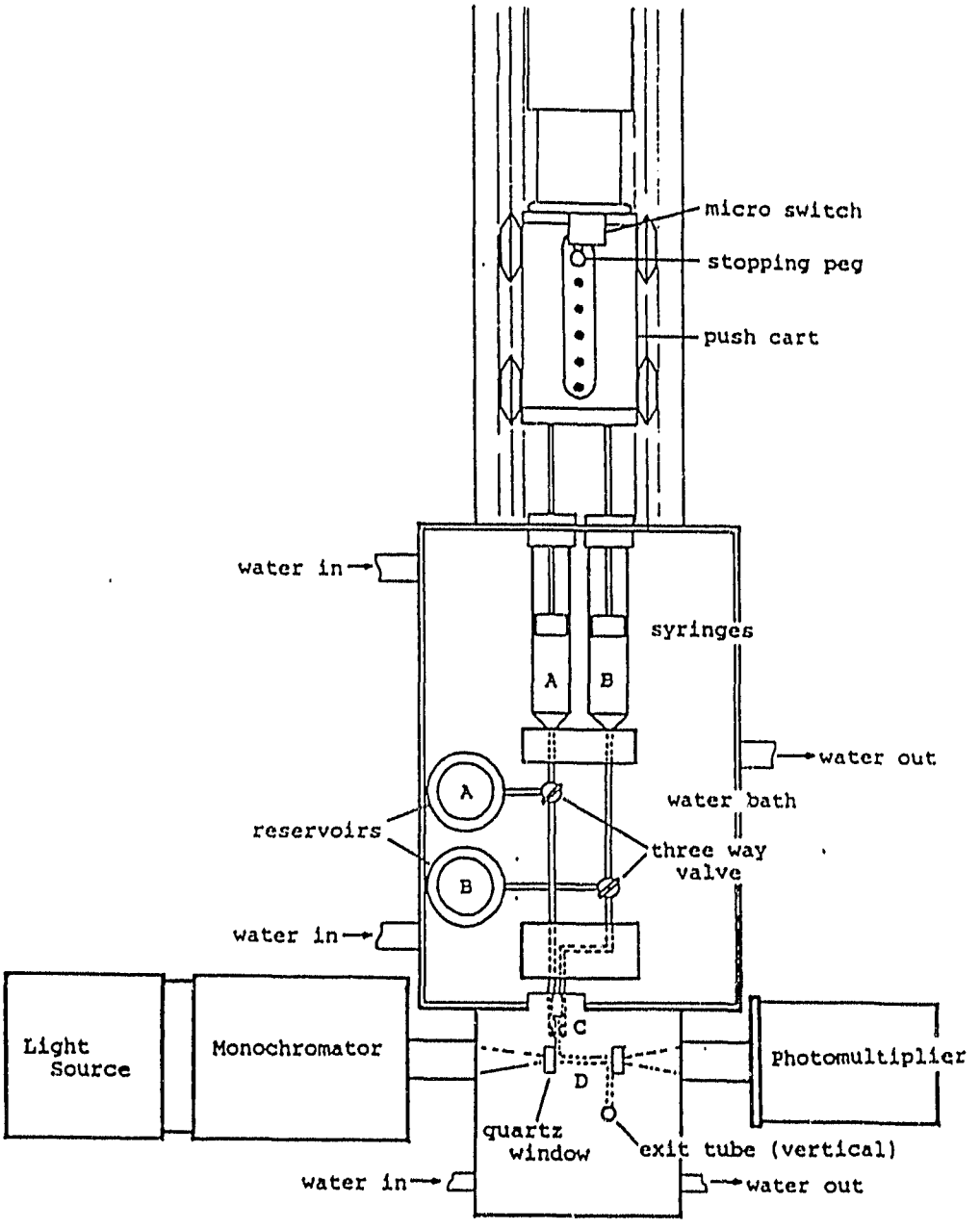

Fig. 2.1 Stopped-flc ; Apparatus.[75b]

the solution to be mixed and injected into the observation chamber. This is the "dead-time" (*ca.* 4 ms) which ultimately limits the observable reaction rate. When the flow of this reacting solution is suddenly stopped, the segment within the observation chamber will continue to react and the rate of reaction of this solution may then be monitored.

The monochromatic light used in the observation is detected by a photomultiplier which converts the observed intensity of light to voltage by a linear amplifier with variable gain settings and noise filters to a value between 0 to +10 V. The output is fed to an oscilloscope for visual display and to an IBM personal computer through a Techmar PC-Labmate, which performs the analogue-to-digital conversion (it is also the source of the electronic clock). The data are manipulated by the computer to give the variation of voltage versus time, and subsequently, to give the variation of Ln(ΔOD) with respect to time. A more detailed description of the mathematical relationships and the instrumentation can be found in ref. 75.

2.2.2 Cyclic Voltammetry:

Cyclic voltammetry is a controlled potential technique. It is performed at a stationary electrode which is in contact with an electrolyte solution containing the species of interest. The potential, E, at the electrode is varied linearly with time, t, and at some predetermined value of E

the scan direction reversed. The current which flows through the cell is measured continuously during the forward and reverse scans and it is the analysis of the resulting *i*-E response, and its dependence on the scan rate dE/dt, which provides a considerable amount of information. There are several excellent articles which deal with the theoretical and experimental aspects of cyclic voltammetry at both introductory[76] and more sophisticated levels.[77,78] The introduction provided here will only outline the basic terms involved in application of cyclic voltammmetry technique.

Consider a typical cyclic voltammograme (CV) of species Ox_1, Fig. 2.2. The forward scan commences at the *initial potential* of -0.75 V and very little current is obtained until about -1.15 V where Ox_1 begins to be reduced to the product Red_1:

$$Ox_1 + ne \underset{k_b}{\overset{k_f}{\rightleftharpoons}} Red_1 \qquad (2.1)$$

The current increases as the rate of reduction increases at more negative potentials but eventually a maximum is reached (-1.25 V) and thereafter the current decreases steadily. The cathodic peak in the CV results from the competition of two factors: (a) the increase in the (net) rate of reduction as the potential becomes more negative and (b) the development of a thickening depletion layer across which reactant has to diffuse. At potentials more than 100/n mV past the peak,[79] the reactant concentration at the electrode surface is small

compared to the concentration far from the electrode, and the current is controlled by the rate of diffusion of reactant through the depletion layer (diffusion controlled current).

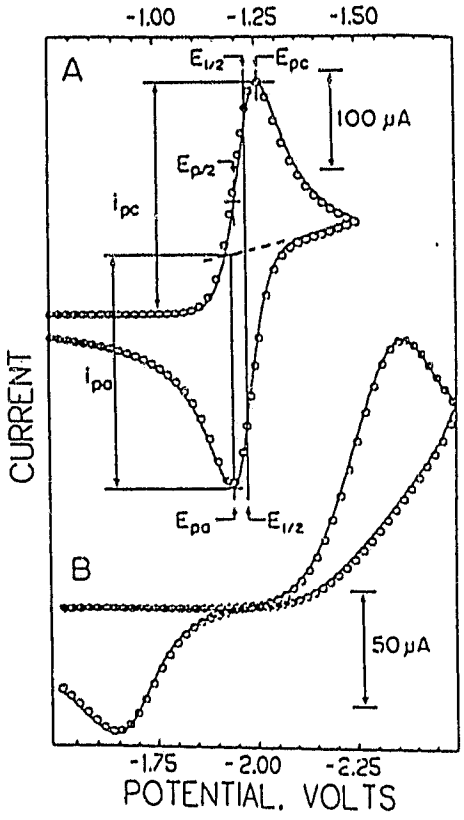

Fig. 2.2 Cyclic Voltammogramme

The scan direction is reversed at -1.50 V, and the diffusion-controlled reduction continues until about -1.25 V, where net oxidation of Red_1 back to Ox_1 occurs. The layer from which Ox_1 has been *depleted* is an *accumulation* layer for Red_1 and some of this Red_1 can diffuse back to the electrode and be oxidized. An anodic peak in the CV is obtained for reasons analogous to those underlying the cathodic peak: the surface

concentration of Red_1 becomes small and the current is limited by the rate of return of Red_1 to the electrode.

In general, the CV is characterized by several important parameters:[80] the cathodic (E_{pc}) and anodic (E_{pa}) peak potentials, the cathodic (i_{pc}) and anodic (i_{pa}) peak currents, the cathodic half-peak potential ($E_{p/2}$) and the half-wave potential ($E_{1/2}$). The definition of $E_{1/2}$ is borrowed from classical polarography according to eq. 2.2,

$$E_{1/2} = E^\circ + (RT/nF)\ln(D_{Red}/D_{Ox})^{1/2} \qquad (2.2)$$

E° is the formal potential pertaining to the ionic strength of the solution used, D_{Ox} and D_{Red} are the diffusion coefficients of the oxidized and reduced forms respectively, and n is the number of electrons in the half reaction. F is Faraday constant (96,486 Coulombs/mole). Because D_{ox} is usually very close to D_{Red} in value, $E_{1/2}$ is often considered to equal to E° ($[E_{1/2} - E^\circ]$ is normally only few mV).[79]

The above example is a ideal case for the *reversible* electrochemical process. In this type of reaction, the electron transfer reaction at the electrode surface is so fast that equilibrium ($K = k_f/k_b$) is maintained even with a substantial net current and a rapidly changing potential, that is, the Nernstian equation prevails throughout the entire process (giving rise to a Nernstian CV curve). In some cases, the electron transfer at the electrode surface is not fast. That is, the speed of electron transfer is not able to compete with the net current or the potential change. Processes of

this sort are termed electrochemically *quasi-reversible* (if k_f and k_b are of the same order of magnitude over most of the potential range) or totally *irreversible* (if $k_f \gg k_b$ for the cathodic peak and $k_b \gg k_f$ for the anodic peak). The characteristics of a Nerstian CV wave are:

1) $|E_{pc} - E_{p/2}| = 2.2RT/nF = 57/n$ mV at 298 K;

2) $E_{pc} - E^\circ = 1.1RT/nF = 28.5/n$ mV at 298 K;

3) $\Delta E_p = |E_{pc} - E_{pa}| = 2.2RT/nF = 57/n$ mV at 298 K;

4) $i_{pc} = i_{pa}$;

5) E_{pc} and ΔE_p independent of scan rate.

Depending on the experimental conditions, the observed ΔE_p may vary from 57 to 80 mV.

The diagnostic criteria for an irreversible CV wave are:

1) $|E_{pc} - E_{p/2}| = 1.8RT/\alpha nF = 48/\alpha n$ mV at 298 K;

2) $\Delta E_p > 60$ mV at 298 K;

3) $E_{pc} - E^\circ = -(RT/\alpha nF)\{0.78 + \ln(D_{Ox}^{1/2}/k_s) + \ln[(\alpha nFv)^{1/2}/RT]\}$;

4) $\Delta E_{pc}/(\Delta \log v) = -30/\alpha n$ mV at 298 K;

5) $i_p(irrev)/i_p(rev) = 1.1\alpha^{1/2}$.

α is the *charge-transfer* parameter, and associated with the degree of the irreversibilty. k_s is the electron transfer rate at E°. v is the scan rate. In the case where $\alpha = 0.5$, the CV obtained will have a symmetrical shape, and E° is at the midpoint of E_{pc} and E_{pa}, as shown in fig. 2.2b. For the process where $\alpha \neq 0.5$ the mean potential of E_{pc} and E_{pa} is displaced from the true E°, to negative values if $\alpha < 0.5$ and positive

values if $\alpha > 0.5$.[76d]

The processes discussed above are all purely electrochemical reactions (no chemical reaction involved). For such a system, cyclic voltammetry can provide information about: (i) the reversibility of process; (ii) the formal potential, E° ($= E_{1/2}$) for the reversible (and quasi-reversible when $\alpha = 0.5$) reactions; (iii) the number of electrons, n, involved in the process. In addition, application of quasi-reversible CV in obtaining the rate of eletron-transfer has also been attempted both theoretically and experimentally.[81]

For the transition metal complexes, an electron transfer reaction, E, is sometimes followed by a chemical process, C, which may be either a structural rearrangement to a more stable form or a reaction to form a totally different species. A example for such system is shown in eq. (2.3):

$$Oxd_1 + ne \underset{k_{b1}}{\overset{k_{f1}}{\rightleftharpoons}} Red_1 \underset{k_2}{\overset{k_1}{\rightleftharpoons}} Red_2 \qquad (2.3)$$

The processes involved in eq. 2.3 are normally called an EC system. If both Red_1 and Red_2 are stable, and both the electron-transfer and the chemical reactions proceed very rapidly in comparison with the current and scan rate, a Nernstian wave will appear on the CV, and the system is called both electrochemically and chemically reversible. However, if k_{f1} and k_{b1} are fast enough but k_1 and k_2 are not, or Red_2 (or Red_1) is not stable on the cyclic voltammetry timescale, an

irreversible wave will appear, and the system is called electrochemically reversible but chemically irreversible. In some cases, it may also be chemically reversible but electrochemically irreversible.

A general treatment of a variety of systems involving both electrochemical and chemical processes has been introduced by Bond,[82] Rieke,[83] Geiger,[76d,84] and Walton.[85] In their treatment, the stable oxidized form, Ox_1, and reduced form, Red_2, are located at diagonal corners of a "square" scheme:

$$\begin{array}{ccc} Ox_1 + ne & \underset{k_{b1}}{\overset{k_{f1}}{\rightleftharpoons}} & Red_1 \\ k_4 \uparrow\downarrow k_3 & & k_2 \uparrow\downarrow k_1 \\ Ox_2 + ne & \underset{k_{b2}}{\overset{k_{f2}}{\rightleftharpoons}} & Red_2 \end{array}$$

Scheme 2.4 Electrochemical "Square Scheme"

where the species Red_1 and Ox_2 are normally less stable. In this system, as soon as Red_1 is formed from reduction of Ox_1, it is converted to the more stable form, Red_2. After the potential is reversed, the anodic peak is produced by oxidation of Red_2 (instead of Red_1) to form Ox_2, which being unstable, converts to Ox_1 upon formation. As a result, the cathodic and anodic peaks observed on the CV do not correspond to the same redox couple, and often shows quasi-reversible characteristics. By changing temperature and/or scan rate, Red_1 may sometimes be stable enough (or the scan rate is fast

enough) so that the anodic peak for oxidation of Red_1 can be observed on the CV, which then has two anodic peaks. The same can also occur to Ox_2 and the cathodic peaks. Studying this type of quasi-reversible CV, it is often possible to obtain mechanistic details of the reactions involved in a variety of EC and multi EC, $(EC)_n$, systems. Furthermore, Laviron and Roullier[86] have presented a general theoretical treatment for calculation of rate constants and/or equilibrium constants involved in such system. In their presentation, they simulated the cyclic voltammetric curve that should be exhibited for different relative rate constant values. Application of this theoretical approach in some cases has proven to be successful.[87] A more detailed discussion on this subject can be found in the references given above.

The CV's presented in this thesis were recorded with a PAR 273 Potentiostat/Galvanostat interfaced to an IBM PC computer and an EPSON FX-80 dot matrix printer. The electrochemical cell was of the conventional three electrode design with platinum microspheres as the counter and working electrodes (other electrodes such as glassy carbon were employed occasionally) and either a saturated calomel or Ag/AgCl reference electrode. The electrochemical potential of the reference electrodes was checked periodically by the measurement of known systems (e.g. Ferrocene/Ferrocinium, $Frc^{+/o}$, in acetonitrile). The solutions all contained appropriate supporting electrolyte (*vide infra*) to eliminate

migrational and resistance problems. All solutions were degassed by bubbling argon through the solution prior to electrochemical measurement.

2.2.3 Electron Spin Resonance:

When a magnetic field is applied to a sample containing **unpaired** electrons, the interaction of the field and the spin angular momentum produces two energy levels with the magnetic moment aligned with or against the magnetic field. For electrons, the spin state with $m_s = -1/2$ (labelled $|\beta\rangle$) has its spin anti-parallel to the applied field and is lower in energy. Stimulated transitions between the $|\beta\rangle$ and the $|\alpha\rangle$ ($m_s=1/2$) spin state occur when the radiant energy satisfies the equation

$$\Delta E = h\upsilon = g\beta H \qquad (2.8)$$

where υ is the applied frequency, H is the imposed magnetic field, h is Planck's constant, β is the Bohr magneton, and g is the Landé splitting factor, or commonly called the "g-factor".

g has a tensor character. In a magnetically anisotropic molecular environment, the value of g changes as a function of the orientation of molecule relative to the external field. The value of g, in any arbitrary direction, can be expressed as the resultant of the tensor components g_{xx}, g_{yy} and g_{zz}, corresponding to the direction of the x, y and z axes (the axis of highest symmetry in the molecule is conventionally

taken as the z axis). The average value of g, g_o, is equal to one-third of the trace of tensor, given by the relation

$$g_o = (g_{xx} + g_{yy} + g_{zz})/3 \qquad (2.9)$$

Measurements on homogeneous powdered or liquid solution phase samples give only the g_o value, while for single crystals or frozen solution samples the values of g_{xx}, g_{yy} and g_{zz} may be determined. In the case where the molecule has C_{4h} symmetry, $g_{xx} = g_{yy} = g_\perp$ and $g_{zz} = g_{/\!/}$, and eq. 2.9 may then be rewritten as

$$g_o = (2g_\perp + g_{/\!/})/3 \qquad (2.10)$$

For a free electron, the g value, g_e, should be "2.00", but small relativistic effects increase this value to 2.0023. In transition metal complexes (where unpaired electrons are located mainly on the metal center), calculation of g value is somewhat complicated by the fact that orbital moments must also be taken into consideration. Owing to the orbital moment contribution (through spin-orbital coupling), the value of g will differ from that for the free radical. This difference largely depends on orbital occupation, electron configuration, and the nature of the metal ion.

For technical reasons electron spin resonance (esr) spectrometers give the differential of the absorption in a static magnetic field on which a varying field is superimposed. The second integral of this value is proportional to the concentration. The value of the magnetic field corresponding to the symmetry center of absorption gives, by the use of eq. (2.8), the value of g. The absolute

g value of an unknown sample is, however, usually determined by measuring a sample of known g (g_k) value under the same conditions and using eq. 2.11

$$gH = g_kH' \qquad (2.11)$$

where H and H′ are the magnetic resonance fields for the unknown and the known samples respectively.

The external magnetic field is not the sole factor in determining the field strength acting on the unpaired electron, When the unpaired electron is located near a nucleus having $I \neq 0$. In this case the electron will be influenced, as is known, by $(2I + 1)$ different magnetic fields. Thus absorption will be observed at $2I + 1$ different values of the external magnetic field. To a first approximation, the spacings between the component spectral lines will be equal to one another and correspond to the *coupling constant*, A. This coupling constant A is actually a measurement of the residence probability of the electron in the immediate vicinity of the atomic nucleus. In the case of a magnetic field produced by the combined effects of several atomic nuclei at the electron, the nuclei will exert their effects independently from one another. When, for example, there are two atomic nuclei of nuclear spins I_1 and I_2 giving rise to a magnetic-field force, the number of lines in the spectrum will be $(2I_1 + 1)(2I_2 + 1)$. Also the spacing between the lines attributed to identical nuclei will be a measure of the residence probability of the electron. For different atomic nuclei these spacings are, in

general, different, and hence, conclusions can be drawn from these observations regarding the distribution of the electron within the molecule. In the case of transition metal complexes (where the unpaired electron is mainly on metal center), the couplings between the metal nuclei and d electrons are normally called "hyperfine-coupling" (hf-coupling); while the couplings between the donor nuclei and the d electrons are called "superhyperfine coupling" (shf-coupling).

Like g, A also has tensor character. For hf-coupling in the complex of axial (C_{4h}) symmetry, the average of A value, A_o, can be expressed as

$$A_o = (A_{/} + 2A_{\perp})/3 \qquad (2.12)$$

where $A_{/} = A_{zz}$, $A_{\perp} = A_{xx} = A_{yy}$. For shf-coupling, however, it is often possible to observe only either A_o or one of $A_{/}$ and $A_{\perp}$ due to the weakness of coupling. In liquid solution samples, only A_o can be observed for hf-coupling; while $A_{/}$ and $A_{\perp}$ may be observed for hf-couplings, and A for shf-couplings may be obtained only from a single crystal or frozen solution samples.

The introduction given above is only a "brief" outline of some very basic terms involved in esr spectroscopy. There are many books written which provide more detailed discussion on both the theoretical and experimental aspects of this subject.[88] There have also been a number of review articles on transition metal esr spectroscopy.[89] As can be seen from the above discussion, esr technique is very useful in the study of

transition metal complexes where unpaired electrons are present. By analyzing g and A values, esr spectra may offer detailed information about the location of unpaired electrons, the electron configuration of the metal center (and hence the coordination geometry), the occupation of the orbitals, the distribution of the electron density, and the coordination of donor type. Indeed, this technique has been, and still is, frequently used in the study of Ni(III) and Cu(II) complexes, especially when their structures are investigated.

Ni(III) complexes

In its complexes, d^7 Ni(III) frequently has a low-spin octahedral (or, tetragonal) configuration, which gives rise to the highest Crystal Field Stabilization Energy (CFSE). In the case where the metal is surrounded by four nitrogen donors in the equatorial plane, the esr spectra of these complexes often appear with $g_{xx} = g_{yy} = g_{\perp}$ and $g_{zz} = g_{/\!/}$ due to C_{4h} symmetry around metal center. However, relative values of $g_{/\!/}$ and $g_{\perp}$ are dependent on which orbital (d_{z^2} or $d_{x^2-y^2}$) the unpaired electron occupies. If the result of Jahn-Teller effect is the tetragonal elongation of octahedral structure (the unpaired electron occupies the d_{z^2} orbital), the effect of spin-orbital coupling gives rise to $g_{\perp} > g_{/\!/} \approx g_e$; while the tetragonal compression (the unpaired electron is in the $d_{x^2-y^2}$ orbital) causes a reversed order: $g_{/\!/} > g_{\perp}$.[90]

Depending on the nature of the axial donors, the shf-coupling between the electron and a nuclear-active donor may

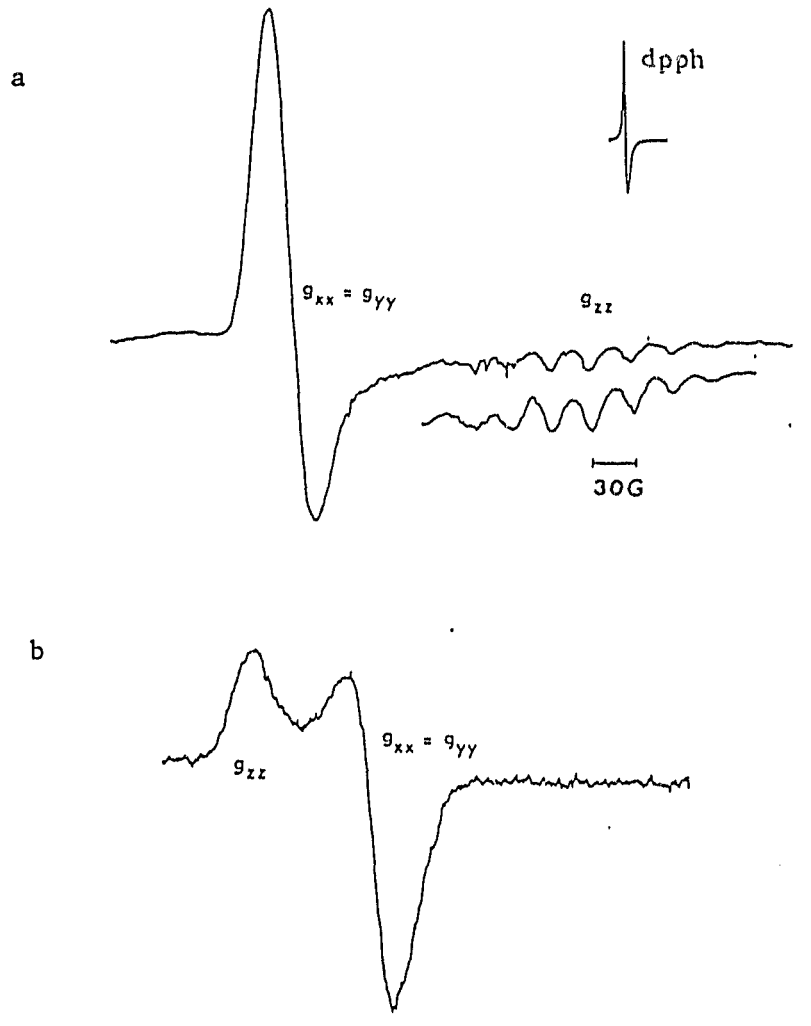

Fig. 2.3 ESR spectra of Ni(III) complexes (in a frozen solution, 77 K): a, in a tetragonally elongated octahedral geometry; b, in a tetragonally compressed octahedral geometry.[91]

---

appear with a center at $g_{\prime}$. The shf-coupling from equatorial donors, however, is usually absent due to the weakness of coupling. The typical esr spectra of these nickel(III)

complexes are presented in the Fig. 2.3.

Cu(II) complexes

In d^9 copper(II) complexes of square-planar, square pyramidal, and/or tetragonally-elongated octahedral geometry, the unpaired electron occupies the $d_{x^2-y^2}$ orbital because of the Jahn-Teller effect. The esr spectra normally appear with the order of g values as $g_{\parallel} > g_{\perp} > g_e$. In the case where the Jahn-Teller effect stablizes the $d_{x^2-y^2}$ orbital (in a tetragonally-compressed octahedral complex), the unpaired electron is in the d_{z^2} orbital, and the order reverses to $g_{\perp} > g_{\parallel} \approx g_e$.

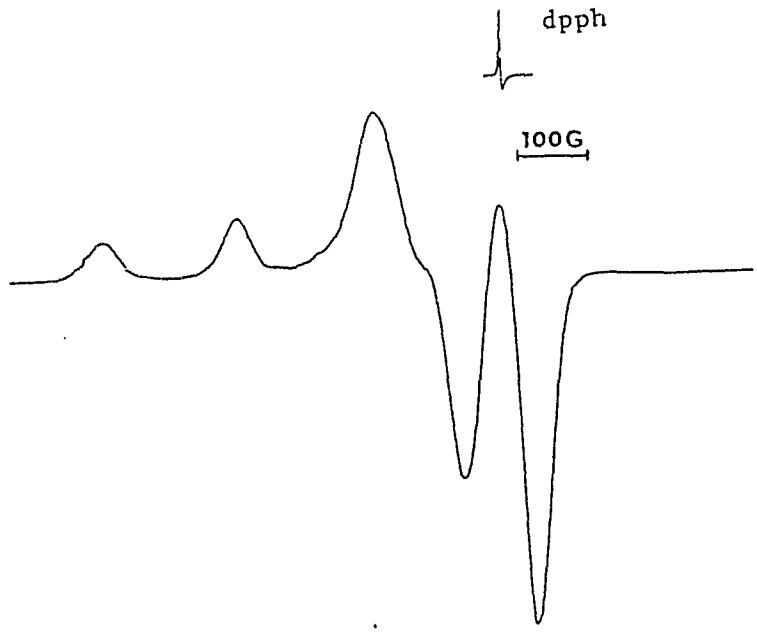

Fig. 2.4 ESR spectrum of Cu(II)cyclem[91b] (in frozen DMF, 77 K). (a typical spectrum for the tetragonally elonged octahedral, or square planar, geometry).

In nature, copper consists of ~61% of ^{63}Cu and ~39% of

^{65}Cu. Both have a nuclear spin of I = 3/2. The hf-coupling between the electron and these nuclei gives rise to eight peaks in their esr spectra. However, because of similar coupling strength of the ^{63}Cu and ^{65}Cu nuclei, the eight hf-coupling peaks frequently merge into four peaks and only the average coupling constant can be resolved.

The shf-coupling from the axial donor is often very weak in the Cu(II) complexes where the electron is in the $d_{x^2-y^2}$ orbital. When it is strong enough so that resolution can be made, the shf-coupling peaks normally appear around the center of $g_{\perp}$. Typical esr spectra of Cu(II) spectra are provided in Fig. 2.4.

The esr spectra presented in this thesis were recorded on a Varian E-6S spectrometer operating in the 3000 gauss range with X-band radiation ($\upsilon \approx 9.5$ GHz). The low temperature spectra were obtained using a quartz insert dewar filled with liquid nitrogen. The g values were calculated using eq. 2. with a known free radical DPPH, diphenylpicrylhydrazyl, (g = 2.0037).

2.2.4 Crystallography:

The theoretical and experimental discussion on the application of X-ray diffraction method in determination of molecular structure can be found in a number of text books, and articles.[92] The crystallographic determination of the molecular structures for the compounds presented in this

thesis were all completed by K.A.Beveridge, Department of Chemistry, University of Victoria. As a general procedure, the crystals were mounted in glass Lindemann tubes and the unit cells and space groups determined by using Weissenberg and precession photography, after which the crystals were transferred to a Picker four-circle diffractometer automated with a PDP11/10 computer. In the case of the ligand salt, $[N_4O(HClO_4)_4]$, the data were collected on a Nonius CAD4 instrument. More detailed descriptions of procedures involved in individual compounds will be provided where appropriate.

2.2.5 Other Instrumentation:

UV/Visible absorption spectra were obtained using a Perkin Elmer Lambda 4B UV/Vis spectrometer, or a Beckman DU-8 spectrometer. All spectra were recorded using a pair of matched 1 cm quartz cells (Hellma). Solution kinetics were monitored by using a two compartment quartz "split-cell" (Helma; 2x4.38 mm). Equal volumes of the reactants were placed in the compartments and mixed rapidly by inversion just prior to observation of the reaction. Note that due to the mixing time necessary, only slower reactions ($t_{1/2}$ > 1 min.) were measured by this technique. Data treatment was by a least squares analysis of the resulting ln(ΔOD) vs time plot on an IBM PC computer. The cell was thermostatted by an external water bath for the Lambda 4B.

High field ^{1}H and ^{13}C nmr spectra were obtained using a

Bruker WM 250 Fourier Transform spectrometer locked to the solvent deuterium resonance. ^{13}C spectra were obtained with broad-band ('noise') irradiation of appropriate frequencies to decouple the protons. Additional ^{1}H nmr spectra were obtained with a Perkin Elmer R-32 nmr spectrometer. All chemical shifts (in ppm) are reported relative to tetramethylsilane (TMS).

Infrared spectra were obtained with a Perkin Elmer 283 Infrared spectrometer using KBr pellets of the relevant species.

The pH of the solutions was measured with a Radiometer 26 pH meter or a Fisher Accumet 610A pH meter using an Orion 91-04 combination glass electrode. The electrode was standardized using standard buffers at pH 4.01 and 6.86 (25 °C) as applicable.

Optical rotation was measured using a Perkin-Elmer 141 Polarimeter at λ = 589 nm (sodium D lamp). All samples were studied in aqueous media at room temperature. The *specific rotation*, $[\alpha]_D$, and *molar rotation*, $[M]_D$, were used as units in data recording and discussions. The two units are defined as[112]

$$[\alpha]_D = \alpha_{\lambda obs}/(Cl_d)$$

$$[M]_D = \alpha_{\lambda obs}/([C]l_m)$$

where $\alpha_{\lambda obs}$ is the observed optical rotation, C is the concentration in grams per milliliter of the solute, l_d is the path length in decimeters, [C] is molar concentration of the solute, and l_m is the path length in meters.

Elemental Analysis were performed by Canadian Microanalytical Services, Vancouver, B.C. Canada.

Chapter 3. Synthesis and Redox Chemistry of the Ni(II)/(III) Complex of Bis Methyl-Substituted [9]aneN_3

3.1 Introduction

Recent developments in the study of the redox behaviour of the nickel(II/III) couple are largely credited to success in the synthesis of polyazamacrocycle complexes, most of which are tetraazamacrocycle complexes. The important property of these complexes is their ability to stabilize the Ni(III) species. As the nickel(II) system favours the formation of the square planar geometry and nickel(III) the pseudo octahedral, the change in geometry at the nickel centre of those complexes during the reaction makes it more complicated to analyze the factors affecting the electron-transfer process. Recently, nickel complexes of oxime, tris-bipyridyl and other di-imine ligands have been prepared,[90,93-99] which were capable of maintaining octahedral geometry in the +2 and +3 states. McAuley[100] and other workers[101] have also reported the preparation of the $[Ni([9]aneN_3)_2](ClO_4)_2$, the first example of a saturated N_6 donor set which is reasonably stable in aqueous media. The crystal structure of this species has been reported,[102] and investigation of its redox reaction also has been attempted.[100]

The present work proposes to extend these studies with synthesis of the (-)-(R)-methyl-1,4,7-triazacyclononane ligand, L1, and the corresponding nickel(II)/(III) complexes. The study of the redox reactions of these complexes is expected to enable a better understanding of the barriers associated with electron transfer, particularly by

investigating whether the presence of the methyl group in the inner sphere of the complex may pose a structural impediment in the self-exchange reaction:

$$Ni^{2+}(L1)_2 + {}^*Ni^{3+}(L1)_2 \rightarrow Ni^{3+}(L1)_2 + {}^*Ni^{2+}(L1)_2 \quad (k_{11}) \qquad (3.1)$$

Considering there are relatively few methods available for directly determining the rate of self-exchange[103] (eq. 3.1), the complex presented here has an advantage in the study of this type of reaction. That is, the asymmetric centre in the complex provides a possibility for such measurement (*vide infra*).[70b,104] Unfortunately, the self-exchange reaction in the present system is too rapid to do so with the equipment available. However, using cross-correlation reactions involving outer-sphere reagents, the self-exchange rate for the [Ni(II)/(III)$(L1)_2$] couple has been determined.

In addition, the ligand L1 has an extra methyl group on its "back-bone" (CH_2 chelate chain) comparing to the [9]aneN_3. It is interesting to see how this substitution on triaza macrocycles affects the electrochemical behaviour of Ni(II) center in comparison with that on the tetraaza macrocycles.

3.2 Synthesis

Ever since the Richman and Atkins procedure was introduced[19] for preparation of saturated nitrogen-containing macrocycles, its use has become common in syntheses of a large variety of polyaza macrocycles.[105] This is largely for the following reasons:

i) It requires moderate dilute conditions, and relatively short times as compared to the high dilute condition method.

ii) It gives rise to a "free" ligand as the product, which is readily usable in preparing any desired metal complexes (while "template" method produces metal-ion complexes, and also choosing an appropriate metal as template ion is sometimes a problem).

iii) Most important of all, it often leads to the best yield among the methods available.[105a]

Indeed, as far as triaza (or N_2X, X = S or O) cycles are concerned, almost all recently successful syntheses have employed this method.[105] For this reason, the Richman and Atkins method was used in synthesis of the target ligand.

In general, there are two possible ways to synthesise methyl-substituted [9]aneN_3 ligands as shown in Scheme 3.1:

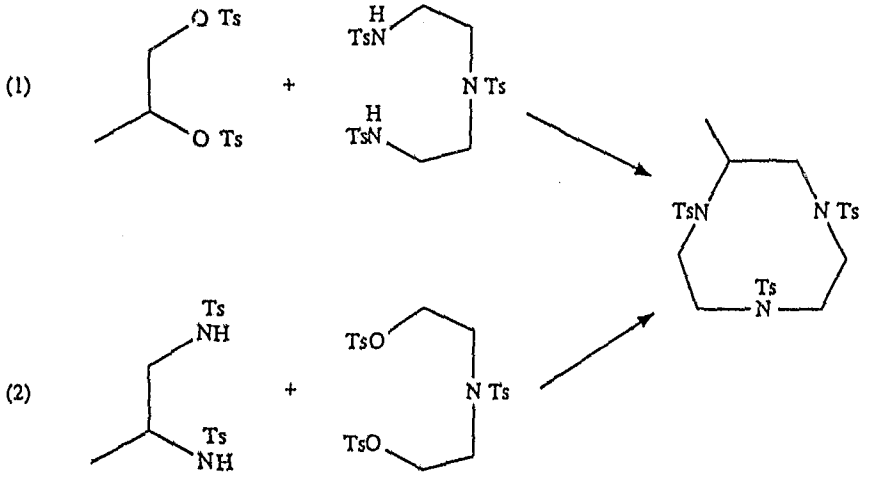

Scheme 3.1

However, Graham *et al*[106] have reported that the tosylated derivatives of the methyl-substituted diols failed to react with the sodium salts of the tosylated triamines, and the tosylated triamines were recovered in almost quantitative yield when route (1) was chosen.[106] These results have been rationalized in part as the inability of the bulky-N^-Ts nucleophile to attack a sterically hindered site such as a secondary C-OTs group.[106] Therefore, route (2) in scheme 3.1 is obviously a better choice for the present synthesis. The procedure involved in the synthesis of the target ligand has been described in section 2.1.

Resolution of (-)-(R)-1,2-diaminopropane was achieved by using the method described by Dwyer and co-workers.[71b] According to this method, the 1,2-diaminopropane isomer mixture was added into an aqueous solution of d-tartaric acid, and the precipitate formed was recrystallized 11 times from an acetic acid/water solution. The resulting tartrate salt gave a specific rotation, $[\alpha]_D$, of -22.5°, which accounted for ~90% optical purity. This salt was then converted to the hydrochloride by reacting with KCl according to the method of Bailar *et al*.[107]

In general, the cyclization of the C-substituted precursor is much more difficult than the unsubstituted analogues, and often leads to a low yield and a greater variety of by-products.[106] Though 2-methyl-[9]aneN_3 has been prepared by other workers,[106,108] the latest work by Graham *et*

al. showed only 20% yield of tritosylate cyclic product.[106] In their procedure, the cyclization was accomplished by using the disodium salt of N,N′-ditosylpropane-1,2-diamine to react with 2-[tosyl(2-tosyloxyethyl)amino]ethyl tosylate:

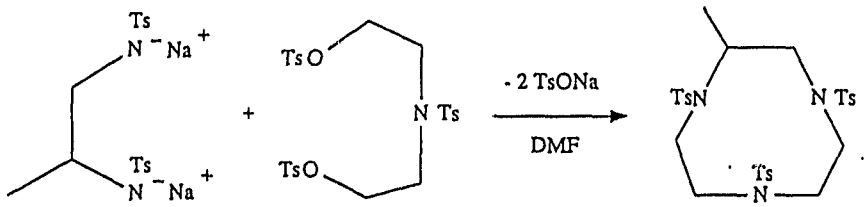

Scheme 3.2

To obtain a better yield, an attempt was made in the present work to carry out the cyclization by two steps (see Scheme 2.1). As the first step, only one amine group was deprotonated, which allowed the reaction to give exclusively the 1:1 product. This was followed by deprotonation of the second amine group, and then intra-molecular reaction to close the ring. The yield (50%) obtained from this procedure was more than double of that (20%) by other workers.[106]

Detosylation of the methyl-substituted macrocycles has also proved to be more difficult than was the case for unsubstituted macrocycles,[97] and often requires more vigorous conditions to completely remove the tosyl groups. For this reason, reactions of this type are frequently carried out in 40% HBr/acetic acid for a long period of time (usually > 24 hours).[106,109] However, in the present work it was discovered that the much better yield (59%) may be obtained using conc.

sulfuric acid at 155 °C for 30 min.. This result is remarkable considering the general difficulty imposed by C-substitution on the detosylation (e.g. 10% yield has been reported by other workers[108a]).

The molar rotation, $[M]_D$, of the free ligand L1 is - 41 deg.$M^{-1}m^{-1}$, which corresponds to $[\alpha]_D$ of -28.7°. This is comparable to the $[\alpha]_D$ of -22.5° from the starting material.

Complexation of Ni(II) with the free ligand L1 was readily achieved (see section 2.1), and the complex may be recrystallised as a perchlorate salt from an aqueous media at pH ≈ 10.5. Because of the presence of the C-substituted methyl group and the chiral centre on the ligand, it is possible that complexation above may result in at least 12 isomers. A tentative attempt was made to separate the isomers using column chromatography, and three pink bands were observed on a Sephadex column. The major band was eluted with 3.5 M $NaNO_3$ (section 2.1). However, no further resolution was pursued, and all chemical studies of this system were carried out using the product isolated from the major band on the column. Although single crystals were obtained from this product, the crystallographic determination of its molecular structure was unsuccessful due to the random orientation of the methyl group in molecular packing.

Oxidation of $Ni(II)(L1)_2^{2+}$ in either aqueous or nonaqueous media gave rise to its Ni(III) analogue. The Ni(III) species is stable, and may be isolated as a solid crystalline material

from nitrate media. However, attempts to determine its molecular structure also failed for the same reason as that in the case of the Ni(II) species.

3.3 Physical Properties

3.3.1 Spectroscopy

UV/Visible

In aqueous media, the UV/Visible spectrum of the pink $[Ni(II)(L1)_2]^{2+}$ solution has two d-d transitions at $\lambda_{max.}$ of 500 nm (ε = 4 $M^{-1}cm^{-1}$) and 798 nm (ε = 11.3 $M^{-1}cm^{-1}$), which is characteristic of the octahedral nickel(II) configuration.[110] The solution is relatively stable at neutral pH, but decomposes in acidic media (*vide infra*). Also in water, the Ni(III) complex showed considerable stability with little decomposition at pH 3 over a 24-hour period. The spectrum of this green solution is dominated by two strong charge transfer bands at maximums 274 and 315 nm ($\varepsilon \approx 8.5 \times 10^3$ $M^{-1}cm^{-1}$). There also is evidence for a weak d-d transfer at 550 nm and of a further feature at 795 nm (ε = 112 $M^{-1}cm^{-1}$).

ESR

The esr spectra of the Ni(III) species were measured in frozen (77 K) matrices. The $[Ni(III)(L1)_2]^{3+}$ ion in either aqueous or nonaqueous media has an esr spectrum characteristic of a low-spin d^7 ion in a tetragonally-elongated octahedral ligand field. The g values ($g_{/}$ = 2.031; $g_{\perp}$ = 2.114; 9.5GHz) are typical for such an ion (see section 2.2.3), and there is

evidence for shf-coupling involving the axially coordinated nitrogen donors, ($A_{/\!/}$ = 18.3G). In this regard, the esr spectrum is closely similar[100,111] to that of the Ni(III)([9]aneN$_3$)$_2^{3+}$ ion ($g_{/\!/}$ = 2.02, $g_\perp$ = 2.14, $A_{/\!/}$ = 23.7 G), and to the Ni(bpy)$_3^{3+}$ ion which also shows NiN_6 coordination ($g_{/\!/}$ = 2.02_7, $g_\perp$ = 2.13_7).[98]

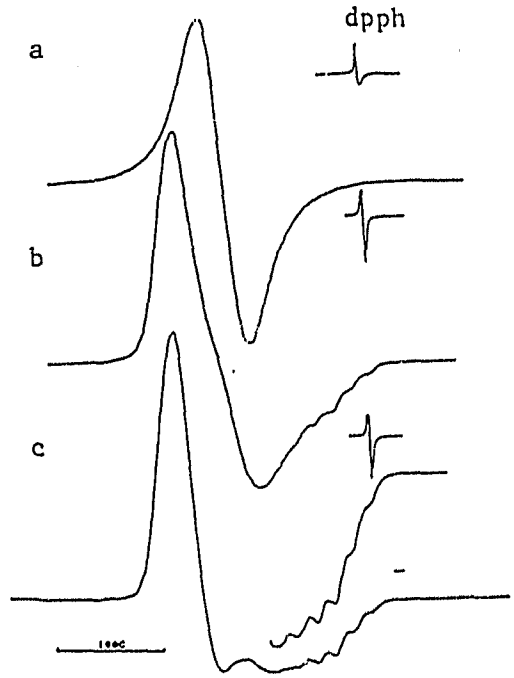

Fig. 3.1 a) ESR spectra of [Ni(III)(L1)$_2$]$^{3+}$ in deionised water (frozen solution, 77 K); b) as (a) in 0.1 M $LiNO_3$; c) as (a) and (b) in 3.0 M HNO_3.

Of interest is the effect of ionic strength on the esr spectrum (Fig. 3.1), which may be related to outer-sphere ion pairing with anions. From the solid Ni(III) complex (nitrate salt) solution was prepared in deionised water that was frozen

immediately. This showed an isotropic spectrum (g_{iso} = 2.0949) at 77 K (Fig. 3.1a). On addition of $LiNO_3$ to yield a NO_3^- concentration of 0.1M, departure was observed toward a pseudoaxial spectrum. Addition of further nitrate (as HNO_3) provided evidence at 1.5 and 3 M concentration (Fig. 3.1c) of the complete separation of the $g_{/\!/}$ and $g_\perp$ features to give an axial spectrum with shf-coupling observed in the parallel signal. The intermediate (0.1 M) spectrum (Fig. 3.1b) may be interpreted as deriving from an equilibrium mixture of the isotropic and axial spectra associated with the free cation and the ion-paired species. Outer-sphere association causes an asymmetry that produces the separation of the g values. This finding is important in considering the reduction by iodide ion where a preequilibrium is postulated prior to the electron transfer (*vide infra*).

3.3.2 Electrochemistry

The electrochemistry of the $[Ni(II)(L1)_2]^{2+}$ complex was studied using cyclic voltammetry in aqueous media with Li^+/H^+-NO_3^- (1.0M) as supporting electrolyte and Hg/Hg_2Cl_2 as the reference electrode. The CV of the Ni(II)/Ni(III) couple shows reversible behaviour with ΔE < 60 mV, i_{pc}/i_{pa} = 1, and a pH-independence in the range 0.1 - 1.0M $[H^+]$. The $E_{1/2}$ of this couple is 0.94 V (vs. NHE).

For the tetraaza macrocyclic complexes of Ni(II), it was observed that dimethyl substitution of the six-membered

chelate ring resulted in an increase of $E_{1/2}$ for the $Ni^{2+/3+}$ couple by ≈ 185 mV.[32] However, the same substitution on the five-membered chelate ring has little effect on the redox potential.[32] Here again, the difference in redox potentials for $Ni^{2+/3+}(L1)_2$ and $Ni^{2+/3+}([9]aneN_3)_2$ (which has $E_{1/2}$ of ~0.95 V[101]) is only ~10 mV. It appears that C-substitution on the **triaza** macrocycles has a similar effect on the redox properties of the metal centre as that on the **tetraaza** macrocycles.

3.3.3 Optical Activity

The optical activity of transition metal complexes has been well documented by other workers.[112,113] The Co(III) complex with the same ligand, L1, was reported, and the optical activity investigation of this complex showed a great conformational contribution to ligand field circular dichroism.[108a] The present $[Ni(II)(L1)_2]^{2+}$ complex provides a possible opportunity for investigation of how the electron-configuration change (from d^6 to d^7) affects the optical properties. However, because of the unavailability of suitable equipment, a detailed optical study of this Ni(II) complex could not be carried out at the present time. However, the optical rotation (OR) at the sodium D line was investigated.

Upon coordination of the ligand to Ni(II), the $[M]_D$ changed from - 41 to - 1.31×10^3 deg·M^{-1}·m^{-1}. This tremendous increase in OR is likely the result of both conformational contribution and structural distortion from perfect octahedron

(as in the case of the $[Co(III)(L1)_2]^{3+}$ complex[108a]), indicating that all six five-membered chelate rings in the complex are in the same conformation (either all λ or all δ), with some octahedral distortion. Oxidation of Ni(II) to Ni(III) led to $[M]_D$ of + 1.90×10^3 deg·M^{-1}·m^{-1}. This large reverse OR possibly resulted from the conformational reversal of all the chelate rings. The higher absolute $[M]_D$ value of the Ni(III) species in comparison with that of Ni(II) probably reflects the higher degree of conformational and structural (lowering pseudo-octahedral symmetry) twist in order for the ligands to better accommodate the smaller highly-charged Ni(III) ion.

The large difference in $[M]_D$ values between Ni(II) and Ni(III) species, 3.21×10^3 units, makes it a sensitive monitor for the change of oxidation-state on the metal center, which is particularly useful in measuring the self-exchange rate of $Ni^{2+/3+}$ couple[104]

$$Ni^{2+}(L1)_2 + {}^*Ni^{3+}(L1)_2 \rightarrow Ni^{3+}(L1)_2 + {}^*Ni^{2+}(L1)_2 \quad (k_{11}) \qquad (3.5)$$

where the ones with "*" are optically active components, and others are the racemic mixtures. It is unfortunate that the rate of the electron-transfer is too high, and could not be measured with the equipment available here.

3.4 Kinetic Investigation of Redox Reactions of $[Ni(II)/(III)(L1)_2]^{2+/3+}$

For all the redox reactions studied, the stoichiometry (to ± 2%) may be represented by a one-electron transfer. No

hydrogen ion dependences were observed over the range 0.02-1.0M $[H^+]$ as expected from the lack of any protonation equilibria exhibited by the reactants.

3.4.1 Hydrolysis of the Nickel(II) complex

The stability of the $[Ni(L1)_2]^{2+}$ complex was investigated in acidic media. Kinetic studies were made over the range 0.2-0.9 M $[H^+]$. The rate of decomposition is unusually slow for an octahedral Ni(II) species confirming the thermodynamic stabilisation imparted in coordination of the two facial N_3 donor ligands and the establishment of the various chelate rings. Rate studies were carried out (I = 1.0M) in acidic perchlorate media. The results are presented in Table 3.1 where it may be seen that a linear dependence is observed with respect to proton concentration. The observed rate law may be expressed in the form

$$R = k_H[Ni(L1)_2^{2+}][H^+] \qquad (3.3)$$

and it may be seen that $k_H = (1.81 \pm 0.09)\times10^{-4}\ M^{-1}s^{-1}$ at 30°C. Thus in 1.0M $[H^+]$, the half-life of the Ni(II) complex is 70 min.. This may be compared with $t_{1/2}$= 10 s for the corresponding $Ni(en)_3^{2+}$ ion under comparable conditions, and is understandable in terms of "macrocyclic effect" In acidic media any reactions in the stopped-flow time scale show negligible decomposition of the $Ni(L1)_2^{2+}$ during the course of the experiment. From the rate law it may be interpreted that protonation at one of the ligand sites leads to relatively

easy access of other hydrogen ions to complete the ligand dissociation which is consistent with the concept of *multiple juxtapositional fixedness* (*vide supra*).

Table 3.1 Rates of Hydrolysis of $[Ni(L1)_2]^{2+}$ in Acidic Media

$[Ni(II)] = 2\times10^{-4}M$; $\lambda = 202$ nm; $I = 1.0$ M; $T = 30°C$

$10^5 k_{obs}/s^{-1}$	3.55	5.56	7.4	8.00	12.5	13.7	16.9
$[H^+]/M$	0.20	0.30	0.40	0.50	0.70	0.80	0.90

Errors in individual rate constants ±1%.

3.4.2 Oxidation of $[Ni(L1)_2]^{2+}$ by $[Co(OH_2)_6]^{3+}$

Addition of $Co^{3+}(aq)$ to the Ni^{2+} solution gives rise to an immediate intense green colouration associated with the Ni(III) ion. Spectrophotometric titration showed a strict 1:1 stoichiometry with an isosbestic point at 224 nm. Kinetic measurements were carried out at λ = 340-600 nm where the absorbance is attributable solely to the Ni(III). The results are summarized in Table 3.2(a) where it is seen that the rate is strongly hydrogen ion dependent. Pseudo-first order conditions revealed a dependence on [Ni(II)] consistent with the rate law

$$d[Ni(III)]/dt = k_1[Ni(II)][Co_{aq}^{3+}] \qquad (3.3)$$

Since there are no proton-related dependences associated with the reductant, the mechanism may be expressed as

$$K_h = [CoOH^{2+}][H^+]/[Co^{3+}]$$

$$Ni(L1)_2^{2+} + Co_{(aq)}^{3+} \rightarrow Ni(L1)_2^{3+} + Co_{(aq)}^{2+} \quad (k_2) \qquad (3.4)$$

$$Ni(L1)_2^{2+} + Co(OH)^{2+} \rightarrow Ni(L1)_2^{3+} + Co^{2+} + OH^- \quad (k_3) \qquad (3.5)$$

The overall second order rate constant may thus be written in the form

$$k_1 = k_2 + k_3K_h/[H^+] \qquad (3.6)$$

and plots of k_1 against $[H^+]^{-1}$ are linear, leading to k_2 = 638 ± 28 $M^{-1}s^{-1}$ and k_3K_h = 251 ± 7 s^{-1} (R^2 = 0.992). On the basis of $K_h = 2x10^{-3}$ M,[74] $k_3 = (1.25 \pm 0.15)x10^5$ $M^{-1}s^{-1}$. The rates are broadly similar to those for the reaction of the $Ni([9]aneN_3)_2^{2+}$ ion (k_2 = 430 $M^{-1}s^{-1}$, $k_3 = 1.35x10^5$ $M^{-1}s^{-1}$) reflecting the almost identical E^o values. The rate constant for the hydroxo pathway, k_3, lies in the range 10^5–10^6 $M^{-1}s^{-1}$ derived previously for reactions of this type.

3.4.3 Oxidation of $Ni(L1)_2^{2+}$ by Ni(IV)oxime

The oxime, 3,14-dimethyl-4,7,10,13-tetraazahexadeca-3,13-diene-2,15-dionedioximate^{2-}, has been shown[93,94] to coordinate to Ni ions with deprotonation of the oxime goups in the Ni(IV) state. Previous studies have shown that there is no hydrogen ion dependence on reduction to Ni(III)[Hoxime] and that the latter species is a strong oxidant which reacts rapidly with a second mole of reductant to give, on protonation, the stable $[Ni(II)(H_2oxime)]^{2+}$ complex. Spectrophotometric titration of $[Ni(L1)_2]^{2+}$ with Ni(IV)oxime showed 2.05 moles of reductant required per mole of Ni(IV)oxime. Kinetic studies were made at $[H^+]$ = 0.5M under conditions of excess reductant. The data

presented in Table 3.2(b) are consistent with the rate law

$$R = k_4[Ni(L1)_2^{2+}][Ni(IV)\,oxime]$$

with k_4 of 40.4 ± 2.2 $M^{-1}s^{-1}$.

3.4.4 Reduction of $Ni(III)(L1)_2^{3+}$ with $Co(phen)_3^{2+}$

Kinetic studies were carried out in nitrate media to assist solubility of the reductant which was present in excess. Spectrophotometric data are consistent with (± 2%) the one-electron transfer

$$Ni(L1)_2^{3+} + Co(phen)_3^{2+} \rightarrow Ni(L1)_2^{2+} + Co(phen)_3^{3+} \quad (k_5) \quad (3.9)$$

There was no observed dependence on [H⁺] and studies were made at various [Co(II)] concentrations in 0.5 M HNO_3. The data (Table 3.2c) are well described by the equation

$$R = k_5[Ni(L1)_2^{3+}][Co(II)]$$

with $k_5 = (3.2 \pm 0.05)\times10^5$ $M^{-1}s^{-1}$ consistent with an outer-sphere electron transfer.

3.4.5 Oxidation of Iodide by $[Ni(III)(L1)_2]^{3+}$

There is a ready oxidation of $I^- \rightarrow I_3^-$ by the nickel(III) complex:

$$2Ni(L1)_2^{3+} + 2I^- \rightarrow 2Ni(L1)_2^{2+} + I_2\ (+ I^- \rightarrow I_3^-) \quad (k_6) \quad (3.11)$$

Kinetic studies were carried out at a variety of hydrogen ion concentrations. Rate data at 0.02 M and 0.2M ($HClO_4$) are presented in Table 3.2d. As may be seen, the dependence on

Table 3.2

a) Hydrogen Ion Dependence of the Rate of Oxidation of $[Ni(II)(L1)_2]^{2+}$ by $Co(III)_{aq}$

λ = 342 nm. $[Ni(II)] = 4\times10^{-4}$M. I = 1.5 M.

$[Co(III)] = 2.5\times10^{-5}$.

$[H^+]$/M (A)	0.10	0.20	0.25	0.30	0.35	0.40
$k_2/M^{-1}s^{-1}$ (B)	3140	1870	1730	1480	1380	1250
(A)	0.45	0.50	0.60	0.75	0.80	1.0
(B)	1230	1090	1080	940	940	780

b) Reaction of $[Ni(II)(L1)]^{2+}$ with Ni(IV)oxim

$[H^+]$ = 0.5 M. I = 1.0 M (ClO_4^-). T = 25°C. λ = 500 nm.

$[Ni(IV)] = 1.9\times10^{-5}$M.

$10^4[Ni(II)]$/M	4.01	8.0	16.01
10^2k_{obs}/s	1.33	3.20	6.24

c) Reaction of $[Ni(III)(L1)_2]^{3+}$ with $[Co(phen)_3]^{2+}$

$[H^+]$ = 0.5 M. I = 1.0 M (NO_3^-). T = 25°C. λ = 500 nm.

$[Ni(III)] = 1.9\times10^{-6}$M

$10^5[Co(II)]$/M	4.0	6.0	8.0	14.0
k_{obs}/s	12.4	19.0	25.9	44.9

d) Reaction of Iodide with $[Ni(III)(L1)_2]^{3+}$

$[Ni(III)] = 2\times10^{-5}$M. I = 1.0 M ($ClO_4^-$). T = 25°C. λ = 340 nm.

i. $[H^+]$ = 0.02 M:

$10^4[I^-]$/M	5	25	100
$k_{obs}/M^{-1}s^{-1}$	0.105	0.536	2.26

ii. $[H^+]$ = 0.2 M:

$10^4[I^-]$/M	5	25	100
$k_{obs}/M^{-1}s^{-1}$	0.106	0.516	2.17

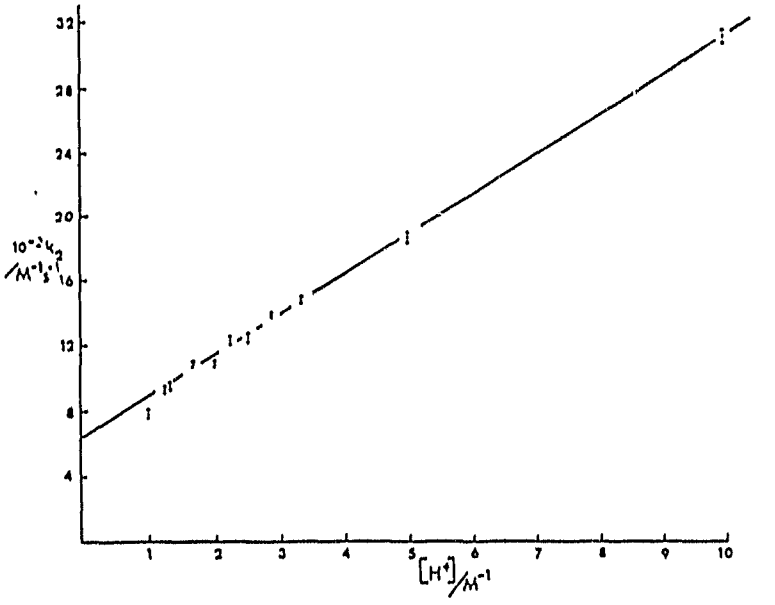

Fig. 3.2 Plots of k_2 against $[H^+]^{-1}$ for the reaction of $Co(III)_{aq}$ with $[Ni(L1)_2]^{2+}$. I = 1.0 M. T = 25 °C.

reductant up to 500 fold excess is strictly first order, in accordance with the hydrogen ion independent rate law

$$R = k_6[Ni(III)][I^-] \qquad (3.12)$$

with $k_6 = 214 \pm 5\ M^{-1}s^{-1}$.

3.4.6 Reaction of $Ni(II)(L1)_2^{2+}$ with $Ni([9]aneN_3)_2^{3+}$:

Although the ΔE value for the reaction is 0.005V, there is still an observable change on mixing of the reagents, enabling rate data to be derived for both the forward and reverse processes. For an equilibrium of this type

$$Ni(L1)_2^{2+} + Ni([9]aneN_3)_2^{3+} \underset{k_b}{\overset{k_f}{\rightleftharpoons}} Ni(L1)_2^{3+} + Ni([9]ane_3)_2^{2+} \qquad (3.13)$$

in conditions of excess of $[Ni(L1)_2^{2+}]$ and $[Ni([9]aneN_3)_2^{2+}$, the equilibrium may be treated as two pseudo-first order

Table 3.3

a) Rate Data for the Reaction of $[Ni(III)([9]aneN_3)_2]^{3+}$ with $[Ni(II)(L1)_2]^{2+}$

$[H^+]$ = 0.5 M. I = 1.0 M (ClO_4^-). λ = 400 nm.

Excess of $[Ni(II)([9]aneN_3)_2]^{2+}$ complexes present as indicated

$[Ni(III)]$ = $1x10^{-5}$M.

$10^4[Ni(II)([9]aneN_3)_2^{2+}]/M$		$10^4[Ni(II)(L1)_2^{2+}]/M$					
		2.0	4.0	6.0	8.0		
						Slope[a]	Int[b]
1.0		0.90	1.48	-	2.72	3042±49	0.28±.03
2.0	k_{obs}	1.16	1.74	2.41	3.02	3125±58	0.52±.03
4.0	$/s^{-1}$	1.55	2.16	2.78	3.46	3175±58	0.90±.03
6.0		2.11	2.76	3.44	3.06	3265±39	1.46±.02

a = $M^{-1}s^{-1}$, b = s^{-1}.

mean slope (k_f) = 3150 ± 40 $M^{-1}s^{-1}$

plot of intercepts against $[Ni([9]aneN_3)_2^{2+}]$ yields k_b = 2301 ± 440 $M^{-1}s^{-1}$.

Table 3.3 (continued)

b) Rate Data for the Reaction of $[Ni(II)(L1)_2]^{2+}$ with $[Ni(III)(cyclam)]^{3+}$

$[H^+]$ = 0.15 M. I = 1.0 M (ClO_4^-). λ = 380 nm.

Excess of $[Ni(II)(cyclam)]^{2+}$ complexes present as indicated.

$[Ni(III)(cyclam)^{3+}]$ = 1×10^{-5}M.

$10^4[Ni(cyclam)^{2+}]$/M		$10^4[Ni(II)(L1)_2^{2+}]$/M					
		3.0	4.0	5.0	7.0	Slope[b]	Int[c]
2.0	k_{obs} /s^{-1}	2.46±0.06	3.23±0.05	4.15±0.12	5.53±0.09	7717±317	0.18±0.16
4.0		3.1 ±0.2	3.95±0.2	4.41±0.05	6.25	7745±600	0.75±0.30
8.0		3.75	4.75	5.20±0.05	7.0	7914±600	1.42±0.30

mean slope (k_f) = 7792 ± 506 $M^{-1}s^{-1}$.

plot of intercepts against $[Ni(cyclam)^{2+}]$ yields k_b = 1602 ± 410 $M^{-1}s^{-1}$.

a) Error limits based on two independent determinations of the rate constant;

b) $M^{-1}s^{-1}$;

c) s^{-1}.

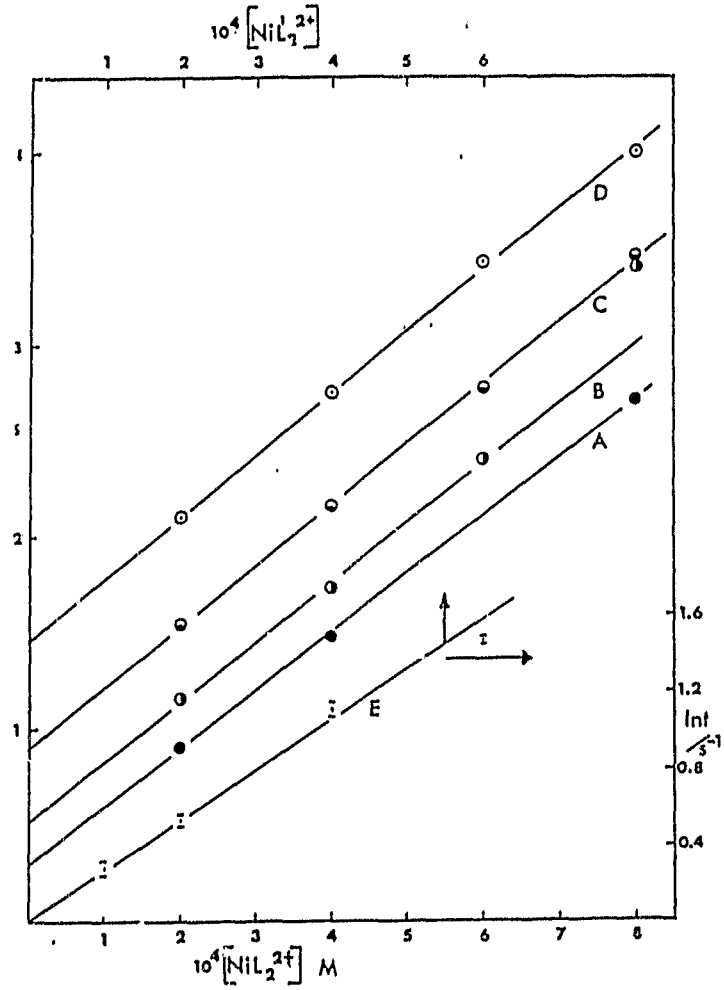

Fig. 3.3 Kinetic data for the reaction of $[Ni(L1)_2]^{2+}$ (NiL_2^{2+}) with $[Ni([9]aneN_3)_2]^{3+}$ ($NiL'_2{}^{3+}$), $[H^+]$ = 0.15 M, I = 1.0 M. Reversibility observed in conformity with eq. (3.14).

A,B,C,D = 2,4,6,8 x 10^4 M $[NiL_2^{2+}]$.

Slopes = k_f = (3.15 ± 0.4)x10^3 M^{-1}.

Right hand and upper ordinates: (E) Plot of intercepts from above against $[NL'_2{}^{2+}]$ yield as slope k_b = (2.3 ± 0.4)x10^3 $M^{-1}s^{-1}$.

reactions. The observed first order rate constant, k_{obs}, may be expressed in the form

$$k_{obs} = k_f[Ni([9]aneN_3)_2^{2+}] + k_b[Ni(L1)_2]^{2+} \quad (3.14)$$

At constant $[Ni(L1)_2^{2+}]$, plots of k_{obs} against $[Ni([9]aneN_3)_2^{2+}]$ should be linear. Intercept of lines of common slope (k_f) should be a linear function of $[Ni(L1)_2^{2+}]$ to yield k_b. Using the data in Table 3.3a it may be seen from Fig. 3.3 that such is the case, with (eq. (3.13)) $k_f = (3.15 \pm 0.04)\times10^3\ M^{-1}s^{-1}$ and $k_b = (2.31 \pm 0.14)\times10^3\ M^{-1}s^{-1}$ respectively. The ratio of the rate constants (K = 1.36) is in excellent agreement with the equilibrium constant (K = 1.22) derived from electrochemical data.

3.4.7 Reaction of $Ni(L1)_2^{2+}$ with $Ni(cyclam)^{3+}$

In view of the similarities in E° values, $\Delta E = 0.037V$, the reactions were investigated as outlined above for the equilibrium situation. The data presented in Table 3.3b are consistent with $k_f = (7.8 \pm 0.2)\times10^3\ M^{-1}s^{-1}$ and $k_b = (1.60 \pm 0.41)\times10^3\ M^{-1}s^{-1}$ respectively leading to an equilibrium constant K = 4.9. This is in reasonable agreement with K = 3.2 calculated from electrochemical measurements.

3.3.8 Discussion

The lack of any $[H^+]$ dependence in the reactions with $Co(phen)_3^{2+}$ and I^- is consistent with no protonation equilibrium for the Ni(II)/(III) couple. Substitution

Table 3.4 Marcus Parameters for the Redox Reaction of $[Ni(L1)_2]^{2+}$

---- at 25 °C using E° (NHE) = 0.940 V for $[Ni(L1)_2]^{3+/2+}$

	Reactant	E°(V)	$k_{11}/M^{-1}s^{-1}$	K_{12}	$\ln K_{12}k_{11}f_{12}$	$k_a/M^{-1}s^{1}$
1)	$Co(phen)_3^{2+}$	0.37[b]	8[b]	4.51×10^{9}	21.15	3.2×10^{5}
2)	$Ni(oxime)^{2+}$	0.65[c,d]	6×10^{4} [d]	1.22×10^{-6}	- 1.41	40.4
3)	Co^{3+}	1.86[e]	10^{-12} [f]	3.9×10^{15}	3.51	6.4×10^{2}
4)	I^{-}	1.40[g]	2×10^{8} [h]	1.61×10^{-8}	- 2.61	30[i]
5)	$Ni(9\text{-ane})_2^{3+}$	0.947[j]	6×10^{3} [k]	1.4	9.00	3.15×10^{3}
6)	$Ni(9\text{-ane})_2^{2+}$ [l]	0.947[j]	6×10^{3} [k]	0.74	8.39	2.31×10^{3}
7)	$Ni(cyclam)^{3+}$	0.97[m]	2×10^{3} [m]	3.9	8.95	7.8×10^{3}
8)	$Ni(cyclam)^{2+}$	0.97[m]	2×10^{3} [m]	0.26	6.25	1.60×10^{3}

---

[a]k_a = second order rate constant for reaction; [b]ref. 116; [c]ref. 117; [d]ref. 95; [e]ref. 74; [f]ref.118; [g]ref. 119; [h]ref. 120; [i]value quoted assumes K_o ion pairing constant = 7 M; [j]ref. 101; [k]ref. 100; [l]Reverse reaction of (3.13); [m]ref. 103.

---

inertness of the octahedral $NiN_6^{3+/2+}$ configuration requires an outer-sphere electron transfer. The Marcus[60,63] theory may be used to estimate the self-exchange rate for the complex. Since for most systems under consideration, reactants and products are of the same charge, work terms are generally small. Equation (1.15) may be re-written as

$$\ln k_{12} - \ln w_{12} = 0.5\ln(k_{22}K_{12}f_{12}) + 0.5\ln k_{11} \qquad (3.15a)$$

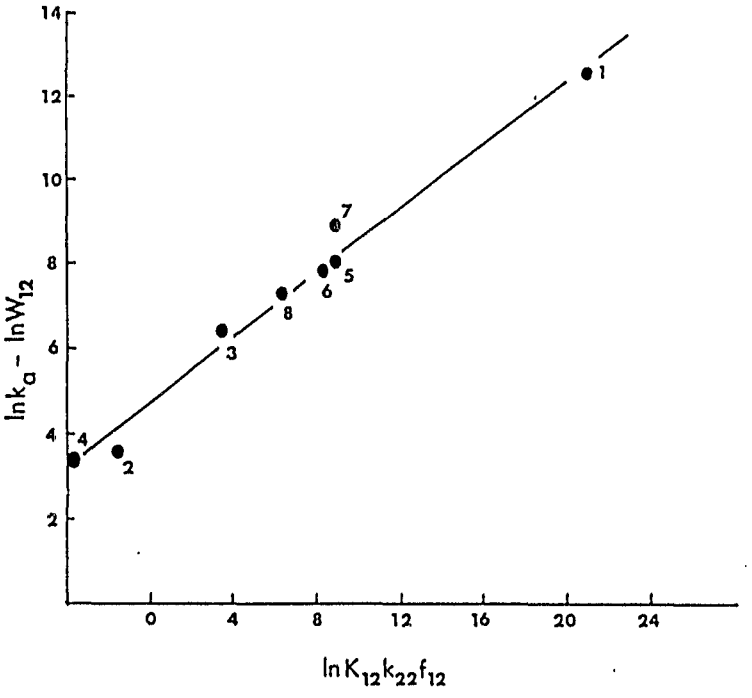

Fig. 3.4 Plot of $\ln k_a - \ln W_{12}$ against $\ln k_{12}k_{22}f_{12}$ for "Marcus Cross-correlation". Reactions identified by number in Table 3.4. Point 4 (reduction of iodide plotted using pre-equilibrium constant K_o = 7 M). Intercept = $0.5 \ln k_{11}$.

---

or

$$\ln k_{12} = 0.5 \ln (k_{22}K_{12}f_{12}) + 0.5 \ln k_{11} \qquad (3.15b)$$

and a plot of $\ln k_{12}$ against $\ln (K_{12}k_{22}f_{12})$ should be linear with slope 0.5 and intercept $0.5 \ln k_{11}$. Using the data in Table 3.4, the plot (Fig. 3.4) may be obtained. The least squares slope is 0.38 ± 0.2 and the self-exchange rate of (1.4 ± 0.5) x 10^4 $M^{-1}s^{-1}$ is obtained. Of interest is the fact that data from both oxidation and reduction reactions are indistinguishable on the

line. The value for the slope is somewhat lower than that expected from the Marcus treatment. This has been encountered previously in similar systems.[100] In the case of the iodide reaction, a pre-equilibrium constant K_o = 7 M^{-1} has been used to obtain the rate constant k_a in the expression $k_6 = K_o k_a$.

For redox couples involving transition metal ions, the wide variation in rates of self-exchange has been interpreted, in part, in terms of the inner-shell reorganisation of the reactions. In the case of the Ni(II)/(III) reactions, there is transfer of $d\sigma^*$ electron between the (d^8) high-spin $Ni(II)(L1)_2^{2+}$ and the low-spin (d^7) Ni(III) species. Attempts have been made recently to describe redox reactivity in terms of M-N bond length changes,[70] but few data are available for the Ni(II)/(III) systems where structural information may be compared with kinetic parameters. This area is actively being pursued in our laboratory. In the case of $Ni([9]aneN_3)_2^{3+}$,[102] the species exhibits Jahn-Teller distortion with the axial bonds 0.139 Å longer than the equatorial. Also the axial bonds are 0.01 Å longer than those of the $Ni([9]aneN_3)_2^{2+}$ where the equatorial bonds are 0.129 Å shorter in the Ni(II) species. The self-exchange rate constant for the bis[9]$aneN_3$ system ($6x10^3$ $M^{-1}s^{-1}$) is similar to that found in this study. For the *trans*-$Ni(cyclam)Cl_2^{+/0}$ exchange ($k = 3.4x10^4$ $M^{-1}s^{-1}$)[114] the corresponding changes are d(Ni-Cl)=0.04 Å and d(Ni-N)=0.088 Å. If the electron is removed from the $d_{x^2-y^2}$ orbital, then contraction in the equatorial plane will be a factor and the

smaller changes in the dichloro complex may contribute to a more rapid exchange. Clearly more data are required prior to a full analysis of these d^8/d^7 reactions. However, it is of note that the presence of the methyl group in the complexes, which might be considered to provide resistance to the necessary ligand framework rearrangement and also to perturb the cavity available to the metal ion through inter-ligand H-H nonbonded repulsions, appears to make little difference to the self-exchange rates. The imposition of greater structural rearrangement, possibly through the use of pendant arm macrocycles,[115] may be required to provide the sort of bond length difference discrimination and, hence, rate variations observed in other systems.[70b]

Chapter 4. Syntheses and Characterization of A Novel Macrobicyclic Cu(II) Complex and Reaction Intermediates

4.1 Introduction

A continuing feature of interest in coordination chemistry is the stability imparted to organic functional groups when bonded to a metal center.[1,121-123] This is true especially of macrocyclic complexes which may contain unsaturated (e.g. imine) linkages.[124-127] Recent studies in our laboratories,[128,129] have been directed towards the formation of bicyclic ligands in which a substituted triazacyclonoane ([9]aneN$_2$X) [X = S, NH, O] is "fused" to the fourteen membered ring cyclam, [14]aneN$_4$. Strategies towards formation of such species have involved (a) extrapolation of derivatives of [9]aneN$_2$X via a Michael addition of acrylonitrile and reduction to the bis-aminopropyl-pendant arm species, followed by (b) ring closure at a complexed copper(II) centre. The interest of such reactions is that they represent some of the few examples of successful cyclization by glyoxal[130] and reduction (BH_4^-) at metal complexes of this type. In the corresponding 14-membered tetra-aza ring systems, similar reduction results in the formation of metallic copper.[131]

A noteworthy feature of template synthesis in which there are five coordination sites, had been the identification and characterization of unexpected intermediates in the cyclization process. In the system where X = NH,[129] an imidate (iminoether) has been isolated which exhibits remarkable kinetic stability towards acid hydrolysis, presumably owing to the binding of the imino nitrogen to the copper center. Also,

as a result of incomplete reduction with borohydride ion, an enamine cation was isolated and characterized crystallographically.

As part of the continuing investigation of this series of complexes, the macrobicycle in which the apical donor is an oxygen atom was synthesized. There is interest as to whether this ether oxygen would be as effective a coordinator as S or N.[132] Previous studies on these and related systems[133] are consistent with square pyramidal configurations at Cu(II). However, in the case of nickel(II),[122] a sixth (perchlorate) ligand is coordinated weakly (also see chapter 6, *vide infra*). Other potentially quinquedentate ligands[134] with O donors have also displayed a tendency for four coordination of the macrocycle if other sufficiently strongly ligating groups are present. In contrast, the present findings demonstrate that the oxygen donor, as a result of ligand geometry, may be held in a bonding position for interaction with the metal center. Thus a template reaction sequence ensues, which provides further information on the mechanistic aspects of reactions of coordinated ligands of this type.

4.2 Syntheses

The strategy used in the synthesis of bicyclic N_4O macrocycle was similar to its N_4S and N_5 analogues.[128,129] The procedure involved the preparation of the nine-membered ring, [9]aneN_2O, using the Richman and Atkins reaction and the ring-

closure of 14-membered ring using a template method. Detailed description of the procedures are provided in section 2.2.

Synthesis of [9]aneN_2O was carried out according to the well-documented procedure,[72,74] with the similar modifications as that in the case of the synthesis of ligand L1. As the result of these modifications, a high yield (~86%) was achieved in the present work at the detosylation step.

For a template ring-closure reaction of tetraaza open-chain, Ni(II) has been, and still is, commonly used as the template ion.[1,121-123] This popular preference of choosing Ni(II) as a template ion in this type of cyclization is for the following reasons:

i) it was Ni(II) ion which was first employed, either accidentally[1,11] or intentionally,[1,122] by pioneers in exploring the field of template synthesis;

ii) the Ni(II) ion, which has a d^8 configuration, often tends to coordinate a tetraaza open chain in a planar fashion, and allows the template effect to operate;

iii) the work-up after a template reaction, such as hydrogenation of C=N bonds, is more facile with Ni(II) as the central ion, while other ions often either lead to decomposition[11,44,45] or pose certain degrees of difficulty in handling.[135]

However, Ni(II) ion proved to be unsuitable as a template in the synthesis of a bicyclic N_4X (X = O, S, or NH) system because of presence of 9-membered ring. All attempts (in both

the present work and in previous similar experiments in o laboratory[129]) to cyclize the pendant arms using Ni(II) ion as the template were unsuccessful. This is probably due to the special structural preference involving in this type of bi-pendant-armed 9-membered ring in coordination with the metal ion of octahedral configuration. The crystal structure of $[Ni(II)(L')(NCCH_3)]^{2+}$,[136] L′ = N,N′-bis(3-aminopropyl)-1-oxa-4,7-diazacyclononane, showed that the two arms are in a "folded" form instead of "in-plane", with a solvent molecule in the equatorial position of its octahedral geometry (structure **1**)

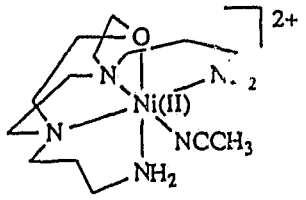

1

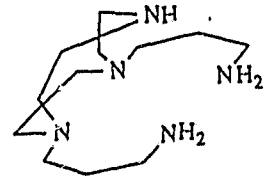

2

The similar observation was made in the case of $[Ni(II)(daptacn)(OH_2)]^{2+}$ (for daptacn see structure **2**) where the two-arm in "folded" form has been suggested as one of the isomers.[137] Consequently, the $[Co(III)(daptacn)(Cl)]^{2+}$ complex was also prepared in our laboratory and its molecular structure showed again that the daptacn ligand was coordinating in the same way as its ether oxygen analogue in structure **2** with two arms in a "folded" form.[137] From the observation above, it appears that this type of bi-pendant-

armed [9]aneN_2X (X = O, S or N) prefers the "folded" form in octahedral coordination environment.

Considering this, the suitable ion for the template cyclization in the present system should be the one which favours square-planar or square-pyramidal configurations over the octahedral so that the two arms can be held in the "in-plane" structure, and a template reaction is, therefore, able to occur. Cu(II) is one of those ions which meets this requirement.[137] It has been observed that in the $[Cu(II)(daptacn)]^{2+}$ complex the two pendant arms were indeed in the same plane and the complex is of square-pyramidal geometry.[137] The previous work in our laboratory has further shown success in using the Cu(II) ion as the template to close the pendant arms of the daptacn ligand.[129] Therefore, Cu(II) ion was considered the obvious choice as the template for the present system. As anticipated, the cycloaddition was successful (see section 2.2).

Hydrogenation of imine group (C=N) of Cu(II) tetraaza mono-cyclic complexes have been investigated by other workers and frequently failed to produce the desired products.[44,45,131] As discussed in section 1.1.4, the problem with this, in part, is that the tetraaza monocyclic ring is not able to keep within its cavity the Cu(I) ion which is formed during the process. However, as a result of the two cyclic rings, the ligand L2 is capable of trapping the Cu(I) ion in the cavity. Also, encouraged by the previous success in similar

experiments with N_4S and N_5 analogues in our laboratory,[128,129] hydrogenation of the template product, Cu(II)(L2), was carried out using $NaBH_4$ as reductant (see section 2.2).

The reduction of $[Cu(II)(L2)]^{2+}$ was investigated under different experimental conditions. When the reaction was conducted under a N_2 atmosphere at low temperature, the initial bluish-pink solution turned to brownish-yellow in colour (which is likely the result of formation of the Cu(I) species) immediately after adding first portion of $NaBH_4$. This solution gradually changed to darker colour (possibly due to the presence of a Cu(0) species) as more $NaBH_4$ was added ($NaBH_4^{total}$:complex > 3:1 in mol). When this was kept for long period (several hours), a lot of black fine powder (Cu(0)) precipitated out. Refluxing the resulting solution afterward did not redissolve this black precipitate back into solution. As a result, only trace amounts of $[Cu(N_4O)]^{2+}$ was obtained (the yield was extremely low). However, when the above dark solution was open to air and refluxed shortly after the addition of $NaBH_4$ was completed, the solution became a light-bluish purple colour, and a high yield of the desired product, $[Cu(N_4O)]^{2+}$, was obtained with only small amount of the black precipitate left. On the other hand, under the condition where no N_2 protection was made, the brownish-yellow colour was observed for only a short period at room temperature (or short period of dark coloration at 0°C) after the addition of $NaBH_4$ and the solution was mainly blueish-purple in colour. It

became more purplish as the reaction progressed, and the solution was refluxed for the rest of reaction period. In this case, the reaction gave rise to mainly the desired product and only a trace amount of black precipitate was produced. A similar observation was also made in the analogous N_5 system at our laboratory.[138]

The results above suggest that $NaBH_4$ is capable of reducing both the Cu(II) centre and the functional groups on the ligand owing to its strong reducing power. Competition between these two reactive centres may be affected by the reaction conditions applied. At a low temperature, the reduction occurs more favourably at the metal centre. Otherwise the reaction on the organic functional group is more competitive. This is understandable in the sense that the driving force for the interaction between Cu^{2+} and BH_4^- is mainly electrostatic, which has little temperature-dependence; however, the driving force for that between the organic functional group and BH_4^- is mostly thermally sensitive. Therefore, a better yield of the product of hydrogenation of the ligand may be obtained at higher temperatures. Furthermore, the intermediates (Cu(I) and Cu(0) species) formed from the reduction of metal centre appeared very air-sensitive, and may be readily oxidised back to Cu(II) (in the case of Cu(0), the oxidative condition has to be applied before it converts to a more stable form). Considering these features, the reaction condition described in section 2.2 was

employed to achieve a high yield of the hydrogenated ligand.

Of interest is that even when Cu(I) was formed at its favourable conditions, most of it may be reversibly oxidised back to Cu(II) upon opening to air. It is well known that Cu(I) is a very unstable ion, and has a strong tendency to undergo disproportionation to form Cu(0) and Cu(II) in the absence of an electron density delocalisation mechanism through metal-to-donor interaction.[13] The present study indicates that these bicyclic type of macrocycles are indeed capable of holding the Cu(I) ion (and probably even Cu(0) ion, diagnosed by the initial dark solution) in its cavity, though it is possible that a potential $d_{metal} \rightarrow d_{donor}$ back-bonding in the system also has some degree of contribution in stabilizing the low oxidation state. As a result of this trapping, the disproportionation of Cu(I) was kinetically slowed down so that it may be converted back to Cu(II). Unfortunately, the Cu(I) species formed was not stable enough to be isolated, and hence, it could not be fully characterized in the present study.

However, isolation of the intermediates from the ring-closure and hydrogenation of the ligand was successful (section 2.2). The complexes of $[Cu(II)(L2)]^{2+}$, $[Cu(L3)]^{2+}$, and the final product, $[Cu(II)(N_4O)]^{2+}$ were isolated and fully characterised. The molecular structures of these complexes and the mechanism involved in the reactions will be discussed later in this chapter. In addition, the free ligand was also

isolated, and its tetra hydroperchlorate salt characterised crystallographically.

4.3 Molecular Structures

4.3.1 Crystallography

The experimental parameters for the three metal complexes and the hydroperchlorate salt of the free ligand are presented on Table 4.1.

$[Cu(L2)](ClO_4)_2$

The unit cell was refined by using 12 pairs of reflections in the 2θ range from 17-45°. The intensity measurements were made by scanning in the θ/2θ mode using 200 steps of 0.01° in 2θ counting for 0.25s/step. Background counting was introduced for 25s at the end of each scan. A set of three standard reflections preceded each batch of 50 measurements, with no noticeable change of intensity observed during the collection.

Solution of the phase problem was achieved by direct methods using SHELX76.[139] The atomic scattering factors were those included in the SHELX76 program together with the Cu f curve from ref. 140. The program used for absorption correction was a local modification of an existing procedure.[141] Completion and refinement of the structure were carried out by difference electron density maps and least squares techniques. All atoms were refined anisotropically except for the hydrogen atoms, only some of which were

observed. The refinement converged with a maximum shift/esd of 0.104 on the final cycle for all atoms except H, (but including one of the perchlorate oxygens, (O(8)). The final difference map showed a maximum peak of 1.53 eA^{-3}. Exclusion of the oxygen atom reduced the shift/esd value to 0.028. Various attempts were made to improve the poor temperature factors on C10, but without success.

$[Cu(N_4O)](ClO_4)_2$

The unit cell was refined by using 21 pairs of reflections in the 2θ range from 16-38°. The intensity measurements were obtained by scanning in the θ/2θ mode using 200 steps of 0.01° in 2θ counting for 0.25s/step. Background counting was introduced for 25s at the end of each scan. Three standard reflections preceded each batch of 50 measurements, with no decomposition during the collection. Details of the solution are similar to those given above. The refinement converged with a maximum shift/esd of 0.017 on the final cycle. The final difference map had a maximum peak of 0.58 eA^{-3}.

$[Cu(L3)](ClO_4)_2$

The unit cell was refined by using 17 pairs of reflections in 2θ range from 17-42°. The intensity measurements were obtained by scanning in the θ/2θ mode using 200 steps of 0.01° in 2θ counting for 0.25s/step. Background counting was introduced for 25s at the end of each scan. Three standard reflections preceding each batch of 50 measurements

Table 4.1 Crystallographic Data

[Cu(L2)](ClO$_4$)$_2$:

Chemical Formula: $CuC_{14}H_{28}N_4O_{10}Cl_2$	T = 22 ± 2 °C
Fw: 546.8	λ = 0.710 69 Å
Space group: $P2_1/c$ (No. 14)	ρ_{obs} = 1.695 g cm^{-3}
a = 10.367(3) Å	ρ_{calc} = 1.665 g cm^{-3}
b = 13.104(5) Å	μ = 12.40 cm^{-1}
c = 8.475(2)Å	$R(F_o)$ = 0.0838
α = 90 (2)°	R_w = 0.0899
β = 93.28(3)°	Z = 4
γ = 90°	trans coeff. = 0.775-0.836
V = 2180.9 Å^3	

[Cu(N$_4$O)](ClO$_4$)$_2$:

Chemical Formula: $CuC_{14}H_{30}N_4O_9Cl_2$	T = 22 ± 2 °C
Fw: 532.8	λ = 0.710 69 Å
Space group: $P2_1/n$ (No. 14)	ρ_{obs} = 1.629 g cm^{-3}
a = 13.880(2) Å	ρ_{calc} = 1.627 g cm^{-3}
b = 15.122(3) Å	μ = 12.31 cm^{-1}
c = 8.475(2)Å	$R(F_o)$ = 0.079
α = 90 (2)°	R_w = 0.073
β = 97.95(1)°	Z = 4
γ = 90°	trans coeff. = 0.811-0.915
V = 2175.2 Å^3	

Table 4.1 (continued)

[Cu(L3)](ClO$_4$)$_2$:

Chemical Formula: $CuC_{14}H_{28}N_4O_9Cl_2$	T = 22 ± 2 °C
Fw: 530.8	λ = 0.710 69 Å
Space group: Pbca (No. 61)	ρ_{obs} = 1.621 g cm^{-3}
a = 16.494(3) Å	ρ_{calc} = 1.646 g cm^{-3}
b = 18.188(3) Å	μ = 13.37 cm^{-1}
c = 14.330(2) Å	$R(F_o)$ = 0.0655
α = 90°	R_w = 0.073
β = 90°	Z = 8
γ = 90°	trans coeff. = 0.716-779
V = 4298.9 Å^3	

[H$_4$(N$_4$O)](ClO$_4$)$_4$:

Chemical Formula: $C_{14}H_{36}N_4O_{17}Cl_4$	T = 22 ± 2 °C
Fw: 690.3	λ = 0.710 69 Å
Space group: $P2_1/n$ (No. 14)	ρ_{obs} = 1.637 g cm^{-3}
a = 13.717(3) Å	ρ_{calc} = 1.645 g cm^{-3}
b = 20.152(5) Å	
c = 10.110(2) Å	$R(F_o)$ = 0.117
α = 90°	R_w = 0.125
β = 94.46(2)°	Z = 4
γ = 90°	
V = 2786.2 Å^3	

showed no change of intensity during the collection.

The structure was solved for the heavy atoms by using MULTAN[142] and refined by least squares using SHELX76.[139] Other procedures were similar to those described above. The refinement converged with a maximum shift/esd of 0.06 on the final cycle. The final difference map showed a maximum peak of 0.698 eA^{-3}.

$[(H_4N_4O)(ClO_4)_4]\cdot H_2O$

Following Weissenberg and precession photography, the crystal was mounted in a Nonius CAD4 diffractometer. Tne cell was refined by using 25 centered reflections in the range θ = 18-35°. No decomposition of the crystal was observed during the data acquisition. Parameters were obtained by using scan speed 10 on the instrument. Absorption corrections were made.[141] The structure was solved by direct methods.[139] The refinement converged with a maximum shift/esd of 0.036 on the final cycle. The final difference map showed a maximum peak of 1.29 eA^{-3}. Considerable disorder was observed in two of the anions.

4.3.2 Results

$[H_4(N_4O)](ClO_4)_4\cdot H_4O$

X-ray quality crystals were obtained from a strongly acidic ($HClO_4$) solution of the ligand. Unfortunately during refinement it was found that there was unresolvable disorder associated with two of the perchlorates, centered on C13 and

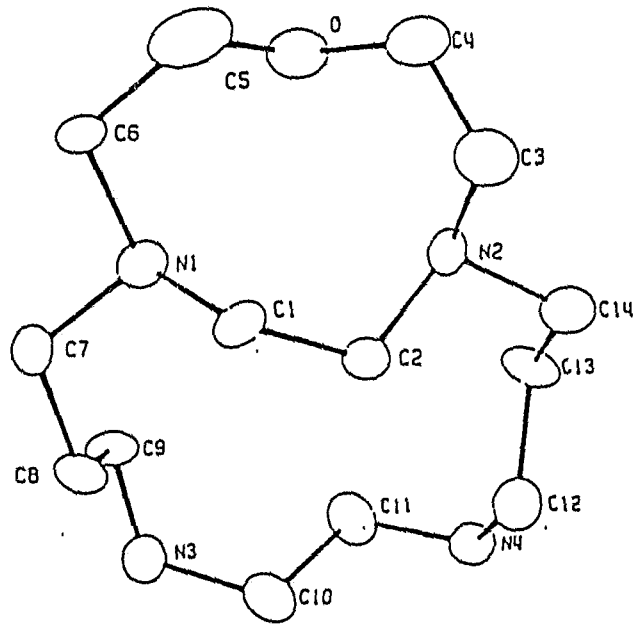

Fig. 4.1 ORTEP diagram of the ligand cation ($[H_4N_4O]^+$) from the tetrahydroperchlorate salt, showing 25% thermal ellipsoids.

C14. For this reason, the final R value of 0.117, (R_w= 0.125) is very high. Relevant data are provided in Table 4.2-4.4. However, sufficient information on the structure is provided that it may be used as a perspective of the framework into which the metal ion is incorporated (Fig. 4.1). There are also surprisingly few ligand structures of this type of ligand available. The closest comparisons are the cage macrobicycles, 5-X-12,17-dimethyl-1,9,12,17-tetraazabicyclo[7.5.5]nonadecane (X = aza or oxa):

3

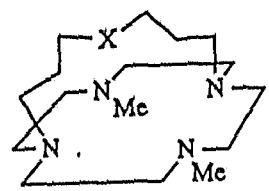

X = NH, or O

Table 4.2 $[H_4(N_4O)]^{4+}$

Fractional atomic coordinates and temperature parameters.

Atom	x/a	y/b	z/c	Ueq
Cl(1)	28121(28)	4387(21)	15709(41)	572(15)
Cl(2)	36149(24)	28622(21)	14709(39)	538(15)
Cl(3)	-10213(27)	14522(23)	23214(43)	580(15)
Cl(4)	-4270(31)	40690(25)	17441(52)	716(18)
O(1)	2054(11)	885(8)	1580(16)	125(7)
O(2)	3096(21)	307(9)	401(18)	219(15)
O(3)	3464(17)	685(15)	2446(25)	243(16)
O(4)	2502(11)	-183(8)	2049(19)	143(9)
O(5)	4616(6)	2843(5)	1109(10)	56(4)
O(6)	3681(10)	2810(8)	2852(11)	120(7)
O(7)	3088(11)	2352(8)	843(17)	136(8)
O(8)	3207(10)	3459(7)	1151(16)	116(7)
O(9)	-1339(11)	1014(9)	1291(19)	147(9)
O(10)	-1757(14)	1814(12)	2763(22)	189(11)
O(11)	-384(22)	1173(13)	3242(27)	272(17)
O(12)	-566(26)	1927(15)	1747(27)	254(18)
O(13)	543(9)	3801(8)	1909(13)	117(7)
O(14)	-958(15)	3714(18)	820(25)	229(17)
O(15)	-307(22)	4563(15)	664(30)	236(17)
O(16)	-739(25)	4423(15)	2579(21)	272(19)
O(17)	7006(8)	503(5)	4913(10)	69(4)
O	5381(8)	4258(5)	1639(12)	73(5)
N(1)	5860(8)	3288(6)	3425(11)	45(4)

Table 4.2 (continued)

N(2)	6491(8)	3386(6)	465(11)	51(5)
N(3)	5607(9)	996(6)	3077(13)	62(5)
N(4)	6347(10)	1118(6)	-494(12)	60(5)
C(1)	6887(9)	3331(8)	2994(14)	50(5)
C(2)	6979(9)	3028(7)	1640(15)	49(5)
C(3)	6800(14)	4101(8)	354(19)	77(7)
C(4)	5992(17)	4553(11)	762(25)	121(11)
C(5)	5599(18)	4510(11)	2987(24)	113(11)
C(6)	5442(13)	3951(8)	3930(17)	70(7)
C(7)	5799(12)	2768(8)	4565(15)	64(6)
C(8)	6104(11)	2064(7)	4179(16)	58(6)
C(9)	5296(10)	1695(7)	3363(15)	52(5)
C(10)	6231(11)	967(8)	1906(16)	62(6)
C(11)	5657(11)	1064(8)	618(15)	59(6)
C(12)	6920(13)	1755(9)	-489(17)	74(7)
C(13)	6230(11)	2317(7)	-988(14)	54(6)
C(14)	6738(12)	3026(8)	-861(16)	65(7)

Estimated standard deviations are given in parentheses.

Coordinates x 10^n where n = 5,4,4,4 for Cl, O, N, C

Temperature parameters x 10^n where n = 4,3,3,3 for Cl, O, N, C

U_{eq} = the equivalent isotropic temperature parameter.

$U_{eq} = 1/3\ \Sigma_i\Sigma_j U_{ij} a_i^* a_j^* (a_i . a_j)$

Table 4.3 Interatomic Distances (Å) for $[H_4(N_4O)]^{4+}$

Atoms	Distance	Atoms	Distance
C(13) -C(12)	1.535(21)	C(10) -N(3)	1.515(20)
C(14) -C(13)	1.591(21)	C(11) -N(4)	1.528(19)
C(4) -O	1.400(21)	C(12) -N(4)	1.505(20)
C(5) -O	1.464(23)	C(2) -C(1)	1.512(19)
C(1) -N(1)	1.508(16)	C(4) -C(3)	1.517(25)
C(6) -N(1)	1.555(18)	C(6) -C(5)	1.504(29)
C(7) -N(1)	1.564(18)	C(8) -C(7)	1.539(21)
C(2) -N(2)	1.502(17)	C(9) -C(8)	1.523(19)
C(3) -N(2)	1.508(20)	C(11) -C(10)	1.481(21)
C(14) -N(2)	1.583(19)	C(9) -N(3)	1.507(19)

Table 4.4 Bond Angles (°) for $[H_4(N_4O)]^{4+}$

Atoms	Angle	Atoms	Angle
C(5) -O -C(4)	110.6(18)	C(4) -C(3) -N(2)	109.8(15)
C(6) -N(1) -C(1)	115.1(12)	C(3) -C(4) -O	113.7(15)
C(7) -N(1) -C(1)	110.8(11)	C(6) -C(5) -O	107.5(17)
C(7) -N(1) -C(6)	106.9(11)	C(5) -C(6) -N(1)	111.2(14)
C(3) -N(2) -C(2)	114.0(12)	C(8) -C(7) -N(1)	113.6(12)
C(14) -N(2) -C(2)	109.8(11)	C(9) -C(8) -C(7)	112.8(12)
C(14) -N(2) -C(3)	107.2(11)	C(8) -C(9) -N(3)	110.8(11)
C(10) -N(3) -C(9)	111.9(12)	C(11) -C(10) -N(3)	112.8(13)
C(12) -N(4) -C(11)	114.2(12)	C(10) -C(11) -N(4)	109.9(12)
C(2) -C(1) -N(1)	112.6(10)	C(13) -C(12) -N(4)	108.6(14)
C(1) -C(2) -N(2)	117.3(12)	C(14) -C(13) -C(12)	112.4(13)
		C(13) -C(14) -N(2)	111.0(11)

Estimated standard deviations are shown in parentheses.

where the axially binding atom is located in the bridge spanning the two tertiary nitrogens of the 12-membered ring. In that pentaaza system,[143] the macrocycle has been shown to take up three hydrogen ions, behaving in the first protonation step as a proton sponge. The structure proposed for the protonated ion involves two hydrogen ions incorporated into the macrocycle as part of a network comprising all five nitrogen centres. Where X = O[144], there is evidence for the proton located as a "quasi metal" complexing agent. These structures are in marked contrast to the present ion, where all four of the nitrogens are protonated. The rings show considerable puckering, with some distortion round the tertiary nitrogens N1 and N2. In this case, the angles C6-N1-C1 (115.1(12)°) and C3-N2-C2 (114.0(12)°) are much larger that the tetrahedral angle in contrast to the other angles aroun these atoms. However, the lack of precise information on the location of the hydrogens, unavailable owing to perchlorate disorder, limits detailed analysis, especially for the other nitrogen centres where slightly larger angles are again observed.

$[Cu(L2)]^{2+}$

X-ray quality crystals were obtained from a solvent mixture of acetonitrile/ether. The structure of the five coordinate ion is shown in Fig. 4.2a. Relevant crystal data are presented in Tables 4.5-4.7. The crystal structure consists of a complex ion packed with two perchlorate counter

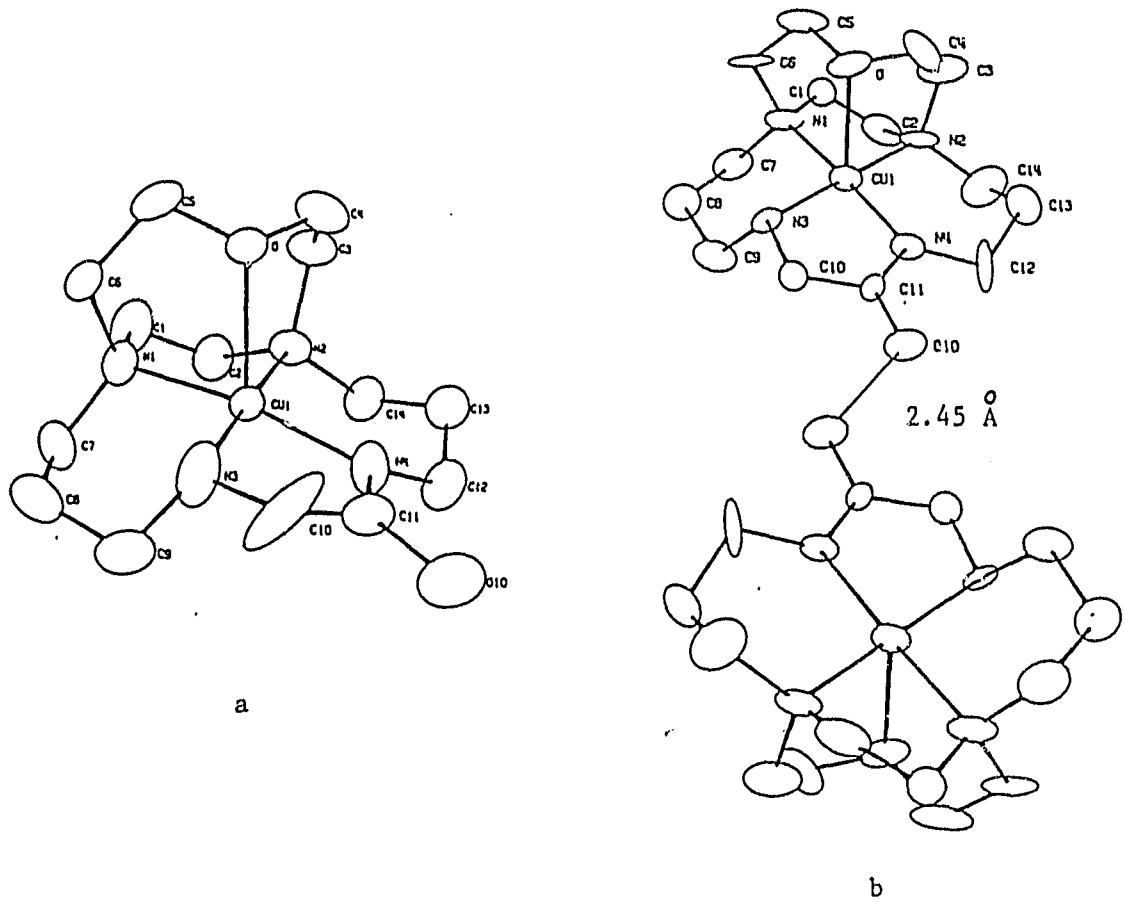

a b

Fig. 4.2 a, ORTEP diagram of the cation $[Cu(L2)]^{2+}$, showing 25% thermal ellipsoids; b, the structure of the hydrogen-bonded $[Cu(L2-H)]_2^{3+}$ dimer.

---

ions. The coordination geometry at the copper centre is square pyramidal and very similar to that of $[Cu(daptacn)]^{2+}$ [137] apart from the additional chelate ring. The ion is virtually identical to the imidate intermediate formed in the pentaaza system from the daptacn precursor.[128] It represents the first example of an amidol complex of this type, and the immediate

Table 4.5 $[Cu(L2)](ClO_4)_2$

Fractional atomic coordinates and temperature parameters.

Atom	x/a	y/b	z/c	Ueq
Cu(1)	-20482(13)	37389(10)	31616(9)	483(5)
Cl(1)	78333(37)	10997(27)	14019(25)	723(13)
Cl(2)	30431(39)	34588(35)	3177(25)	827(16)
O(1)	7027(19)	1683(13)	883(10)	184(9)
O(2)	8651(24)	549(18)	967(11)	232(12)
O(3)	8470(17)	1713(16)	2006(11)	186(9)
O(4)	7135(16)	441(15)	1888(12)	194(10)
O(5)	1756(17)	3631(23)	285(14)	284(16)
O(6)	3702(17)	4248(13)	169(16)	236(13)
O(7)	3044(16)	2709(18)	-252(13)	227(12)
O(8)	3429(31)	3180(24)	1051(13)	376(20)
O	-2495(8)	5238(6)	3776(5)	66(3)
O(10)	1692(15)	2965(11)	526(10)	150(7)
N(1)	-3997(10)	3586(9)	2250(6)	66(4)
N(2)	-2479(11)	4528(8)	2096(6)	59(4)
N(3)	-1618(13)	2878(15)	4157(9)	118(7)
N(4)	-156(12)	3657(10)	3020(10)	100(6)
C(1)	-4686(15)	4006(15)	2478(10)	101(7)
C(2)	-3766(13)	4077(12)	1795(8)	75(6)
C(3)	-2639(17)	5643(11)	2286(10)	85(6)
C(4)	-2108(18)	5947(12)	3146(12)	97(7)
C(5)	-3816(16)	5300(13)	3963(11)	94(7)
C(6)	-4348(15)	4218(13)	4008(11)	90(7)

Table 4.5 (continued)

C(7)	-4342(15)	2461(13)	3359(11)	95(7)
C(8)	-3679(22)	1943(13)	4101(12)	110(9)
C(9)	-2234(22)	1834(16)	4086(11)	111(9)
C(10)	-205(22)	2925(24)	4368(11)	164(13)
C(11)	416(14)	3216(13)	3668(20)	129(11)
C(12)	465(17)	3782(15)	2232(13)	106(8)
C(13)	-179(19)	4617(14)	1711(12)	101(8)
C(14)	-1539(16)	4348(13)	1427(9)	80(6)

Estimated standard deviations are given in parentheses.

The footnotes are the same as those in Table 4.2.

Table 4.6 Bond Angles (°) for $[Cu(L2)]^{2+}$

Atoms	Angle	Atoms	Angle
N(1) -Cu(1) -O	80.0(4)	N(4) -Cu(1) -N(2)	95.8(5)
N(2) -Cu(1) -O	83.4(4)	N(4) -Cu(1) -N(3)	83.4(5)
N(2) -Cu(1) -N(1)	86.5(4)	C(11) -Cu(1) -O	107.5(5)
N(3) -Cu(1) -O	100.6(6)	C(11) -Cu(1) -N(1)	150.3(7)
N(3) -Cu(1) -N(1)	93.7(5)	C(11) -Cu(1) -N(2)	122.6(7)
N(3) -Cu(1) -N(2)	175.9(7)	C(11) -Cu(1) -N(3)	56.8(7)
N(4) -Cu(1) -O	109.0(5)	C(11) -Cu(1) -N(4)	26.8(7)
N(4) -Cu(1) -N(1)	170.9(5)		

Table 4.7 Interatomic Distances (Å) for [Cu(L2)]2+

Atoms	Distance	Atoms	Distance
O -Cu(1)	2.259(8)	N(3) -Cu(1)	1.987(12)
N(1) -Cu(1)	2.044(10)	N(4) -Cu(1)	1.991(12)
N(2) -Cu(1)	2.029(9)		

product of the dehydration of the di-carbinolamine formed in the Schiff-base condensation. The N4-C11 distance, (1.31(3) Å) is much shorter than the other N-C bonds in the ion, (1.146(2)-1.53(2) Å) and must be regarded as a double bond. The distance is almost identical not only with the imidate complex investigated previously[128] (1.28(2) Å), but is also very similar to the values (1.29, 1.30 Å) found for the C=N bonds in a conjugated diimine derived from nickel(II) cyclam, where there is multiple bond character (see Chapter 7). The bond angles at both C11 and N4 also reflect unsaturation. Around C11, two of the angles are 124° and the other 111(2)°. The latter, N4-C11-O10, is probably influenced by a hydrogen bond between O10 and O7 of one of the perchlorates. Although the hydrogen was not locatable, the O10-O7 link (2.507 Å) is consistent with a strong hydrogen bond. At N4, there is some asymmetry with two angles at 125° and 123° and the C11-N4-Cu angle of 109(1)°. The larger angles may reflect the pull exerted by C10 to allow for formation of the five membered chelate ring. The sum of the angles at each center is 359° and 358° respectively indicating approximate planarity. Mean plane

calculations involving atoms Cu, N4, C11, C12, C10, O10 show extensive planarity with the most significant deviation (0.14Å) at N4.

Including the data for the free ligand for the C-O distances observed at the apical oxygen, the average lengths in all the systems under consideration are C5-O, 1.45(3)Å. However, in this ion, the C11-O10 bond (1.39(2) Å) is significantly shorter. This reflects a π-bond character from a resonance form with more amide contribution.

The four equatorial nitrogens do not form a truly idea plane, w ,h N2 and N3 above and N1 and N4 below. The ligand structure is similar to that found in previous complexes of this type. The Cu-N1 and Cu-N2 bonds to the tertiary nitrogens, 2.04(1) Å and 2.03(1) Å respectively are longer than those to the secondary centres (Cu-N3 = Cu-N4 = 1.99(1) Å). The longest bond to copper is the apical Cu-O, which at 2.259(8) Å is somewhat longer than the corresponding Cu-N (2.21(1) Å) in the pentaaza imidate ion.[128] This may reflect the weaker ligating tendency of the ether oxygen. In the present complex ion, the copper is positioned 0.114(10) Å above the N4 plane towards the apical oxygen, much less than the 0.21(2) Å observed for the N5-imidate.[128] The angle between the Cu-O(ap) vector and the normal to the N4 plane is 15.2°. This tilting of the apical atom away from the position directly above the copper is a feature of all the ions studied and is the result of the inability of the ligand to completely

reach over and occupy the orthogonal site.

An unsatisfactory feature of the structure is the rather poor temperature factor associated with atom C10 for which the origin is not known at present. Of interest, however, is the fact that another form of this ion was found under slightly differing experimental conditions. At neutral pH, the ion exists as a dimer where there is deprotonation of one of the amidol hydrogen atoms and a strong hydrogen bond (O10-O10′ = 2.45 Å) between the two inverted complex ions. Structural parameters are virtually identical to these described above with the exception that the C10-C11 distance is 1.45 Å, closer to the single bond value anticipated. Again, of the three perchlorates required for electroneutrality, one is badly disordered.[136] The structure of this ion is shown in Fig. 4.2b.

$[Cu(L3)]^{2+}$

Crystals of the perchlorate salt were grown from a solution of the complex in acetonitrile in an ether atmosphere. The atomic coordinates, bond lengths and angles are listed in Tables 4.8-4.10. The structure consists of a five coordinate copper complex and two perchlorate counter ions. The molecular structure of the cation is shown in Fig. 4.3.

The coordination geometry at the copper centre may be described as square pyramidal with a weak interaction between the copper and O8 of one of the perchlorate ions (2.98 Å). As was seen in the amidol complex above, the bond lengths to the

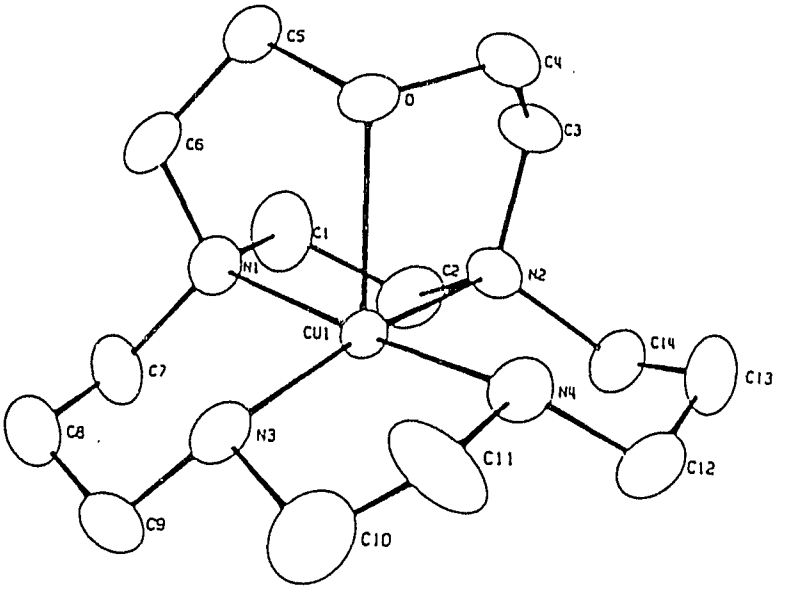

Fig. 4.3 ORTEP diagram of the cation $[Cu(L3)]^{2+}$, showing 25% thermal ellipsoids.

---

tertiary nitrogens (Cu-N1, 2.065(8) Å and Cu-N2, 2.021(7) Å) are somewhat longer than those to the secondary atoms (Cu-N, 2.021(7) Å average). The distance between the metal ion and the apical oxygen, 2.335(6) Å, is longer than that found for the other two cations. The angles subtending atoms in the propyl bridges e.g. C9-N3-Cu are all uniformly in the range 113-114°, significantly different from those (105.0(7)° and 105.5(7)°) within the five membered ring containing the double bond. The value of 1.34(2) Å for the C10-C11 distance is consistent with unsaturation within this ring.

Of the three copper complexes examined in this study, the four "planar" nitrogens in this cation are the most distorted towards a pseudo-tetrahedral arrangement. In the enamine, the

Table 4.8 $[Cu(L3)]^{2+}$

Fractional atomic coordinates and temperature parameters.

Atom	x/a	y/b	z/c	Ueq
Cu(1)	12676(7)	40914(5)	25524(7)	412(4)
Cl(1)	-6632(17)	19689(14)	-3056(18)	630(10)
Cl(2)	33460(18)	-4280(15)	77703(20)	677(10)
O	154(4)	3419(3)	2113(4)	57(2)
O(1)	75(5)	1954(5)	-54(5)	97(4)
O(2)	-1139(5)	1941(5)	512(6)	106(4)
O(3)	-836(7)	2616(5)	-790(7)	134(5)
O(4)	-814(5)	1355(5)	-879(6)	106(4)
O(5)	2881(6)	-955(5)	8302(8)	134(5)
O(6)	3549(8)	-709(7)	6930(7)	163(6)
O(7)	4021(6)	-307(7)	8321(7)	145(6)
O(8)	2841(6)	181(4)	7680(6)	108(4)
N(1)	1766(6)	3055(4)	2556(6)	68(3)
N(2)	1461(5)	4089(4)	1147(5)	58(3)
N(3)	1260(6)	4153(4)	3962(6)	68(3)
N(4)	661(6)	5047(4)	2582(6)	74(4)
C(1)	2098(8)	2902(7)	1586(8)	93(5)
C(2)	2217(6)	3630(6)	1093(7)	72(4)
C(3)	778(7)	3724(7)	610(7)	72(4)
C(4)	2(6)	3680(6)	1164(7)	70(4)
C(5)	349(7)	2631(5)	2165(8)	77(5)
C(6)	1056(8)	2554(6)	2800(9)	83(5)
C(7)	2476(8)	2972(7)	3210(8)	92(5)

Table 4.8 (continued)

C(8)	2239(8)	3148(8)	4246(9)	96(6)
C(9)	2041(9)	3931(8)	4446(7)	96(6)
C(10)	1082(12)	4948(8)	4178(10)	124(8)
C(11)	509(10)	5208(9)	3626(11)	137(8)
C(12)	996(7)	5649(7)	1958(13)	97(6)
C(13)	1021(8)	5425(8)	972(11)	98(6)
C(14)	1670(8)	4840(6)	765(8)	83(5)

Estimated standard deviations are given in parentheses.

The footnotes are the same as those in Table 4.2.

Table 4.9 Bond Angles (°) for $[Cu(L3)]^{2+}$

Atoms	Angle	Atoms	Angle
N(1) -Cu(1) -O	81.6(3)	N(4) -Cu(1) -N(2)	96.0(4)
N(2) -Cu(1) -O	82.1(3)	N(4) -Cu(1) -N(3)	85.9(4)
N(2) -Cu(1) -N(1)	86.3(3)	C(2) -Cu(1) -O	96.2(3)
N(3) -Cu(1) -O	107.0(3)	C(2) -Cu(1) -N(1)	59.2(3)
N(3) -Cu(1) -N(1)	92.9(3)	C(2) -Cu(1) -N(2)	32.9(3)
N(3) -Cu(1) -N(2)	170.6(3)	C(2) -Cu(1) -N(3)	140.8(4)
N(4) -Cu(1) -O	92.6(3)	C(2) -Cu(1) -N(4)	124.9(4)
N(4) -Cu(1) -N(1)	173.4(4)		

Table 4.10 Interatomic Distances (Å) for $[Cu(L3)]^{2+}$

Atoms	Distance	Atoms	Distance
O -Cu(1)	2.335(6)	N(3) -Cu(1)	2.023(8)
N(1) -Cu(1)	2.065(8)	N(4) -Cu(1)	2.020(7)
N(2) -Cu(1)	2.041(7)		

Estimated standard deviations are given in parenthesis.

copper centre is only 0.0325 Å above the N4 plane, which is less than the nitrogens forming the base of the square pyramid. The degree of tugging of the apical oxygen, is reflected by the angle of incidence between the Cu-O vector and the mean N4 plane at 14.8°.

$[Cu(N_4O)]^{2+}$

The structure of this ion is shown in Fig. 4.4. In this case, the four atoms of the N4 plane show only minor deviations (0.006 Å maximum) from coplanarity. The trans-basal angles are N3-Cu-N2 178.0(6)° and N1-Cu-N4, 177.5(6)° respectively. The copper atom is located 0.0396 Å above the plane, but there is a strong bond with the apical oxygen 2.275(9) Å confirming the square pyramidal nature of the complex cation. As in the enamine case, there is a weak interaction between O5 of one of the perchlorates and the sixth site of the copper coordination sphere (2.866 Å). This is shorter than the corresponding electrostatic interaction in the $[Cu(L3)]^{3+}$ ion, presumably owing to the closer coplanarity of the copper in the fully saturated ring. Unlike the other

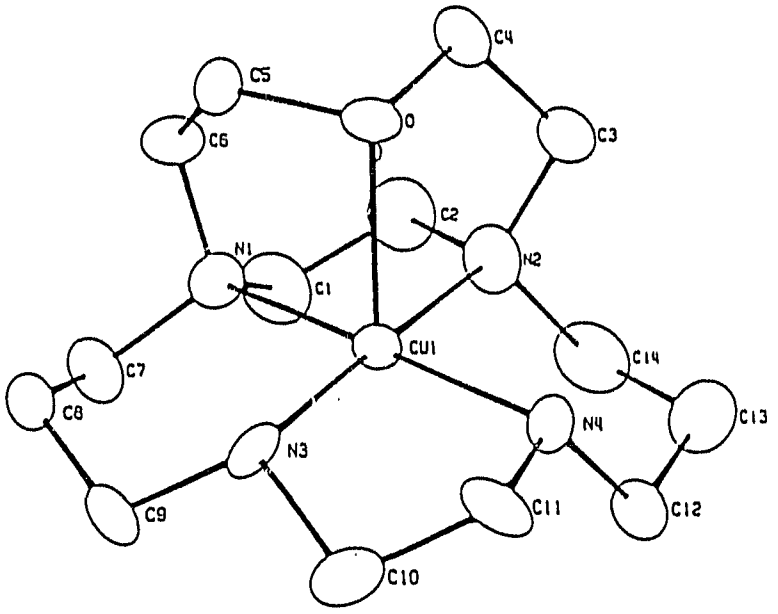

Fig. 4.4 ORTEP diagram of the cation $[Cu(N_4O)]^{2+}$, showing 25% thermal ellipsoids.

---

two copper complex ions under consideration, the Cu-N bonds are all 2.04 Å within experimental error. This is identical to the average distances found for the $[CuN_4S]^{2+}$ macrobicycle and is typical of N4 ligands coordinated in planar fashion around copper(II).[145] In other respects, the ion is closely similar to the enamine, except for the lengthening of the C10-C11 bond to 1.51(2) Å consistent with a single bond. The "tugging" angle 13.4° is lower than for the other two ions, presumably owing to the better encapsulation of the copper ion to the N_4 plane.

4.4 Discussion

4.4.1 Mechanisms

While in Schiff-base condensations of tetraaza open-chain

Table 4.11 $[Cu(N_4O)]^{2+}$

Fractional atomic coordinates and temperature parameters.

Atom	x/a	y/b	z/c	Ueq
Cu(1)	-6678(13)	24536(14)	27528(17)	405(6)
Cl(1)	20712(39)	2442(32)	30757(48)	647(20)
Cl(2)	62747(36)	20683(36)	23817(46)	658(20)
O(1)	2625(9)	-360(8)	3887(14)	91(6)
O(2)	1257(14)	-190(11)	2418(15)	150(9)
O(3)	1694(9)	897(8)	3821(13)	95(6)
O(4)	2629(16)	584(12)	2272(20)	209(14)
O(5)	7253(11)	2315(11)	2299(17)	141(9)
O(6)	6295(11)	1560(11)	3499(14)	122(8)
O(7)	5971(11)	1559(11)	1314(13)	126(8)
O(8)	5694(12)	2811(10)	2429(15)	135(8)
O	921(7)	2834(7)	2781(10)	55(4)
N(1)	-881(10)	3750(9)	2200(14)	60(6)
N(2)	-520(12)	2207(10)	868(13)	75(7)
N(3)	-858(9)	2674(8)	4624(11)	48(5)
N(4)	-513(9)	1164(8)	3248(14)	60(6)
C(1)	-1371(15)	3651(15)	849(18)	83(9)
C(2)	-742(16)	3051(15)	107(17)	88(9)
C(3)	569(13)	1944(13)	844(18)	72(8)
C(4)	1239(13)	2645(13)	1527(16)	73(8)
C(5)	911(12)	3781(10)	3133(17)	63(8)
C(6)	74(13)	4242(12)	2274(18)	69(8)
C(7)	-1589(14)	4269(12)	2887(20)	75(9)

Table 4.11 (continued)

C(8)	-1285(13)	4242(11)	4347(20)	68(8)
C(9)	-1517(14)	3375(13)	4994(19)	82(9)
C(10)	-1198(14)	1811(12)	5131(18)	72(8)
C(11)	-532(12)	1115(12)	4706(19)	71(8)
C(12)	-1239(13)	594(13)	2450(22)	80(9)
C(13)	-1032(16)	550(16)	1048(25)	103(12)
C(14)	-1214(16)	1457(19)	320(18)	96(11)

Estimated standard deviations are given in parentheses.

The footnotes are the same as those in Table 4.2.

Table 4.12 Bond Angles (°) for $[Cu(N_4O)]^{2+}$

Atoms	Angle	Atoms	Angle
N(1) -Cu(1) -O	82.2(5)	N(4) -Cu(1) -N(2)	92.9(6)
N(2) -Cu(1) -O	80.3(5)	N(4) -Cu(1) -N(3)	86.3(5)
N(2) -Cu(1) -N(1)	86.1(6)	C(1) -Cu(1) -O	95.1(5)
N(3) -Cu(1) -O	101.6(4)	C(1) -Cu(1) -N(1)	31.8(6)
N(3) -Cu(1) -N(1)	94.7(5)	C(1) -Cu(1) -N(2)	59.9(6)
N(3) -Cu(1) -N(2)	178.0(6)	C(1) -Cu(1) -N(3)	120.3(6)
N(4) -Cu(1) -O	99.9(4)	C(1) -Cu(1) -N(4)	146.1(6)
N(4) -Cu(1) -N(1)	177.5(6)		

Estimated standard deviations are given in parentheses.

Table 4.13 Interatomic Distances (Å) for $[Cu(N_4O)]^{2+}$

Atoms		Distance	Atoms		Distance
O	-Cu(1)	2.275(9)	N(3)	-Cu(1)	2.038(12)
N(1)	-Cu(1)	2.054(12)	N(4)	-Cu(1)	2.021(13)
N(2)	-Cu(1)	2.045(14)			

Estimated standard deviations are given in parentheses.

type of complexes, the primary product is generally expected to be the diimine, evidence has been presented previously[128,131] for imine-carbinolamine species. Hydrated material produced from a nickel(II) amine/glyoxal reaction, which was difficult to characterise, gave infra-red data consistent with an imine-carbinolamine.[131] However, in the present study, while an intermediate dicarbinolamine must be formed, the initial complex identified was an amidol species $[Cu(L2)]^{2+}$ (Scheme 4.1) which is tautomeric with an amide. This species is similar to the imidate complex formed in methanolic media in the condensation of the corresponding daptacn system.[128]

In Scheme 4.1 is presented a mechanism whereby the amidol may be formed. It is proposed that the initial product of the glyoxal condensation is the bis-carbinolamine (1) which, upon elimination of water, yields an imine-carbinolamine (not shown). Subsequent base-catalysed proton shift yields the unsaturated enolic species (2) which is converted to the $[Cu(L2)]^{2+}$ ion by a tautomeric proton rearrangement. Alternatively, (1) loses a water molecule as shown to yield

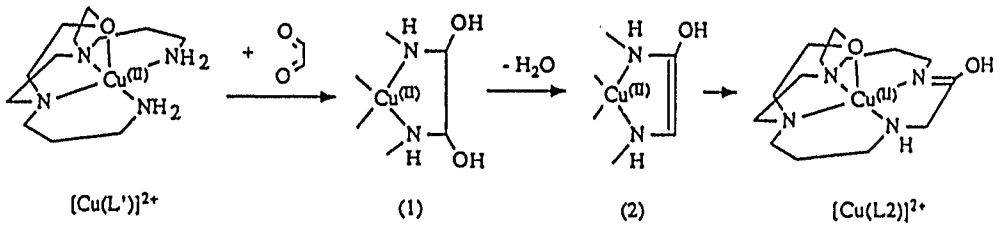

Scheme 4.1

the C=C bond (2) which then undergoes tautomeric change. The ionization of methylene protons adjacent to an imine in a five membered ring is well documented.[146] The amide may be produced under basic conditions. In this regard it is similar to the system observed for the $[Cu(N_5)]^{2+}$ ion formed on base hydrolysis of the corresponding imidate.[9] Interaction with a second mole of $[Cu(L2)^{2+}]$ results in the formation of the hydrogen-bonded dimer (scheme 4.2), the structure of which is also characterised (Fig. 4.2b).

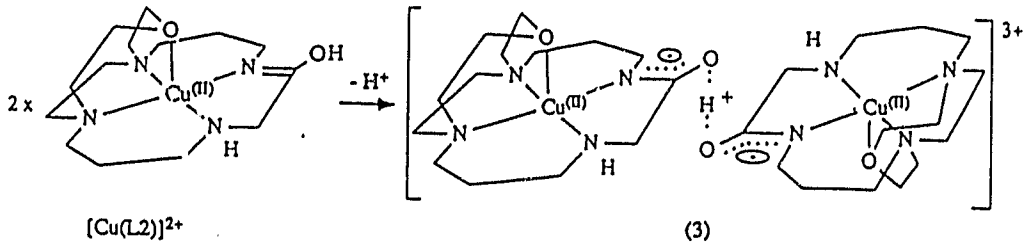

Scheme 4.2

Incomplete reduction of the amidol with BH_4^-, results in the enamine $[Cu(L3)]^{2+}$. Further reaction with an excess of reductant yields the macrocyclic ion $[Cu(N_4O)]^{2+}$. In the present experiment the enamine was the only intermediate

isolated in hydrogenation process, which is similar to that in the case of $[Cu(N_5)]^{2+}$.[128] As shown in scheme 4.3,

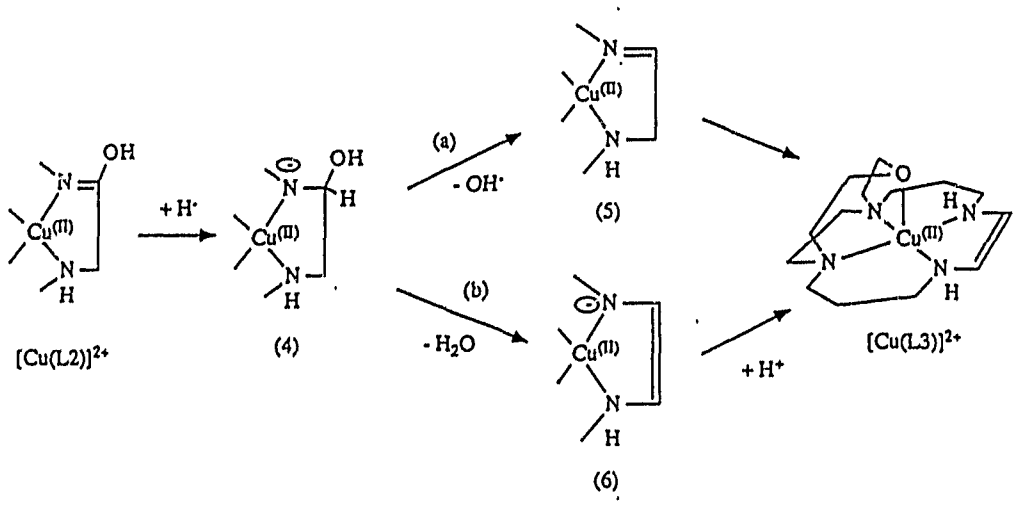

Scheme 4.3

it is likely that the first step of hydrogenation is H^--attack on the unsaturated β-carbon to give rise to the species **4**. From **4** to enamine $[Cu(N_4O)]^{2+}$, there are two possible pathways: (a), which has an imine intermediate **5**, and (b), which forms a intermediate **6** (scheme 4.3). The pathway (a) has been suggested by other workers[147] for this type of hydrogenation, but it is unlikely the case in the present system. Comparing the condensation product $[Cu(L2)]^{2+}$ with the most probable intermediate **2** (see scheme 4.1), it appears that the double bond on the five-numbered ring favours N=C form rather than C=C form as far as the structural preference is concerned. This structural preference should be the same in the case of **5** and $[Cu(L3)]^{2+}$, though the absence of -OH group may change

the proference slightly. That is, the structural energy of $[Cu(L3)]^{2+}$ should not be lower than that of **5** so much that the species **5** is forced to converted itself to the former in *almost 100 %*! In other words, if pathway (a) were the case, the species **5** should be, at least, produced if not the major product. However, *no* imine species was observed whatsoever in both present and previous experiments.[128] Therefore, pathway (b) is more likely the case. The doubly charged copper(II) ion is likely able to stabilise the negatively charged secondary amine to some extent so that the intermediate **4** prefers to lose H_2O (forming **6**) and then pick up a proton to give the enamine product instead of losing OH^- (forming **5**) and then converting to the product through a hydrogen 1,3-shift. In this pathway no **5** is formed, and the species **6** is not stable enough to be isolated, particularly in *acidic* media, and hence, the enamine $[Cu(L3)]^{2+}$ is the only intermediate which can be isolated in the hydrogenation of $[Cu(L2)]^{2+}$.

4.4.2 Intermediates

The amidol functional group in the condensation product $[Cu(L2)]^{2+}$ exists only when the ligand is coordinated to a copper(II) ion. Discharging the Cu(II) ion from the ligand framework led to formation of an amide ligand (L"), which was isolated and identified (see section 2.2). It appears that the five-membered ring on the $[Cu(L2)]^{2+}$ prefers to have two sp^2 atoms rather than one so that the ring can be more planar.

There is an interesting comparison between the amidol species and the mono-oxo-tetraamine complexes described previously by Kimura[148]. In the case of mono-oxo-cyclam (4),

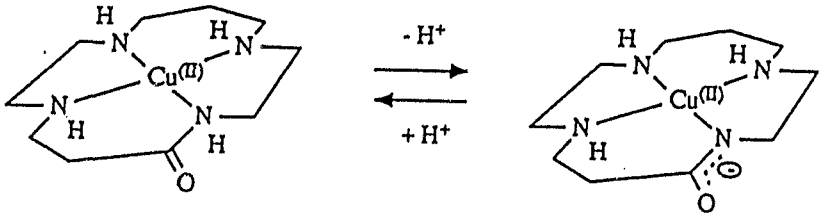

4

where the ring contains one amido group, there is no evidence for the amidol, and a significant thermodynamic preference is observed for the square-planar forms of the nickel(II) and copper(II) complexes, even in the presence of potential axially coordinating donors. In the present system, although the ether oxygen is a weak binder, it is a sufficiently good σ donor, both in the copper case, and, in the corresponding nickel complex which is high spin (see chapter 6), that oxygen coordination is observed. Perhaps it is noteworthy that there is no ready deprotonation of the amidol implying its weaker in-plane field than that of the amido nitrogen. What is clear is that there are subtle effects of the ring field which can be transmitted to the metal center and which are exhibited by the facility to change coordination number.

A weak Cu-O(ether) bond (2.47(2) Å) has been reported in the copper(II) complex of the potentially ditopic receptor, 1,4,7,10-tetraoxa-13,16,19,22-tetraazacyclotetracosane (5).[149] This bond is considerably longer than the corresponding bonds

(2.25-2.33Å) found in the present study.

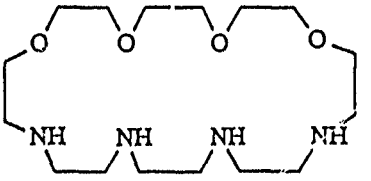

5

The present ligand framework is related to the ligand 1-oxa-4,7-diazacyclononane, [9]aneN$_2$O. Thermodynamic studies[72] show that there is considerable stabilization of octahedral complexes relative to other similar systems. It is suggested that this relates to the conformation of the 9-membered ring favoring coordination to the octahedral face of a small metal ion. Of the first row elements, Cu^{2+} forms the strongest complex, log K_2([Cu([9]aneN$_2$O)$_2$]$^{2+}$) = 10.86.[72] In this system the ether oxygens are both bound to the copper ion. However, with the additional cyclam framework in the bicyclo-ligands, the stability constant for [Cu(L2)]$^{2+}$ undoubtedly will be considerably higher.

The molecular structure of each complex ion is best described as a distorted square pyramid. In some instances the copper ion lies above the mean plane of the four nitrogens, with the apical oxygen atom tilted away from a position directly above the copper. In the case of the ion [Cu(L3)]$^{2+}$, the four nitrogen centres are perfectly planar with a displacement of the metal from the plane of 0.0396 Å towards

the oxygen donor, The angle between the Cu-O(apical) and the perpendicular to the N4 plane is 13.4°, as a result of the inability of the apical donor to reach over completely and occupy the position normal to the plane. For the saturated ligand and the amidol, the corresponding values are 14.82° and 15.23° respectively. As the copper ion is located further out of the plane, the degree of "tugging" increases.

Chapter 5 Spectroscopic and Electrochemical Properties of Square Pyramidal Cu(II) Complexes of BicycloN_4X (X = O, S and N) ----- Axial Donor Effect

5.1 Introduction

The chemistry of copper complexes has long been, and still is, a very active field both spectroscopically and electrochemically. The interest in this is largely stimulated by the observation of the unique properties of the copper-containing enzymes and proteins in their spectroscopy and redox chemistry. Examples of these are Type I copper(II) proteins,[150] which are characterized by a very intense absorption at about 600 nm (ε = 3000 - 5000 $M^{-1}cm^{-1}$) in their electronic spectra and very small $A_{\parallel}$ values (30 - 90 G) in their esr spectra; and galactose oxidase, which contains copper as a active centre in catalyzing the two-electron transfer reactions.[151] To understand the unusual behaviour of the copper(II) in biological systems, the investigations carried out by chemists have focussed mainly on how the change in the coordination environment affects the copper centre by using wide variety of synthetic molecule models. The majority of these model complexes are of tetra coordination, which are normally square planar (SP1) (or tetrahedrally distorted) in geometry, and it is now clear that both spectroscopic and electrochemical nature of copper(II) are strongly influenced by the changes on the tetragonal plane (such as different donor types, tetrahedral distortion, rigidity of ligand framework etc.). Recently, there is growing interest in the penta and hexa coordinated copper(II) complexes as to how the axial donors affect the copper centre.[35,133,152-156]

As a contribution to this latter development in understanding of copper chemistry, a series of pentadentate bicyclic ligands (Structure 1) has been synthesised in our laboratory[128,129] (also see chapter 2 and 4). For these ligands, the four amines on the cyclam moiety plus the apical donor on the nine-membered ring are all expected to be able to bind the copper(II) upon complexation, so the square pyramidal coordination geometry can be achieved. Furthermore, the change of the apical donor from oxygen to sulfur and nitrogen is expected to result in different degrees of displacement of copper from the N_4 plane towards the apical donor.[153] This is indeed the case, at least in the solid state. The crystal structures of their copper(II) complexes have revealed that the copper ion is fully encapsulated in the ligand by the five donors, and sits above the N_4 plane towards the axial donor[128,129] (*vide infra*), adopting a square pyramidal geometry. The distance of copper to the plane decreases as the apical donor changes from N, S to O. In solution, these copper(II) complexes are very stable, and no detectable decomposition was observed even in 4.0M $HClO_4$ for several days. Hence, these complexes provide a good model for studying the effect of the apical donor on the spectroscopy and electrochemistry of the copper centre. In addition to this, the complex of L2 (Structure 1) offers an opportunity to examine the effect of different tetragonal planes under the square pyramidal coordination environment in comparison with that of N_4O.

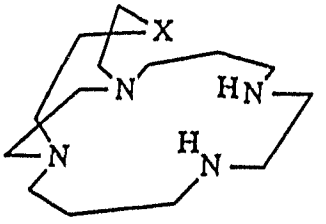

N_4X

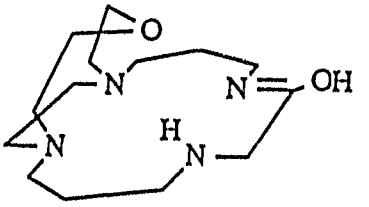

L2

X = O, S or N

1

Another important common feature shared by the ligands presented here is the strong rigidity imposed by the bicyclic rings. It has been reported that because of its d^{10} electron configuration, copper(I) complexes have quite a strong tendency to adopt a geometry different from that of copper(II) complexes.[87] In an investigation of macrocyclic polythia-copper complexes using cyclic voltammetry, Rorabacher *et. al.*[87] have observed that upon reduction of Cu(II) centre, the Cu(I) complex formed underwent self-rearrangement to adopt a geometry which differed from that of the original Cu(II) complex, and a "square scheme" was observed. This observation has been used to explain the discrepancy which appeared frequently in the self-exchange rates of the $Cu^{2+/+}$ complexes of small molecular weight when the different approaches were made in the kinetic study of their redox reations.[69a,157] With the intrinsic rigidity, the title ligands may provide alternative means to prevent the coordination or geometrical

rearrangement associated with the electron transfer process at the copper centre, and as well to enhance the self-exchange rate due to the smaller changes in both inner coordination sphere and solvation sphere during the redox reaction.[150]

5.2 UV/Visible Spectra

In CH_3CN, all of the complexes presented have a d-d band envelope peak in the range from 500 to 600 nm, and a charge transfer absorption in the range from 250 to 300 nm (Table 5.1). A typical spectra are shown in Fig. 5.1. For the complex Cu(II)(L2), the extra peak at 198 nm and a shoulder peak at about 660 nm were observed (Fig. 5.1b). The former is likely due to the $\pi \rightarrow d$ charge transfer and the latter probably results from the solvent-coordinated octahedral complex (*vide infra*), since the coordination at the axial position lowers the energy of the d-d transitions.[152] The peak for the possible solvent-coordinated complexes, which is expected to appear at near or higher than 600 nm, was very weak (Fig. 5.1a) for the complexes of N_4X (X = O, S, and N) and cyclam.

The spectra taken in H_2O solvent are also given in Table 5.1. For the Cu(II) complexes of N_4X and cyclam, the spectra are almost identical in both solvents, consistent with the statement made above, that is, the species concerned remain in a mainly unsolvated square pyramidal geometry in solution.[153] For the copper complex of L2, the absorption at about 534 nm also remains almost intact under solvent change, but, a slight

Table 5.1 Results from UV/Visible Spectra of Cu(II)(L)

L	$\lambda_{max.}$(nm) (ε, $M^{-1}cm^{-1}$) in CH_3CN	$\lambda_{max.}$(nm) (ε, $M^{-1}cm^{-1}$) in H_2O
N_4O	272(6630), 525(86)	274(6800), 522(102)
L2	198(4590), 269(5700), 533(73), 660(39)[a]	199(9103), 271(5950), 533(70), 673(26)[a]
N_4S	280(6370), 533(98)	281[b], 532(143)[b]
N_5	274(6370), 565(155)	276(5700),[b] 567(145)[b]
cyclam	253(7330), 507(90)	251(6984), 504(72)

[a]shoulder peak; [b]from ref. 137.

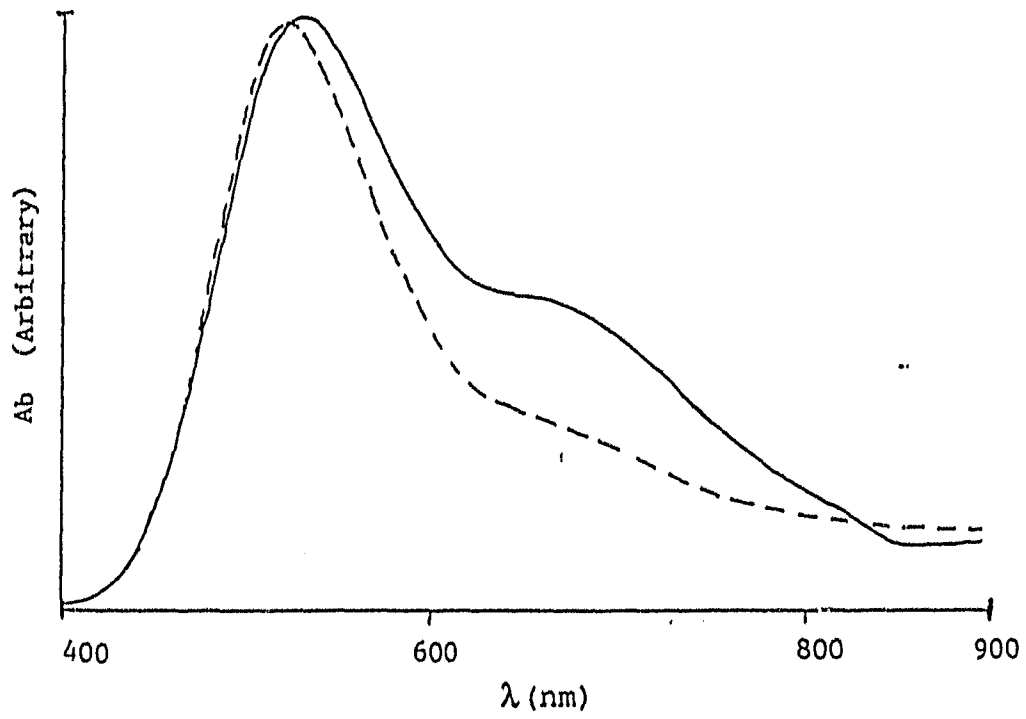

Fig. 5.1 Visible spectra in CH_3CN: a) ··· Cu(II)(N_4O); b) – Cu(II)(L2).

"red shift", from 660 to 673 nm, of the shoulder peak was observed on going from CH_3CN to H_2O, indicating correspondence of the solvent coordination to the shoulder peak.

The "red shift" of the d-d band envelope maximum in the order of cyclam, N_4O, N_4S to N_5 likely results from both σ donation of the axial donor and the movement of copper ion out the N_4 plane. It has been well recognized[152,153] that the energy difference of the *d* orbitals on the copper(II) can be reduced by the axial donor, and the stronger σ donor tends to cause a greater reduction. Lowering the energy of the d-d transition by displacing the copper ion from the tetragonal plane has been investigated by Addison *et al.*,[153] and it has been observed that the extent to which the copper is displaced from the plane depends on the strength of the axial donor.[153] The stronger the donor, the further the copper ion is removed from the plane. Thus, the "red shift" observed may be rationalized in terms of both the strength of σ donation and the displacement of the copper ion out the plane.

It is interesting to notice that as the ligand is changed from N_4O, N_4S and N_5, the molecular absorption coefficient, ε, increases steadily, from 86 to 155 $M^{-1}cm^{-1}$ in CH_3CN and from 102 to 145 $M^{-1}cm^{-1}$ in water. This is consistent with the degree of displacement of copper from the N_4 plane, since the further the copper is pulled out of the plane, the lower the symmetry of the complex, and, hence, the stronger the absorption. The observation is in accordance with the order of the

displacement of the copper ion from the plane in the solid state. The large ε value for the complex of cyclam, in comparison with that for the complex of N_4X, may originate from the strong p-d bonding between the in-plane nitrogens and the copper.

The "red shift", about 10 nm, of the d-d transition for the complex of L2 in comparison with that for the complex of N_4O is likely due to the weaker tetragonal plane field imposed by the ligand L2, resulting from both the sp^2 hybridization of one of the four in-plane nitrogen donors and the electron-withdrawing group on the ligand L2.

5.3 ESR Spectra

The esr spectra of all complexes concerned are characteristic of square pyramidal or tetragonally-elongated octahedral geometries with the unpaired electron in the $d_{x^2-y^2}$ orbital of the copper(II). The results from mixed solvent of CH_3CN/DMF (1:1) are all presented in Table 5.2. The values for $g_{/\!/}$ and $A_{/\!/}$ were determined at 77 K, g_o and A_o at ambient temperature. The values for $g_\perp$ and $A_\perp$ were estimated by application of the simple first-order relationships:[159,160] $g_\perp = (3g_o - g_{/\!/})/2$ and $A_\perp = (3A_o + A_{/\!/})/2$ (g_o and A_o assumed temperature independent[161]). The typical spectra are shown in Fig. 5.2.

For all of the complexes investigated, N-shf coupling was observed only in solvated complex Cu(II)(L2)(CH_3CN), which showed eleven small peaks corresponding to the five nitrogens

coordinated to the copper with $^{N}A_{\perp}$ = 14 G (Fig. 5.2b). It has been documented that for polyaza Cu(II) complexes, "N-shf coupling is observable only if the percentage of s character contributed to the bonding MO by the nitrogen donors exceeds critical value of 20.0% s".[162] For the Cu(II) complexes of N_4X and cyclam, the nitrogens are all of sp^3 hybridization, and the detection level is near or below the borderline for N-shf coupling, and could not be detected in esr spectra. In the case of Cu(II)(L2) complex, however, the solvent-coordinated species is likely of presence in the solution (*vide infra*), the N-shf coupling is strengthened by (a) the sp^2 donor from the ligand, and (b) the sp donor from the CH_3CN.[162] In turn, the eleven lines in the esr spectrum, though weakened by the equilibrium between the solvent-coordinated and the non-solvent-coordinated species, is evidence for the coordination of CH_3CN, and suggests that the solvent coordinated octahedral complex may be a component of the equilibrium. In accord with this is the observation that the $g_{\perp}$ for L2 is smaller than that for N_4O. Without the presence of the solvent-coordinated species, as observed frequently for other Cu(II) comlexes,[153,163] $g_{\perp}$ is expected to increase as the ligand changes from N_4O to L2 owing to the more cationic N_4 tetragonal plane on L2. However, it is not the case in the present investigation.

The values for A_o, $A_{/}$ all decrease as the axial donor become weaker (from N, S to O) (Table 5.2), as anticipated on the basis that a stronger donor orbital tends to mix more with

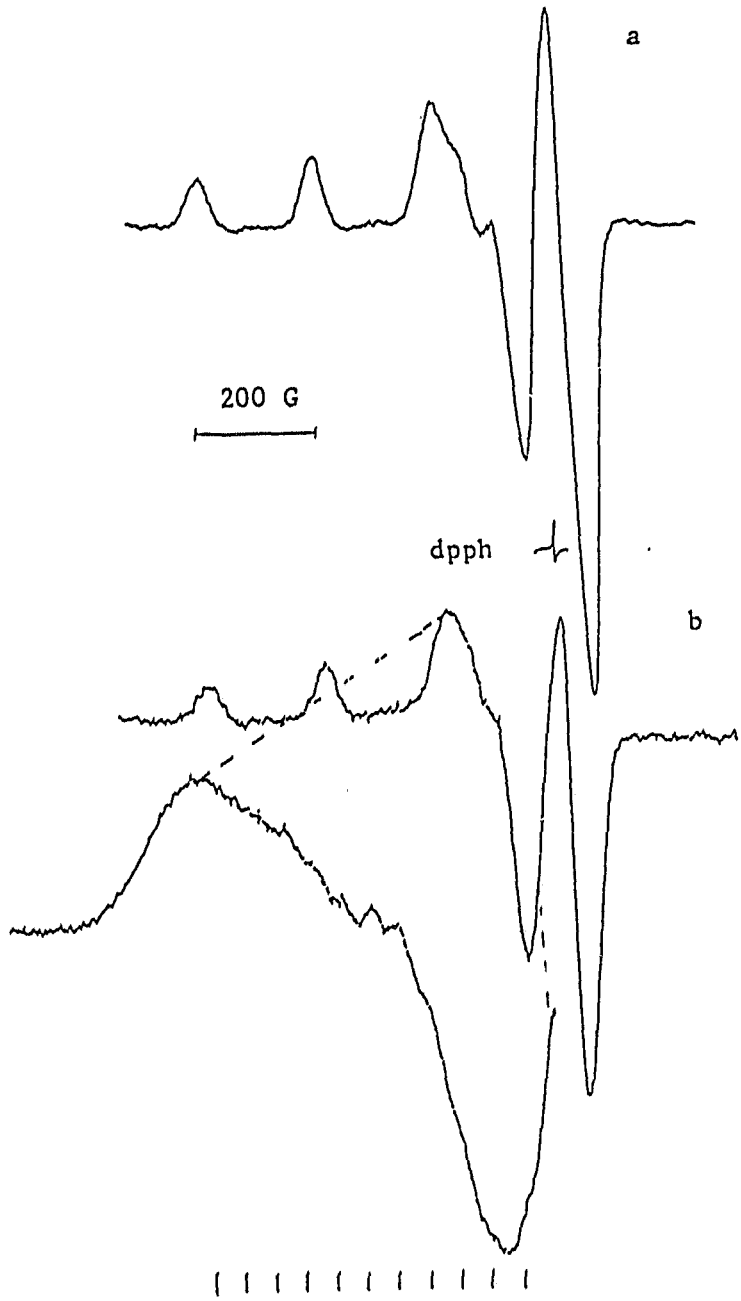

Fig. 5.2 ESR spectra of Cu(II)(N_4O) (a) and Cu(II)(L2) (b) in CH_3CN/DMF (1:1) at 77 K.

Table 5.2 Results from ESR Spectra of Cu(II)(L)

L	$g_{/\!/}$	$A_{/\!/}^{b}$	g_o	A_o^{b}	$g_\perp^{c}$	$A_\perp^{b,c}$
N_4O	2.204	190	2.099	87	2.047	35.5
L2[e]	2.194	188	2.094	85	2.043	33.5
N_4S	2.201	185	2.096	86	2.044	36
N_5	2.208	180	2.105	77	2.053	25.5
cyclam	2.198	200	2.097	90	2.046	35

[a]in CH_3CN/DMF (1:1); [b]in Gauss; [c]calculated from equation $g_\perp = (3g_o - g_{/\!/})/2$; [d]calculated from equation $A_\perp = (3A_o - A_{/\!/})/2$; [e]presence of eleven N-shf coupling peaks with $^{N}A_\perp$.

the orbital of the metal centre, and delocalize electron-density to the donor orbital, and hence, a smaller amount of the density is left on the metal centre (see section 2.2.3).

Although the correlation between $g_{/\!/}$ and $A_{/\!/}$ has been widely recognized for the tetrahedrally distorted square planar Cu(II) complexes,[164] the correlation for the square pyramidal Cu(II) complexes where copper is displaced from the tetragonal plane, has proved to be very poor.[153] Here again, no correlation between $g_{/\!/}$ and $A_{/\!/}$ is evident in the present system. The correlation between g_o and A_o in the complexes of N_4X is very poor, though this correlation has been observed for the other square pyramidal Cu(II) complexes.[153] The reason for this poor correlation is not clear. The relation between $g_\perp$ and $A_\perp$

can be correlated for the complexes of N_4X. However, the position for N_4S is lower than that for N_4O in the correlation. Reason for this is not clearly understood, and probably has to do with the d_{Cu}-d_s interactions between the apical sulfur and the central copper (*vide infra*).

In comparison with the results from the UV/Visible spectroscopy, both $A_{/\!/}$ and $A_{\perp}$ can be correlated with the energy of the d-d transitions in terms of the σ-bonding strength, which is common to both square planar and square pyramidal Cu(II) complexes.[150,153]

For the complexes of N_4O and N_5, the g and A values are all similar to that observed from the monocyclic Cu(II) complexes[155] of [15]aneN_4O and [15]aneN_5 respectively, consistent with their similarity of inner-shell coordinations.

5.4 Electrochemistry

The electrochemistries of all the complexes were studied using cyclic voltammetry. The CV's were obtained at ambient temperature in CH_3CN/0.1M $[(t\text{-}Bu)_4N](ClO_4)$ with $Ag/AgNO_3$ (0.01M) as the reference electrode, unless specified otherwise. The measured potentials are referenced to $Frc^{+/0}$ at 0.1 V.

5.4.1 Cu(II) (N_4O)

Oxidation

In CH_3CN, oxidation of Cu(II) (N_4O) complex was a symmetric

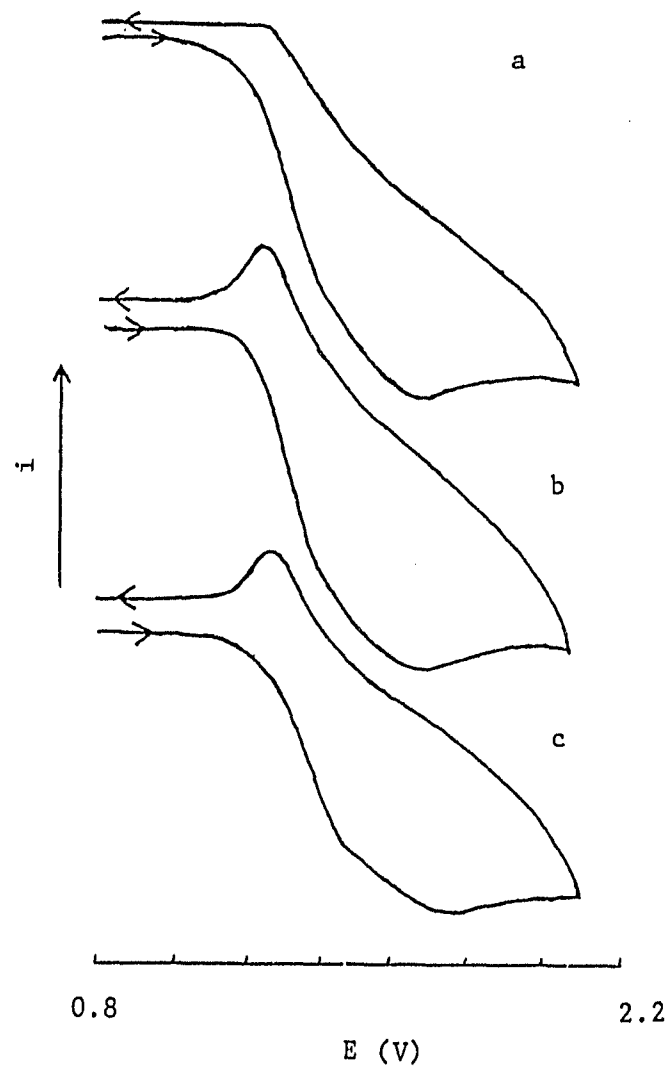

Fig. 5.3 CV of $[Cu(N_4O)]^{3+/2+}$ in CH_3CN at the scan rate of a, 200; b, 1000; c, 3500 mV/s.

quasi-reversible process (α = 0.5) at high scan rates ($\geq$ 1000 mV/s), having $E_{1/2}$ of 1.3 V (Fig. 5.3b,c). When scanning slowly, however, it became irreversible (Fig. 5.3a). There was

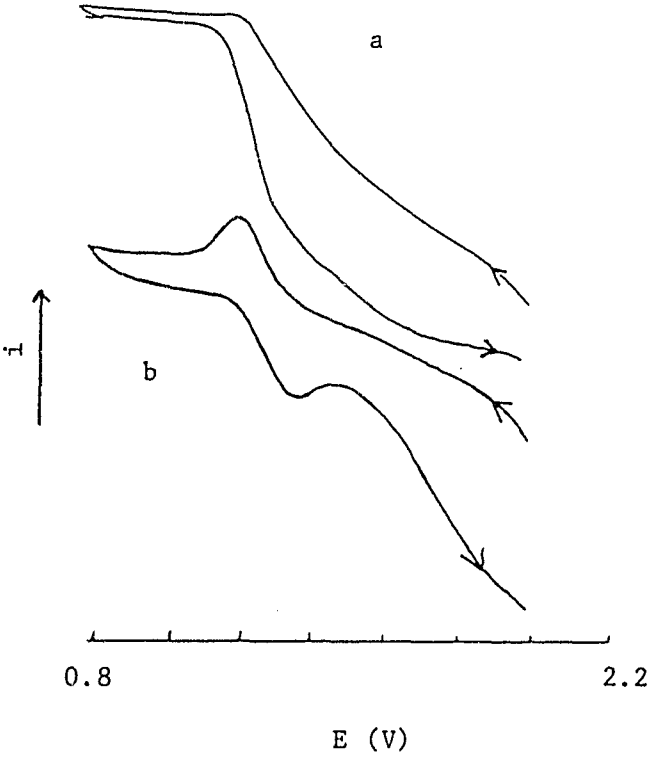

Fig. 5.4 CV of $[Cu(N_4O)]^{2+/3+}$ in CH_3CN at the scan rate of: a, 200; b, 3000 mV/s.

---

also another EC process apparent in the CV (Fig. 5.3) with a anodic peak at a higher potential (E_{ap} = 1.60 V). This second anodic peak disappeared when the CV was scanned cathodically, at a high rate (Fig. 5.4b), though it was observed at a lower rate (Fig. 5.4a).

Reduction

Electrochemical reduction of the square pyramidal complex was a EC process. Upon reduction the initial Cu(I) complex, I,

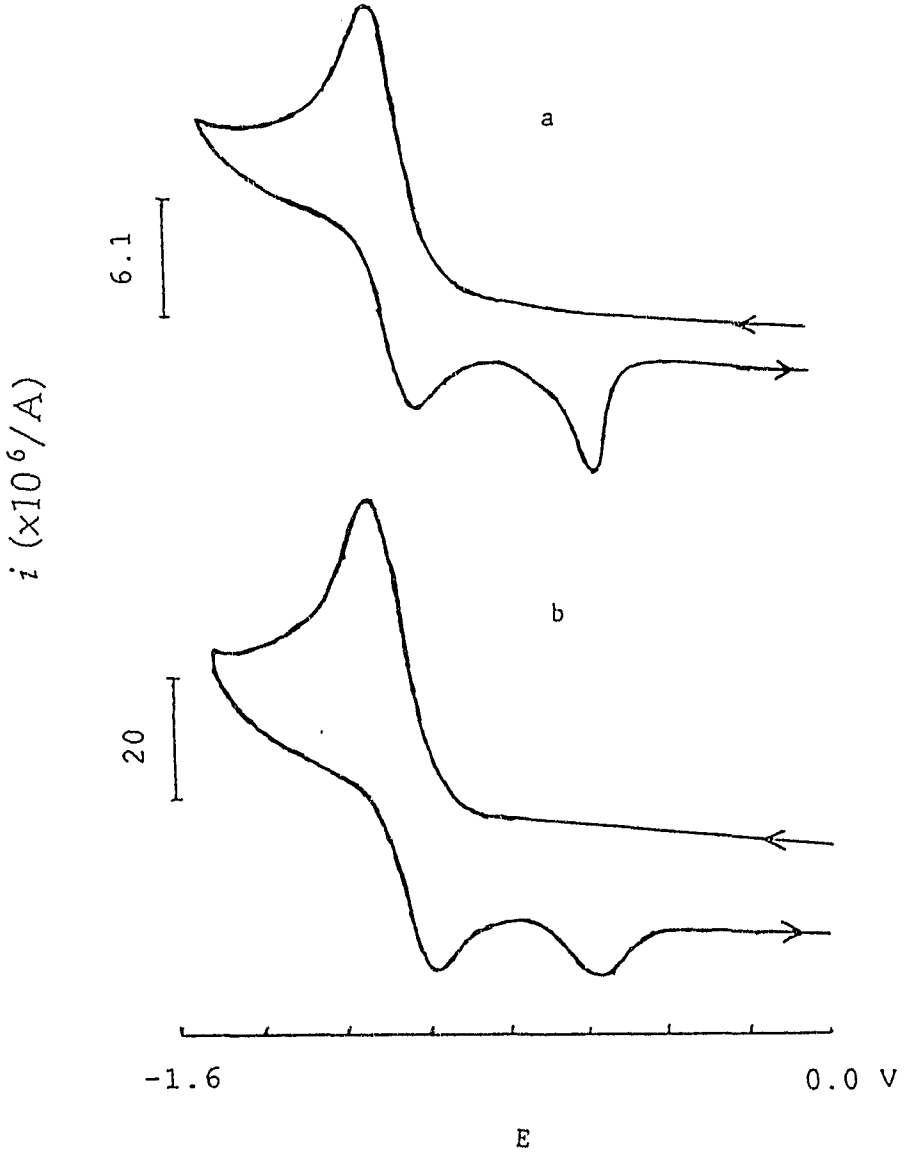

Fig. 5.5 CV of $[Cu(N_4O)]^{2+/+}$ in CH_3CN at the scan rate of: a, 100; b, 1000 mV/s.

---

rapidly equilibrated with its structural isomer II, giving rise to two anodic peaks at ~ -1.0 and -0.58 V respectively

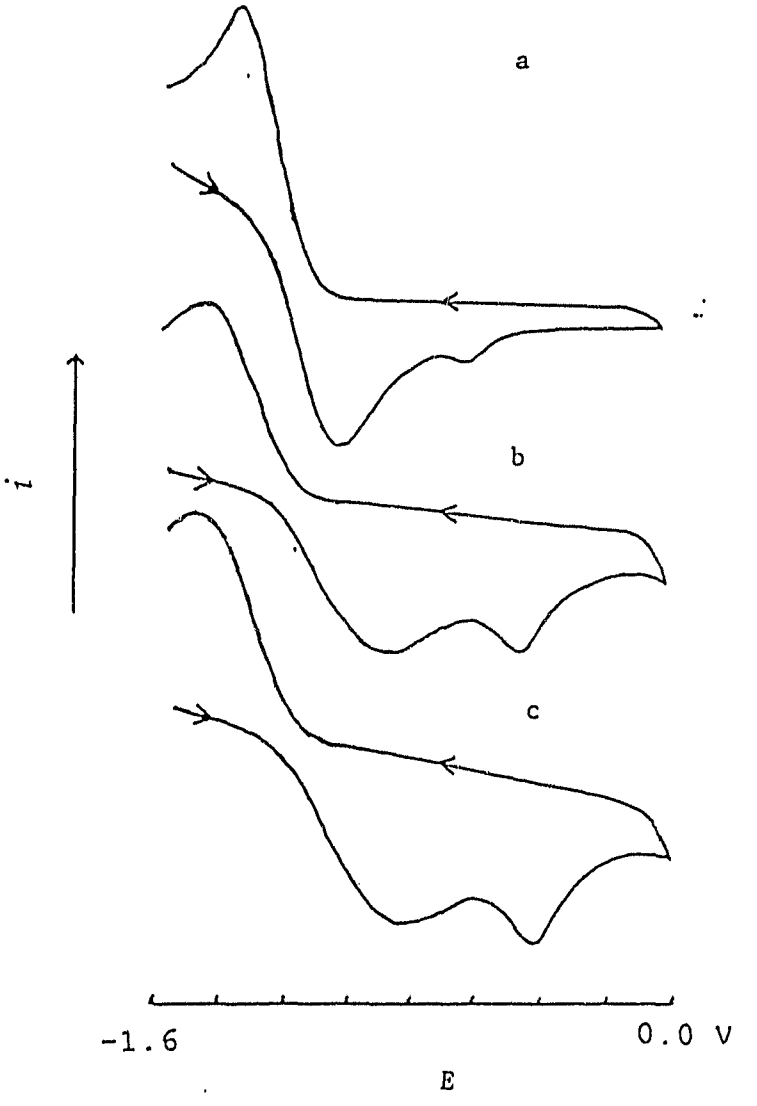

Fig. 5.6 CV of $[Cu(N_4O)]^{+/2+}$ at -20 °C, with the scan rate: a, 200; b, 2000; c, 3000 mV/s.

(Fig. 5.5). The origin of II from I is shown by the fact that, the sum of the heights of two anodic peaks, $i_{ap,1}$ for I and $i_{ap,2}$ for II, always equals the height of the cathodic peak, $i_{cp,1}$ (from reduction of the unsolvated complex), and the ratio of $i_{ap,2}/i_{ap,1}$ decreased as the scan rate increased (Fig. 5.5).

Detailed study of the CV's obtained by scanning from -1.5

to 0.0 V at low temperature (-20 °C) indicates the conversion between I and II is a true equilibrium (Fig. 5.6). It is likely that 250 ms of pre-run rest time (pre-set on the instrument) could enable any reasonable fast equilibration to be established. As shown in Fig. 5.6, ratio of $i_{ap,1}/i_{ap,2}$ increases as the scan rate increases from 200 mV/s (Fig. 5.6a) to 3000 mV/s (Fig. 5.6c), indicating there must be a process operating to convert II to I, otherwise the ratio at the slower scan rate ought to be smaller than that at the higher, since there would be more complex II accumulated for the longer time. With recognition of existence of this equilibrium, the observations above can be readily understood. When the scan rate is low in comparison with the equilibration process, the complex I lost by electrochemical oxidation can be compensated at the expense of complex II through the equilibration, and hence, a small amount of V is left when the potential reaches about -0.57 V. At high scan rate, a lower concentration of II is available for the conversion to I because of the shorter time, and hence, more complex II is left when its oxidation potential arrives. The faster the scan rate, the more complex II remains, and consequently the lower ratio of $i_{ap,1}/i_{ap,2}$ is to be expected.

The electrochemical nature of the initial square pyramidal complex was studied by scanning anodically from -1.4 to -0.8 V (Fig. 5.7). As scan rate increased by 10 fold (from 100 to 1000 mV/s), the peak separation, $\Delta E_{a,c}$, remained almost

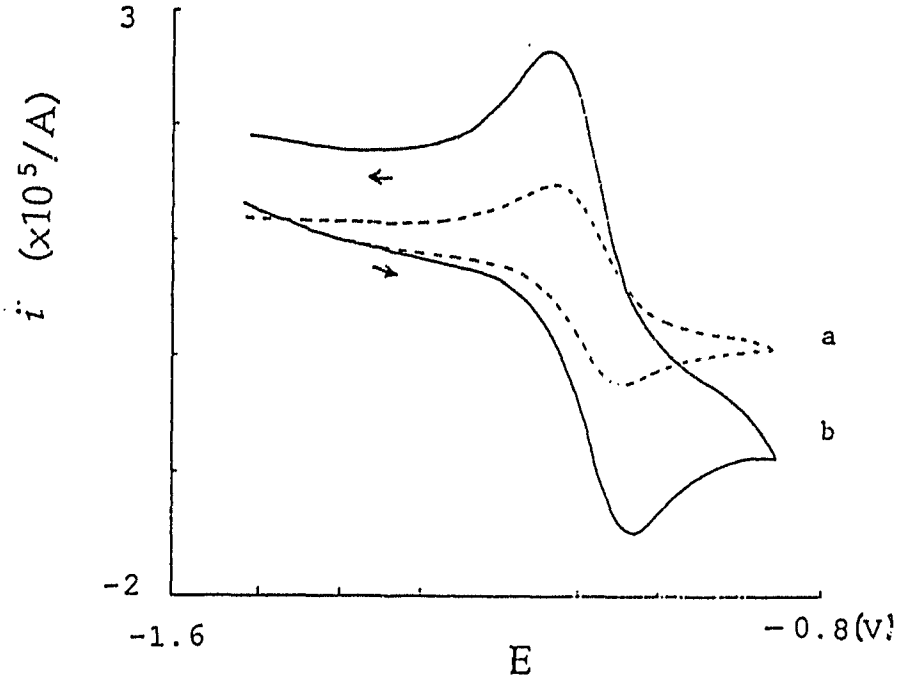

Fig. 5.7 CV of $[Cu(N_4O)]^{+/2+}$ in CH_3CN at the scan rate of: a, 100; b, 1000 mV/s.

intact being a value of ~70 mV, together with $i_{ap,1}/i_{cp,1} = 1$, reflecting a reversible (both electrochemical and chemical) nature of the process. The redox potential of the $Cu^{2+/+}(N_4O)$ couple, $E_{1/2}$, is -1.04 V.

For the species II, no cathodic peak corresponding to its oxidized form could be detected even with the scan rate of 3000 mV/s at -20 °C (Fig. 5.6c). Considering the higher oxidation potential (indicating possible higher effective charge on the metal centre) and sharper anodic peak (indicative of possibly a lower Franck-Condon barrier, or in other words, a less bond-rearrangement during the electron-

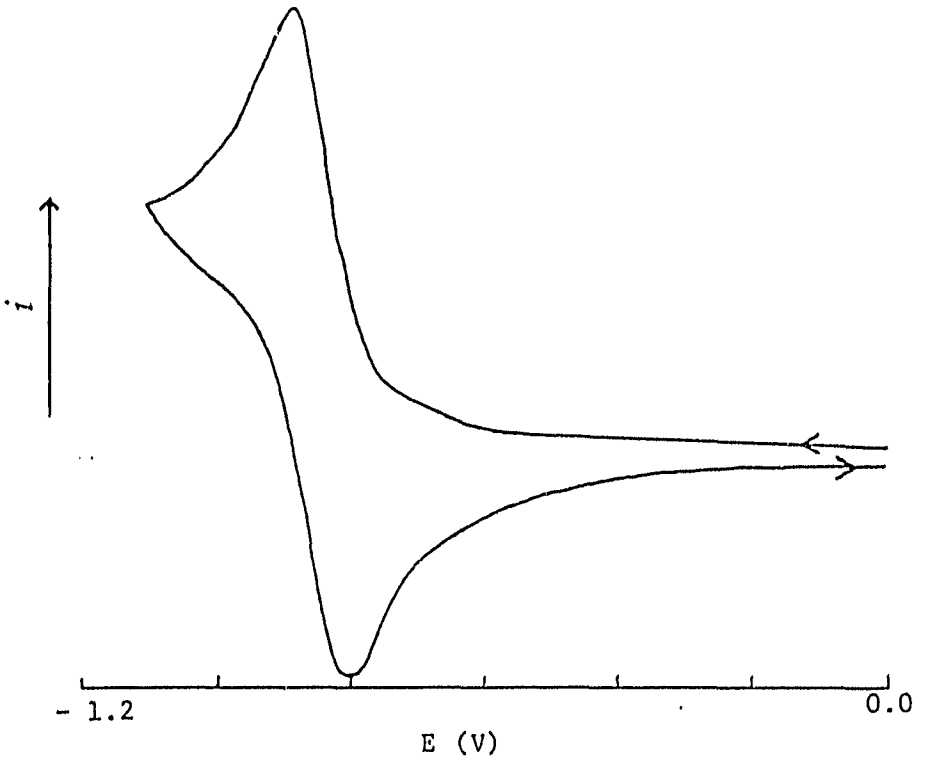

Fig. 5.8 CV of $[Cu(N_4S)]^{2+/+}$ in CH_3CN at the scan rate of 200 mV/s.

transfer) than that of the penta-coordinated complex I, it is very likely that it is a tetra-coordinated species and formed by dissociation of one of the bicyclic ligand donors from the inner-shell coordination in the penta-coordinated species I.

Among the five base donors in the complex I, the ether oxygen is the hardest base, whereas Cu(I) is a very soft acid. Theoretically, the oxygen is likely to be the one that is removed from the coordination sphere on going from the complex I to II. In order to confirm this, it is better to compare the CV of Cu(II) (N_4O) with that of Cu(II) (N_4S). If it is one of the

four nitrogens which is removed from the coordination in the N_4O complex, it is expected that the reduction of Cu(II)(N_4S) should also give rise to two complexes analogous to I and II, where one having the five donors coordinating and another only S and three N's. But, this is not the case. The CV of Cu(II)(N_4S) shows only one reversible $Cu^{2+/+}$ couple with $E_{1/2}$ of -0.85 V (Fig. 5.8), suggesting that in this case all of the donor atoms remain attached before and after electron transfer and only one species exists after reduction. This can be rationalized by the greater strength of the Cu-S bond (soft base, soft acid) and the expected rigidity of the cyclam moiety holding the four nitrogens coordinated. If the four nitrogens can remain coordinated in the complex Cu(I)(N_4S), it is difficult see why they can not in the complex I. Based on this reasoning, the structure of species II is likely to be the one which has the ether oxygen removed from the coordination sphere.

At this stage, it is impossible to determine the exact structure of the complex I. However, it is likely to be somewhere between tetrahedral and square planar, or, in other words, a tetrahedrally distorted square planar. The cavity of the *trans*-I cyclam moiety is probably too small to hold Cu(I) right in the middle of N_4 plane. The very rapid conversion of the tetra-coordinated Cu(II), III (the oxidized form of II), to the initial penta-coordinated complex, on the other hand, suggests it can not be a perfect tetrahedral, because it would

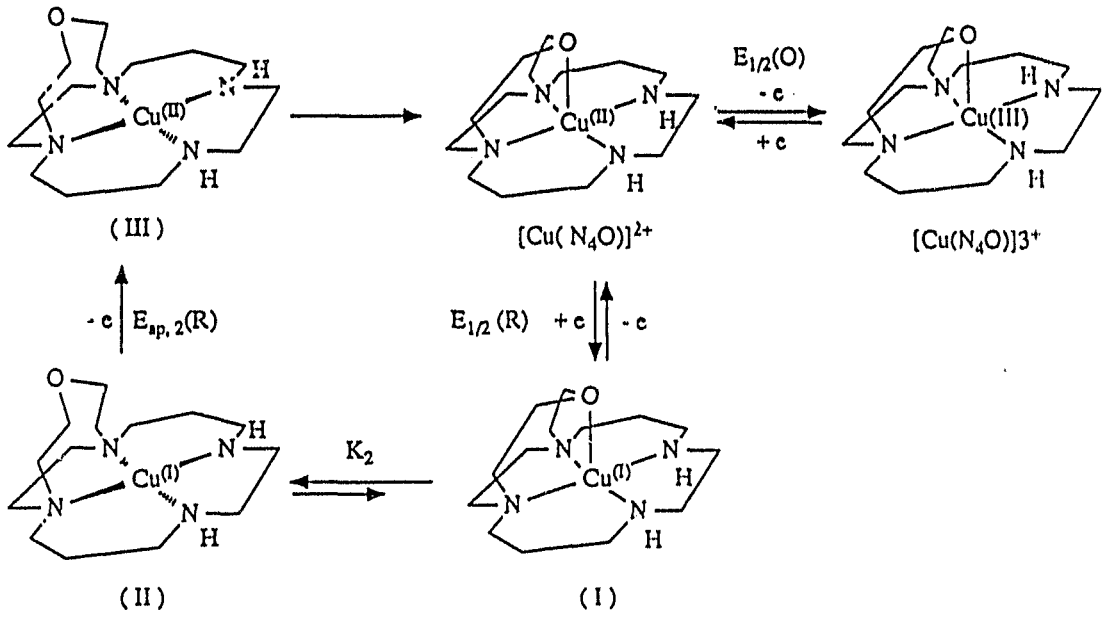

Scheme 5 1 Electrochemical Reaction Scheme of $[Cu(N_4O)]^{3+,2+,+}$

involve a lot of bond rearrangement during the electron-transfer, and the rate of the conversion is expected to be much slower (giving rise to a broader anodic peak).

All of the processes involved in the electrochemical redox reactions of the complex Cu(II)(N_4O) are shown schematically in Scheme 5.1. For the reduction process, a "square scheme" is observed. It demonstrates again that the Cu(I) centre has a very strong tendency towards adopting a structure which is different from that which the Cu(II) centre prefers.[87]

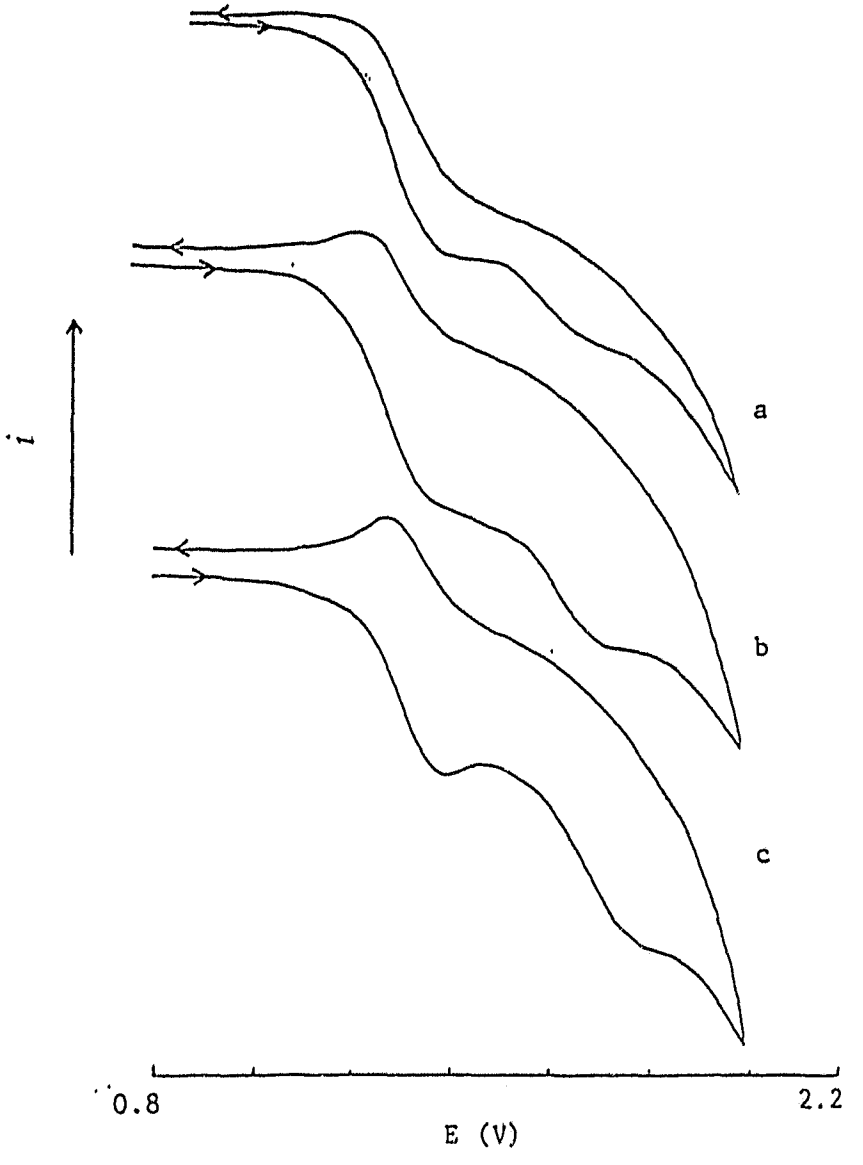

Fig. 5.9 CV of $[Cu(L2)]^{2+/3+}$ in CH_3CN at the scan rate of: a, 20; b, 200; c, 1000 mV/s.

5.4.2 Cu(II)(L2)

Oxidation

In CH_3CN, it is likely that Cu(II)(L2) exists in

equilibrium with its solvated counterpart, Cu(II)(L2)(CH_3CN) (as indicated from both the esr and visible spectroscopic studies, *vide infra*). Oxidation of the unsolvated square pyramidal complex showed symmetric quasi-reversible characteristics with $E_{1/2}$ of 1.32 V at high scan rate (≥ 500 mV/s) (Fig. 5.9c), and was an EC process at low scan rate ($i_{cp}/i_{ap} < 1$ at ≤ 200 mV/s) (Fig. 5.9a). The CV of the solvated octahedral complex was characteristic of an EC process at all scan rates ranging from 20 to 3000 mV/s (absence of cathodic peak), but showed an electrochemically reversible and chemically irreversible nature at low scan rates (≤ 200 mV/s) with an anodic peak at ~ 1.75 V (Fig. 5.9a,b, and Table 5.3).

The equilibrium between the solvated and unsolvated species was also confirmed by scanning cathodically from 2.0 to 0.8 V (Fig. 5.10). At a low scan rate (200 mV/s), two anodic peaks were observed (Fig. 5.10a). However, only one anodic peak at the lower potential (corresponding to the solvated species) was detected at a high scan rate (4000 mV/s, Fig. 5.10b).

Reduction

The reduction of solvated complex Cu(II)(L2)(CH_3CN) has $E_{1/2}$ of -1.40 V, with electrochemically quasi-reversible characteristics ($\Delta E \approx 100$ mV, $\alpha = 0.5$) (Fig. 5.11). At the scan rate of 50 mV/s, the ratio of i_{cp}/i_{ap} is > 1, indicating Cu(I)(L2)(CH_3CN) is not very stable. The ratio approached to unity when the scan rate was 1000 mV/s or faster (Fig. 5.11).

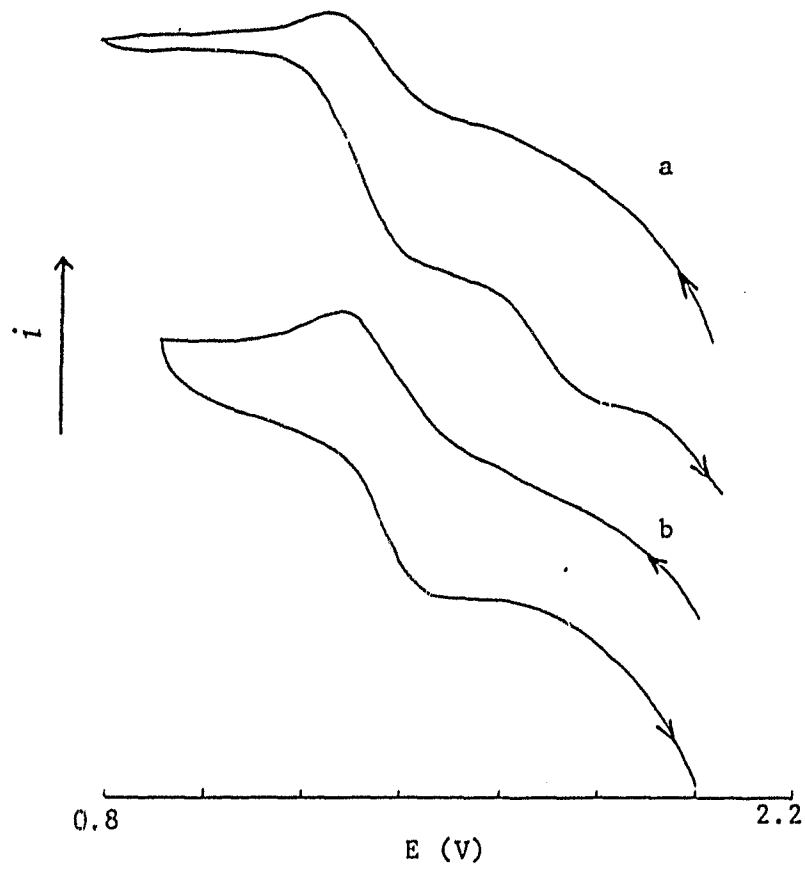

Fig. 5.10 CV of $[Cu(L2)]^{3+/2+}$ in CH_3CN at the scan rate of: a, 200; b, 4000 mV/s.

Unlike Cu(II)(N_4O), the CV of the unsolvated complex Cu(II)(L2) showed a cathodic peak and only one anodic peak (Fig. 5.11). Both cathodic and anodic peaks were relatively insensitive to the scan rate when scanning slowly (reflecting the electrochemically reversible nature of the process at a low scan rate). At 200 mV/s, E_{cp} was -0.96 V, and E_{ap} -0.46 V (Table 5.3). In comparison with the CV of Cu(II)(N_4O), the cathodic peak, E_{cp}, is assigned for the reduction of

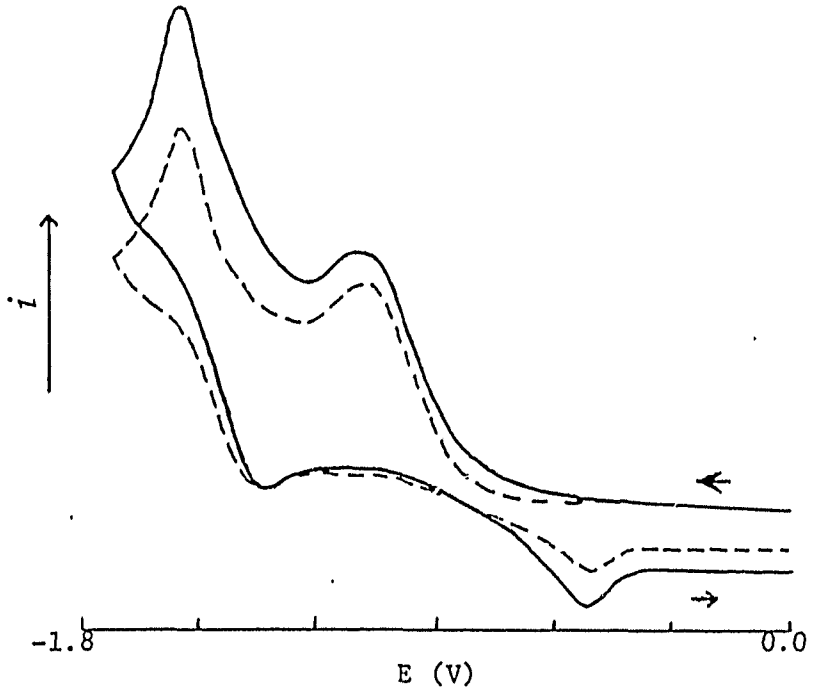

Fig. 5.11 CV of $[Cu(L2)]^{2+/+}$ in CH_3CN at the scan rate of: a, "…" 1000; b, "-" 2000 mV/s.

Cu(II)(L2), and the anodic peak, E_{ap}, for the oxidation of the four-nitrogen-coordinated Cu(I)(L2). That the anodic peak is missing for the oxidation of the penta-coordinated Cu(I)(L2) suggests that the ether oxygen donor detached away from the axial coordination much more rapidly than that in the case of Cu(I)(N_4O) (I).

Molecular modeling shows that the hydrogen atoms on the two side chains of ether ($-CH_2CH_2OCH_2CH_2-$) must, to greater or lesser extent depending on the size of Cu(I) and how high Cu(I) sits above the N_4 plane, overcome the barrier from the bulky electron density cloud of Cu(I) in order for the ether oxygen to turn away from the apical position. For the Cu(I)(L2) complex, the ligand cavity is bigger (one of

nitrogen is of sp^2 hybridization), the electron density cloud of the Cu(I) is smaller (due to the electon-withdrawing group on the ligand) and more coplanar with the N_4 plane (to obtain better d_{Cu}-π_L interaction), compared with that in the case of Cu(I)(N_4O). Therefore, the conversion of penta-coordinated to tetra-coordinated species has lower barrier and is able to proceed faster. At ambient temperature, the conversion proceeds so rapidly that no Cu(I)(L2) can be detected at the scan rates applied. Thermodynamically, the stability of the tetra-coordinated species also depends on the size and the position of Cu(I). When the Cu(I) has a smaller electron density cloud and is closer to the N_4 plane, the repulsion between the hydrogens mentioned above and the Cu(I) is smaller, and hence, the tetra-coordinated species is more stabilized.

The irreversible nature of $Cu^{2+/+}$(L2) couple makes it difficult to esti..ate the $E_{1/2}$ for the reduction. However, it is reasonable to say that the value should be ~ -(0.96-0.028) = -0.93 V, which is higher than that, -1.04 V, for the $Cu^{2+/+}$(N_4O) couple. This increased stability of the Cu(I) centre on going from N_4O to L2 may be attributed mainly to d_{Cu}→π_L interaction between the copper(I) and the electron-withdrawing amidol functional group on the ligand L2. Consistent with this is that the increase, ~ 0.11 V, in $E_{1/2}$ for reduction of the penta-coordinated species is similar to that, ~ 0.12 V, in E_{ap} for oxidation of the tetra-coordinated ones.

5.4.3 Cu(II)(N_4S) and Cu(II)(N_5)

The CV's obtained from oxidation of Cu(II)(N_4S) and Cu(II)(N_5) also showed two anodic peaks, like in the case of N_4O. When the CV's were scanned at a fast speed (>2000 mV/s for $[Cu(II)(N_4S)]^{2+}$, and >200 mV/s for $[Cu(II)(N_5)]^{2+}$, quasi-reversible peaks were identified for both redox couples with $E_{1/2}$ of 1.36 V for $Cu^{3+/2+}(N_4S)$ and $E_{1/2}$ of 1.21 V for $Cu^{3+/2+}(N_5)$ (Table 5.3). In both cases, the unsolvated penta-coordinated complex is the dominant component, and the unidentified species (corresponding to the higher anodic peaks) are the minor components in the solutions.

For the N_4S complex, the oxidation likely took place at the copper centre, instead of the ligand. This is supported by the observation that the $[Co(III)(N_4S)]^{3+}$ shows no oxidation peak in the range from 0.5 to 1.8 V.[166]

The CV's of the reduction of both Cu(II) complexes showed only one reversible couple (ΔE = 60 mV, $i_{cp} = i_{ap}$) for the unsolvated square pyramidal complexes, and no peak (neither cathodic nor anodic) for the solvent-coordinated complex was observed (Fig. 5.8, and 5.12). The $Cu^{2+/+}(N_4S)$ couple has $E_{1/2}$ of -0.85 V, and $E_{1/2}$ for $Cu^{2+/+}(N_5)$ is -1.16 V (Table. 5.3). In both cases, no tetra-coordinated complex was detected. As discussed above, the absence of a tetra-coordinated complex of Cu(I)(N_4S) can be readily understood in terms of "soft base and soft acid". In the case of Cu(I)(N_5), compared with the Cu(I)(N_4O), the Cu(I) sits higher above the N_4 plane (*vide*

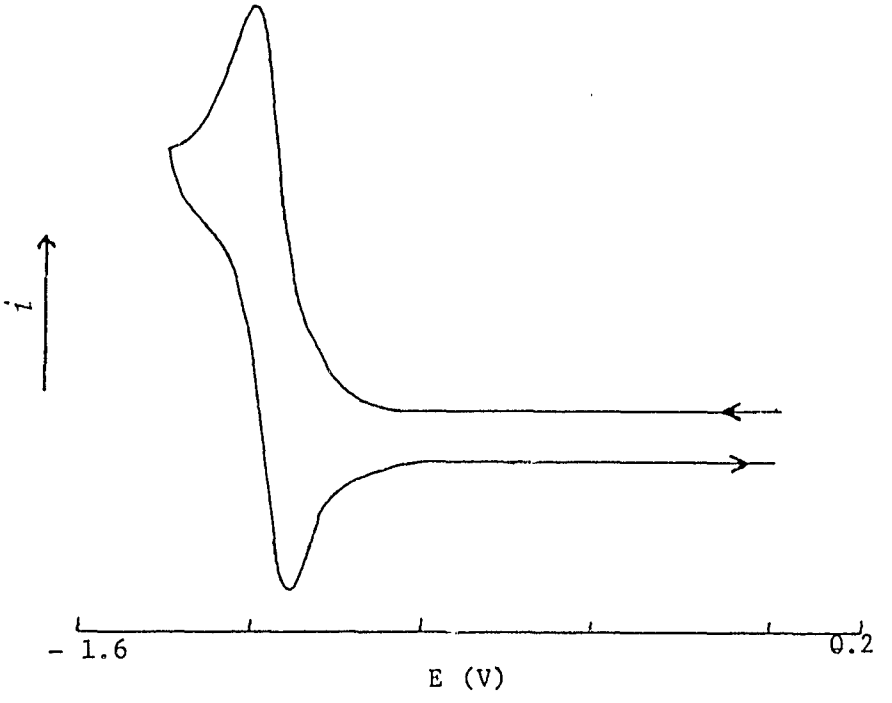

Fig. 5.12 CV of $[Cu(N_5)]^{2+/+}$ in CH_3CN at the scan rate of 50 mV/s.

supra), which leads to increasing both the barrier for the conversion and the instability of the tetra-coordinated species (if it did form), as addressed previously in the case of $[Cu(II)(L2)]^{2+}$. It is possible that the barrier is so high for the conversion of a penta-coordinated to a tetra-coordinated complex that it eventually prevents the axial nitrogen from deflecting. As a result, only a reversible redox of the $Cu^{2+/+}(N_5)$ couple was observed.

5.4.4 Cu(II)cyclam:

For reason of comparison, the redox chemistry of

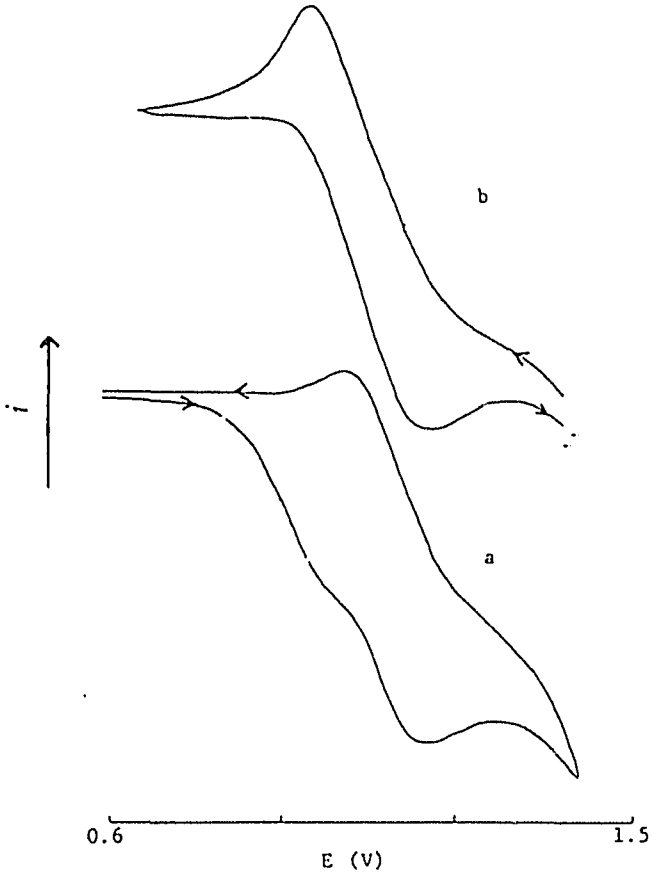

Fig. 5.13 CV of $[Cucyclam]^{3+/2+}$ in CH_3CN at the scan rate of: a, 100; b, 200 mV/s.

$[Cu(II)cyclam]^{2+}$ in CH_3CN was also studied eletrochemically under the same conditions to those above. For $Cu^{3+/2+}$ couple, CV showed reversible characteristics with $E_{1/2}$ of 1.08 V, ΔE = 60 mV, and $i_{cp} = i_{ap}$. There was also evidence for the solvent coordinated species. The CV's obtained by scanning anodically always showed a small shoulder peak at about 0.95 V (Fig. 5.13a). This shoulder peak disappeared when the CV was scanned cathodically (Fig. 5.13b), indicating the solvent may not be

able to remain in the coordination sphere due to stronger tetragonal distortion when the charge of copper centre changed from 2^+ to 3^+.[35,167]

The reduction of [Cu(II)cyclam]$^{2+}$ was an EC process, giving rise to only one cathodic peak. At the scan rate of 200 mV/s, E_{cp} for the reduction is -1.12 V. The instability of Cu(I)cyclam likely results from the small cavity of the ligand, which fits much better for small ion like Cu(III). Without an extra ring to help hold the metal ion in the cage, it is easier for the big Cu(I) ion to dissociate from the cyclam ring. This observation also confirms that the species converted from unsolvated [Cu(I)(N_4O)]$^+$ and [Cu(I)(L2)]$^+$ complexes (*vide supra*) are *not* from solvation.

5.4.5 Axial Donor Effect

Substitution of NH by S raises the oxidation potential by 0.15 V, which is three-fold amount of the difference, 0.05 V, between the $E_{1/2}$'s for $Cu^{3+/2+}$(dioxo[16]aneN$_5$) and (dioxo[16]aneN$_4$S) complexes.[35]

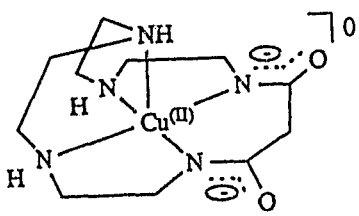

dioxo[16]aneN$_5$

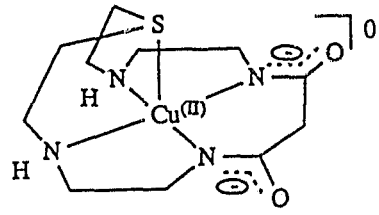

dioxo[16]aneN$_4$S

It appears that the extent to which the oxidation potential of copper is influenced by the axial donor is very much dependent

Table 5.3 Results from Cyclic Voltammetry of Cu(II)(L)[a]

L	Reduction (V)[b]	Oxidation (V)[b]
N_4O[c]	$E_{1/2}$= -1.04[d]; $E_{ap,2}$= 0.58[f]	$E_{1/2}$= 1.30[e]; $E_{ap,2}$= 1.60[f]
L2[c]	$E_{1/2}$= -1.40[e]; E_{cp}= -0.96[f]; E_{ap}= -0.46[f]	$E_{1/2}$= 1.32[e]; $E_{ap,2}$= 1.75[f]
N_4S[g]	$E_{1/2}$= -0.85[d]	$E_{1/2}$= 1.36[e]; $E_{ap,2}$= 1.55[f]
N_5[g]	$E_{1/2}$= -1.16[d]	$E_{1/2}$= 1.21[e]; $E_{ap,2}$= 1.45[f]
cyclam[g]	E_{cp}= -1.12[f]	$E_{ap,1}$= 0.95[f]; $E_{1/2}$= 1.08[d]

[a]in CH_3CN with $Ag/AgNO_3$ (0.01 M) as the reference electrode; [b]potentials refered to $Frc^{+/0}$ at 0.1 V; [c]$(Et)_4N(ClO_4)$ (0.1 M) as surporting electrolyte; [d]reversible process; [e]symmetric quasi-reversible process (α = 0.5); [f]chemically irreversible process, the value obtained under approximantly electrochemically reversible condition at scan rate of 200 mV/s (E_{ap} is not sensitive to the scan rate); [g]$(t\text{-But})_4N(ClO_4)$ (0.1 M) as surporting electrolyte.

on the strength of the tetragonal plane field through the mechanism of tetragonal distortion. The negatively charged N_4 plane in the dioxo complexes is known to have a much stronger in-plane field than the neutral ones in the present complexes, and expected to cause a larger tetragonal distortion.[35,167] This distortion, consequently, reduces the interaction between the axial donor and copper, and hence, the redox reaction at the copper centre is less sensitive to the change at the axial position. It is also possible that the interaction between the axial donor and copper is enforced by the more rigid bicyclic

ligand over the monocyclic ones. The limited data here make it impossible to separate these two effects. However, it is likely that both of them have their roles to play.

As the axial donor is changed from S to O, the oxidation potential at the central Cu(II) decreases by ~ 60 mV, reflecting the preference of the "hard-acid" Cu(III) for the "hard-base" oxygen over the "soft-base" sulfur. Consequently, the oxidation potential increases in the order of N, O and S, which is, qualitatively speaking, similar to that in the Ni(II) analogues in CH_3CN solvent (*vide infra*).

For the reduction of the Cu(II) centre, replacement of N by O increases the potential by 0.12 V, which is comparable with that, 0.16 V, observed for the copper complexes of [15aneN_5] and [15aneN_4O].[155] This is not much different from that, 0.09 V, for $E_{1/2}$'s in the case of oxidation, and consistent with the nature of σ donation of N and O to the copper. This increased stability of Cu(II) towards reduction by a better σ donor such as nitrogen is to be expected,[153,155] and can be understood readily in terms of lowering the effective charge in the Cu(II) centre. In the case of $[Cu(II)(N_4S)]^{2+}$, the reduction potential increases dramatically to -0.85 V, significantly above that for both N_4O and N_5 complexes. This great stabilization of Cu(I) towards oxidation by the S donor should obviously be ascribed to the strong $d_{Cu} \rightarrow d_s$ back-bonding. In general, the strength of this $d_{Cu} \rightarrow d_s$ back-bonding depends, in part, on the effective charge of the

copper. The 3d orbitals of Cu(I) have higher energy, and are able to overlap much better with (hence, give away more electron density to) the 3d orbitals of S than that of Cu(II). Therefore, for the lower charged copper centre, the $d_{Cu} \rightarrow d_s$ back-bonding shows a strong influence on the redox chemistry, but for the highly charged copper centre, the σ donation plays a major role. As a result, the $d_{Cu} \rightarrow d_s$ interaction process stabilizes Cu(I) (by 0.19 V) much more than Cu(II) (by 0.06 V) towards the oxidations, in comparison with that in the case of the O donor (Table 5.3).

The substitution of N by S leads to an anodic shift of 0.31 V in the reduction potential of Cu(I)/(II) couple (Table 5.3). Compared with this, the largest positive shift observed in the reduction potential caused by the similar substitution in the tetragonal plane of the Cu(II) complexes with macrocyclic ligands of [14]ane$S_{(m-n)}N_n$ (m = 4, n = 0, 1, 2, 3) is about 0.24 V.[158] Considering the general recognition that the redox potential of Cu(II) is much more sensitive to the changes in the tetragonal plane than that in the axial positions (especially when the unpaired electron is in the "$d_{x^2-y^2}$" orbital), the result obtained here seems surprising. At first, one may rationalize this in terms of the rigidity of the bicyclic ligand framework, which might force the apical S donor close to copper, and hence, strengthen the interaction. This argument, however, is unlikely to be valid. The crystal structure of Cu(II)(N_4S) shows the Cu-S bond length is

2.549(Å),[129] which is longer than all of the Cu-S bonds (2.2 - 2.4(Å)) observed in the [14]ane$S_{(m-n)}N_n$ system,[158] though the situation may be slightly different in solution. On the contrary, this comparison (in terms of the bond length) makes the result above even more surprising. The better explanation is probably that the $d_{Cu} \rightarrow d_S$ back-bonding operates much more efficiently when the S donor sits in the axial position than in the plane. When it is in the equatorial position, the stabilization of $d_{x^2-y^2}$ electrons in the Cu(I) center by the S donor is achieved mainly by withdrawing the electron density, and hence, increasing the effective charge through $d_{ij(Cu)} \rightarrow d_{ij(S)}$ (i, j = x, y, z; i ≠ j) interactions. However, when the S donor is in the axial site, it has not only similar interactions to the above, but its $3d_{x^2-y^2}$ orbital is able to directly interact with the $d_{x^2-y^2}$ orbital of copper center. It is the latter which lowers the energy of $d_{x^2-y^2}$ electrons in Cu(I) to a much greater extent, and hence, stabilizes the metal center more toward oxidation than that in the equatorial position.

5.4.6 Effect of Tetragonal Plane Field

The tetra-coordinated square planar Cu(II)cyclam has much lower oxidation potential, 1.08 V, than the square pyramidal complexes (Table 5.3). The similar observation has also been made for the nickel analogues (see Chapter 6, *vide infra*). This strong ability of stablizing Cu(III) towards reduction by

cyclam may be attributed to the strong in-plane field generated by the four coplanar nitrogen donors. It has been documented that for a similar increase in the strength of the plane field, the gain in CFSE for Cu(III) is more than that for Cu(II),[167] that is, as the planar field is strengthened, the Cu(III) will be stablized to a greater extent than the Cu(II). Therefore, the oxidation potential for Cu(II) decreases. It has also been well documented that the tetraazamacrocycles tend to take coplanar coordination,[168,169] and the coplanar cyclam is considered to fit best with Cu(II).[29] It appears that for the system studied here, the copper ion is pulled out of the N_4 plane so much that the stabilization energy gained from the axial coordinations by H_2O can not compensate for that lost by weakening the tetragonal plane field caused by displacing the copper from the plane. The differences in tetragonal nitrogens (secondary or tertiary), and conformation of cyclam (*trans* I over *trans* III) may also contribute in stabilizing the Cu(III) centre. But, there is lack of direct evidence supporting this argument. Even if it is true, their contributions are likely to be minor in comparison to that from the change in the tetragonal field.[167]

5.4.7 Correlation with ESR and Electronic Spectra

It is not surprising to see the oxidation potentials of the Cu(II) complexes of N_4X (X = O and N) (Table 5.3)

correlate with both $A_{//}$ or A_o in their esr spectra (Table 5.2) and the "red-shift" in their electronic spectra (Table 5.1), since all of these are, in one way or another, related to the strength of the axial donor. As the oxidation potential increases, the energy of the d-d transition decreases, which is in contrast to that in the case of the square planar copper(II)-peptide complexes where the potential and the energy changed in the same direction.[167] This difference may be qualitatively explained in the following terms. The stronger σ donor is always able to increase the energy of the $d_{x^2-y^2}$ orbital in the copper, from which the electron is lost during the electrochemical process, no matter whether it is at the apical site or in the tetragonal plane, though the mechanism involved may be different (donating electron density for the apical bonding and strengthening the tetragonal plane field for the in-plane coordination[167]). However, as far as the energy gap of the d_{Cu} orbitals is concerned, the strong donor has different effects depending on the position of its coordination. When at the apical site, it increases the energy of the d_{xz} and d_{yz} orbitals much more than that of the $d_{x^2-y^2}$ orbital, and hence, **reduces** the energy of the d-d transitions; when in the tetragonal plane, it promotes, in terms of energy, the $d_{x^2-y^2}$ orbital much more than the d_{xz} and d_{yz} orbitals, and, hence, **increases** the energy of the d-d transitions. As a result, at the axial position, the stronger donor lowers the oxidation potential and causes the "red shift" in the visible

spectrum; in the plane, it also lowers the potential, but leads to the "blue shift" in the spectrum.

For the complexes of N_4O and L2, the correlation between the oxidation potentials and the λ_{max} values of the d-d envelope peak is as expected (Table 5.1, 2 and 3), and can be readily understood in terms of the strength of the in-plane field.[167] The performance of cyclam can also be explained in a similar way.

The correlation between the reduction potentials and $A_{\parallel}$ or λ_{max} for N_4O/L2 pair or N_4O/N_5 pair (Table 5.1, 2 and 3) can all be rationalized on the same basis as discussed above, and is in accord with observations made from the other copper complexes.[153,155]

It is interesting to examine how the sulfur donor affects the central Cu(II) (Table 5.1, 2 and 3). As far as the σ-donation ability is concerned, the sulfur is intermediate of the ether oxygen and the amine nitrogen. On the other hand, the sulfur is also capable of acting as an electron-withdrawing group through the d(Cu)→d(S) interactions. When the sulfur is at the apical position, this d(Cu)→d(S) interaction has its most influence on the d (except d_{z^2}) orbitals of the central copper and the chemical properties associated with these orbitals. Therefore, the redox chemistry (associated mainly with the $d_{x^2-y^2}$ orbital) of the Cu(II) in the N_4S complex has a large influence from the d(Cu)→d(S) interaction; whereas the $A_{\parallel}$, A_o and the d-d envelope peak are

mainly dominated by the σ-donation or combination of the both (which still leads to the domination of σ-donation), and can be readily correlated in terms of the σ-bonding strength.

5.5 Conclusions

In this chapter, spectroscopic and electrochemical properties of series Cu(II) macrobicyclic complexes were described. In general, both the properties at the copper centre are sensitive to the nature of the apical donor, and can be correlated with its σ-bonding strength. As the apical donor changes from O to N, the d-d envelope band manifests a "red-shift", the A_{Cu} values decrease , and the Cu(III) centre becomes more stabilized. The effect of the S donor may be rationalized in terms of both σ donating and d(Cu)→d(S) withdrawing nature of the sulfur.

For N_4X (X = O, S, or N) complexes, the inner-shell reorganization upon reduction at the copper centre was observed only in the case of X = O, where a "square scheme" was obtained. In the case of X = S, or N, the bicyclic ligands appeared rigid enough to hold the Cu(I) centre in square pyramidal coordination (at least in CV time scale), implying that with appropriate donor this type of macrobicyclic ligand is indeed capable of maintaining inner-shell coordination during the process of reduction of the Cu(II) centre, and has a potential application in investigation of electron-transfer reaction of Cu(II)/Cu(I) couple.[162]

The reduction potential of the Cu(II) centre depends on both σ-bonding strength and d_{Cu}-d_{donor} interactions. It appears that the latter is the more dominant factor in the case of the N_4S complex. In addition, it is recognized that the S donor at the axial position is able to stabilize more the central Cu(I) ion towards oxidation than at the equatorial, which is attributed to the direct influence on the reacting electron through the $d_{x^2-y^2}(Cu^I) \rightarrow d_{x^2-y^2}(S)$ interaction in the former case.

Chapter 6. Characterization and Reactivity of Ni(II) and Ni(III) BicycloN_4O Complexes

6.1 Introduction

Although the stabilisation of nickel(III) by tetraazamacrocycles has now been recognised for more than two decades[1,11,33,122,170-175] and the metal-based nature of the unpaired spin confirmed,[176] there have been relatively few kinetic investigations of substitution at this metal centre.[171,173,177] In part, this is the result of the rather unstable higher valence complexes in acidic media. However, when the inner coordination sphere of the nickel is fully ligated, (e.g., in [9]aneN$_3$ complex[101,178]) species of greater kinetic robustness are formed such that they find use as outer-sphere electron transfer reagents.[100] In attempting to overcome the problem of ready self decomposition, we have prepared a series of ligand systems, where by incorporation of derivatives of the nine-membered ring onto the tetraazacyclic ring, a N$_4$X square pyramidal donor set (X = N, S, or O) (for the ligand structures see structure 1 in chapter 5) is formed leaving a single site for substitution in the octahedral ion (see Chapter 4, and ref. 128, 129).

In a previous investigation, Hancock[72] described the interaction of the coordination of an ether oxygen with metal center in the nickel(II) ([9]aneN$_2$O)$_2^{2+}$ ion and concluded that, in the solution, the ether oxygen was coordinated owing to the facial conformation adopted by the ligand. Equilibrium data were consistent with reasonably strong binding. In the present investigation, we present crystallographic evidence for ether

coordination. In some respects, the complex under investigation is similar to that the 5-oxa-12,17-dimethyl-1,9,12,17-tetraazabicyclo[7.5.5]nonadecane ligand[144] where the oxygen donor, being part of a bridging unit between two nitrogens, is held in a suitable axial interaction site. In both systems, the metal centre is encapsulated sufficiently strongly that it is possible to recrystallise the complexes from acidic media without any observable decomposition. The formation of $[Ni(L2)(H_2O)]^{2+}$ is consistent with spectroscopic data for octahedral nickel(II) and with the finding that a perchlorate ion is bound in the solid state. Oxidation to nickel(III) is achieved with use of aquocobalt(III) in aqueous media and by NO^+ in acetonitrile or nitromethane. Under the former conditions, the complexed metal ion is sufficiently stable in acidic solutions that kinetic studies of substitution at the sixth position may be undertaken.

In addition to interest of substitution reactions, these Ni(III) N_4X complexes may also serve as a good model for the kinetic investigation of electron-transfer reactions. By changing X from O to N and then to S, the axial donor becomes softer, and the Ni-X bond length is expected to be less affected by the variation of oxidation-state of the central ion ($Ni^{3+/2+}$), resulting in an increase in the self exchange rate of electron-transfer reaction at the metal centre.[70]

6.2 Molecular Structure

Crystallography

The experimental parameters for the nickel complex are shown in Table 6.1. The unit cell was refined by using 17 pairs of reflections in the 2θ range 16-44°. The intensity measurements were obtained by scanning in the θ/2θ mode using 160 steps of 0.01° in 2θ counting for 0.25s/step. Background counting was introduced for 20s at each end of the scan. A set of three standard reflections preceeded each batch of 50 measurements, with no noticeable change in intensity observed during the collection.

Solution of the phase problem was achieved via application of the direct-methods MULTAN.[179] Subsequent least squares refinements were carried out with the SHELX76 program package.[139] The atomic scattering factors were those included in the SHELX76 program together with the Ni f curve.[140] The program used for absorption correction was a local modification of an existing procedure.[141] Completion and refinement of the structure were carried out by difference electron density maps and least square techniques. All atoms were refined anisotropically. The refinement converged with a maximum shift/esd of 0.057 on the final cycle. The final difference map showed a maximum peak of 0.597 $eÅ^{-3}$.

Results and Discussion

The structure of $[Ni(L2)(ClO_4)]^+$ is shown in Fig. 6.1. The atomic coordinates are provided in Table 6.2. As has been in

Table 6.1 Crystallographic Data

Chemical Formula: $NiC_{14}H_{30}N_4O_9Cl_2$	T = 22 ± 2 °C
Fw: 527.85	λ = 0.710 69 Å
Space group: $P2_1/n$ (No. 14)	ρ_{obs} = 1.612 g cm^{-3}
a = 13.580(6) Å	ρ_{calc} = 1.625 g cm^{-3}
b = 15.400(8) Å	μ = 11.91 cm^{-1}
c = 10.418(4)Å	$R(F_o)$ = 0.0672
α = 90 (2)°	R_w = 0.0672
β = 97.91°	Z = 4
γ = 90°	trans coeff. = 0.824-0.871
V = 2178.0 Å^3	

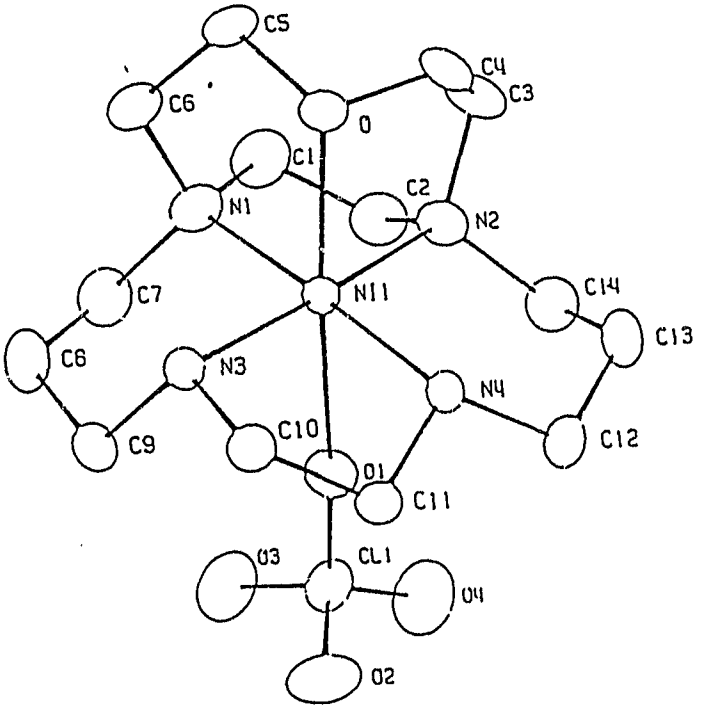

Fig. 6.1 ORTEP drawing of the molecular structure of $[Ni(II)(N_4O)(ClO_4)]^+$

previous studies,[128] the cyclam ring adopts the *trans*-I configuration, adopting the terminology of Bosnich et al.[180] In this conformation, the hydrogen atoms or substituent groups are all located on the same side of the ligand framework. Details of the bond lengths and angles within the inner coordination sphere are presented in Table 6.3. The average Ni-N bond lengths, (2.064(7) Å) are almost identical to those in the corresponding $[Ni(N_4S)(ClO_4)]^+$ ion, 2.070(10) Å, and may represent a compromise between the calculated M-N distance for cyclam in the *trans*-I configuration (2.01 Å)[33,122,181] and the idea Ni(high spin)-N bond length (2.10 Å).[182] Owing to the moderately strong metal to perchlorate interaction, ($Ni-O_1$ = 2.373(7)Å) the geometry at the metal center must be viewed as pseudo-octahedral. The distance to the coordinated perchlorate is considerably smaller than that in the sulfur analogue, (2.563(2) Å) in part because whereas in that system the nickel atom is displaced 0.111 Å towards the apical sulfur, in the present complex the metal centre lies 0.0049 Å below the virtually co-planar nitrogen donor set in the direction of the perchlorate. This is significantly different from the situation predicted by Hancock and co-workers[183] where the nickel is calculated to reside 0.06 Å above the N_4 plane in the *trans*-I configuration of cyclam. The distance between the nickel and the apical ether oxygen is remarkably short (2.109(6)Å) for a ligand framework of this type. In the sulfur analogue, the bond length is 2.385 Å, which is similar to

Table 6.2

Fractional atomic coordinates and temperature parameters.

Atom	x/a	y/b	z/c	Ueq
Ni(1)	56623(7)	25594(6)	22382(10)	340(4)
Cl(1)	84824(18)	28346(17)	25863(24)	608(9)
Cl(2)	28756(19)	48013(14)	19460(25)	564(9)
O	4140(4)	2281(4)	2216(6)	49(2)
O(1)	7423(5)	2653(4)	2546(7)	71(3)
O(2)	8603(7)	3354(6)	1482(8)	106(4)
O(3)	8791(6)	3342(6)	3699(8)	107(4)
O(4)	9010(7)	2063(6)	2578(9)	116(4)
O(5)	2340(5)	5398(4)	1082(7)	78(3)
O(6)	3242(5)	4115(5)	1250(8)	86(3)
O(7)	3737(7)	5220(6)	2590(9)	118(4)
O(8)	2280(9)	4522(7)	2789(12)	175(7)
N(1)	5552(6)	2835(6)	4149(8)	63(3)
N(2)	5828(5)	1273(5)	2826(8)	52(3)
N(3)	5483(5)	3847(4)	1719(7)	43(3)
N(4)	5761(5)	2342(4)	312(6)	38(2)
C(1)	5767(9)	2005(8)	4945(10)	78(5)
C(2)	6318(8)	1347(7)	4176(10)	68(4)
C(3)	4833(7)	835(6)	2787(11)	64(4)
C(4)	4024(7)	1362(6)	1871(10)	57(4)
C(5)	3762(7)	2495(7)	3437(10)	64(4)
C(6)	4500(7)	3131(7)	4169(10)	66(4)
C(7)	6273(8)	3541(8)	4654(10)	79(5)

Table 6.2 (continued)

C(8)	6117(8)	4422(7)	3900(12)	79(5)
C(9)	6242(7)	4420(6)	2449(11)	63(4)
C(10)	5488(7)	3890(5)	264(9)	51(3)
C(11)	6121(7)	3171(5)	-200(9)	48(3)
C(12)	6401(7)	1614(6)	-55(10)	60(4)
C(13)	6175(8)	772(6)	628(12)	70(4)
C(14)	6503(8)	748(6)	2067(12)	71(5)

Estimated standard deviations are given in parentheses.

Coordinates x 10^n where n = 5,5,4,4,4 for Ni, Cl, O, N, C

Temperature parameters x 10^n where n = 4,4,3,3,3 for Ni, Cl, O, N, C

Table 6.3 (a)

Bond Angles(°)

Atoms			Angle	Atoms			Angle
O(1)	-Ni(1)	-O	169.2(2)	N(3)	-Ni(1)	-O(1)	93.3(3)
N(1)	-Ni(1)	-O	81.4(3)	N(3)	-Ni(1)	-N(1)	92.0(3)
N(1)	-Ni(1)	-O(1)	93.6(3)	N(3)	-Ni(1)	-N(2)	178.0(3)
N(2)	-Ni(1)	-O	82.9(2)	N(4)	-Ni(1)	-O	98.7(2)
N(2)	-Ni(1)	-O(1)	87.2(3)	N(4)	-Ni(1)	-O(1)	86.7(3)
N(2)	-Ni(1)	-N(1)	86.0(3)	N(4)	-Ni(1)	-N(1)	177.4(3)
N(3)	-Ni(1)	-O	96.4(2)	N(4)	-Ni(1)	-N(2)	96.5(3)
				N(4)	-Ni(1)	-N(3)	85.5(3)

(b)

Interatomic Distances(Å)

Atoms		Distance	Atoms		Distance
O	-Ni(1)	2.109(6)	N(2)	-Ni(1)	2.077(7)
O(1)	-Ni(1)	2.373(7)	N(3)	-Ni(1)	2.061(6)
N(1)	-Ni(1)	2.061(8)	N(4)	-Ni(1)	2.057(7)

Estimated standard deviations are given in parentheses

those in less strained homoleptic thioether complexes $[Ni([9]aneS_3)_2]^{2+}$, 2.386 Å[184] and $[Ni([18]aneS_6)]^{2+}$, 2.388 Å[185] respectively. Unfortunately there are very few systems with which comparison can be made. In the open chain precursor complex prepared prior to the ring closure the ether oxygen is *trans* to a primary nitrogen, the Ni-O bond length is 2.19(1) Å.[136] In the *trans*-Ni(cyclam)$(NO_3)_2$ complex, where the macrocycle is in the *trans*-III configuration, the Ni-O distance is 2.169 Å.[183] In the corresponding $[Cu(II)(N_4O)]^{2+}$ macrobicyclic complex, which has the *trans*-I configuration but is five coordinate, the Cu-O distance is 2.259 Å, although in this ion the copper is located 0.21 Å above the N_4 plane. In this case the angle between the Cu-O(ap) vector and the normal to the N_4 plane is 15.2°, reflecting the inability of the nonane ring to reach over fully and encapsulate the axial site. In the present complex, this "tugging" angle is reduced considerably to 10.8°, owing to the better emplacement of the metal center within the N_4 plane. The structure is somewhat closer to octahedral although the $O-Ni-O_1$ angle at 169.2(2)° is the result of the tugging of the nine-membered ring. Unfortunately the hydrogen atoms associated with the secondary nitrogens were not located in the structure. Such data would have provided information in any possible hydrogen bonding between these atoms and the ether oxygen.

6.3 ESR Spectra

The nickel(III) complexes are esr active, yielding spectra characteristic of a low spin d^7 ion in a distorted octahedral environment of axial symmetry.[171,176,177] Oxidation of the nickel(II) complex in acidic perchlorate media by use of $Co(III)_{aq}$ yields a species with $g_{/}$ = 2.028 and $g_{\perp}$ = 2.200 features (Fig. 6.2a) where there is no evidence of any shf-coupling as expected owing to the presence of only oxygen donors (one from ligand, one from coordinated perchlorate or water, *vide infra*) at the axial sites. These data may be compared to those from the *trans*-III $[Ni(III)cyclam]^{3+}$ [171] ($g_{/}$ = 2.033 and $g_{\perp}$ = 2.219) respectively. A detectable shift is observed in the perpendicular feature. Upon the addition of chloride ion, the spectrum observed is consistent with only a single halide coordinated in the axial site ($g_{/}$ = 2.033 and $g_{\perp}$ = 2.189, $A_{\perp}$ = 29 G) (Fig. 6.2b). The formation of a mono-fluoro-complex ion is confirmed (Fig. 6.2c) in aqueous solution with, in this instance, evidence for splitting of both the perpendicular and parallel signals, $g_{/}$ = 2.027, $A_{/}$ = 212 G, $g_{\perp}$ = 2.189, $A_{\perp}$ = 71 G. These values are similar to those derived previously for other macrocyclic complexes.[171,128] Despite attempts at forcing a second axial ion into the primary coordination sphere of the nickel, there was no evidence for displacement of the ether oxygen. In the reaction with thiocyanate, although the overall process involves a redox reaction, the kinetic data for an inner sphere

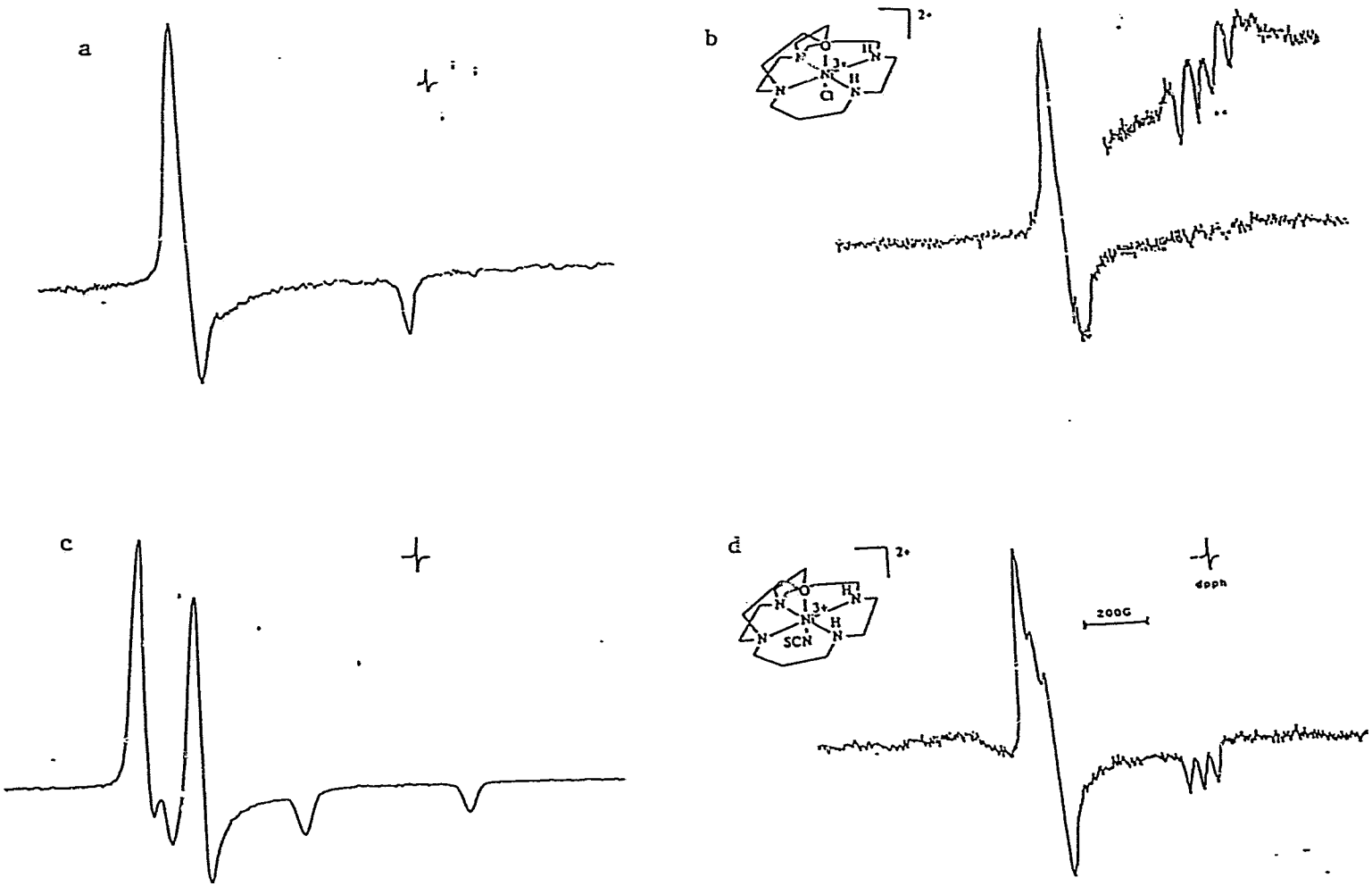

Fig. 6.2 ESR Spectra of $[Ni(N_4O)]^{3+}$ in Aqueous Media (77 K). (a) ClO_4^- ; (b) Cl^- ; (c) F^- ; (d) SCN^-.

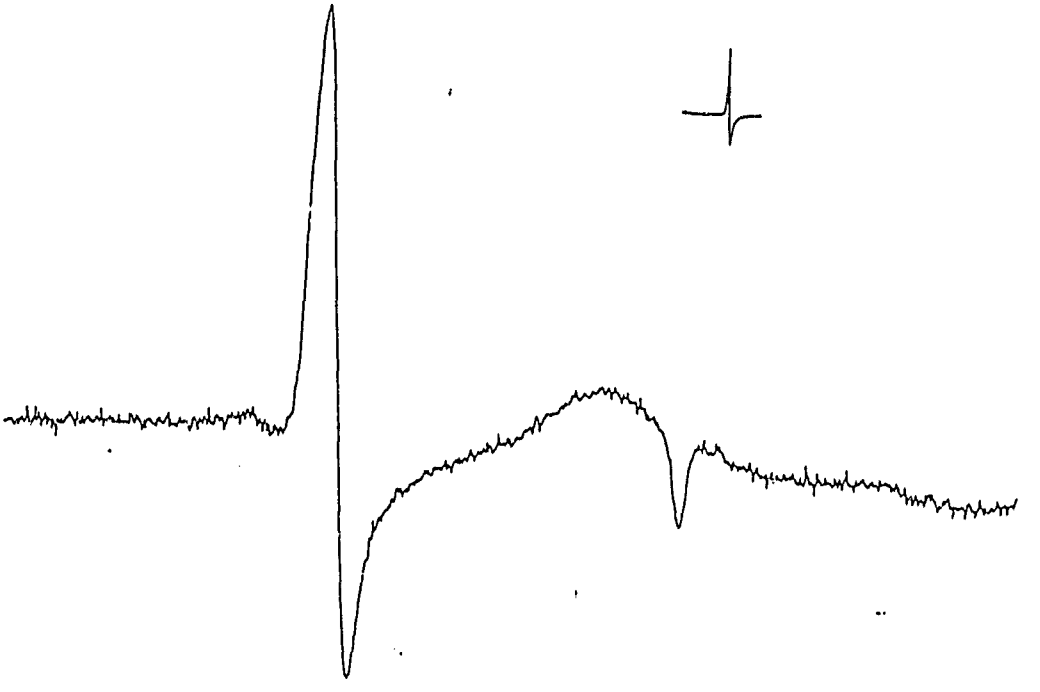

Fig. 6.3 ESR spectrum of $[Ni(III)([9]aneN_3)_2]^{3+}$ in 0.5 M NaF aqueous medium (frozen, 77 K).

intermediate complex (*vide infra*) are reinforced by the observation from the esr spectra of a N-bonded axially coordinated intermediate (Fig. 6.2d). The spectrum for this complex is consistent with delocalisation of the unpaired electron, since both the $g_{/} = 2.029$ and $g_{\perp} = 2.181$ shown shf-coupling, $A_{/} = 23$ G, and $A_{\perp} = 24$ G. The latter feature is comparatively rare and is found where there is unsaturation at the nitrogen center. In this regard, the spectrum is similar to that obtained for the [*bis*-thiocyanatonickel(III)]$^{+}$ ion, $g_{/} = 2.048$, $g_{\perp} = 2.208$, $A_{/} = 26$ G(q), $A_{\perp} = 21$ G(q).[171,178]

In order to examine the strength of binding of the ether

oxygens, esr experiments were carried out using the nickel(III) ion prepared from the nickel(II) species with $[Ni([9]aneN_2O)_2]^{2+}$ where the geometry of the ligand is such that the O-donors are in the *trans* (axial) positions. Oxidation of the complex, either by $NOBF_4$ in CH_3CN in the presence of excess F^- (Fig. 6.3) or by Co_{aq}^{3+} in 0.5 M NaF yield identical spectra, with no evidence for any ligation of the fluoride. This is consistent with maintenance of coordination of the ether in the inner coordination sphere of the oxidized ion. This result has implications in the interpretation of the hydrogen ion dependences observed in the substitution reactions (*vide infra*).

6.4 Electrochemistry:

In Aqueous Media

Cyclic voltammetry of the $[Ni(N_4O)(H_2O)]^{2+}$ ion in 1.0 M $HClO_4$ displayed a reversible wave, independent of scan rate, which, when corrected for the Ag/AgCl reference electrode gave a potential at 1.17 V *vs* NHE. This is remarkably higher than that for the $[Ni(cyclam)]^{3+/2+}$ couple (0.97 V)[170,177] and may reflect either strain in the oxidant or a greater thermodynamic stability of the nickel(II) ion. There is confirmation of the complex formation with other anions from the shifts in potential in solutions 1.0 M in the ligating ion. In all cases, good reversibility was observed with peak separations of the order 60-80 mV. When corrected for the

reference, the redox potentials are (vs NHE) NO_3^- 1.13 V, Cl^- 1.01 V, and SO_4^{2-} 1.04 V, respectively.

Table 6.4 Oxidation Potentials of $[Ni(N_4X)]^{2+}$ in Aqueous Media ----- from Cyclic Voltammetric Study

1.0 M of NaL (*vs* NHE)

$E_{1/2}$(V) X = / L =	O	S[a]	N[b]
NO_3^-	1.12	1.06	1.00
Cl^-	1.01	1.01	0.98

[a]0.67 V *vs.* SCE in 0.5 M $NaSO_4$ (ref. 137); [b]0.63 V *vs.* SCE in 0.5 M $NaSO_4$ (ref. 137).

***Trans*-Influence**

It is interesting to compare the present N_4O system with its N_5 and N_4S analogues. As shown in Table 6.4, in 1.0 M NO_3^- the oxidation potential decreases as apical donor changes from O to S and to N, which is consistent with σ-donating ability of these donors and similar to that in the case of the Cu(II) analogues (section 5.4). While the similar trend also exists in 1.0 M Cl^- media, the amount of decrease in the oxidation potential by replacing the ligating anion nitrate with chloride is also reduced in the order of 0.11, 0.05 to 0.02 V. This phenomenon may be best interpreted in terms of *trans*-influence. That is, as the $M-X_{ap}$ bond strength increases from

X = O, S to N, the bond *trans* to X is weakened. This *trans*-influence is also helpful in understanding much more rapid substitution reaction in N_5 and N_4S complexes than that in N_4O case (*vide infra*).

In CH_3CN Solvent

Electrochemical properties of the $[Ni(N_4O)]^{3+}$ ion were also investigated in acetonitrile media (in 0.1 M Et_4NClO_4) with reference electrode $Ag/AgNO_3$ (0.01 M) (and external reference $Frc^{+/0}$). The potential used below are all *vs.* $Frc^{+/0}$ = 0.0 V, unless specified otherwise.

Oxidation of the Ni(II) complex was both chemically and electrochemically reversible, having $E_{1/2}$ of 0.76 V with $\Delta V \approx$ 60 mV and i_{pa}/i_{pc} = 1. This oxidation potential is ~ 0.01 V *lower* than that of N_4S analogue (Table 6.5), which is somewhat surprising considering the reversed difference in aqueous media. The reason for this is not clearly understood, probably having to do with solvation effects.

Reduction of the Ni(II) complex was a EC process. At low scan rates ($\leq$ 100 mV/s), it was electrochemically reversible but chemically irreversible with a cathodic peak at ~ -1.84 V and an anodic peak at ~ -1.48 V, both of which were not sensitive to the scan rates, Fig. 6.4. When the scan rate was higher ($\geq$ 200 mV/s), the two peaks started to shift, indicating an electrochemically irreversible nature. Comparing these with the results from the Cu(II) analogue, it is likely that the ether oxygen donor was removed from the inner

coordination sphere upon formation of the Ni(I), which coordinated with the remaining four nitrogens in a distorted square planar geometry due to both the Jahn-Teller effect and the weak interaction between "hard-acid" (O) and "soft-base" (Ni^{I}) (see the "square scheme" in scheme 5.3.1).

Considering the electrochemically reversible nature of the species at low scan rate, the reduction potential of $[Ni^{II}(N_4O)]^{2+}$ may be estimated as (-1.84) + 0.029 = -1.81 (V), and oxidation potential of the square planar species as (-1.48) - 0.029 = -1.51 (V). Thus, the difference between oxidation and reduction potentials of $[Ni^{II}(N_4O)]^{2+}$ is ~ 2.57 V, which is greater than that generally observed in NiN_4 macrocyclic complexes[186] and also that in N_4S analogue,[129] 2.46 V, reflecting somewhat a stabilization of the Ni(II) state in the present bicyclic ligand system. This stabilization is probably derived from a relatively lower reduction potential (noting that in N_4S analogue is -1.68 V), owing to the factors such as the *trans*-I configuration of the cyclam moiety[183] and the "hard-acid" nature of the apical ether oxygen).

6.5 Kinetic Investigations

6.5.1 Subsitution Reactions

The nickel(II) $(N_4O)^{2+}$ perchlorate salt in water yields a solution of considerable stability with spectroscopic charateristics of an octahedral ion, $\varepsilon_{222} = 2.42 \times 10^3$, $\varepsilon_{337} = 17$, $\varepsilon_{515} = 10$, and $\varepsilon_{681} = 5\ M^{-1}cm^{-1}$. Some decomposition is observed in

strongly acidic (4 M) media. However, this was sufficiently slow as not to impede any kinetic investigations. Titration with Co_{aq}^{3+} in 2.0 M $HClO_4$ provided absorbance changes consistent with a one-electron oxidation to a nickel(III) ion, (isosbestic point at 222 nm) with the final product ε_{326} = (6.6 ± 0.2)x10^3, ε_{374}(sh) = (5.3 ± 0.3)x10^3, and ε_{634} = 37 ± 2 $M^{-1}s^{-1}$ respectively. The extinction coefficients were obtained by extrapolation to zero time of kinetic plots since some decomposition of the nickel(III) ion was observed over the time required for the spectrophotometric titration.

The kinetic stability of the Ni(III) was monitored as a function of hydrogen ion concentration. As is shown in Table 6.5, the decomposition rate is independent of $[H^+]$ over the range 0.1 - 1.0 M, the half life of the species being of the order of 50 minutes. In this regard, the complex ion differs in behavior from [Ni(III)cyclam]$^{3+}$ where an increasing decomposition rate is observed with increasing pH.

Table 6.5

Rate data for decomposition of $[Ni(N_4O)(H_2O)]^{3+}$ in acidic media: T = 25°C, I = 1.0M, ($H^+/Li^+, ClO_4^-$)

$[H^+]$/M	0.10	0.40	0.60	0.80	1.0
$10^4 k_{obs}/s^{-1}$	2.07	2.12	2.51	2.15	2.11

mean (2.19±0.13)x$10^{-4}s^{-1}$

Results

i) Reaction with Cl^-

Kinetic study of substitution reaction of Ni(III) complex ion with Cl^- was carried out in various supporting electrolytes, namely H/$LiClO_4$, H/$NaNO_3$ and H/Li triflate at 10.0 ± 0.2 °C. Chloro complex formation was confirmed in separate experiments where mixing the metal ion complex with Cl^- showed an increased absorbance at 313 nm, a decrease in the 385 nm and an isosbestic point at 452 nm. In all the experiments, Cl^- concentrations were ≥ 100 fold of [Ni(III)] so that a pseudo-first order reaction condition was achieved. The Ni(III) ion was prepared immediately prior to the experiment by oxidizing corresponding Ni(II) species with a deficiency of Co_{aq}^{3+}.

Under constant ionic strength of I = 1.0 M, the observed reaction constant, k_{obs}, was dependent of proton and Cl^- concentrations. The nature of supporting electrolyte also has significant influence on the kinetics. The experimental data are provided in Table 6.6.I, and shown in Fig. 6.4. In general, k_{obs} has an empirical form

$$k_{obs} = k_i + k_{ii}/[H^+] + (k_{iii} + k_{iv}/[H^+])[Cl^-] \qquad (6.1)$$

The values for the four constants, k_n (n = i - iv), in different media were presented in Table 6.7 (the units are omitted).

Table 6.6 Kinetic Results from the Substitution Reactions

$T = 9.0 \pm 0.2°C$; $I = 1.0$ M; $\lambda = 400$ nm.

I. Cl^- Substitution in Common Supporting Electrolyte:

(a) in $H/LiClO_4$

i, $[H^+] = 0.2$ M

$[Cl^-]$ ($x10^3$/M)	5	10	20	30	40
k_{obs} (s^{-1})	6.08(6)	7.48(4)	10.5(4)	13.6(1)	16.5(4)

ii, $[H^+] = 0.25$ M

$[Cl^-]$ ($x10^3$/M)	4	10	20	30
k_{obs} (s^{-1})	5.04(24)	6.85(7)	10.2(4)	13.0(6)

iii, $[H^+] = 0.6$ M

$[Cl^-]$ ($x10^3$/M)	4	8	12	16	32	60
k_{obs} (s^{-1})	3.9(2)	5.4(1)	6.5(4)	7.5(6)	11.7(3)	19.2(5)

iv, $[H^+] = 1.0$ M

$[Cl^-]$ ($x10^3$/M)	4	10	20	30	50
k_{obs} (s^{-1})	3.7(2)	5.1(1)	8.06(9)	11.0(1)	16.1(3)

$$k_{obs} = 2.23 + 0.442/[H^+] + (260 + 9.43/[H^+])[Cl^-]$$

(b) in H/Li Triflate

i, $[H^+] = 0.2$ M

$[Cl^-]$ ($x10^3$/M)	2	6	10	15
k_{obs} (s^{-1})	6.07(36)	9.95(21)	12.80(36)	18.49(34)

ii, $[H^+]$ = 0.25 M

$[Cl^-]$ ($x10^3$/M)	2	6	10	15
k_{obs} (s^{-1})	5.68(36)	8.40(15)	12.10(23)	16.18(36)

iii, $[H^+]$ = 0.6 M

$[Cl^-]$ ($x10^3$/M)	2	8	15
k_{obs} (s^{-1})	4.77(30)	8.48(25)	12.28(36)

iv, $[H^+]$ = 1.0 M

$[Cl^-]$ ($x10^3$/M)	3	6	10	20	40
k_{obs} (s^{-1})	5.2(2)	6.7(2)	8.7(1)	13.8(2)	24.1(4)

$k_{obs} = 3.35 + 0.1411/[H^+] + (418 \pm 102.2/[H^+])[Cl^-]$

(c) in $H/NaNO_3$

i, $[H^+]$ = 0.2 M

$[Cl^-]$ ($x10^3$/M)	1.5	3	6	10
k_{obs} (s^{-1})	5.86(5)	7.83(51)	9.72(49)	11.88(97)

ii, $[H^+]$ = 0.25 M

$[Cl^-]$ ($x10^3$/M)	1.5	3	6	10
k_{obs} (s^{-1})	6.60(62)	6.51(71)	8.44(60)	10.09(40)

iii, $[H^+]$ = 0.6 M

$[Cl^-]$ ($x10^3$/M)	1.5	3	6	10
k_{obs} (s^{-1})	5.61(43)	5.95(18)	7.05(11)	8.70(21)

iv, $[H^+]$ = 1.0 M

$[Cl^-]$ ($x10^3$/M)	1.5	3	6	10
k_{obs} (s^{-1})	4.64(20)	5.29(37)	6.00(22)	7.32(3)

$k_{obs} = 3.98 + 0.282/[H^+] + (217 + 84.7/[H^+])[Cl^-]$

II Cl^- Substitution in Mixed Supporting Electrolytes:

in $HClO_4$/Triflic acid (HT); I_{total} = 1.0 M; $[H^+]$ = 1.0 M.

i, [HT] = 0.0 M

$[Cl^-]$ ($x10^3$/M)	4	10	20	30	50
k_{obs} (s^{-1})	3.7(2)	5.1(1)	8.1(1)	11.0(1)	16.1(3)

ii, [HT] = 0.3 M

$[Cl^-]$ ($x10^3$/M)	5	10	15	20
k_{obs} (s^{-1})	4.63(14)	6.14(15)	7.46(18)	9.18(15)

iii, [HT] = 0.65 M

$[Cl^-]$ ($x10^3$/M)	6	12	18
k_{obs} (s^{-1})	5.83(11)	8.73(30)	10.50(4)

iv, [HT] = 1.0 M

$[Cl^-]$ ($x10^3$/M)	3	6	10	20	40
k_{obs} (s^{-1})	5.1(2)	6.7(2)	8.7(1)	13.8(3)	24.1(2)

$k_{obs} = 2.73 + 1.02/[HT] + (250 + 244/[HT])[Cl^-]$

III Cl^- Substitution in Different Ionic Strength:

in $H/LiClO_4$

(a) I = 1.5 M

i. $[H^+]$ = 0.2 M.

$[Cl^-]$ ($x10^3$/M)	2	5	10	20
k_{obs} (s^{-1})	4.00(28)	4.30(13)	5.14(7)	7.26(8)

ii, $[H^+]$ = 0.25 M

$[Cl^-]$ ($x10^3$/M)	2	5	10	20
k_{obs} (s^{-1})	3.52(10)	4.17(12)	5.10(13)	6.88(4)

iii, $[H^+]$ = 0.6 M

$[Cl^-]$ ($x10^3$/M)	5	10	20
k_{obs} (s^{-1})	3.44(15)	4.36(2)	5.99(18)

iv, $[H^+]$ = 1.0 M

$[Cl^-]$ ($x10^3$/M)	2	5	10	20
k_{obs} (s^{-1})	2.82(44)	3.38(18)	3.85(19)	5.30(27)

$k_{obs} = 2.32 + 0.225/[H^+] + (136 + 11.0/[H^+])[Cl^-]$

(b) I = 2.0 M

i. $[H^+]$ = 0.2 M.

$[Cl^-]$ ($x10^3$/M)	2	5	10	20
k_{obs} (s^{-1})	2.7	3.00	3.88	5.47

ii, $[H^+]$ = 0.25 M

$[Cl^-]$ ($x10^3$/M)	2	5	10	20
k_{obs} (s^{-1})	2.77	3.43	3.79	5.25

iii, $[H^+]$ = 0.6 M

$[Cl^-]$ ($x10^3$/M)	2	5	10	20
k_{obs} (s^{-1})	2.07	2.43	3.02	4.37

iv, $[H^+]$ = 1.0 M

$[Cl^-]$ ($x10^3$/M)	2	5	10	20
k_{obs} (s^{-1})	2.02	2.06	2.65	3.76

$k_{obs} = 1.53 + 0.156/[H^+] + (98.4 + 10.8/[H^+])[Cl^-]$

IV. SCN^- Substitution:

in $H/LiClO_4$; I =1.0 M;

(a) $[H^+]$ = 1.0 M

$[SCN^-]$ ($x10^3$/M)	2	4	6	10
k_{obs} (s^{-1})	4.6(1.3)	6.5(4)	8.4(6)	12.3(6)

(b) $[SCN^-] = 4.0x10^{-3}$ M

$[H^+]$ (M)	1	0.6	0.4	0.3	0.2
k_{obs} (s^{-1})	6.5(4)	6.6(2)	7.1(3)	7.6(2)	8.2(1)

$k_{obs} = 2.14 + 0.450/[H^+] + 968[SCN^-]$

$$\text{rate} = 2.23 + 0.442[H^+]^{-1} + (260.2 + 9.43[H^+]^{-1})[Cl]$$

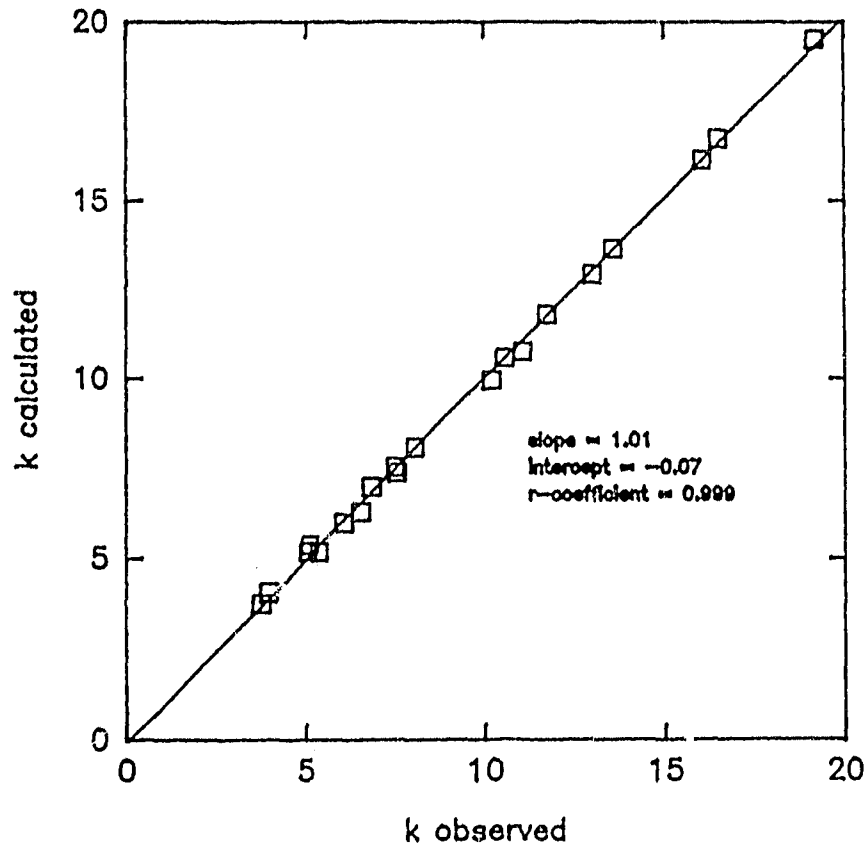

Fig. 6.4 (a) Correlation of k_{obs}(calc.) with k_{obs}(exp.) for the results from 1.0 M H/$LiClO_4$ solution.

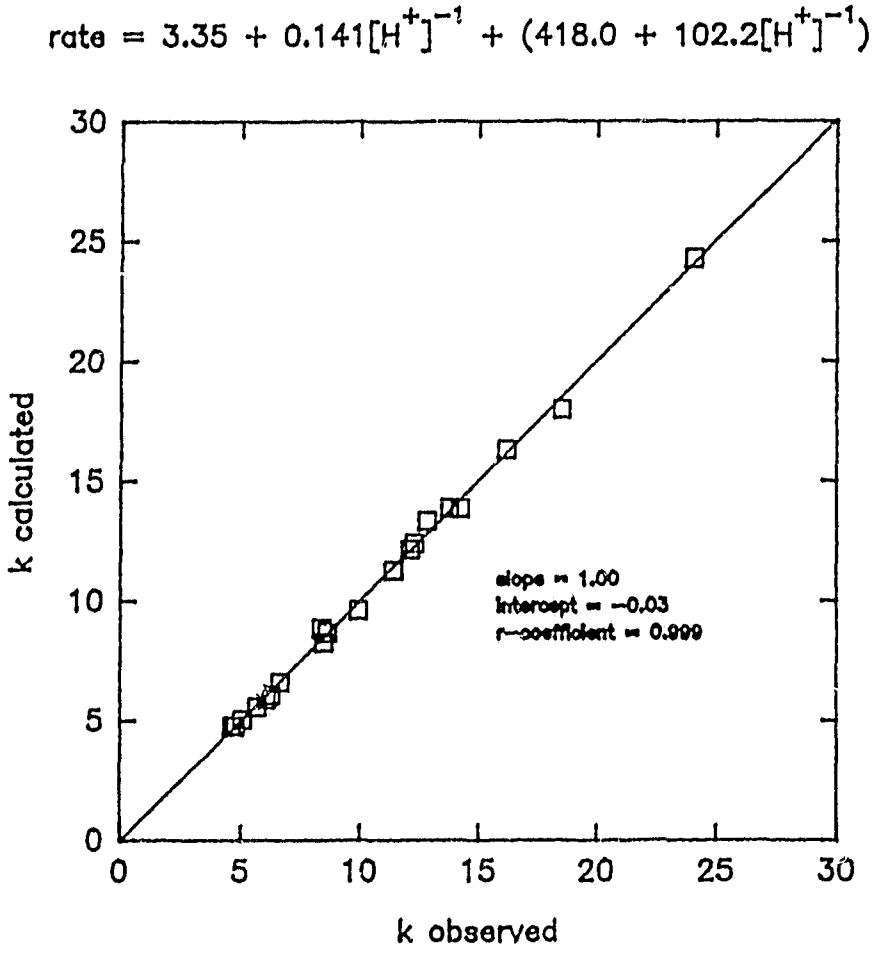

Fig. 6.4(b) Correlation between k_{obs}(calc.) with k_{obs}(exp.) for the results from 1.0 M H/Li triflate solution.

Fig. 6.5

Dependence of observed rate constants on media for a perchloric acid / triflic acid mixture (note: $[H^+] = 1.0$ M)

rate = 2.73 + 1.02[triflate] + (249.6 + 243.6[triflate])[Cl]

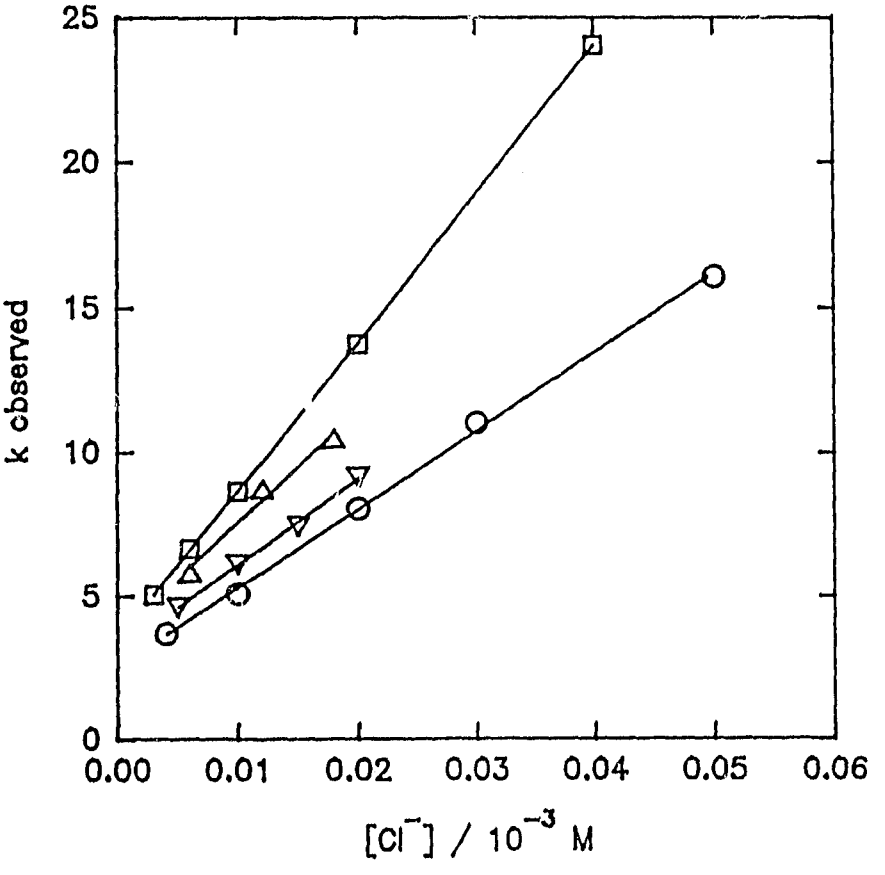

$$k_{obs} = 2.32 + 0.225[H^+]^{-1} + (136.3 + 11.00[H^+]^{-1})[Cl^-]$$

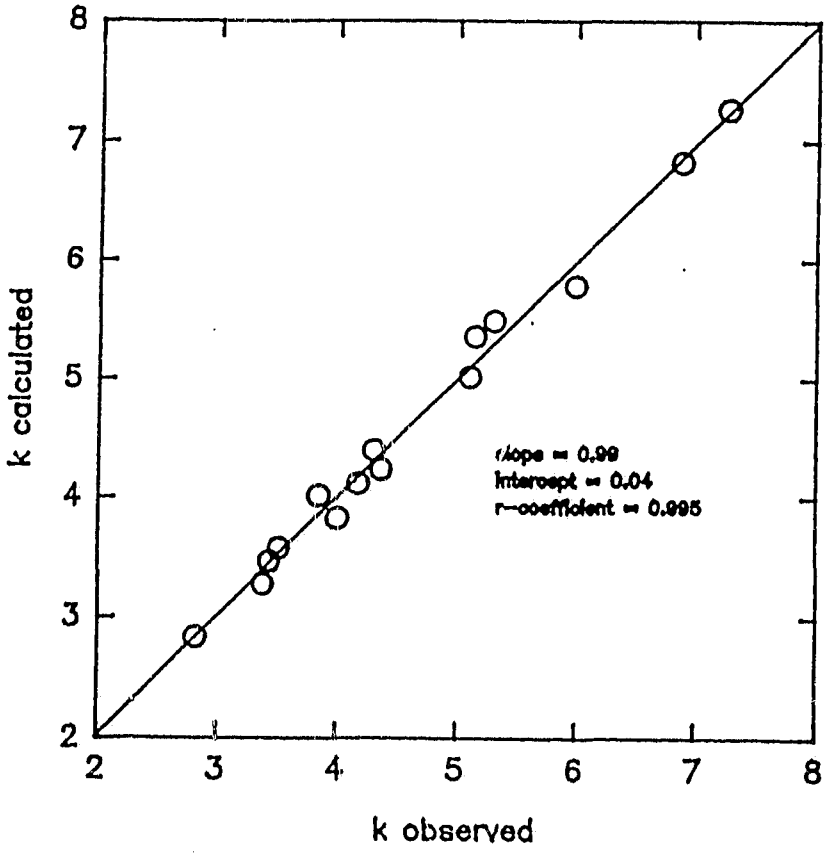

Fig. 6.6 (a) Correlation of k_{obs}(calc.) with k_{obs}(exp.) for the results from 1.5 M H/$LiClO_4$ solution.

$$\text{rate} = 1.526 + 0.156[H^+]^{-1} + (98.39 + 10.75[H^+]^{-1})[Cl^-]$$

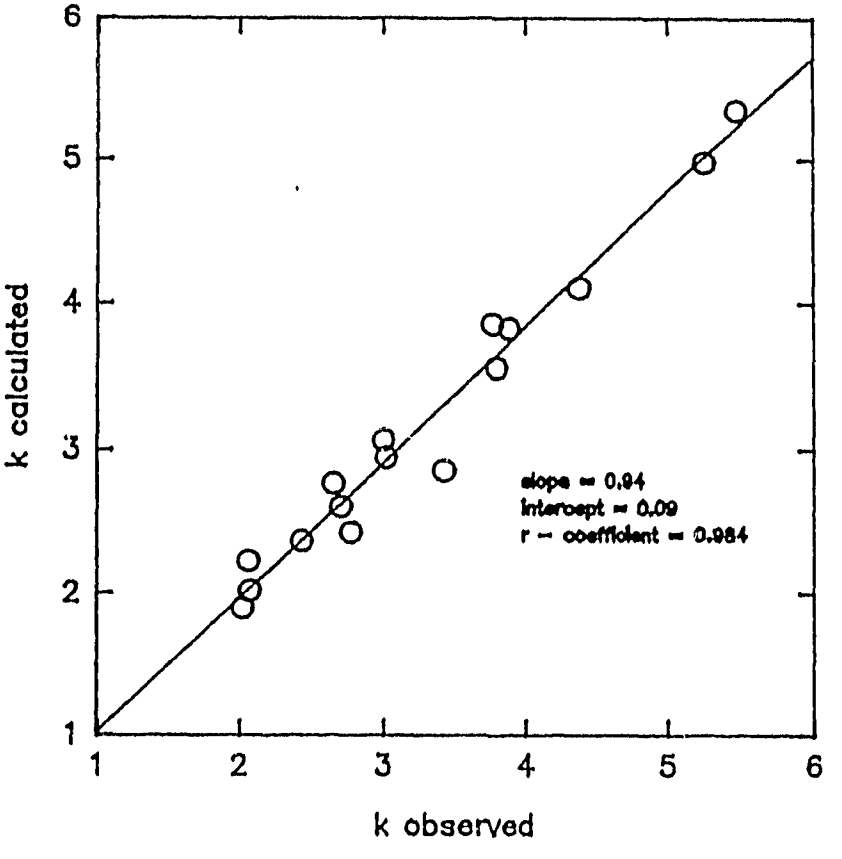

Fig. 6.6 (B) Correlation of k_{obs}(calc.) with k_{obs}(exp.) for the results from 2.0 M H/$LiClO_4$.

Table 6.7 Rate Constants in Different Media

	k_i	k_{ii}	k_{iii}	k_{iv}
Perchlorate	2.23	0.442	260	9.43
Nitrate	3.98	0.282	217	84.7
Triflate	3.35	0.141	418	102

With maintaining the ionic strength of 1.0 M, the

substitution reaction was also investigated using mixture of perchloric and triflic acids ($[H^+]_{total}$ = 1.0 M), and the results are listed in Table 6.6.II, and shown in Fig. 6.5. The observed rate constant, k_{obs}, from this experiment may be expressed as (in a form of the triflate concentration dependence)

$$k_{obs} = 2.73 + 1.02[HT] + (250 + 244[HT])[Cl^-] \qquad (6.2)$$

where HT stands for triflic acid.

The effect of a concentration change of the supporting electrolyte, X, on the four rate constants in eq.(6.1) was also investigated with X = perchlorate, and the data are presented in Table 6.6.II, and are shown in Fig. 6.6. Dependences of k_n (n = i - iv) on [X] are demonstrated in Table 6.8.

Table 6.8 Rate Constants in Different [X] from Perchlorate Media

	k_i	k_{ii}	k_{iii}	k_{iv}
1.0 M	2.23	0.442	260	9.43
1.5 M	2.32	0.225	130	11.0
2.0 M	1.53	0.156	98.4	10.8

ii) Reaction with SCN^-

Reaction conditions were employed similar to those described above (X = perchlorate, I = 1.0 M). Sufficient

aquocobalt(III) was added to a solution of the nickel(II) to provide approximately 90% of the metal ion in the higher oxidation state and an excess of the ligand was reacted in the stopped-flow spectrometer. The reaction was observed to be biphasic, with the formation of an intermediate followed by a redox process. As in the case of Cl^- system, k_{obs} has a expression

$$k_{obs} = k_i + k_{ii}/[H^+] + k_{iii}[SCN^-] \qquad (6.3)$$

where (the units are omitted for the sake of simplicity) k_i = 2.14, k_{ii} = 0.45, and k_{iii} = 968. The absence of k_{iv} term (corresponding to that in eq. (6.1)) is due to insufficient experimental data (Table 6.6.IV, and Fig. 6.7).

The subsequent redox reaction was significantly slower and could be studied independently at higher temperatures. The reduction of the thiocyanato complex was investigated at 29 ± 2 °C. The data (Table 6.9) are consistent with two pathways resulting from thiocyanate independent and dependent steps, both of which are independent of proton concentration.

$$[Ni(N_4O)(NCS)]^{2+} \xrightarrow{k_a} [Ni(N_4O)]^{2+} + NCS \qquad (6.4)$$

$$[Ni(N_4O)NCS]^{2+} + NCS^- \xrightarrow{k_b} [Ni(N_4O)]^{2+} + (NCS)_2 \qquad (6.5)$$

The rate constants are for the former is 3.65 ± 0.15 s^{-1} and for the latter 0.33 ± 0.05 $M^{-1}s^{-1}$ respectively. No attempt was made to identify the postulated thiocyanogen product from the bimolecular reaction owing to the low concentrations of the reagents involved and the ready hydrolysis of this species

in the acidic media employed.

Table 6.9

Rate data for the second (redox) step in the reaction between [Ni(III)] and SCN^-, T = 29±2°C, $[Ni(III)]_t = 5\times10^{-5}M$

$10^3[NCS^-]$	1.00	2.00	4.00	6.00	9.00	9.00
k_{obs}/s^{-1}	4.00	4.26	5.04	5.86	6.64	6.55[a]

Data at $[H^+]$ = 0.25M except for (a), $[H^+]$ = 0.75M.

In addition to the N_4O complex, the substitution reactions of the N_5 and N_4S macrobicyclic complexes were also investigated under experimental conditions similar to the above. In both the cases, the reactions appeared very rapid, and an attemp to lower the reaction rates by reducing the reactant concentrations failed due to the fact that the changes in the visible range for the reaction were too small under the high dilution conditions. Studies using a stopped-flow apparatus equipped with an UV light source are in progress.

Discussion

The substitution reaction of the present d^7 Ni(III) complex is, as shown above, very complicated, and affected by factors such as the proton concentration, the supporting anion, and the entering ligand. At the present time, our understanding of the reaction is provided in a tentative mechanism accounting for the kinetic results, which is

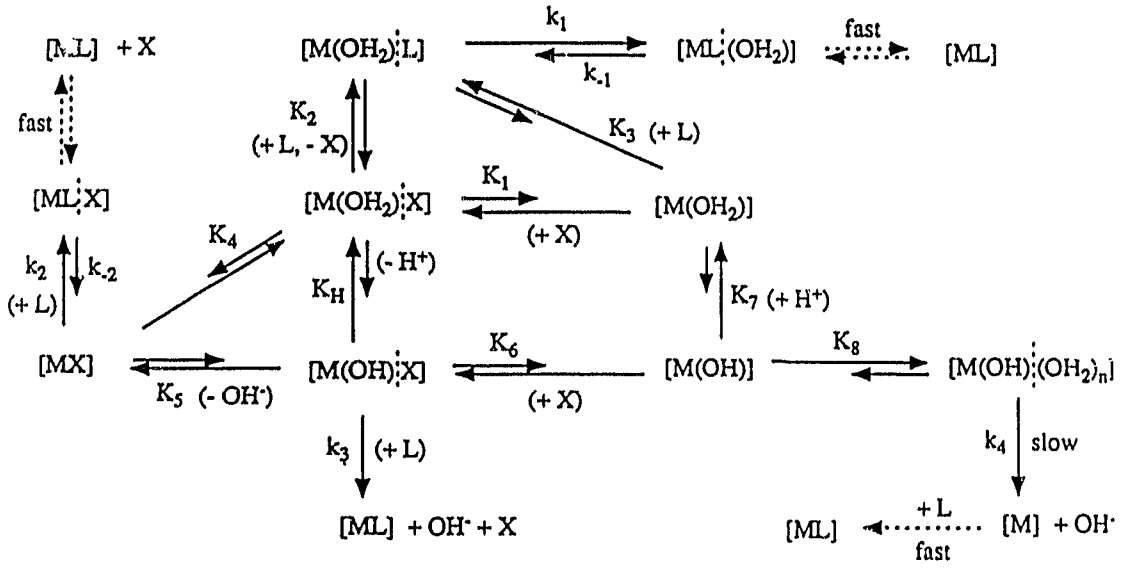

Scheme 6.1 Mechanistic Scheme of the Substitution Reaction of $[Ni(III)N_4O)(OH_2)]^{3+}$ in Aqueous Medium.

proposed in Scheme 6.1. The mechanism involves a number of equilibria including an aquo complex, an anion-coordinated species, a hydrolysed ion, and ion-pairs of both the supporting anion and the entering ligand. The mathematical expressions for these equilibria are as follows:

$$K_1 = [M(OH_2)]/[M(OH_2):X] \quad (6.6)$$

$$K_2 = [M(OH_2):L][X]/[M(OH_2):X][L] \quad (6.7)$$

$$K_H = [M(OH_2):X]/[M(OH):X][H^+] \quad (6.8)$$

$$K_3 = [M(OH_2):L][X]/[M(OH_2):X][L] \quad (6.9)$$

$$K_4 = [MX]/[M(OH_2):X] \quad (6.10)$$

$$K_5 = [MX][OH]/[M(OH):X] \quad (6.11)$$

$$K_6 = [M(OH)][X]/[M(OH):X] \quad (6.12)$$

$$K_7 = [M(OH_2)]/[M(OH)][H^+] \quad (6.13)$$

$$K_8 = [M(OH)\,!\,(OH_2)_n]/[M(OH)] \quad (6.14)$$

where M represents for the penta-coordinated $[Ni(III)(N_4O)]^{3+}$ ion, L the entering ligand, and X is the supporting anion. The symbol "!" is for ion-pair formation, and "n" is either 1 or 2 for the number of the hydrogen-bonded water(s) with the coordinated hydroxide.

As far as the kinetics are concerned, there are four pathways which may be considered rate-determining, among which two are the reversible processes and the other two irreversible

$$Rate_1 = (k_1 + k_{-1})[M(OH_2)\,!\,L] \quad (6.15)$$

$$Rate_2 = (k_2[L] + k_{-2})[MX] \quad (6.16)$$

$$Rate_3 = k_3[L][M(OH)\,!\,X] \quad (6.17)$$

$$Rate_4 = k_4[M(OH_2)\,!\,(OH_2)] \quad (6.18)$$

Under the conditions that *all the equilibria of (6.6) to (6.14) remain throughout the kinetic process*, the equations above may be rewritten as

from eq. (6.7) and (6.15):

$$Rate_1 = (k_1 + k_{-1})K_2[L][M(OH_2)\,!\,X]/[X] \quad (6.19)$$

from eq. (6.10) and (6.16):

$$Rate_2 = (k_2[L] + k_{-2})K_4[M(OH_2)X]/[H_2O \quad (6.20)$$

from eq. (6.8) and (6.17):

$$Rate_3 = k_3[L][M(OH_2)\,!\,X]/(K_H[H^+]) \quad (6.21)$$

from eq. (6.8), (6.11), (6.14), (6.12), and (6.18):

$$Rate_4 = k_4K_6K_8[M(OH_2)\,!\,X][H_2O]^n/(K_H[X][H^+]) \quad (6.22)$$

Combining eqns. (6.19) to (6.22), the total rate may be

expressed as

$$Rate_{total} = Rate_1 + Rate_2 + Rate_3 + Rate_4$$

$$= \{(k_1 + k_{-1})K_2[L]/[X] + (k_2[L] + k_{-2})K_4 + K_3[L]/(K_H[H^+]) + k_4K_6K_8/(K_H[X][H^+])\}[M(OH_2)\,X] \quad (6.23)$$

Under the condition that *$[M(OH_2)\,X]$ is the dominant component in the system*, that is

$$[M]_{total} \approx [M(OH_2)\,X] \quad (6.24)$$

the observed total rate constant, k_{obs}, may be represented as

$$k_{obs} = (k_{-2}K_4) + (k_4K_6K_8/K_H[X])(1/[H^+]) + \{(k_2K_4 + (k_1 + k_{-1})/[X]) + (k_3/K_H)(1/[H^+])\}[L] \quad (6.25)$$

Comparing eq. (6.25) with eq. (6.1), one has

$$k_I = k_{-2}K_4' \quad (6.26)$$

$$k_{II} = k_4K_6K_8'/K_H[X] \quad (6.27)$$

$$k_{III} = k_2K_4' + (k_1 + k_{-1})/[X] \quad (6.28)$$

$$k_{IV} = k_3/K_H \quad (6.29)$$

With the limited data available, it is impossible to calculate the accurate values for all the constants. However, the equations (6.25 - 6.29) derived from the mechanism tentatively proposed here do allow us to examine the experimental results qualitatively. In Table 6.7, as the supporting anion is changed from perchlorate to nitrate and triflate, (a) because of the decrease of the K_6 term in eq. (6.27), the k_{II} value is reduced; (b) There is an increase of the k_3 term in eq. (6.29), resulting in an increase of k_{IV}; (c) the highest value for the k_I and the lowest value for k_{III} in

nitrate media are likely due to the highest k_{-2} and the lowest k_2 values for the nitrate, which has the strongest binding power among the three anions.

In Table 6.8, it is seen that as the perchlorate concentration increases, k_{II} and k_{III} decreases according to eq. (6.27) and (6.28) (due to the inverse relationship of [X] with the two terms. The values for the k_I and k_{IV} terms in the table may be regarded as being constant (since its variation with the concentration is subject to experimental errors, in particular the k_I term was derived from the intercept of the kinetic plots and, hence, has a larger amount of uncertainty).

The results from the different entering ligand are also consistent with the expressions described in eqns. (6.26-29). The replacment of Cl^- by SCN^- does not affect the k_I and k_{II} terms (about 2.2 and 0.44 units respectively in both the cases) due to eq. (6.26) and (6.27), but changes the k_{III} remarkably (from 260 to 968 units), as a result of the increase in the k_2 and $(k_1 + k_{-1})$ terms of eq. (6.28).

The results from the mixed supporting-anion (perchlorate/triflate) may also be interpreted in the similar way as above.

In the mechanistic scheme proposed, consistent with the pre-condition made above (that is, the equilibria prevail throughout the kinetic process), is that most of the equilibria involved are either ion-pairing or deprotonations, which are, in general, very rapid processes, except K_4 and K_5.

Under the experimental condition (acidic media), the equilibrium of K_5 may be ignored. The equilibration process for K_4 might be slow compared with those ion-pairing and deprotonation processes, but is probably faster than the following rate-determining step, and hence, may be treated as an "true" equilibrium throughout the kinetic process (in other words, the [MX] is in a kinetic "steady-state" during the process).

Theoretical treament of a reversible individual kinetic process such as $Rate_1$ and $Rate_2$ has been well discussed in ref. 187(a and b). The irreversible nature of $Rate_3$ and $Rate_4$ is a result of the acidic conditions employed in the experiment. The hydroxy complex [M(OH)] is, theoretically speaking, also capable of undergoing substitution process, but the rate is expected to be very small due to its low concentration and kinetic inertness (such as that in the case of Co(III) complex). Even taking its possible pathway into account, the final expression for the kinetics will not be much different from that provided above (eq. (6.25)). The same is also applicable for the pathway $Rate_3$ where the substitution might involve an ion-pair intermediate like [M(OH)⋮X⋮L] which subsequently gives rise to the product [ML]. Pathway $Rate_4$ is somewhat different from the rest, being a dissociative process. This may be explained in terms of hydrogen-bonding between the coordinated hydroxy group and one or two water molecules, which blocks the path where the entering group

might come into the inner-sphere. Therefore, the entering group has to "wait" for the hydroxy to depart from the inner-sphere before coming in, resulting in a very low rate constant (k_{11} is indeed the lowest among the four). Surely, it is also possible for [M(OH)⁞X] to be hydrogen-bonded in the same way as [M(OH)]. However, this process may be either disfavoured by the presence of the ion-paired X group, or could not compete kinetically with $Rate_3$. Again, even taking this possibility into account, the final kinetic expression will be similar to the above (eq. (6.25)).

In addition, there are a number of alternative kinetic treatments involving other possible equilibria which may exist in the system. The treatment presented above is, by no means, the "only answer" to the kinetic results. Another approach to the kinetic expression of the substitution process is to treat all the "equilibria" in the system as reversible kinetic processes which are in a dynamic equilibration state during the reaction. Under this treatment, the kinetic process could not be subdivided into a number of individual pathways, and the total reaction rate may be expressed as

$$\begin{aligned} d[ML]/dt = {} & k_1[M(OH_2)⁞L] - k_{-1}[ML⁞(OH_2)] + k_2[L][MX] \\ & - k_{-2}[ML⁞X] + k_3[L][M(OH)⁞X] \\ & + k_4[M(OH)⁞(OH_2)_n] \end{aligned} \qquad (6.30)$$

The full coverage of the mathematical treatment of eq. (6.30) is not detailed in this thesis. Nevertheless, the final kinetic expression for the observed rate constant is similar

to eq. (6.25) (differing only in the number and nature of the k or K terms), and also consistent with the empirical formula (eq. (6.1)).

It is also not possible to discuss all the alternative treatments of the kinetic results in terms of the mechanism here, and a full examination of every detail of the present mechanism would lead to an unacceptable length of this section. Such discussions will be presented in a future publication, and only several mechanistic features are considered in the following discussion.

Except for $Rate_4$ which is obviously a dissociative process, the exact nature of "intimate mechanism" (section 1.2.1) is not clear for the other three pathways. The treatment of $Rate_3$ above is, to some extent, oversimplified, and could involve some sort of reaction intermediate like [M(OH)|X|L] (*vide supra*). The detailed mechanism may not be determined at this stage, though the expression in eq. (6.17) "appears" like an associative process. The pathway $Rate_1$ and $Rate_2$ are the **I** process, indicated by the sensitivity of k_i and k_{iii} towards the replacement of the supporting anion and/or entering ligand (*vide supra*).

With the mechanism proposed above, it appears that the intimate mechanism for the substitution reaction at the Ni^{3+} centre is dependent of the bond strength of the leaving group and the metal centre. When either Cl^- or SCN^- (which both form strong metal-donor bond) is the leaving group (k_{-2} process in

$Rate_2$), the k_1, or k_{-2} (since K_4' is independent of L, see Scheme 6.1) is insensitive towards the replacement of Cl^- by SCN^-, and sensitive towards the nature of the supporting anion (Table 6.7), indicating the I_a nature. The substitution of the coordinated water in the pathway $Rate_1$, however, appears to be an I_d process. Although the replacement of Cl^- by SCN^- as an entering ligand increased the value for k_{111} from 260 to 968 units (*vide supra*), this increase is a combination of both k_2K_4 and $(k_1 + k_{-1})$ terms (eq. (6.28)), and ratio of $k_1(SCN^-)/k_1(Cl^-)$ is likely less than $968/260 \approx 3.5$, which is not much different from that in the case of Ni(III)cyclam ($k_f(SCN^-)/k_f(Cl^-) \approx 1.5$),[171] and much smaller than that observed in the "classical" I_a process, such as $Cr(OH_2)_6^{3+}$, 62,[187c] and $Mo(OH_2)_6^{3+}$, 59,[187d] indicating a possible I_d nature in the present system.

6.5.2 Redox Reactions

The kinetic effect of the apical donor change on the electron transfer reaction was investigated using $[Ni(III)(N_4X)]^{2+}$ (X = O, S, or N) to react with $[Ni(II)([9]aneN_3)_2]^{2+}$. The experiments were carried out at 12 ± 0.1 °C in 1.0 M $H/NaClO_4$ ($[H^+]$ = 0.5 M) with excess $[Ni(II)([9]aneN_3)_2]^{2+}$ over the N_4X complexes. The experimental data were listed in Table 6.10. For all these reactions, the rates were pseudo-first order in the form

$$k_{obs} = k_{12}[Ni^{II}([9]aneN_3)_2]$$

The individual rate constants, k_{12}, together with $E_{1/2}$'s used

Table 6.11 Kinetic Results from Redox Reactions of $[Ni^{III}(N_4X)]^{3+}$ with $[Ni^{II}([9]aneN_3)_2]^{2+}$

T = 12 ± 0.2 °C; I = 1.0 M ($H/LiClO_4$); $[H^+]$ = 0.5 M; λ = 400 nm.

(A) X = O: $[Ni(III)(N_4O)]$ = 1.0×10^{-5} M

$[Ni^{II}([9]aneN_3)_2]$ ($\times10^4$ M^{-1})	1.0	2.0	3.0	4.0
k_{obs} (s^{-1})[a]	11	17	25	32

[a]uncertainties < 10%.

$k_{obs} = k_{12}[Ni^{II}([9]aneN_3)_2]$, $k_{12} = 1.4\times10^5$ $M^{-1}s^{-1}$.

(b) X = S: $[Ni(III)(N_4S)]$ = 1.0×10^{-5} M

$[Ni^{II}([9]aneN_3)_2]$ ($\times10^4$ M^{-1})	2.0	3.0	4.0
k_{obs} (s^{-1})[a]	18.7	25.3	35.7

[a]uncertainties < 10%.

$k_{obs} = k_{12}[Ni^{II}([9]aneN_3)_2]$, $k_{12} = 1.8\times10^5$ $M^{-1}s^{-1}$.

(c) X = N: $[Ni(III)(N_5)]$ = 1.0×10^{-5} M

$[Ni^{II}([9]aneN_3)_2]$ ($\times10^4$ M^{-1})	2.0	3.0	4.0
k_{obs} (s^{-1})[a]	2.1	3.0	4.2

[a]uncertainties < 10%.

$k_{obs} = k_{12}[Ni^{II}([9]aneN_3)_2]$, $k_{12} = 1.1\times10^4$ $M^{-1}s^{-1}$.

Table 6.12 Self-Exchange Rates of $[Ni(N_4X)]^{3+/2+}$ [a]

X =	O	S	N
k_{12} ($x10^{-4}$ $M^{-1}s^{-1}$)	1.4	1.8	0.11
$E_{1/2}$ (V, *vs.* NHE)	1.17[b]	1.06[c]	1.00[c]
k_{11} ($x10^{3}$ $M^{-1}s^{-1}$)	0.4	50	2

[a] using simplified "Marcus cross-relation": $k_{12} = (k_{11}k_{22}K)^{1/2}$, where $\log K = (E_{11}^{\circ} - E_{22}^{\circ})F/RT$, E_{22}° of $[Ni([9]aneN_3)_2]^{3+/2+}$ = 0.947 V *vs.* NHE, $k_{22} = 6x10^{3}$ $M^{-1}s^{-1}$ (from ref. 101); [b] in 1.0 M $NaClO_4$; [c] from Table 6.4.

---

for the calculation of k_{11} and k_{11}'s from simplified "Marcus cross-relation" (eq. 1.16), are provided in Table 6.11.

A significant feature of these results is that the self-exchange rate, k_{11}, decreases in the order of S > N > O. Although there is lack of information about the exact structural change in the metal-donor bonds in the present system, this decrease is, qualitatively speaking, in conjunction with the degree of the Ni-X bond length variation as the nickel centre converts from the (II) to the (III) state. A "softer" donor (such as S) is less sensitive to the change of oxidation state ($2^{+} \rightleftharpoons 3^{+}$) at the metal ion ("hard-acid") than a "harder" donor (such as O) in terms of the metal-donor bond length. Here again, the results demonstrate that the inner-shell reorganization plays very important role

in determining the self-exchange rate of electron-transfer reaction at a coordinated transition metal centre.[70]

Chapter 7. Synthesis, Characterization and Reactivity of Ethylene-bridged Binuclear Ni(II) Complex

7.1 Introduction

Interest in transition metal macrocyclic complexes are, in large part, derived from mutual impact of the coordinated metal ion and the ligand, as far as chemistry is concerned. For this reason, the study of macrocyclic complexes has been, and still is, focussed almost exclusively on activities of either the metal centre or coordinated ligand. Along with this, interpretation of the results is mostly based on some sort of "interaction" between the ligand to metal or vice versa, and separation between metal centre and ligand is usually, if not always, clear in rationalization. While it is often the case when the metal centre is only to *affect*, or *influence*, a ligand-based reaction (where the reactive site is beyond the reach of the metal), or the ligand can only *perturb* the reactivity at the metal centre (acting as a σ-donor and/or π-acceptor/donor in the metal-based reaction), this consideration may not be helpful for the situation where the highest ligand orbital and/or the lowest unoccupied orbital are comparable with that at the metal centre in terms of energy, and are able to mix with and form a metal-ligand molecular orbital (MLMO) which is the centre of chemical activity. The earliest report on such a system is probably 11,13-dimethyl-1,4,7,10-tetraazacyclotrideca-10,12-dienatonickel(II) perchlorate, [NiAT]ClO_4 (1), by Richardson and Sievers.[188] The molecular structure of this complex shows a high (relatively speaking) aromaticity on its six-membered

dieno(-) ring (*vide infra*). Unfortunately, the aromatic nature of this complex was ignored, and no chemical reactivity of this species was mentioned in their report.

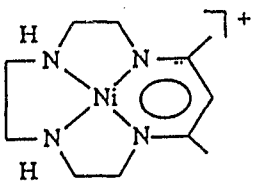

1

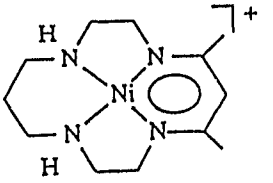

2

After this report, redox reactions of $[NiAT]^+$ and $[Ni(Me_2[14]4,7-[14]-dieno(-)N_4]^+$, $[NiAT']^+$ (2) were investigated by Endicott et al..[189] The oxidation potentials (E_{pa}) of 0.62 V ($[NiAT]^+$) and 0.55 V ($[NiAT']^+$), together with that of $[Co(AT')(NCS)_2]^\circ$, $\leq$ 0.4 V (*vs.* SCE in DMF), are difficult to attribute solely to either "metal-based" or "ligand-based" oxidation. Furthermore, observations from the kinetic study of metal-β-dieno(-) complexes also did not imply that the metal and ligand "sites" are wholly independent.[189]

It was not until recently that the term "quasi-aromatic", which combines metal and ligand factors as a whole, was used in the report by Murmann and Vassian.[190] In their report molecular structures of (2,2,3,9,10,10-hexamethyl-5,7-dioxa-6-hydra-1,4,8,11-tetraazacyclotetradec-3,8,11,13-tetraene)Ni(II), [Ni(PnAO-6H)]° (3), and its derivatives were described. These also show high aromatic character on the unsaturated six-membered ring as was observed from $[NiAT]^+$. Although "quasi-aromatic" was used to describe the ring and the

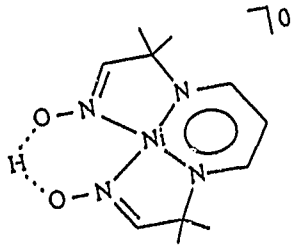

3

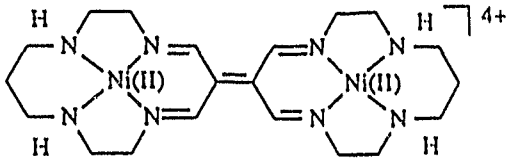

4

data from crystallography, ^{13}C and ^{1}H NMR, and EHMO calculation all provided evidence for a delocalization of electron density on this ring, no aromaticity was discussed in the report. Systematic investigation on the reactivity of this "quasi-aromatic" ring showed that the β-carbon on the six-membered ring is very active and behaves as a nucleophile, and a number of reactions (mostly organic in nature) were reported at this carbon.[190] However, again no aromaticity was invoked in the interpretation of the results, which may, indeed, be explained readily in terms of the aromatic nature of the ring system. Nevertheless, their work was probably the first effort made in exploring the chemistry of this type of metal-ligand "quasi", or "pseudo", aromatic ring.

In examining the results from molecular structure and initial investigation on chemistry (particularly redox chemistry) of the unsaturated binuclear complex, $[Ni^{II}_2(L4)]^{4+}$, (**4**), it was recognized that for six-membered ring where atoms all have free p_z orbitals, there is a strong tendency for it to form an aromatic (or "quasi" aromatic) system. This tendency is, indeed, so strong that even in the situation where the number of $3p_z$ electrons ($4p_z$ from metal is always

empty) is less than (4x2 +2), the system still wants to reach to some degree of aromatization by gaining electron density from the metal through $4p_z$-d_{xz}, d_{yz} mixing. This recognition was found to be very helpful in understanding not only all the structural features and the chemical nature of the unsaturated dimer in the present work, but the property of other related systems (e.g., $[NiAT]^+$ and [Ni(PnAO)-6H]°) as well. Thus, for a system like this, any chemical reactivity on the aromatic ring (and/or its conjugated neighbour) may not be attributed solely to the metal or ligand, but a combination of both. As to more fundamental aspects, the present work might probably be regarded as an initial step toward understanding a new aspect of transition metal coordination chemistry, that is, the chemistry of truly "combination" of metal and ligand.

One of important aspects of this "combination" chemistry is the electron transfer reactions. Interest of electron-transfer reactions of most coordination complexes has been, and still is, metal-based which may be well described by considering the perturbation imposed by coordinating donors on the electron density and orbital energy of central metal ion. However, interest of electron tranfer on the ligand site was recently stimulated by Dolphin's report[191] in which he proposed that π-cation radical ligand states mediate electron-transfer reactions of some cytochromes. Other relevant evidence for this proposal was the discovery[192] that the site of oxidation (*i.e.*, at the metal or ligand) of ruthenium porphyrins can be

altered merely by changing the axial ligands.

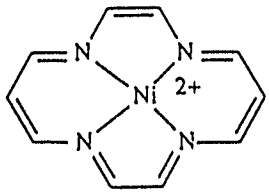

5

For the synthetic macrocyclic complexes, Holm and Millar[193] have reported that oxidation of Ni(II) complex with highly conjugated [14]aneN$_4$ ligand (5) is predominantly ligand-based. Internal electron transfer from ligand to metal centre has also been reported by Endicott et al.[189,194] for Co(III) complex with a β-diiminato type ligand such as $[Co(AT')(NCS)_2]^0$, where Co(III) oxidized the β-diiminato chelate to form a ligand radical species which subsequently dimerized to give a binuclear complex. However, kinetic investigation of such "ligand-based" electron transfer was rare, and where it was attempted, the rate of such transfer was found to be "diffusion-limited".[189]

Thus, with very fast electron transfer (normally $k \geq 10^9$ $M^{-1}s^{-1}$) on one side (ligand-based) and relatively slow electron transfer (normally $k \leq 10^4$ $M^{-1}s^{-1}$) on another (metal-based), it is possible that metal-ligand "combination" system offers a compromise between the two, and may, at least potentialy, serve as a model in the study of electron transfer reactions in biological systems.

7.2 Formation of $[Ni(II)_2(L4)]^{4+}$

The procedure involved in the preparation of $[Ni(II)_2(L4)]^{4+}$ has been described in section 2.1.3. The dimerization process may be easily monitored by color change. The initial yellow solution of Ni^{II}cyclam turned green (formation of Ni(III)) shortly after H_2O_2 was added at approximately 60 °C. This green colour persisted and then underwent a sudden change, through a very short period of dark brownish-yellow (which was likely due to mixing of green and purple colors), to deep purple. The resulting solution was not stable and converted to a brownish-yellow colour (decomposition mixture) if kept at high temperature for more than one minute. However, placing the deep purple solution in ice/water bath immediately after it was formed gave rise to red precipitate of the dimeric product when the counter ion was perchlorate. The dimeric complex can also be obtained using $[Ni(III)(cyclam)]^{3+}$ as starting material.

The dimerization of Ni(II)cyclam was investigated under various conditions. In order for the deep purple dimer product to form, the solution has to be acidic with $[H^+] \geq 0.2$ M (the acids used in the present work were H_2SO_4, HNO_3 and $HClO_4$). At a higher pH, no dimerization was observed. The temperature is also very important for the formation of the dimer. The dimerization occured only at the temperatures above 50 °C (but the best yield was obtained at ~ 60 - 70 °C), otherwise only a green Ni(III) solution was produced. As far as oxidising

reagents are concerned, sodium peroxodisulfate was the only other one besides hydrogen peroxide which is capable of oxidizing Ni(II)cyclam to generate the dimeric species under the same conditions. Other oxidizing reagents such as conc. HNO_3 ($\geq$ 3.0 M), Ce^{4+}, Co_{aq}^{3+}, etc. all failed to produce the dimerized product. and led only to a Ni(III) green solution. The effect of the metal centre on the dimerization was also investigated by replacing Ni(II) with Cu(II). Only Cu(II)cyclam was isolated after the reaction was subjected to the same conditions as those for the Ni(II).

While sodium peroxodisulfate may be used to produce the dimeric species, isolation of the product from the resulting deep purple solution turned out to be very difficult (probably due to presence of sulfate ion). Even when the solution was saturated with perchlorate, no precipitate was formed even after being refrigerated for several days. The procedure described in section 2.1.3 was found to give the best yield (~ 25%) of the isolated dimeric product among all alternatives.

Attempts were also made to isolate the reaction intermediates by analysing either the final reaction mixture or the solution obtained before the deep-purple coloration formed. In both cases, the only species which were isolated and characterised were either the starting material or the dimer product (sometimes also [Ni(III)cyclam]$^{3+}$ in HNO_3 media). Reaction with insufficient amounts of H_2O_2 only gave rise to a green solution, and Ni(II) and/or Ni(III) species were the

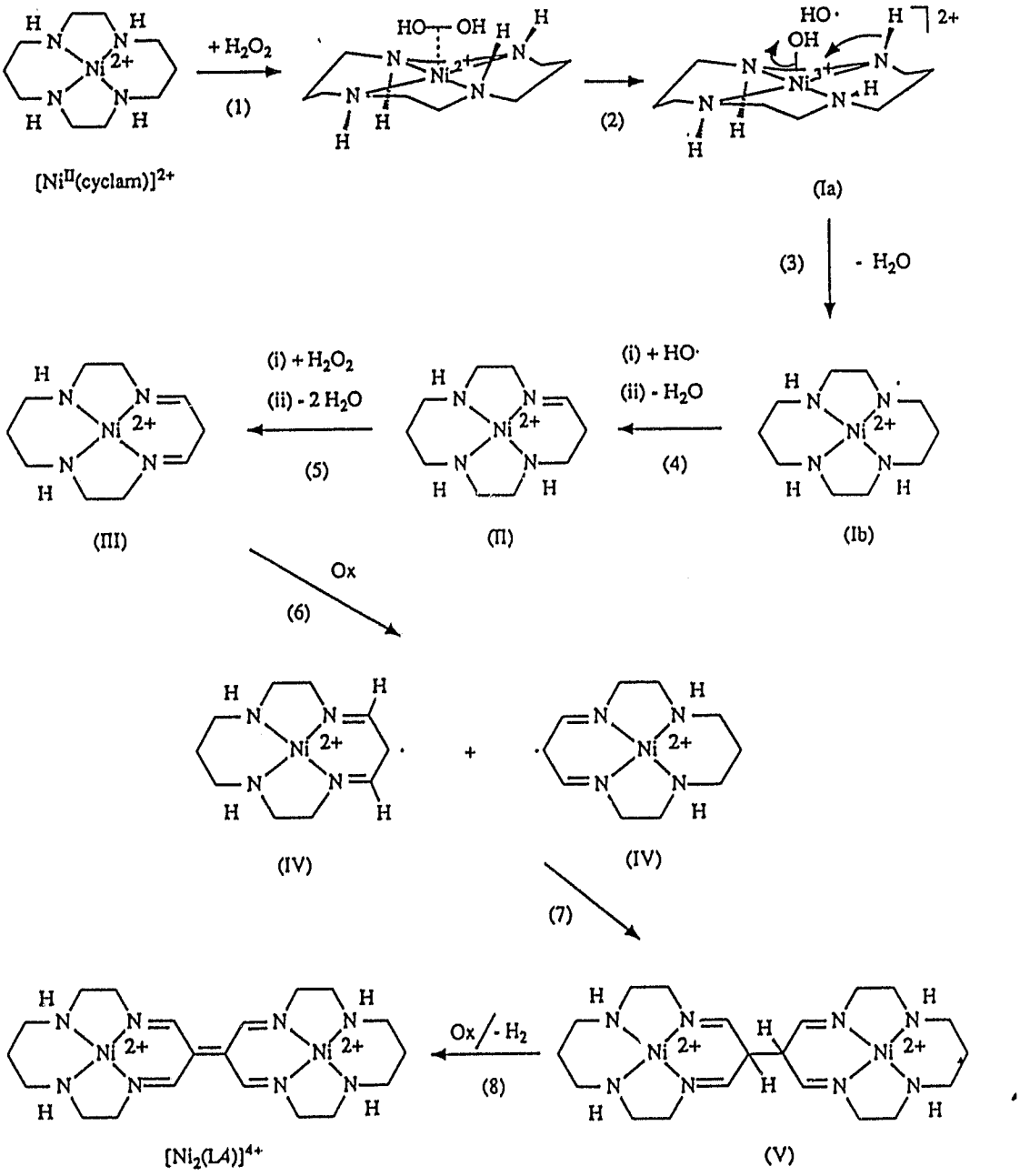

Scheme 7.1 Mechanistic Scheme of the Formation of $[Ni_2(L4)]^{4+}$

only products. It appeared that depending on how much oxidant was used the reaction either ended at green coloration or went to completion to give a deep-purple solution.

Our present understanding of the observations decribed above is provided in a possible mechanism involved in the process from Ni(II)cyclam monomer to $[Ni(II)_2(L4)]^{4+}$ dimer (Scheme 7.1). From the results obtained it appears that the formation of Ni(III) must be the initial step towards the dimerization, indicated by the green-coloration and failure of Cu(II) replacement. The processes, as suggested by other workers (Scheme 1.3 in section 1.1.4) for a general mechanism in the oxidative dehydrogenation of coordinated ligand is unlikely the case in the present system due to the high acidic conditions. $[Ni(III)cyclam]^{3+}$ is not stable in acidic solution at high temperature and oxidizes water solvent to give $[Ni(II)cyclam]^{2+}$ which then acts as a catalyst (like Fe^{2+} in Fenton's reagent) in converting H_2O_2 to HO· radical (step (1) and (2) in Scheme 7.1). The imine group is probably formed by an intramolacular electron-transfer from the coodinated secondary amine to the Ni(III) to give a Ni(II) ligand-N· radical (**Ib**) and then (or at the same time) a HO· attack on the hydrogen atom on the adjacent α-carbon, (step (3) and (4) in Scheme 7.1). Indeed, it has been known that many reactions involving H_2O_2 in solutions are free-radical based, and homolysis of hydrogen peroxide can be catalysed by metal ions.[195] The radical mechanism proposed here for the formation

of the imine function is consistent with the experimental results described above (that is, (a) only the oxidants with peroxo group are effective; (b) a high temperature is necessary). This proposed radical mechanism is also supported by the pulse-radiolysis study of HO· radical oxidation of Ni(II) complexes of methyl-substituted tetraazamacrocyclic ligands where formation of the Ni(II) ligand-N· radical species was suggested as the initial step in the oxidative dehydrogenation of the coodinated ligand.[196]

The second imine functional group may be formed in the similar way as above, and could take place at either the same six-membered ring of the first one (step (5) in Scheme 7.1), or another one at the opposite side, which accounts for the low yield of the dimeric product (the best yield obtained was 25%).

The six-membered diimine ring on the species **III** may be oxidized by either the Ni(III) species or the H_2O_2 present in the solution to give diimine radical **IV** which then dimerizes to form **V** (step (7) in Scheme 7.1). Further oxidative dehydrogenation of **V** leads to the C=C bridged dimer, $[Ni_2(L4)]^{4+}$ (step (8) in Scheme 7.1).

The necessary requirement of a high acidic condition for the dimerization is probably because of following reasons. The oxidising power of hydrogen peroxide is pH-dependent.[195] It has its highest oxidation potential, 1.77 V *vs* NHE, in acidic environment. In basic media, however, it has a low E° value of

0.87 V which is not strong enough to oxidise both Ni(II) centre (E° for $Ni^{III/II}$cyclam couple is 0.97 V *vs* NHE) and the ligand. Secondly, decomposition of H_2O_2 according to equation

$$2H_2O_2 = 2H_2O + O_2 \qquad (7.2)$$

is also very much dependent on pH, and proceeds rapidly in basic media upon heating.[195] Therefore, without protection of acid, H_2O_2 might be destroyed well before it can produce HO· radical for the dimerization.

Oxidative dehydrogenation provides another means to synthesize unsaturated polyazamacrocyclic complexes, which are of biological significance.[122] Although there have been a good number of reports on oxidative dehydrogenation of tetraazamacrocyclic complexes of transition-metal, the mechanism involved has never been clearly understood in most of the cases, and still is a subject of debate.[36-40] Obviously, more work needs to be done in this area. The investigation presented here is helpful in this respect. Recently, Murmann and Vassian[190] reported that in 1.0 M NaOH solution [Ni(PnAo)-H]$^+$ may be oxidised by a variety of reagents (O_2 or $NaIO_3$ were

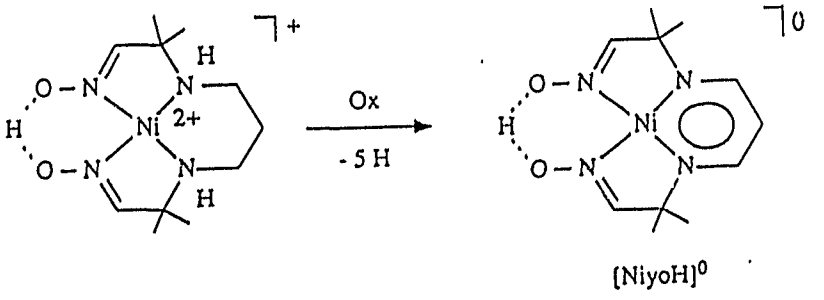

Scheme 7.2

said to be the best) to give a dieno(-) product, [Ni(PnAo)-6H)]° (NioylH), in high yield with no discernible intermediates. NioylH species may be oxidised in aqueous solution by air or electrochemically to producing a C-C bridged dimer $(Niyol)_2$. However, no mechanistic investigation was mentioned. The $[Ni(PnAo)-H]^+$ species has the same six-membered ring as Ni(II)cyclam, and further study of both complexes may lead to a better understanding of the reactions of this type.

7.3 Molecular Structure

As described in section 2.1.3, an X-ray quality crystal of $[Ni_2(L4)](ClO_4)_4$ was obtained from its saturated aqueous solution in the presence of $HClO_4$. Crystallization was achieved by slow evaporation, otherwise only a fine precipitate was produced.

Crystallography

The unit cell was refined by using 21 pairs of reflections in the 2θ range 22 - 39°. Three standard reflections preceded each batch of 50 measurements, with no decomposition during the collection. Details of the solution are similar to those given for the crystallographic structures presented in previous chapters. The refinement converged with a maximum shift/esd of 0.011 on the final cycle. The final difference map showed a maximum peak of 0.755 $eÅ^{-3}$. The rest processes were the same as those described in section 6.2.

Crystallographic data are listed in Table 7.1, and the results for interatomic distances, bond angles, and atomic coordinates are presented in Table 7.2, 7.3, and 7.4 respectively. An ORTEP drawing of molecular structure is shown in Fig. 7.1.

Table 7.1 Crystallographic Data

Chemical Formula: $[NiN_4C_{10}H_{16}O_8Cl_2]_2$	$T = 22 \pm 2$ °C
Fw: 899.7	$\lambda = 0.710\ 69$ Å
Space group: PT (No. 2)	$\rho_{obs} = 1.807$ g cm^{-3}
a = 8.557(1)Å	$\rho_{calc} = 1.818$ g cm^{-3}
b = 13.382(2)Å	$\mu = 14.72$ cm^{-1}
c = 8.475(2)Å	$R(F_o) = 0.0665$
$\alpha = 107.45(2)°$	$R_w = 0.0654$
$\beta = 116.62(2)°$	Z = 2
$\gamma = 76.21(1)°$	
V = 821.5 Å^3	

Results

The dimer molecule has a centre symmetry at the middle point of its bridge, C(2)-C(2′). As shown in Table 7.2, the bond length between the two bridging carbons is 1.402 Å, which is intermediate between the normal distances for a single C-C bond (~ 1.50-5 Å) and a double C=C bond (~ 1.34 Å) (For a more direct comparison, single bond bridge found in bis-Ni(II)cyclam is 1.542 Å,[199] and localized double bond bridge in

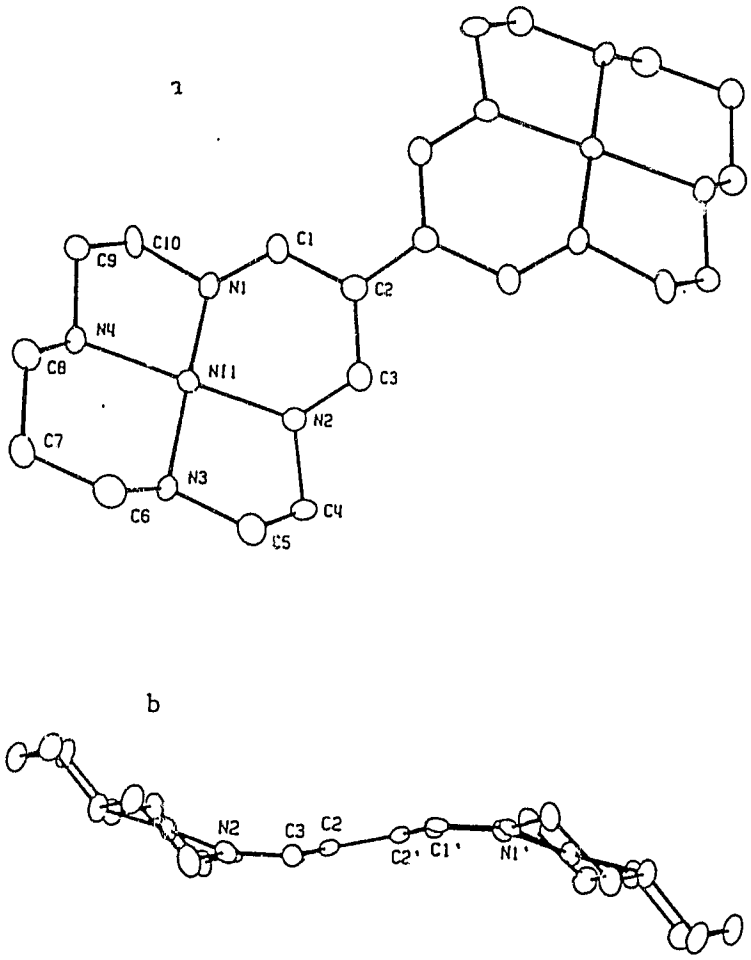

Fig. 7.1 ORTEP drawing of the molecular structure of $[Ni_2(L4)]^{4+}$.

Table 7.2

Interatomic distances (A).

Atoms		Distance	Atoms		Distance
N(1)	-Ni(1)	1.849(9)	C(3)	-N(2)	1.290(13)
N(2)	-Ni(1)	1.851(8)	C(4)	-N(2)	1.473(13)
N(3)	-Ni(1)	1.926(8)	C(5)	-N(3)	1.497(14)
N(4)	-Ni(1)	1.940(8)	C(6)	-N(3)	1.495(14)
O(1)	-Cl(1)	1.390(10)	C(8)	-N(4)	1.489(15)
O(2)	-Cl(1)	1.386(11)	C(9)	-N(4)	1.497(13)
O(3)	-Cl(1)	1.377(10)	C(2)	-C(1)	1.459(14)
O(4)	-Cl(1)	1.388(12)	C(3)	-C(2)	1.459(15)
O(5)	-Cl(2)	1.422(9)	C(2)	-C(2)	1.401(20)
O(6)	-Cl(2)	1.404(8)	C(5)	-C(4)	1.547(16)
O(7)	-Cl(2)	1.390(11)	C(7)	-C(6)	1.528(16)
O(8)	-Cl(2)	1.393(12)	C(8)	-C(7)	1.524(16)
C(1)	-N(1)	1.303(12)	C(10)	-C(9)	1.532(16)
C(10)	-N(1)	1.523(13)			

Estimated standard deviations are given in parentheses.

Table 7.3

Bond angles (d).

Atoms			Angle	Atoms			Angle
N(2)	-Ni(1)	-N(1)	91.5(4)	C(10)	-N(1)	-C(1)	116.5(9)
N(3)	-Ni(1)	-N(1)	176.6(4)	C(3)	-N(2)	-Ni(1)	128.6(8)
N(3)	-Ni(1)	-N(2)	86.8(4)	C(4)	-N(2)	-Ni(1)	113.1(7)
N(4)	-Ni(1)	-N(1)	86.2(4)	C(4)	-N(2)	-C(3)	118.0(9)
N(4)	-Ni(1)	-N(2)	176.6(4)	C(5)	-N(3)	-Ni(1)	108.3(6)
N(4)	-Ni(1)	-N(3)	95.4(4)	C(6)	-N(3)	-Ni(1)	118.8(7)
O(2)	-Cl(1)	-O(1)	113.3(7)	C(6)	-N(3)	-C(5)	110.1(9)
O(3)	-Cl(1)	-O(1)	110.3(8)	C(8)	-N(4)	-Ni(1)	118.3(7)
O(3)	-Cl(1)	-O(2)	107.6(8)	C(9)	-N(4)	-Ni(1)	108.3(6)
O(4)	-Cl(1)	-O(1)	108.7(8)	C(9)	-N(4)	-C(8)	109.5(9)
O(4)	-Cl(1)	-O(2)	108.3(9)	C(2)	-C(1)	-N(1)	119.3(10)
O(4)	-Cl(1)	-O(3)	108.5(10)	C(3)	-C(2)	-C(1)	121.6(9)
O(6)	-Cl(2)	-O(5)	111.4(6)	C(2)	-C(3)	-N(2)	121.4(9)
O(7)	-Cl(2)	-O(5)	110.2(7)	C(5)	-C(4)	-N(2)	103.8(9)
O(7)	-Cl(2)	-O(6)	109.2(7)	C(4)	-C(5)	-N(3)	105.5(9)
O(8)	-Cl(2)	-O(5)	109.2(7)	C(7)	-C(6)	-N(3)	110.4(10)
O(8)	-Cl(2)	-O(6)	108.9(8)	C(8)	-C(7)	-C(6)	114.3(9)
O(8)	-Cl(2)	-O(7)	107.8(10)	C(7)	-C(8)	-N(4)	110.7(10)
C(1)	-N(1)	-Ni(1)	130.0(7)	C(10)	-C(9)	-N(4)	105.2(9)
C(10)	-N(1)	-Ni(1)	113.0(6)	C(9)	-C(10)	-N(1)	102.3(9)

Estimated standard deviations are given in parentheses.

Table 7.4

Fractional atomic coordinates and temperature parameters.

Atom	x/a	y/b	z/c	Ueq
Ni(1)	20137(18)	26854(12)	-28659(18)	302(7)
Cl(1)	48223(38)	34320(26)	56042(42)	443(17)
Cl(2)	-1538(47)	18381(27)	-4783(44)	518(19)
O(1)	6021(14)	3776(9)	5254(16)	97(8)
O(2)	5110(15)	2357(9)	5514(18)	107(8)
O(3)	3132(13)	3659(10)	4380(19)	124(9)
O(4)	4943(23)	3958(13)	7330(17)	155(12)
O(5)	-1596(12)	1337(7)	-811(12)	70(6)
O(6)	3(13)	1765(8)	-2090(12)	82(6)
O(7)	-362(20)	2895(8)	366(18)	124(10)
O(8)	1396(16)	1359(13)	682(18)	136(10)
N(1)	236(11)	3779(7)	-3489(10)	27(4)
N(2)	3002(11)	3440(7)	-501(11)	32(4)
N(3)	3965(11)	1601(7)	-2178(11)	35(4)
N(4)	970(11)	1969(7)	-5391(11)	36(4)
C(1)	-415(14)	4534(8)	-2482(14)	31(6)
C(2)	455(13)	4677(8)	-518(13)	28(5)
C(3)	2260(15)	4207(9)	376(14)	36(6)
C(4)	4830(14)	3014(10)	502(15)	45(6)
C(5)	4819(16)	1804(9)	-155(16)	47(6)
C(6)	3647(16)	471(10)	-2958(17)	51(7)
C(7)	2818(16)	250(9)	-5025(16)	49(6)
C(8)	957(16)	807(9)	-5832(16)	48(6)
C(9)	-869(14)	2492(9)	-6225(14)	38(6)
C(10)	-735(16)	3678(9)	-5527(14)	41(6)

Estimated standard deviations are given in parentheses.
Coordinates $x10^n$ where n = 5,4,4,4 for P,O,N,C.
Temperature parameters $x10^n$ where n = 4,3,3,3 for P,O,N,C.

$[NiATH]_2^{4+}$, *vide infra*, is 1.344 Å[200]). This reflects delocalization of electron density on the π orbital. The delocalization also occurs to imine double bonds in the six-membered rings, average of which (1.301 Å) is longer than that (~ 1.26-1.27 Å) for π-electron-localized C=N bonds, but shorter than the average of single C-N bonds in the molecule (1.495 Å) and those (1.47-1.48 Å) frequently found in organic compounds. These imine bonds are more comparable with that, ~ 1.35 Å, found in heterocyclic system, e.g. pyridine, where nitrogen is in sp^2 hybridization, and its p_z orbital is used in the formation of molecular π orbitals. These delocalization characteristics are in accordance with a lower energy shift of C=N (1600 from 1650 cm^{-1}) and C=C (1410 from 1600 cm^{-1}) stretches in the IR spectrum. Consistently, carbon-carbon single bonds (C(1)-C(2) and C(2)-C(3)) on the diimine ring are shortened, in average, by ~ 0.074 Å in comparison with the rest of C-C bonds in the molecule ($d_{av}(C-C_{delocal})$ of 1.459 Å against $d_{av}(C-C_{local})$ of 1.533 Å). Average length of $C-N_{im}$ bonds, 1.498 Å, is slightly shorter than that of $C-N_{sec}$ bonds, 1.495 Å. The slight elongation (by ~ 0.010-0.015 Å in average, *vide supra*) of C-N single bonds compared with those in organic molecules is common for all transition-metal polyazamacrocyclic compounds, and occurs as a result of losing electron density from secondary nitrogen to the positively-charged metal ion. Bond lengths on other parts of the organic framework are all in agreement with what is generally

expected. The atomic distances in each one of four perchlorate groups are also in the normal range.

Ni(II) is coordinated in square planar geometry by four nitrogens in each macrocycle, with a very weak interaction from an oxygen atom in one of perchlorate groups (at a distance of 2.734 Å). Average bond distance between Ni and imine nitrogens, $d_{av}(Ni-N_{im})$, is 1.850 Å. This is shorter not only than that (1.933 Å) between Ni and secondary amine nitrogen, $d_{av}(Ni-N_{sec})$, in the molecule (as generally expected), but also, most significantly, than all $Ni-N_{im}$ bonds (in *neutral six-membered diimine ring*) so far documented in the literature. The average bond length of $Ni-N_{sec}$ is also somewhat slightly shorter than that (1.54-1.55 Å) observed in square planar Ni(II)cyclam and its derivatives (e.g., spiro-bis(Ni(II)cyclam)[201]).

As shown in Table 7.3, the angles around the three carbons in the diimine ring are all close to 120°, in agreement with in-plane sp^2 hybridization at these carbon centres. While sums of the bond angles around N(1) and that around N(2) are 359.5° and 359.7° respectively (again in accordance with in-plane sp^2 configuration), C(1)-N(1)-Ni (130.0°) and C(3)-N(2)-Ni (128.6°) angles are much expanded from 120°, accompanied by a decrease in C(10)-N(1)-Ni (113°) and C(4)-N(2)-Ni (113.1°) angles from 120°. The bond angles around Ni sum to 359.9°, consistent with the fact that the Ni atom is placed almost perfectly in the N_4 plane. However, the

91.5° of N(1)-Ni-N(2) angle is somewhat larger than expected considering that relative short C(1)-C(2) and C(2)-C(3) bonds and small N(1)-N(2) "bite", 2.651 Å, should give a reduced angle from ~ 92-93° observed in Ni(II)cyclam and its derivatives. Angles at atoms of the organic framework are all close to 109° (as expected for sp^3 tetrahedral configuration) except that of C(6)-N(3)-Ni(1) and C(8)-N(4)-Ni(1) which are somewhat larger (118° for both). In the four perchlorate anions the angles are normal for a tetrahedral structure of the Cl centre.

As a whole, the molecule may be regarded as a series of planes, which bend slightly (but not *twist*) from one and another. Fig. 7.1b shows an ORTEP drawing of this molecule at an angle of ~ 90° different from that in Fig. 7.1. From this figure, it can be seen clearly that the structure starts (from left to right) from plane(1) of C(6), C(7) and C(8), and then bends significantly to give plane(2) of N(3), C(6), C(8), and N(4). After plane(2), plane(3) with N(1), N(2), N(3), and N(4) turns back a little and is joined to plane(4) of N(1), C(1), C(3) and N(2) and the centre plane(5) of C(1), C(2), C(3), C(1′), C(2′) and C(3′) to continue to fold in this direction. The molecule then bends back to maintain its centre of symmetry, and in the end gives an "S" shape. In this view, the two N_4 planes are parallel to each other at a distance of 2.13 Å.

In the centre plane, (5), the six carbons are all almost

perfectly co-planar (estimated standard deviations are less than 0.012 Å), as expected from sp^2 hybridization at C(2) and C(2′). Similarly, four nitrogens show very little, if any, tetrahedral deviation from their mean plane, (3), (displacement of ≤ 0.003 Å), which is somewhat unusual since most square planar tetraazamacrocyclic Ni(II) complexes have some degree of tetrahedral distortion except those in highly conjugated systems. The distance of Ni^{II} to the plane is only 0.046 Å, consistent with the in-plane form derived from the above bond-angle analysis.

Discussion

It is very interesting to compare the structure of the present molecule with that of $[NiAT]^+$,[108] and $[Ni(II)_2(1,1'$-bi(2,13-dimethyl-3,6,9,12-tetraazacyclotridecan-2,12-dienylidene))], $[NiATH]_2^{4+}$ (6):[200]

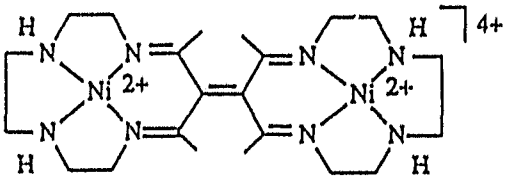

6

The common feature among these three molecules is that they all have a six-membered ring which contains six p_z orbitals ($4p_z$ from Ni and five $2p_z$'s from two N_{im}'s and three carbons). As far as this six-membered ring is concerned, the structural features in the present dimer lie very well between those of

the other two, which represent two extremes of delocalized (in $[NiAT]^+$) and localized (in $[NiATH]_2^{4+}$) diimine rings. Data concerned are listed below in Table 7.5.

Table 7.5

	$[NiAT]^{+\,188}$	$[NiATH]^{4+\,200}$	$[Ni_2(L4)]^{4+}$
d_{av} of Ni–N_{imino} (Å)	1.83	1.887	1.850
d_{av} of C=N (Å)	1.34	1.271	1.297
d_{av} of C–C (Å)	1.40	1.501	1.459
d_{total} (Å)	9.14	9.316	9.214

In addition, while the ring in $[NiAT]^+$ was found to be almost perfectly planar, the corresponding ring in the present compound is in a "boat" shape with about 150° angle between plane(5) and plane(3). Although the accurate shape of the sp^2 ring in $[NiATH]_2^{4+}$ is not reported in the literature, from the displacement of 0.55 Å of the β-carbon out of the C=N plane it is reasonable to estimate that the angle between the plane of Ni and two imine nitrogens and that of three carbons is less than 150°, in other words, the ring is much more severely bent (which has been ascribed to the steric effect between the methyl groups across the bridge) than that in the present case.

These results and the structural features in the present dimer complex may be best interpreted in terms of aromatization of $^{Ni}4p_z$ and five $2p_z$ orbitals. In $[NiATH]_2^{4+}$,

there are six electrons on conjugated p_z orbitals of the chelate, and large electron density cloud on the chelate makes it easy for $4p_z$ to overlap with ligand π orbital. Thus, the empty $4p_z$ orbital of Ni can readily take part in the conjugation, giving rise to stable (4x2 + 2) system. To gain the best overlap and aromatic stabilization energy, Ni stays in the ring plane and gains net electron density (as evidenced by short $Ni-N_{im}$ length). Indeed, the stabilization energy it gains from aromatization is so great that it distorts all the bond angles of the chelate ring (the angle is enlarged from 120° to 124 - 128°) in order to accommodate the Ni into the ring plane (the angle of $N_{im}-Ni-N_{im}$ is also enlarged to 99.7°, which is unusually high for a NiN_4 system). Similar results were also observed in other Ni(II)-dieno(-) systems, such as [Ni(PnAO)-6H]°.

In the present molecule, although it has the orbital requirements needed for an aromatic system, the number of electrons (five on the chelate) is less than 6. Clearly, in order to form a stable aromatic system, the π orbital on the ring has to derive some electron density from the Ni through $4p_z-3d_{xz}, 3d_{yz}$ mixing (indeed, EHMO computation performed on the conjugated π ring orbital of [Ni(PnAO)-6H]° showed the metal orbitals used in overlap are the 4p and $3d_{xz}$, $3d_{yz}$ orbitals[190]).

Evidence for the electron density donation from Ni to the "quasi" aromatic π orbital in the present system is provided from the bond length calculation of total six-membered ring.

In an approximate way, removal of electron density from one bond to another will increase the length of the former and decrease that of the latter, but the total length should not change, at least not much. In comparison with the total ring length in $[NiATH]_2^{4+}$ (which is assumed to be "totally" localized), the total ring length in present molecule decreases by ~ 0.102 Å (Table 7.5). Even after taking account of delocalization on the bridge (which shares the electron density with the ring), it still gives a difference of about 0.0735 Å, which is a quite significant amount considering that the total ring length in $[NiAT]^+$ (which gains one electron in the chelate) decreases ~ 0.074 Å from that in the present molecule and 0.176 Å from that in $[NiATH]_2^{4+}$. This decrease is obviously due to an increase of the electron density in the ring, which must come from the Ni through $4p_z-\pi_{chelate}$ mixing, or overlap.

A consequence of this donation is that it is necessary for the Ni to gain (or the molecule has to organize itself to offer) some "more" electron density to compensate for the loss (or "assists" in the aromatization) through other means. For this, an in-plane form is chosen for the four nitrogen donors so that the Ni is able to provide the best overlap. Also to serve this purpose, a bond-angle of ~ 90° for N(1)-Ni-N(2) is required in order for Ni to receive electron density via σ bonding through the optimum overlap (which is also partially responsible for short $Ni-N_{im}$ bondlength). Furthermore, the Ni

also requires to gain electron density from the two secondary nitrogens. Although the five-membered chelate rings on the two sides prevent the formation of an optimum bond angle at the Ni (N(3)-Ni-N(4) angle is 95.4°, table 7.3), this requirement does shorten the length of Ni-N_{sec} (*vide supra*). This shortening causes N_{sec} to mix more s component into its sp^2 orbital which is bonding with the Ni atom. For the same reason described below, this mixing leads to some degree of increase in the Ni-N_{sec}-C angle, which is indeed observed (*vide supra*).

In order for the ring to form an aromatic system, the $^{Ni}4p_z$ orbital has to overlap with tne chelate π orbital made of the five $2p_z$ orbitals. However, the bond distance between the Ni and the N_{im} is likely too distant for a conventional p-p parallel overlap. Therefore, the Ni atom "bends" so that at least one side of its $4p_z$ is able to overlap largely with the chelate π orbital. Thus, the six-membered ring adopts a "boat" shape rather than a "chair" shape, as a result of uneven distribution of the π electron density on two sides of the ring plane (note that without Ni-ligand interaction and the uneven distribution, the two nitrogens and three carbons should be in the same plane to reach better conjugation, and hence, the ring should be, at least, a "L" shape instead of "boat" shape, which is not observed).

The "abnormal" angles around the imine nitrogens may be explained in the following terms. To draw the Ni atom as close as possible to the chelate so that the aromatization can be

maximized, the nitrogen reorganizes its sp^2 orbitals in such a way that the sp^2 orbital bonding to the Ni atom gains more s component and the sp^2 orbital forming the N-C single bond has more p component. There are two consequences from this reorganization: the first is reducing the length of the N-Ni bond, and increasing that of the N-C single bond (indeed this $N(sp^2)$-C single bond has a average of 1.498 Å which is even slightly, but significantly, longer than the average length, 1.495 Å, of the $N(sp^3)$-C single bonds in the molecule); the second is that with a smaller amount of p component the Ni-N bond tends to have an angle closer to the sp type bonding. Also with less of an s component, the N-C single bond tends to have an angle closer to the sp^3 type bonding, both with regard to the C=N bond. Therefore, the angle between the N-Ni and N=C bonds increases and that between the N-C and N=C decreases. It appears that the five membered ring on the N-C side prevents it from bending too close to the C=N bond so that a decrease in C-N=C angle from 120° can not match up with the increase in Ni-N=C angle, which then results in a larger increase (~ 10°) in the Ni-N=C angle from 120° and a smaller decrease (~ 7°) in the Ni-N-C angle from 120°. The average length of $N(sp^2)$-C is longer than that of $N(sp^3)$-C, and can also be interpreted accordingly.

One of most common features in aromatic system is that "longer" bonds are reduced and "shorter" ones increased. The amount of this change is often indicative of aromaticity. The

larger the change, the higher the aromaticity. It is considered that the structure of $[NiATH]_2^{4+}$ represents the bond lengths for the "normal" C-N, C=N and Ni-N (which are totally "localized") bonds, which is probably the case. The changes in these bond lengths in the "totally aromatic" ring system, $[NiAT]^+$, are - 0.101, + 0.069, and - 0.056 Å ("-" for decrease and "+" for increase), and in the present molecule are - 0.042, + 0.026, - 0.035 Å in the order of the C-N, C=N and Ni-N bonds. This comparison, though very much simplified, suggests that the ring in the present system has about 50% aromaticity against that in $[NiAT]^+$ system. This is roughly in agreement with the electron contributions. That is, if one looks at the way that for a six-membered ring/four-electron system (which is the case in $[NiATH]_2^{4+}$) has no aromaticity and the six-electron system (which is the case in $[NiAT]^+$) has the maximum of aromaticity (100%), then the five electron system (in present case) is intermediate (Although the five p_z electrons from the chelate can not contribute totally to the aromatization in present system (*vide supra*), the electron density donated from the Ni centre may compensate so that electron density of about five can be achieved).

Of interest also is the comparison between the molecular structure of the present dimer species with those of Ni(II) cyclidene complexes where the molecule has two six-membered dimine ring opposite to each other on the ligand. In recent years, Busch et al.[202-204] have synthesized and

crystallographically identified a number of such complexes in their effort to mimic the biological function of dioxygen-carriage. For those complexes, there is no aromatization between $4p_z$(Ni) and ligand π_p orbitals because it is structurally forbidden. Therefore, the structural features in those ligands are all typical of ligand-based delocalization with average of Ni-N bond length about 1.875 Å[202] (which is slightly, but significantly, longer than 1.850 Å in the present system). Further, even where the chelate on the cyclidene is deprotonated to give a dieno(-) type chelate, the electron density is very much delocalized on the chelate (from bond-length and bond-angle analyses) and the average bond length of Ni-N is ~ 1.860 Å[202] (which is even longer than that in the present *neutral* system!). Here again, the evidence is supportive of the presence of aromaticity in the present unsaturated dimer (and as well as $[NiAT]^+$).

Much of the discussion above is focussed on the "quasi" aromatic nature of two unsaturated cyclic rings of the molecule. However, it is also important to realize that the "quasi" aromatic system is, indeed, "quasi". That is, the stabilization energy gained from aromatization is not very large (due to deficiency of electron density, < 6), and could not totally convert the conjugation on the ligand to two "cyclic" π rings. As result of this, taking the molecule as a whole, molecular π, π_M, system in the molecule actually adopts a form which is a compromise between ligand-based conjugation

π, π_L, orbital (one extreme) and two aromatic π, π_{ar}, orbitals (another extreme). In other words, the π_M may be regarded as combination of two components: π_{ar} and π_L. Because of electron deficiency, the two components are comparable, and therefore, one sees unusually shortened Ni-N bonds due to aromaticity (from π_{ar} component, or contribution) and a double-bond character on the bridge (from π_L component, or contribution). This combination also manifests itself in its chemical behavior, which will be discussed later.

7.4 UV/Visible Spectra and Solution Chemistry

7.4.1 UV/Visible Spectra

In aqueous media, electronic spectrum of $[Ni_2(L4)]^{4+}$ dimer species was characterized by a very intense absorption band at visible region ($\lambda_{max} \approx 520 - 550$ nm, and $\varepsilon > 10^3$ $M^{-1}cm^{-1}$), together with the first UV band at 280 nm ($\varepsilon \approx 1.5x10^4$ $M^{-1}cm^{-1}$), and the second at ~ 200 nm ($\varepsilon \approx 1.7x10^4$ $M^{-1}cm^{-1}$). Accurate ε values, particularly that of the visible band, may be obtained only in acidic media because of instability of the species in near neutral and basic media (*vide infra*). In 1.0 M $HClO_4$, $\varepsilon_{520\ nm} = 6.5x10^3$ $M^{-1}cm^{-1}$.

The wavelength maximum, λ_{max}, of the visible band was, to some extent, influenced by the nature of counter-ion present. The results from solutions of different anions are presented in Table 7.6. In presence of anions such as NO_3^-, SO_4^{2-}, or F^- the λ_{Max} of the visible band was little difference from that in

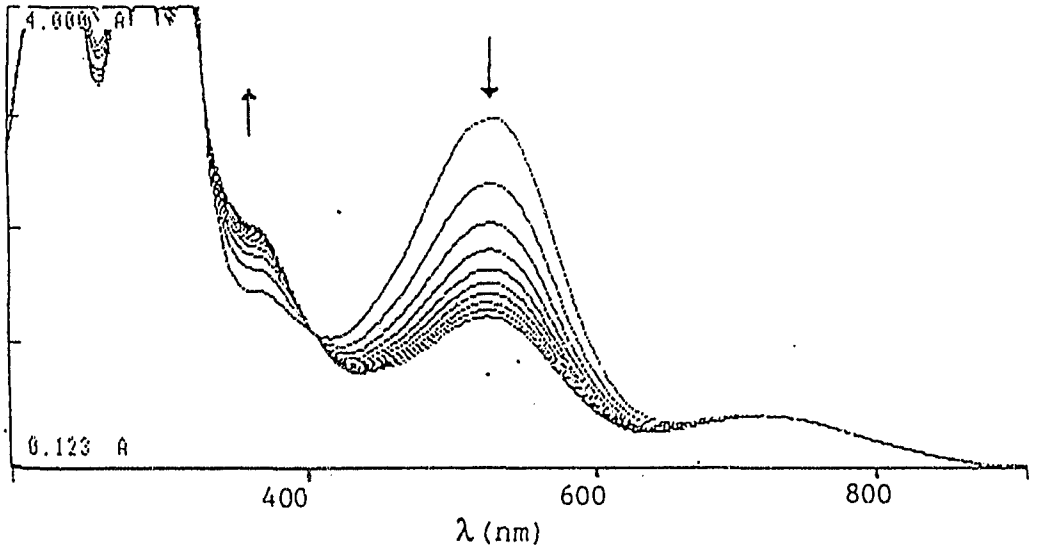

Fig. 7.2 UV/Visible spectra of $[Ni_2(L4)]^{4+}$ in H_2O (scan/5 min.)

Table 7.6 Results from Visible Spectropic Study in H_2O

X^{-n} (1.0 M) (a):	H_2O	ClO_4^-	NO_3^-	SO_4^{2-}	F^{-a}
λ_{max} (nm) (b):	528	520	526	526	528
(a):	SCN^-	Cl^-	Br^-	I^-	CH_3CN^b
(b):	534	534	539	547	515

[a]0.5 M; [b]in CH_3CN.

the water-only solvent. However, as the halide anion was changed from F^- to I^-, the λ_{max} underwent steady "red-shift" from 528 to 547 nm, consistent with the normal spectrochemical order.[5] This not only indicates the presence of an axial

coordination on Ni(II) centres with these halides (including SCN^-), but also implies that the absorption is probably due to electron excitation from the metal d_{z^2} orbital to the lowest unoccupied π_M orbital (π_{LUMO}), since a increase in the axial bonding (as the anion changes from Cl^- to I^-) leads to a increase in the orbital energy of d_{z^2} and, hence, reduces the transition energy of $d_{z^2} \rightarrow \pi_{LUMO}$. In the case where nitrate, sulfate, or fluoride ion was used, the axial coordination was relatively weaker.

The λ_{max} of 520 nm obtained in perchlorate media is the highest (in energy) among all, in aqueous solutions. The reason for this is not clear, and has perhaps to do with the special preference of perchlorate as counter anion by the dimer during its crystallization.

The results from CH_3CN solvent are also presented in the table 7.6. The "blue-shift" of the visible band, λ_{max} = 515 nm, in this organic solvent is likely due to a difference either in solvent coordination, or solvation from that in the case of aqueous media.

7.4.2 Hydrolysis of $[Ni^{II}_2(L4)]^{4+}$ in Aqueous Solution:

In neutral aqueous solution and without the presence of any supporting electrolyte, the dimer species was not stable, and slowly ($t_{1/2}$ of ~ 25 min.) converted to a yellow species with a relatively very weak shoulder peak at λ_{max} of 380 nm, Fig. 7.2. The isosbestic point at 405 nm indicates the

conversion does not have any intermediate and/or any decomposition involved. Addition of perchloric acid *before*, or *shortly* after, the purple solution totally disappeared, reversed the process of conversion and about 100% starting material was recovered. The spectra from the process showed the same isosbestic piont, reflecting a reversible nature of this process. However, when the yellow solution formed was left to stand for a long period, only partial recovery of the initial dimer species was possible by acidification.

A detailed study of the solution chemistry of $[Ni^{II}_2(L4)]^{4+}$ species was carried out spectroscopically in varous media. In H_2SO_4/Li_2SO_4 (**I** = 1.0 M), as the pH was increased from <1 to ~ 6, the spectra showed a steady decrease of both the visible peak and the first UV peak with two isosbestic points at about 405 and 310 nm respectively, and a new shoulder peak emerged at about 380 nm (Fig.7.3a). From pH of ~ 6 upwards, both peaks continued to diminish, and the isosbestic piont at 310 nm was not observed. The absorption at this wavelength started to decrease, indicating another chemical process which begins to occur at pH of ~ 6. At pH ≈ 8.5, the visible band at 530 nm disappeared, but the first UV band still has about one third of its initial intensity (Fig. 7.3a). As pH was increased to ~ 12, the absorption at 310 nm decreased and the shoulder peak mentioned above gradualy shifted to lower wavelength and appeared as a clean peak at ~ 320 nm (Fig. 7.3a, b). Further increase of pH above 12 did not affect the peak at 320 nm, but

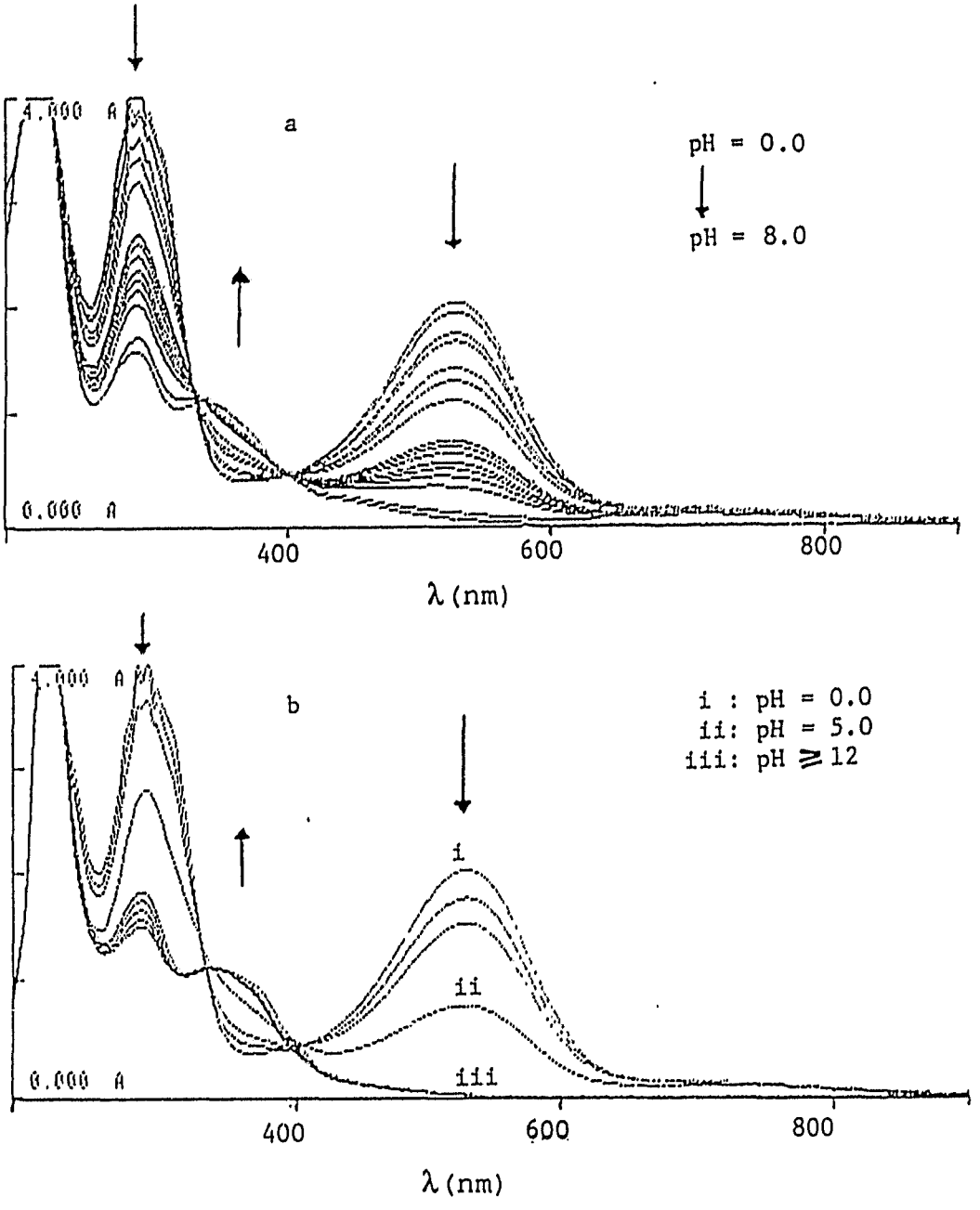

Fig. 7.3 UV/Visible spectra of $[Ni_2(L4)]^{4+}$, pH-dependent studies in H_2/Na_2SO_4 media (I = 1.0 M): (a) pH = 0.0 to 8; (b) pH = 0.0 to >12.

only decreased slightly the first UV peak at 280 nm (Fig. 7.3b).

The observation described above may be understood in terms of H_2O hydrolysis on the C=C bridge. As shown in Scheme 7.3, addition of H_2O on the C=C bridge forms a species **VI**, which has two diimine rings with a C-C single-bonded bridge. This hydration, together with a following deprotonation (Scheme 7.3), accounts for the disappearence of the visible band (the π_M orbital is destroyed by this process) in the weakly acidic media (pH of ~ 1 - 6). At higher pH, the deprotonated dieno(-) species **VII** becomes dominant. For this species, the aromatic ring (or dieno(-) chelate) generates a stronger in-plane field than the diimine ring, and hence, moves the d-d band (380 nm) from **VI** to higher energy, or lower wavelength, (320 nm). In a very basic solution of pH ≥ 12, the hydroxyl group on **VII** may be deprotonated, which does not affect significantly the d-d band at 320 nm.

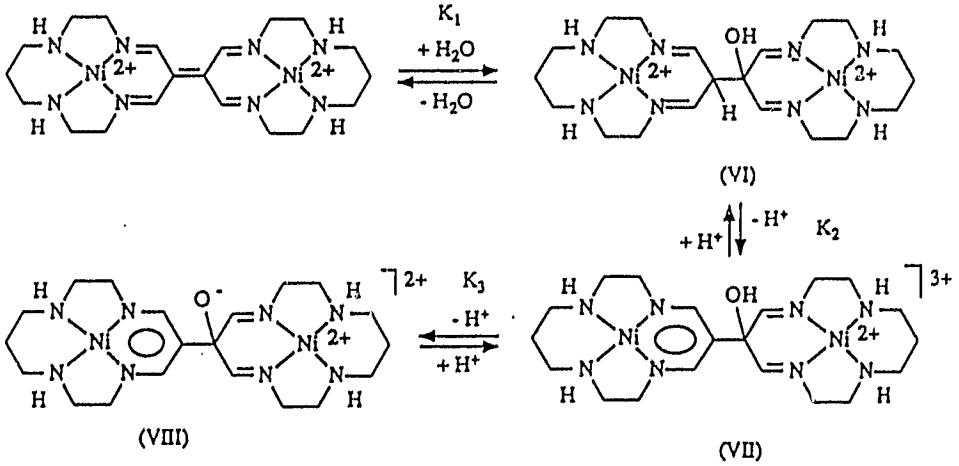

Scheme 7.3 Mechanistic scheme of hydrolysis of $[Ni_2(L4)]^{4+}$

Apparently the first UV band at ~ 280 nm is due to a charge transfer (CT) between metal centre and the imine nitrogens. The H_2O hydrolysis affects much on this transition by destroying the π_M system. The deprotonation process is also expected to influence this band to some extent since it changes the diimine ring to an aromatic ring (dieno(-) chelate). The effect of deprotonation of the hydroxyl group on this band is likely to change the electron-density on the diimine ring.

A detailed study showed that the hydrolysis process of $[Ni^{II}_2(L4)]^{4+}$ appeared to be influenced by the presence of different supporting electrolytes. In perchlorate media, the purple conjugated dimer was stabilized at pH $\leq$ 3 by increasing $[H^+]$ concentration, but disappeared quickly at pH $\geq$ 5.5. However, in both sulfate and nitrate media the hydrolysis was apparently base-catalyzed in the pH region 2 - 6.

Attempts were also made to obtain the pK_a values for the two deprotonation processes using both spectroscopic and potentiometric titrations. Unfortunately, the inertness of the first-step during the hydrolysis and instability of the deprotonated species **VII** and **VIII** resulted in a lack of success. Nevertheless, the results obtained above do allow us to estimate the $pK_{a,1}$ of the first deprotonation to be in the neighbourhood of 5 (or 4 - 6), and $pk_{a,2}$ of the second ~ 12, which are consistent with the results from electrochemical investigations (*vide infra*).

7.5 Electrochemistry:

Electrochemistry of $[Ni^{II}_2(L4)]^{4+}$ was studied using cyclic voltammetry in both CH_3CN and water. In CH_3CN, $(t\text{-}Bu)_4NClO_4$ (0.10 M) was used as supporting electrolyte and $Ag/AgNO_3$ (0.010 M $AgNO_3$) as reference electrode. The study in aqueous media was carried out using Ag/AgCl (in saturated KCl) as reference electrode. Unless specified otherwise, the potentials used in following discussion are referenced to $Fc^{+/0}$ (0.400 V *vs* NHE) for those from acetonitrile solvent studies, and Ag/AgCl (0.222 V *vs* NHE) for those from aqueous studies.

7.5.1 Oxidation:

In water, only a weak anodic shoulder peak at about 0.9 V was observed from oxidation at metal centre, and no cathodic wave was present, indicative of a EC process with rapid chemical decomposition following the electrochemical oxidation. This electrochemical behaviour is common for metal-centred oxidation of diimine chelated Ni(II) complexes.[189] Electrochemical behavior of the dimer compound towards oxidation may be better studied in CH_3CN. In this solvent a quasi-reversible wave with characteristics of $\alpha = 0.5$ (symmetric waves, see section 2.3) appeared at $E_{1/2}$ of 1.06 V (Fig. 7.7). These redox peaks were sensitive to scan rate even at low scan rate (< 20 mV/s), indicating the redox was likely metal-centred. The highly conjugated ligand makes it difficult for the inner-shell reorganization of donors around nickel

centre to occur, and hence, the electron transfer at the metal centre was not able to compete with the current flow and scan rate.

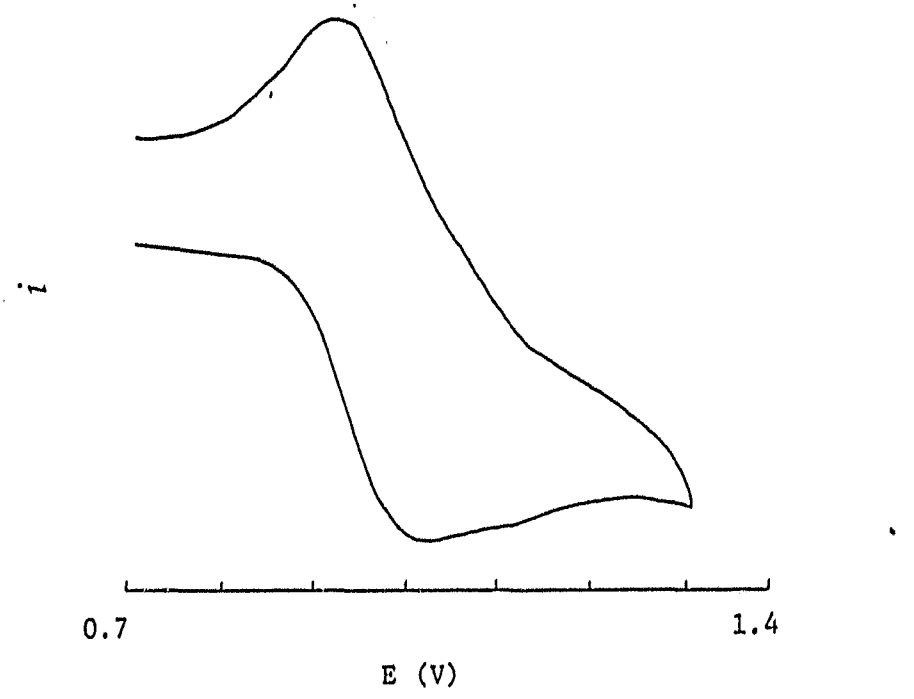

Fig. 7.4 CV of oxidation of $[Ni_2(L2)]^{4+}$ in CH_3CN.

The most interesting feature in the CV is that only one redox peak was observed in the range from 0.5 to 1.4 V. It was known that for a molecule with two reactive centres, M-M, if the electron tranfer processes on these two centres are both reversible, the difference in the redox potentials, ΔE, for

$$M\text{-}M \overset{E^\circ_1}{\rightleftharpoons} M\text{-}M^+ + e \overset{E^\circ_2}{\rightleftharpoons} M^+\text{-}M^+ + 2e \qquad (\Delta E = E^\circ_2 - E^\circ_1)$$

is related to the equilibrium constant K_c of the comproportionation equation

$$M\text{-}M + M^{+}\text{-}M^{+} \overset{K_c}{\rightleftharpoons} 2\,[M\text{-}M^{+}]$$

by

$$K_c = 2\,[M\text{-}M^{+}] / ([M\text{-}M]\,[M^{+}\text{-}M^{+}]) = \exp(\Delta E F/RT)$$

In the case of two equivalent non-interacting metal ion centres, undergoing successive one-electron oxidations, ΔE should be 35.6 mV, *i.e.* $K_c = 4$. The value of K_c reflects the stability of the mixed valence species, $M\text{-}M^{+}$, in the situation where the interaction occurs.

Considering this, the appearance of only one coupled-wave may result from two possible processes. Either, the binuclear species underwent a two-electron one-step quasi-reversible process which shewed a wider peak-separation, ΔE_p, than that, $58/2 \approx 29$ mV expected; or, it proceeded through one-electron two-step electron transfer with interaction of the two reaction centres, which destabilized the intermediate to give a small ΔE value so that the two peaks merged into one. Considering the presence of a highly conjugated system between the two Ni(II) centres, the latter possibility is more likely. However, more work is needed to further distinguish these two possible mechanisms (e.g. differential pulse polarographic and coulometric experiments).

7.5.2 Reduction

Reduction of the conjugated dimer complex gave rise to two reversible couples in both CH_3CN and H_2O media (a typical CV is showed in Fig. 7.5), and the results are provided in the

Table 7.7 Results from Cyclic Voltammetry
(for conditions see section 7.4)

	Reduction		Oxidation
	$E_{1/2}^1$ (V)	$E_{1/2}^2$ (V)	(V)
$[Ni^{II}_2(L4)]^{4+}$ in CH_3CN[a]	0.19	-0.03	$E_{1/2}$ = 1.06[b]
$[Ni^{II}_2(L4)]^{4+}$ in H_2O[c]			
1.0 M NO_3^-	0.18[c]	-0.01[c]	E_{ap} = 0.96[d]
1.0 M Br^-	0.18	-0.03	
VII in 1.0 M $NaNO_3$ (pH ≈ 6 - 12)			E_{ap} = 0.6[d]
VIII in 1.0 M $NaNO_3$ (pH ≥ 12)			$E_{1/2}$ = 0.45[b]

[a]vs. Ferricinium/Ferrecene; [b]quasi-reversible with $\alpha \approx 0.5$; [c]vs. Ag/AgCl in saturated KCl (~ 0.22 V vs. NHE); [d]irreversible peak, and only anodic peak was observed.

Table 7.7. As discussed later, both of these reductions were on the π conjugated system and a reaction scheme accounting for the electron-transfer processes is presented in Scheme 7.4. In water solvent, potentials for the first reduction ($E_{1/2}^1$ = 0.18 V) were the same in both Br^- and NO_3^- media, consistent with the structure suggested for the one electron-reduced species, **IX**, in Scheme 7.4 where the electron was delocalized in π_M orbital.

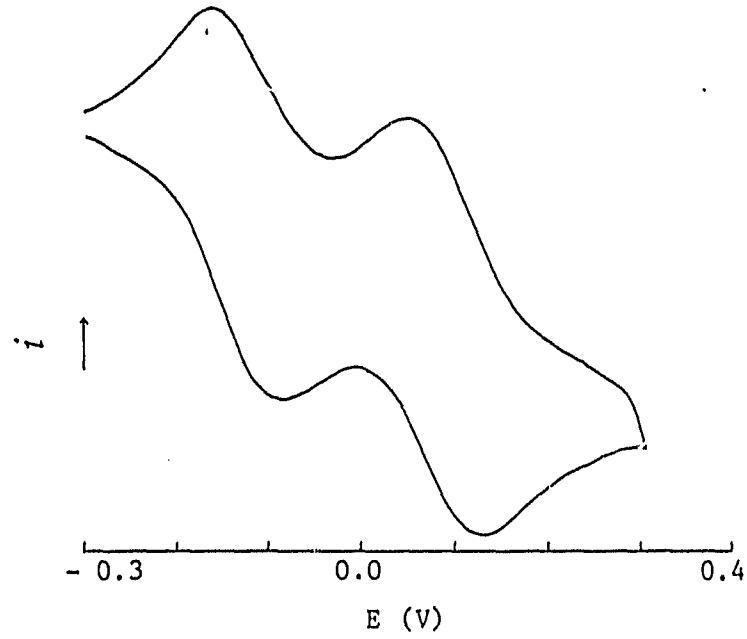

Fig. 7.5 CV of reduction of $[Ni_2(L4)]^{4+}$ in CH_3CN.

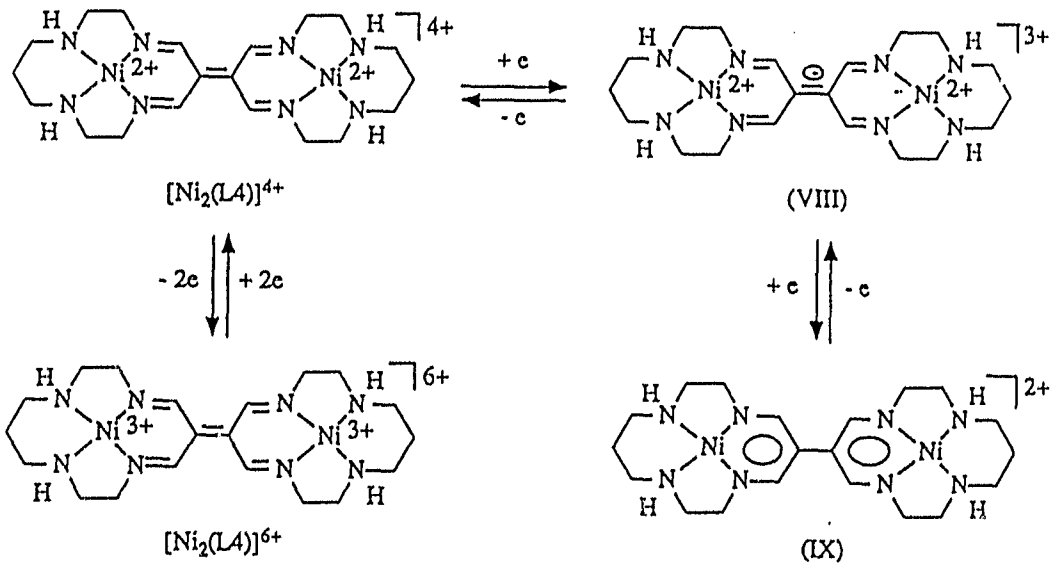

Scheme 7.4

However, the potential for the second reduction ($E_{1/2}^2$) varied from -0.03 V for Br^- to -0.01 V for NO_3^-, shifting about 20 mV. This shift is supportive for the structure proposed forthe second-reduction product, **X**, (Scheme 7.4) in which two electrons are separately located in two "aromatic" rings. Formation of these "aromatic" rings changes the ligand field around the metal centre, and the axial coordination change of Ni(II), therefore, may affect the reduction potential. It was observed spectroscopically (*vide supra*) that bromide ion showed a stronger axial coordination than nitrate ion. This axial stronger coordination, in general, tends to weaken the in-plane field (as in the case of the Cu(II) complexes, see section 5.4), which makes it more difficult for a stronger in-plane field to be formed. As a result, the second reduction (which leads to stronger in-plane field) became more difficult as the axial donor changed from nitrate to bromide, and in presence of the latter ion **IX** is stabilized by ~ 20 mV against reduction.

In CH_3CN, reduction of the unsaturated dimer showed the first redox couple with $E_{1/2}^1$ of 0.19 V and the second with $E_{1/2}^2$ of - 0.03 V. Considering the redox potential of $Fc^{+/0}$ is 0.40 V *vs* NHE, the first reduction potential of the complex gives a $E_{1/2}^1$ of 0.59 V vs NHE, which shows that the unsaturated dimer may be regarded as a moderate oxidizing reagent (indeed, it can oxidize I^- easily in CH_3CN solvent). There was no further reduction observed as the CV was performed from - 0.1

to - 1.4 V, consistent with the stable two-aromatic-rings structure of **X** and also indicating that the nickel(II) centres were very much stabilized by these two rings.

7.5.3 pH-Dependent Study

To compare the results obtained from spectroscopic studies and also confirm the mechanism proposed in Scheme 7.2, the electrocemical behaviour of the unsaturated dimer $[Ni^{II}_2(L4)]^{4+}$ in water was also investigated at different pH using cyclic voltammetry (in a range from - 0.2 to 0.9 V) in $H/NaNO_3$ media (1.0 M). At low pH ($\leq$ 4), only two reversible peaks for the reductions of the unsaturated dimer were observed, see Fig. 7.8a. From pH 4 to 6 these two peaks gradually disappeared, indicating a diminution of the starting material and increase in concentration of species **VI**, and/or more likely, **VII**. In the range of pH = 6 to 12, a peak corresponding to oxidation of the deprotonated dieno(-) species **VII** began to grow at ~ 0.6 V without association of any cathodic peak, Fig. 7.8b. After pH reached to ~ 12, the prevous irreversible peak was replaced by symmetric quasi-reversible coupled peaks at ~ 0.45 V (Fig. 7.8c), resulting from oxidation of hydroxyl-deprotonated species **VIII**. Reversing the process by adding nitric acid stepwise until pH $\leq$ 1 gave the similar changes at all related pH regions. The pH-dependent study in H_2/Na_2SO_4 media showed a similar electrochemical behaviour for the dimer species. The processes

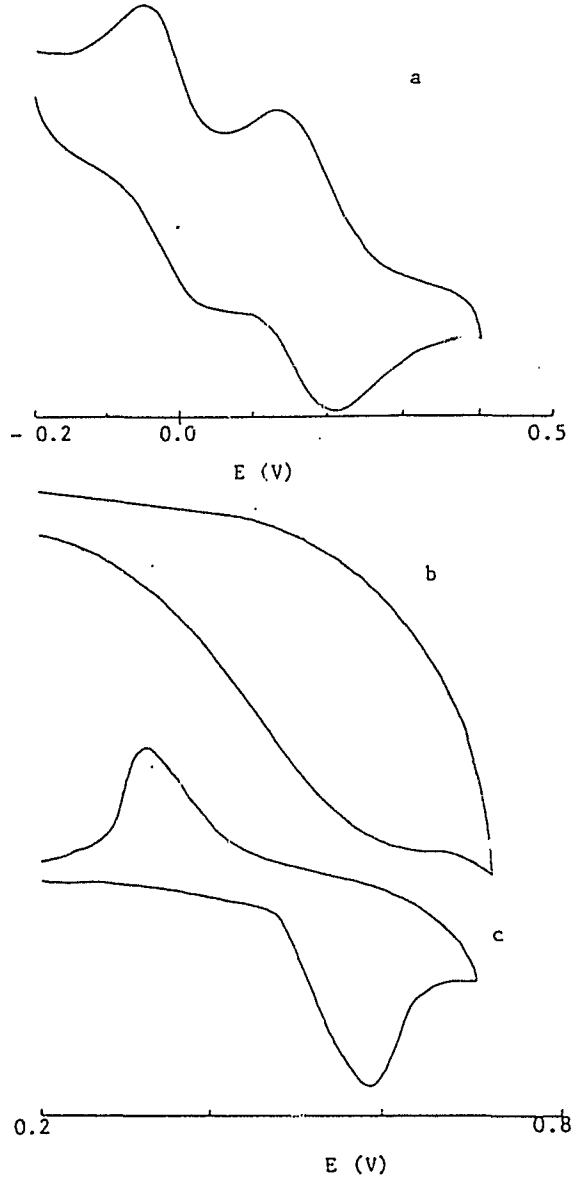

Fig. 7.6 CV from pH-dependent studies: pH = (a) 3; (b) 10; (c) 12.

involved in this system are illustrated schematically in Scheme 7.5.

The fact that no redox reaction was observed from the species **VI** in the potential region of study was consistent with both its low concentration and the results obtained from other similar diimine Ni(II) complexes (e.g. CV of $[Ni(II)(Me_2[14]4,7\text{-dieneN}_4)]^{2+}$ showed only one anodic peak at 10.04 V in chloride media and 10.12 V in perchloride media,[189] which are outside the range in the present study). The electrochemistry observed for the species **VII** is of normal expectancy for dieno(-)-type aromatic complexes of this type (which usually have a ligand-based oxidation at $E_{1/2}$ = ~ 0.4 - 0.8 V *vs* NHE, or E_{pa} = ~ 0.5 - 1.0 V *vs* NHE, as discussed in section 1.1.4). Perhaps, the best comparable example for this is complex ion of $[Ni(II)(Me_2[14]4,7\text{-dieno(-)N}_4]^+$. Cyclic voltammetry of this species give a single irreversible anodic peak at 0.55 V *vs* SCE in DMF (~ 0.8 V *vs* NHE),[189] which is very comparable with E_{pa} of ~ 0.82 V *vs* NHE in the present case. The species **XI**, formed from oxidation of **VII** (Scheme 7.5), is generally unstable, and probably undergoes decomposition or dimerization to a unreactive product. As a result, a EC process with a chemically irreversible pathway was observed. It was somewhat surprising to see that the doubly deprotonated species **VIII** showed a *quasi-reversible* behaviour with i_{pc}/i_{pa} ≈ 1. The possible explanation for this is that the electron-transfer was followed by a chemical process, that is, the

oxidation product **XIIa** was stabilized by internal O^- attack on the radical carbon forming a negatively charged epoxy ring, **XIIb** (Scheme 7.5), which was probably stable enough in the CV time scale and gave $i_{pa}/i_{pc} \approx 1$. The lower oxidation potential

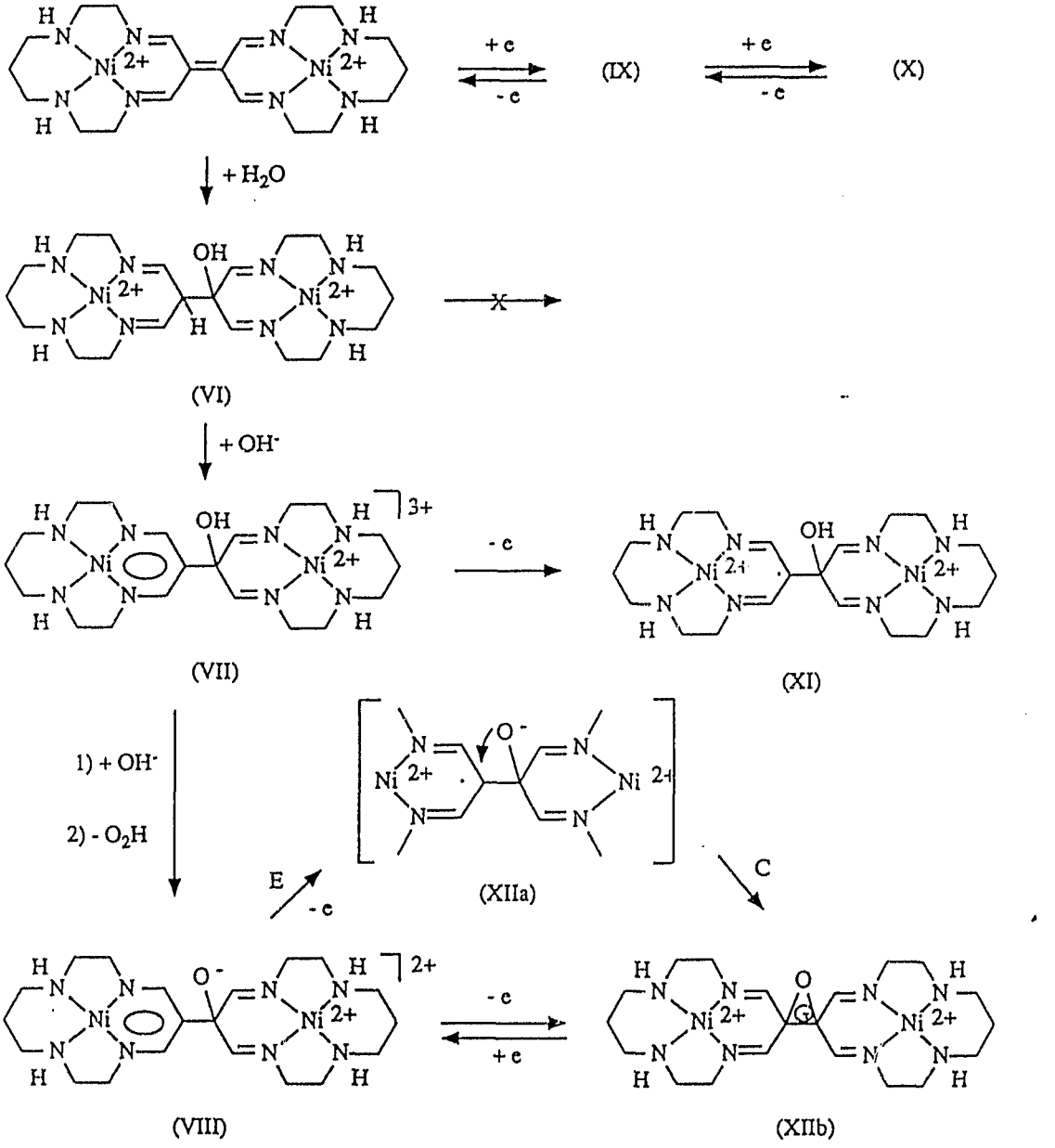

Scheme 7.5 Scheme for the electrochemical pH-dependent study.

of **VIII** than that (estimated from E_p) of **VII** is probably due to greater negative-charge on the ligand framework. Nowever, $E_{1/2}$ = 0.45 V in **VIII** still comparable with that in other similar systems.

The results above obtained from both electrochemical and spectroscopic investigations are all consistent with the mechanism proposed in Scheme 7.5 for the hydrolysis of $[Ni_2(L4)]^{4+}$ dimer in water solvent. Furthermore, the observations from the electrochemical investigation are also consistent with the estimations made for the two deprotonation constants, that is, $pK_{a,1} \approx 5$, and $pK_{a,2} \approx 12$.

7.6 Chemical Redox Reactions

7.6.1 Oxidation

The Ni(II) dimer can be oxidized either electrochemically (as already described above) or chemically. For the chemical oxidation, the oxidizing reagents may be Co_{aq}^{3+} or $Na_2S_2O_8$ in acidic aqueous media and NO^+ in acetonitrile. Consistent with the result from electrochemical study, the esr spectrum of this oxidation product in both solvents was characteristic of a tetragonal-elongated low-spin Ni(III) (indicating that the oxidation was of metal-based) without appearence of metal-metal interaction. In CH_3CN, the spectrum showed five shf-coupling peaks ($A_{\parallel}$ = 20 G) from two axially-coordinated solvents, and was almost identical to that of Ni(III)cyclam under the same conditions (both having $g_{\parallel}$ = 2.025, $g_{\perp}$ = 2.177

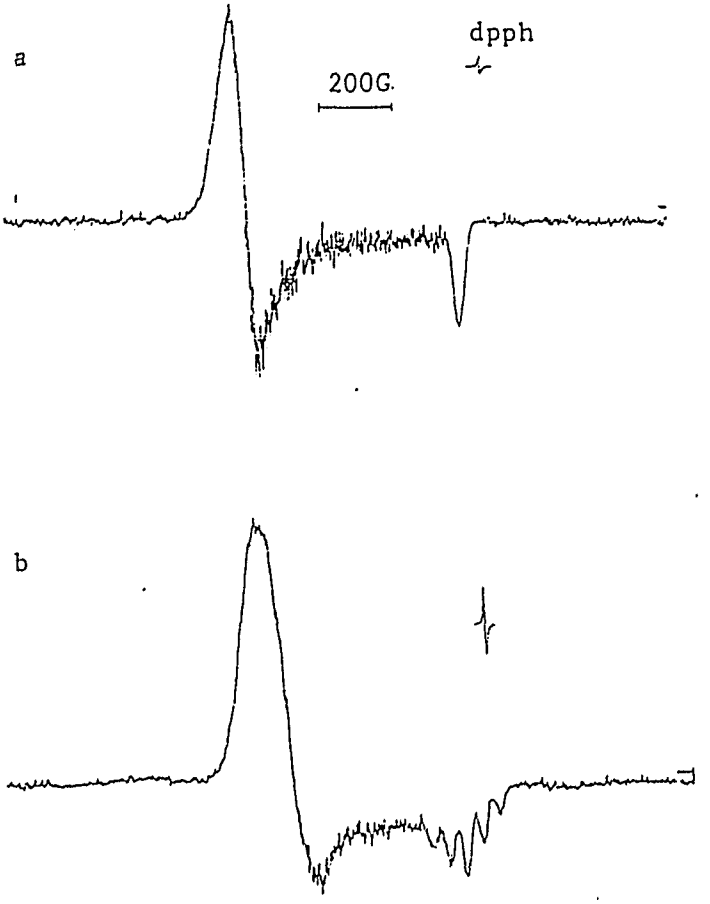

Fig. 7.7 ESR spectra of $[Ni(III)_2(L4)]^{6+}$ (frozen solution, 77 K) in: (a) 1.0 M HNO_3; (b) CH_3CN.

and the same shf-coupling constant) (Fig. 7.7a). The esr from 1.0 M nitric acid solution also contained axial symmetry, with $g_{/} = 2.022$ and $g_{\perp} = 2.287$ (Fig. 7.7b).

The oxidation product from both solvents was not stable, and the green color disappeared usually in less than a minute. This highly unstable nature makes it difficult to further investigate its chemical reactivity.

7.6.2 Reduction

Chemical reduction of the unsaturated dimer, characterized by deep-green coloration, can be readily achieved using reducing reagents such as ascorbic acid, Zn dust, Fe^{2+}, $[Co(phen)_3]^{3+}$ etc. in aqueous media, or ferrocene, I^- (in the form of $(t\text{-}Bu)_4N^+$ salt) in CH_3CN. The reduction product has very strong visible band at ~ 720 nm ($\varepsilon \approx 1.3 \times 10^4$ $M^{-1}cm^{-1}$, which is twice that of the purple $[Ni_2(L4)]^{4+}$ species) in both solvents. There is also a weak visible band at 380 nm in water solution. It was stable in aqueous media under Argon atmosphere, but diminished slowly upon opening to air with a $t_{1/2}$ of from 15 min. to several hours depending on the nature of the supporting electrolyte and the concentration of the species itself (saturated NaBr solution was found to stabilize the green species for a relatively longer period of time). The UV/Visible spectroscopic study of the air-oxidation showed four isosbestic points on-going from the green reduced form to the original purple dimer (Fig. 7.8), reflecting a reversible

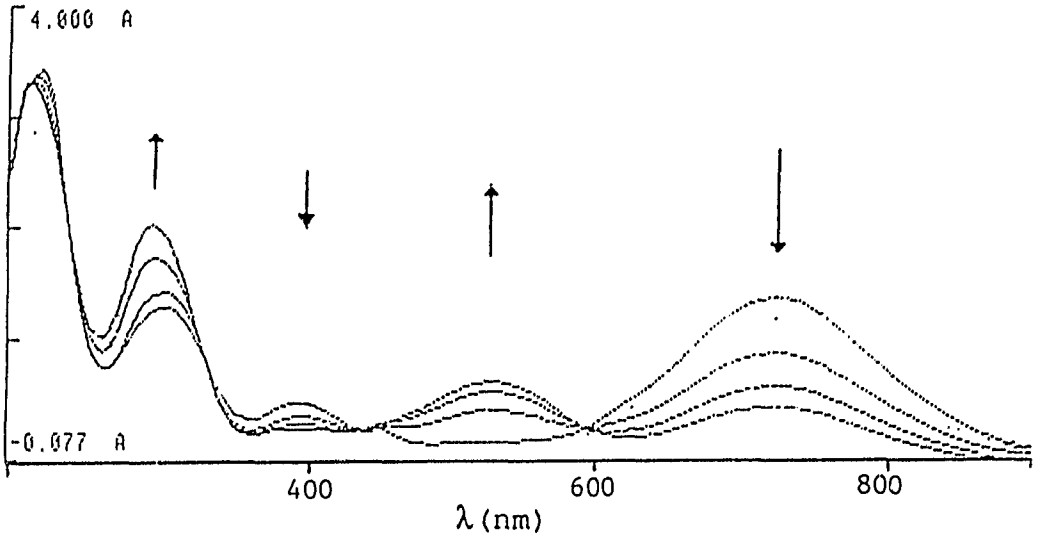

Fig. 7.8 UV/Visible spectra of oxidation of **VIII** in H_2O.

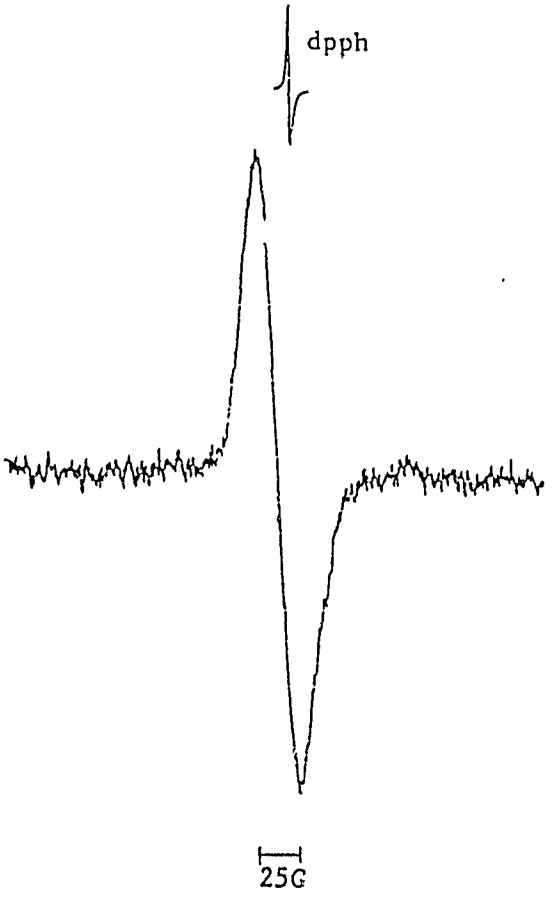

Fig. 7.9 ESR spectrum of **VIII** in CH_3CN (77 K).

nature of the process.

Esr spectra of the green solution of the reduction product in both water and acetonitrile solvents showed a symmetric radical-type peak with g = 2.007 and peak-width of ~ 25 G, which is slightly larger than that, ~ 5 G, normally observed for the organic radicals (Fig. 7.9), suggesting that the green species was a product of one electron-transfer reduction. Much effort has been made to understand how the unpaired electron delocalizes on **IX**. Variations of solvent, supporting electrolyte, and temperature all failed to produce any nitrogen coupled esr spectrum. Similarly, no metal coupling was able to be detected when ^{61}Ni was used as the met in **IX**.

ically, strong reducing reagents, such as Zn n be able to reduce the purple dimer further to th **X**. Unfortunately, even if it does exist, the natu pecies makes it difficult to be detected and chara by conventional techniques available, apart from electrochemical means. The only success in identifying **X** formed chemically was from kinetic studies (*vide infra*).

7.6.3 Kinetic Studies

Reduction of $[Ni_2(L4)]^{4+}$

A kinetic study of the reduction of the conjugated dimer complex was performed using $Co^{2+}(phen)_3$ as reductant in 1.0 M $H/NaNO_3$ aqueous media at 9 °C. Under the conditions where large

excess of the reductant over the dimer was used, k_{obs}, obtained by monitoring disappearence of the visible band at 520 nm, showed a linear dependence of the reductant concentration, and may be expressed as

$$k_{obs} = k_1[Co(II)] \qquad (7.2)$$

where $k_1 = 7.8 \times 10^4\ M^{-1}s^{-1}$. The experimental data are provided in the Table 7.8a.

Considering the moderate driving force of this cross-reaction ($\Delta E \approx 0.09$ V), the simplified Marcus cross-relation, equation 1.16 in section 1.2.2, was used to calculate the self-exchange rate of $[Ni_2(L4)]^{4+/3+}$, which gives k_{11} of 5.1×10^6 $M^{-1}s^{-1}$.

Reduction of IX

In the experiments described above, it was observed that when the reaction was monitored by tracing increase of the band at 720 nm, the reaction trace was of biphasic character, which tended to a maximun and then decreased later. However, there was no such change in the band at 520 nm, suggesting it was not due to oxidation of **IX**, but to a second reduction reaction between **IX** and the [Co(II)] species. Further study by monitoring the reaction at the isosbestic point (591 nm) of the first reaction revealed a first order reaction trace. k_{obs} of this second reaction was not linearly dependent of the reductant concentration, but in the form of

$$k_{obs} = k_1[Co(II)]/(1 + K[Co(II)]) \qquad (7.3)$$

Treatment of those kinetic data (Table 7.8b) by a "best

fitting program" and conversion of eq. 7.3 to

$$1/k_{obs} = K/k_1 + 1/k_1[Co(II)] \qquad (7.4)$$

give rise to an average value of $k_1 = 7.65\times10^4\ M^{-1}s^{-1}$ and that of $K = 5.05\times10^3$.

The possible mechanism involved in this second reduction is consistent with the two reactants forming an ion pair before the electron transfer takes place, as shown in equation (7.5)

$$\mathbf{IX} + [Co(phen)_3]^{2+} \underset{k_{-2}}{\overset{k_2}{\rightleftharpoons}} \{\mathbf{IX}\cdots[Co(phen)_3]^{2+} \xrightarrow{k_3} \mathbf{X} + [Co(phen)_3]^{3+} \qquad (7.5)$$

which has a rate law

$$d[\mathbf{IX}]/dt = \{k_2k_3/(k_{-2} + k_3)\}x \{k_{-2}/(k_{-2} + k_2[Co(II)])\}[Co(II)][\mathbf{IX}]$$

or, under the conditions of $[Co(II)] >> [\mathbf{IX}]$

$$k_{obs} = \{k_2k_3/(k_{-2} + k_3)\}\{1/(1 + K_2[Co(II)])\}[Co(II)] \qquad (7.6)$$

where $K_2 = k_2/k_{-2}$. Compare eq.(7.6) with eq. (7.5), one has

$$k_1 = k_2k_3/(k_{-2} + k_3)$$

$$K_2 = K$$

It is likely that $k_{-2} >> k_3$, therefore

$$k_1 = K_2k_3$$

which gives K_2 of $5.05\times10^3\ M^{-1}$ and k_3 of 15 s^{-1}. The self-exchange rate, k_{22}, of **IX/X** couple can be calculated using the equation (1.16), which gives k_{22} of 180 $M^{-1}\ s^{-1}$.

At first sight, it is perhaps difficult to see how the two positively charged species could form an "ion-pair", which

Table 7.8 Kinetic Data from Reaction of

$[Ni^{II}_2(L4)]^{4+}$ + $Co^{II}(phen)_3$

T = 9.0 ± 0.1 °C; I = 1.0 M (H/$NaNO_3$); $[H^+]$ = 0.1 M;

(a) $[(Ni^{II}_2(L4))^{4+}]$ = 8.0x10^{-6} M; λ = 528 nm.

$[Co^{II}]$ (x10^5 M^{-1})	8.0	11.0	14.0	16.0
k_{obs} (s^{-1})	6.20(18)	8.48(32)	10.83(16)	12.42(11)

$k_{obs} = k_1[Co^{II}]$, k_1 = 7.8x10^4 $M^{-1}s^{-1}$

(b) $[(Ni^{II}_2(L4))^{4+}]$ = 8 ~ 16 x10^{-6} M; λ = 591 nm.

$[Co^{II}]$ (x10^4 M^{-1}) [A]	0.6	0.8	1.0	2.0
k_{obs} (s^{-1}) [B]	3.61(28)	5.28(13)	5.95(32)	7.05(22)
[A]	2.5	3.0	3.2	4.0
[B]	8.09(11)	8.68(14)	9.19(41)	9.47(31)
[A]	5.0	6.0	8.0	10.0
[B]	10.94(54)	12.12(17)	13.25(41)	13.56(43)

$k_{obs} = k'[Co^{II}]/(1 + K[Co^{II}])$

is obviously against electrostatic nature. However, if one takes consideration of large amount of Cl^- anion brought into the solution by $[Co(phen)_2]Cl_2$ salt used (2 times of Co(II) concentration which was already in larger excess over the concentration of **IX**) and the likelihood of axial coordination of chloride on the Ni(II) centers (which was indeed shown in the aqueous solutions of $[Ni_2(L4)]^{4+}$), it is easy to realize that under the condition of the present study, **IX** actually exists in the form of

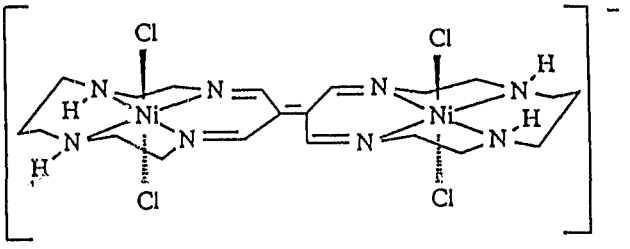

(VIII)

which has an overall of one negative charge.

Even though, the value of $5.05x10^3$ still seems somewhat too high for an ion-pair consisting of -1^- and 2^+ ions if the driving force is solely electrostatic. The additional contibution to this "abnormally" high equilibrium constant may be from interaction of the large parts of organic framework on both complex ions, which are hydrophobic in nature. After the ion-pair is formed, these bulky hydrophobic components are able to act against solvation, and hence, lower the rate of departure. As a result, although the rate of ion-pair

formation is probably not high, the rate of dissociation is even lower, resulting in a net increase in the overall equilibrium constant.

7.7 Discussion

Both structural features and chemical reactivities of $[Ni^{II}_2(L4)]^{4+}$ may be best described by its delocalized electron density on its largely unsaturated and conjugated system. As already pointed out in section 7.2, the π_M orbital on this system is combination of two components, namely π_{ar} and π_L, and these two components are comparable due to their similar stabilization energy. A consequence of this combination is that structurally, as discussed in section 7.2, it adopts a form which has some degree of aromaticity on the two unsaturated six-membered rings and also delocalization charater in its unsaturated ethylene bridge, and chemically it manifests reactivities which are both of ethylene-type and/or aromatic in nature.

Hydrolysis of this compound is simply a typical addition reaction of ethylene. However, the apparently anion-dependent and hydroxide-catalyzed behavior in this hydrolysis suggests it is a nucleophilic rather than electrophilic addition commonly observed in organic unsaturated system. This behavior is, in part, the result of aromatization which draws some of the electron density from the "double" bond into the two rings so that the "double" bond shows electron deficiency and

prefers to accept a nucleophile rather than a electrophile in its initial step of addition reaction.

As far as the redox chemistry is concerned, the unsaturated dimer may be compared with tetracyanoethylene,

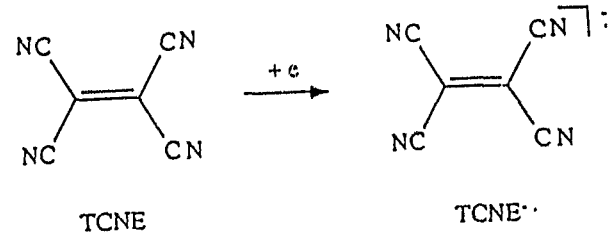

TCNE TCNE·⁻

8

TCNE (8), where ethylene is conjugated with four cyano groups and high delocalization of electron density on its conjugated molecular plane has been demonstrated from the esr spectrum of its reduced form $[TCNE\cdot]^-$.[205-207] Indeed, TCNE may serves as the best model for the organic π delocalization case which bears very close resemblance of the π_L system in present case. Thus, by comparison the redox reactivity of the two species it is possible to comment on the aromaticity in the present compound.

It is well known that TCNE is a strong π-acceptor (as evidenced by the large equilibrium values for its complex formation with organic π-bases).[205] It may be readily reduced by metals such as potassium, sodium, copper etc..[205,207] which are all very strongly reducing to the present compound, though the ease of these reductions is very impressive from an organic point of view. The reduction potential of TCNE is

0.152 V *vs.* SCE in acetonitrile,[205] which is equivalent to ~ 0.39 V *vs.* NHE. This is lower than that (~ 0.6 V *vs.* NHE) of the dimer complex by about 0.2 V. Even more remarkable is that the reduction potential of $[TCNE\cdot]^-$ is reported to be - 0.56 V *vs.* SCE (in the same solvent as above),[205] giving rise to ~ - 0.32 V *vs.* NHE, which is much lower than 0.37 V *vs.* NHE for the reduction of **IX**.

These differences may all be understood in terms of aromaticity present in the dimer complex. The increase in oxidizing power in the complex is very much the result of two effects: the first is the decrease of electron density on π_L "component" due to aromatization on the unsaturated two cyclic ring, and the second is the strong requirement of two "quasi" aromatic rings in obtaining more electron density so that the optimum aromaticity can be achieved. For the initial one electron reduction, it is possible that the first effect is dominant due to overall electron deficiency of the ring system, consistent with the conjugation on the ligand still remaining to some extent after reduction, and the unpaired electron being delocalized on both π_L and the two aromatic π_{ar} orbitals. As a result, approximate 0.2 V of increase in oxidizing power was observed, which is moderate. However, the second reduction provides an opportunity for the two rings to form two "ideal" aromatic system which gain much more stabilization energy than does the ligand-based π_L . Therefore, a large increase in reduction potential for the

second reduction was observed. Indeed, as indicated from initial kinetic results, the aromaticity is so strong in **X** that appearently it almost *totally destroys* the ligand-based π_L orbital, and *converts* all the electron density to the two aromatic π_{ar} orbitals.

This interpretation is consistent with the different anion effects on the two redox potentials of the dimer complex. Little, if at all, effect on the first reduction potential from axial donor replacement of Br^- to NO^- indicates π_M still has much of π_L component. However, the detectable increase in the second reduction potential by this replacement is in conjunction with formation of two aromatic rings, which draws most of the electron density into the rings and greatly changes the in-plane field.

The initial kinetic study of the dimer complex showed the rate of self-exchange for the first one electron reduction is 5.1×10^6 $M^{-1}s^{-1}$, which is ~ 40 times smaller than that, 2.1×10^8 $M^{-1}s^{-1}$, in the case of TCNE.[206] This amount of decrease in the dimer case clearly results from the rigidity of the complex and contribution of π_{ar} conponents in the π_{MO} orbital. It is likely that change on the MO is large but not significant enough to suggest any profound change in the π_M orbital during the electron transfer process. However, self exchange rate of the second reduction is remarkably lower than the first one, reflecting a very large change in the structure of the dimer molecule as **IX** was converted to **X**. For the species **X** which has

12 electrons in the p_z orbitals, it is reasonable to say that the energy system gains from totally delocalizing its p electron density into two aromatic rings is much greater than that from ligand-based conjugation. Therefore, the π_M orbital is dominated by π_{ar} component with probably very little, if any, amount of π_L contribution. A result of this is that the bridging carbon to carbon bond is left almost no π_L density and becomes a more likely a single bond. This single bond allows two cyclic rings to rotate so they becomes more independent of one another. In this way, the system gains best aromatic stabilization energy, and also the "2⁻" charge may be more remotely separated. All these processes involve substantial bond changes in the dimer molecule, and hence, the rate is reduced dramatically.

Of interest is a comparison of the esr spectrum of the reduced dimer radical **IX** with that of organic radical $[TCNE^{\cdot}]^{-}$. the g value of the dimer radical is 2.007 which is slightly higher than that of the organic radical, 2.0036,[206] reflecting influence of the metal orbital through π_{ar} component in π_M orbital. Much greater evidence of metal orbital contribution to the HOMO is from the peak width (~ 25 G). In general, organic radicals have a very sharp peak with a width about 5 G. Delocalization of the electron may broaden the peak such as in the case of $[TCNE^{\cdot}]^{-}$, which is ~ 10 G wide.[206] However, even in much more highly delocalized situation, without the metal orbital contribution the width is usually less than 10 G. For

example, in [Ni(Me$_4$[14]hexaenatoN$_4$)]$^+$ cation radical (9) where electron is highly delocalized in 14-membered ring system, the esr peak width is < 10 G.[193] Considering this, the large peak width observed from the dimer radical **IX** must be from a metal orbital contribution.

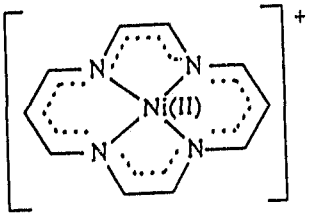

9

Despite that it is obvious that the orbital the unpaired electron occupies has metal-orbital contribution, the metal-radical coupling is, however, too small (if any) to be detected in the dimer. The failure to observe this coupling may be interpretated as follows. In the π_{ar} component of the π_M orbital, the 4p$_z$(Ni) has lower energy than the other p$_z$ orbitals from the carbons, therefore the higher the π_{ar} orbital, the smaller the contribution from the 4p$_z$. The orbital the unpaired electron occupies is the highest which should be expected to have a largely-reduced amount of the 4p$_z$ contribution. In addition, this highest π_{ar} orbital has to mix with that from "ligand-based component" (π_L), which reduces the 4p$_z$ contribution even more. Furthermore, as mentioned above, the orbitals the metal uses in the π_{ar} system are 4p with some d$_{xz}$ and d$_{yz}$. This means there is little, if any,

Fermi-Contact (which mainly operates through interaction between s orbital and nucleus) between the π_{ar} and the Ni nucleus even if the electron totally localizes in this orbital. In part, this should also be responsible to the weakness of the possible metal-radical coupling (if there is any). Consequently, no metal-coupling but a metal-influence was observed.

Another possible reason for the failure to observe the metal coupling is a fast spin-spin relaxation (through a "exchange relaxation" mechanism). It is likely that the electron configuration at the two Ni(II) centres in the dimer is not purely low-spin but rather a mixure of both high-spin and low-spin (due to the axial coordination which was observed in the UV/Visible spectroscopic study, *vide supra*). Considering the π_{MO} the unpaired electron occupies has the π_{ar} contribution, this high-spin component may relativly easily communicate with the spin of the unpaired electron, and hence, the spin-spin relaxation becomes a relatively rapid process with regard to the esr time scale. As a result, the possible metal-radical couplings are averaged, giving rise to a single broad peak (spin-spin "exchange broadening").

The absence of the nitrogen coupling may also be explained in similar way. Indeed, many conjugated radical systems containing p(N) ortibals fail to show N-coupling. For example, the esr spectrum of $[Ni(Me_4[14]hexaenatoN_4]^+$ shows no N-coupling at all, though participation of ^Np_z's in the highly-

delocalized ligand-based π orbital was clearly shown.

It is also interesting to compare the kinetics of electron transfer in the present case with those in "classical" metal-based and ligand-based systems. Generally speaking, electron transfer processes at organic centres (even if coordinated to a metal ion) are fast, and often of diffusion-limited. The process at a metal-centre, on the other hand, is relatively slow due to a relatively larger inner shell reorganization barrier. For example, the rate of ligand-based electron transfer in $[Co(Me_2\text{-}[14]aneN_4\text{-}dieno(-))]^+$ is found to be diffusion-limited ($\geq 10^9$ $M^{-1}s^{-1}$)[189], and that of the metal-based electron transfer in Ni(II)cyclam is 2×10^3 $M^{-1}s^{-1}$.[103] Compared with these two systems, the rate, 5.1×10^6 $M^{-1}s^{-1}$, in the present quasi-aromatic system is intermediate. This comparison not only reflects an aromatic nature of the system, but also suggets that there is a potential application of this metal-ligand mixing mechanism in "tuning" the rate of electron transfer.

7.7 Future Work

The present investigation of the chemistry of the ethylene-bridged macrobicyclic system has shown a unique feature of the "combination" chemistry of metal and ligand, based on which all the structural features and chemical reactivities of this dimer complex can be rationalized. Obviously, there is very rich chemistry in such a system,

which may be derived from either the π_L or π_{ar} components. The chemistry of the π_{ar} component is characterized by the aromaticity in the two six-membered rings, and that of the π_L by the "π-acidity" of the ethylene-bridge. Because of the orbital overlap beween the metal and the chelate, it is possible that the reactivity of both the components may be monitored by variation of the coordinated metal ion (in terms of electron configuration and oxidation state).

In addition to the theoretical significance (which has been mentioned in the introduction and discussion sections above), this ethylene-bridged dimer system may also, at least potentially, serve as a catalyst in activation of organic or inorganic π molecules. For instance, by selecting a suitable metal ion for the dimer complex, it is possible to increase the π-acidity at the ethylene-bridge such that it is able to "absorb", and hence, activate a "π-molecule", such as N_2, O_2 and CO, through π-π interaction.

REFERENCES

1. G.A.Melson, "*Coordination Chemistry of Macrocyclic Compounds*" G.A.Melson Ed., Plenum press, New York 1979, p.2.

2. F.H.Moser and A.L.Thomas, "*Phthalocyanine Compounds*", Reinhold Publishing Corp., New York (1963).

3. E.Antonini and M.Brunori, *Hemoglobin and Myoglobin in their Reactions with Ligands*, North-Holland Publishing Co. Amsterdam (1971).

4. G.S.Marks, "*Heme and Chlorophylls*", Van Nostrand, London (1969).

5. D.R.Willians, "*The Metals of Life*" Van Nostrand-Reinhold, London (1971).

6. N.F.Curtis, *J. Chem. Soc.*, 4409 (1960).

7. D.A.House and N.F.Curtis, *Chem. Ind.*, 42, 1708 (1961).

8. M.C.Thompson and D.H.Busch, *J. Am. Chem. Soc.* 86, 3651 (1964)

9. G.N.Schrauzer, *Chem. Ber.* 95, 1438 (1962).

10. F.Umland and D.Thierig, *Angew. Chem.*, 74, 388 (1962).

11. N.F.Curtis, *Coord. Chem. Rev.*, 3, 3 (1968).

12. R.F.Gould (Ed.) "*Bioinorganic Chemistry*", *Advances in Chemistry* Series No. 100, American Chemical Sociaty, Washington (1971).

13. D.K.Cabbinus and D.W.Margerum, *J. Am. Chem. Soc.*, 91, 6540 (1969).

14. D.H.Busch, K.Farmary, V.Goedken, V.Katovic, A.C.Melnyk, C.R.Sperati, and N.Tokel, *Adv. Chem. Ser.*, 100, 44 (1971).

15. J.-M.Lehn and J.P.Sauvage, *J. Am. Chem. Soc.*, 97, 6700 (1975).

16. C.O.Dietrich-Buchecker and J.P.Sauvage, *Angew. Chem.*, Int. Ed. Engl., 28, 189 (1989).

17. D.H.Busch and N.A.Stephenson, *Coord. Chem. Rev.* 100, 119 (1990).

18. S.Karbach, W.Löhr and F.Vögtle, *J. Chem. Res.*(s) 314 (1981).

19. J.E.Richman and T.J.Atkins, *J. Am. Chem. Soc.*, 96, 2268 (1974).

20. D.S.C.Black, "*Reaction of Coordinated Ligands*", *Comprehensive Coordination Chemistry*, Sir. G.Wilkison Ed.-in-Chief, Pergaman Press, Oxford (1987), Vol. 1, p.415.

21. L.Fabbrizzi, P.Paoletti and A.B.P.Lever, *Inorg. Chem.*, 15, 1502 (1976).

22. M.Micheloni, P.Paoletti and A.Sabatini *J. Chem. Soc. Dalton Trans.*, 1189 (1983).

23. R.D.Hancock and A.Martell, *Comments Inorg. Chem.*, 6, 237 (1988).

25. D.H.Busch, *Helv. Chim. Acta.*, Fasciculus Extraordinarius Alfred Werner. 174 (1967).

26. L.Y.Martin, L.J.DeHayes, L.J.Zompa and D.H.Busch, *J. Am. Chem. Soc.*, 96, 4046 (1974).

27. L.Y.Martin, C.R.Sperati and D.H.Busch, *J. Am. Chem. Soc.*, 99, 2968 (1977).

28. Y.Huang, L.Y.Marin, S.C.Jackels, A.M.Tait and D.H.Busch, *J. Am. Chem. Soc.*, 99, 4029 (1977).

29. V.J.Thöm, J.C.A.Boeyens, G.J.McDougall and R.D.Hancock, *J. Am. Chem. Soc.*, 106, 3198 (1984).

30. T.F.Endicott and B.Durham, "*Coordination Chemistry of Macrocyclic Compounds*" G.A.Melson Ed., Plenum press, New York 1979, p.393.

31. A.M.Tait and D.H.Busch, *Inorg. Chem.*, 14, 1881 (1975).

32. F.V.Lovecchio, E.G.Gore and D.H.Busch, *J. Am. Chem. Soc.*, 96, 3109 (1974).

33. D.H.Busch, *Acc. Chem. Res.*, 11, 392 (1978).

34. L.Fabbrizzi and D.M.Proserpio, *J. Chem. Soc., Dalton Trans.* 229 (1989).

35. E. Kimura, *J. Coord. Chem.*, 15, 1 (1986).

36. C.J.Hipp, L.F.Lindoy and D.H.Busch, *Inorg. Chem.*, 11, 1988 (1972).

37. N.F.Curtis, *Chem. Commum.*, 1966, 881 (1966).

38. J.C.Dabrowiak, F.V.Lovecchio, V.L.Goedken and D.H.Busch, *J. Am. Chem. Soc.*, 94, 5502 (1972).

39. J.C.Dabrowiak and D.H.Busch *Inorg, Chem.*, 14, 1881 (1975).

40. V.L.Doedken and D.H.Busch, *J. Am. Chem. Soc.*, 97, 4238 (1975).

41. J.A.Switzer and J.F.Endicott, *J. Am. Chem. Soc.*, 102, 1181 (1980).

42. J.A.Cunningham and R.E.Sievers, *J. Am. CHem. Soc.*, 95, 7183 (1973).

43. F.Z.McElroy and J.C.Dabrowiak, *J. Am. Chem. Soc.*, 98, 7112 (1976).

44. E.Ahmed, M.L.Yucker and M.L.Tobe, *Inorg. Chem.* 14, 1 (1975).

45. N.F.Curtis, *J. Chem. Soc. (A)*, 1971, 2834 (1971).

46. M.L.Tobe, *Inorganic Reaction Mechansim*, Nelson, New York, 1972.

47. C.H.Langford and H.B.Gray, *Ligand Substitution Processes*, W.A.Berjamin, Ontario, 1974.

48. J.K.Burdett, *J. Chem. Soc. Dalton Trans.* 1725 (1976).

49. Y.Ducommum, D. Zbinden and A.E.Merbach, *Helv. Chim. Acta.*, 65, 1385 (1982).

50. Y.Ducommum, K.E.Newman, and A.E.Merbach, *Inorg. Chem.*, 19, 3690 (1980).

51. S.Lanza, D.Minniti, P.Moore, L.Sachinidis, R.Romeo and M.L.Tobe, *Inorg. CHem.*, 23, 4428 (1984).

52. M.L.Tobe, "*Reaction of Coordinated Ligands*", *Comprehensive Coordination Chemistry*, Sir. G.Wilkison Ed.-in-Chief, Pergaman Press, Oxford. 1987, Vol. 1, p. 295.

53. D.W.Wargerum, G.R.Cayley, D.C.Weatherburn and G.K.Pagenkopt, "*Kinetics and Mechanisms of Complex Formation and Ligand Exchange*", *in "Coordination Chemistry"*, A.E.Martell Ed., ACS Monograph, 1978, Vol. 2, p. 1-120.

54. A.Werner, *Z. Anorg. Allgem. Chem.*, 3, 267 (1893).

55. (a) I.I.Chernyaev, *Ann. Inst. Platine (UUSR)*, 4, 261, (1926);

(b) I.I.Chernyaev, *Inst. Obshch. i neorgan. Khim. Acad. Nauk (USSR)*, 5, 118 (1927).

56. A.A.Grinberg, *Ann. Inst. Platine (USSR)*, 5, 109 (1927).

57. J.Chatt, J.A.Dunsanson and L.M.Venanzi, *Chem. and Ind.* (London), 749 (1955).

58. J.Chatt, J.A.Dunsanson and L.M.Venanzi, *J. Chem. Soc.*, 4456 (1955).

59. L.E.Orgel, *J. Inorg. Chem.* 2, 137 (1956).

60. R.A.Marcus:
(a) *Trans. N. Y. Acad. Sci.*, 19, 423 (1957);

(b) *Annu. Rev. Phys. Chem.*, 15, 155 (1964);

(c) *J. Chem. Phys.* 43, 679 (1965).

61. N.S.Hush, *Trans. Faraday Soc.*, 57, 557 (1961).

62. (a) J.Ulstrup, *Charge Transfer Process in Condensed Media*, Spronger Verlage, Berlin, 1979;

(b) N.R.Kestner, J.Logan and J.Jortner, *J. Phys. Chem.*, 78, 2148 (1974).

63. (a) M.D.Newton and N.Sutin, *Annu. Rev. Phys. Chem.*, 35, 441 (1983);

(b) N.Sutin, *Acc. Chem. Res.*, 15, 275 (1982);

(c) N.Sutin, *Prog. Inorg. Chem.*, 30, 441 (1983);

(d) T.Guarr and G.McLendon, *Coord. Chem. Rev.*, 68, 1 (1985).

64. D.DeVault, *Q. Rev. Biophys.* 13, 387 (1980).

65. T.J.Meyer, the same to ref.(20), Vol. 1, p. 331.

66. (a) M.Chou, C.Creutz and N.Sutin, *J. Am. Chem. Soc.* 99, 5615 (1977);

(b) M.J.Weaver and E.L.Lee, *Inorg. Chem.*, 19, 1936 (1980).

67. A.Haim, *Acc. Chem. Res.* 8, 264 (1975).

68. A.Haim, *Prog. Inorg. Chem.*, 30, 273 (1983).

69. (a) J.M.Martin, J.F.Endicott, I.A.Ochrymowyca and D.B.Rorabacher, *Inorg. Chem.*, 26, 3012 (1987);

(b) M.M.Bernardo, P.V.Rbandt, R.R.Schroeder, D.B.Rorabacher, *J. Am. Chem. Soc.*, 111, 1224 (1988).

70. (a) B.S.Bruschwiy, C.Creutz, D.H.Macartney, T.K.Sham and N.Sutin, *Faraday Discuss. Chem. Soc.*, 74, 113 (1982);

(b) H.-J.Küppers, N.Ademiro, C.Pomp, D.Ventur, K.Wieghardt, B.Nuber and J.Weiss, *Inorg. Chem.*, 25, 2400 (1986).

71. (a) S.F.Mason and R.D.Peacock, *Inorg. Chim. Acta*, 19, 75 (1976);

(b) F.P. Dwyer, F.L.Peacock and A.Shulman, *J. Am. Chem. Soc.*, 81, 290 (1959).

72. V.J.Thöm, M.S.Shaikjee and R.D.Hancock, *Inorg. Chem.*, 25, 2992 (1986).

73. (a) H.Koyama and T. Yoshino, *Bull. Chem. Soc. Japan*, 45, 481 (1972);

(b) E.Buhleier, W.Rasshofer, W.Wehner, F.Lupportz and F.Vögtle, *Justus Liebigs Ann. Chem.*, 1344 (1977).

74. G.Davies and B.Warngvist, *Coord. Chem. Rev.*, 5, 349 (1970).

75. T.Whitcombe, *Ph.D. Dissertation*, University of Victoria, 1988.

76. (a) D.H.Evans, K.M.O'Connell, R.A.Petersen and M.J.Kelly, *J. Chem. Educ.*, 60, 290 (1983);

(b) R.N.Adams, *Electrochemistry at Solid Electrodes*, Marcel Dekker, New York, 1969, Chapter 5.;

(c) W.R.Heinenman and P.T.Kissinger, *Amer. Laboratory*, November 1982, p. 29;

(d) W.E.Geiger, *Prog. in Inorg. Chem.*, 33, 275 (1985).

77. A.J.Bard and L.F.Faulkner, *Electrochemical Methods*, John Wiley and Sons, New York, 1980, Chapter 6.

78. D.D.McDonald, *Transient Techniques in Eletrochemistry*,

Plenum Press, New York, 1977, Chapter 6.

79. U.Svanholm and V.D.Parker, *J. Chem. Soc. Perkin trans.*, 2, 755 (1975).

80. R.S.Nicholson and I.Shain, *Anal. Chem.*, 36, 706 (1964). This paper summarizes earlier theoretical work and presents theoretical results for a number of important reaction schemes with coupled chemical reactions.

81. (a) R.S.Nicholson, *Anal. Chem.*, 37, 1351 (1965);

(b) M.L.Olmstead and R.S.Nicholson, *Anal. Chem.*, 38, 150 (1966).

82. (a) F.L.Wimmer, M.R.Snow and A.M.Bond, *Inorg. Chem.*, 13, 1617 (1974);

(b) A.M.Bond and K.B.Oldham: *J. Phys. Chem.*, 87, 2492 (1983) and 89, 3739 (1985).

83. (a) R.D.Rieke, H.Kojima and K.Öfele, *J. Am. Chem. Soc.*, 98, 6735 (1976);

(b) *Ibid Angew. Chem. Int. Ed. Engl.*, 19, 538 (1980);

(c) R.D.Rieke, W.P.Henry and J.S.Arney, *Inorg. Chem.*, 26, 420 (1987).

84. J.Moraczewski and W.E.Geiger, *J. Am. Chem. Soc.*, 101, 3407 (1979).

85. K.A.Conner and R.A.Walton *Inorg. Chem.*, 25, 4422 (1986).

86. E.Laviron and L.Roullier, *J. Electroanal. Chem.*, 186, 1 (1985).

87. M.M.Bernardo, P.V.Robandt, R.R.Schroeder and D.B.Rorabacher, *J. Am. Chem. Soc.*, 111, 1224 (1989).

88. e.g.
(a) P.W.Atkins and M.C.R.Symons, *the Structure of Inorganic Radicals*, Elsevier, Amsterdam, 1967;

(b) P.B.Ayscough, *Electron Spin Resonance in Chemistry*, Methuen, London, 1967;

(c) M.Bersohn and J.C.Baird, *Electron Paramagnetic Resonance*, Benjamin, New York, 1966;

(d) M.C.R.Symons, *Advan. Phys. Org. Chem.*, 1, 284

(1963);
(e) A.Carrington and A.D.McLachlan, *Introduction to Magnetic Resonance*, Harper and Row, New York, 1967;

(f) W.B.Lewis *Inorg. Chem.*, 6, 1737 (1967);

(g) C.P.Poole, *Electron Spin Resonance*, Wiley (Interscience), New York, 1967;

(h) C.R.Slichter, *Principles of Magnetic Resonance*, Harper, New York, 1963.

89. (a) S.Fujiwara *Spectroscopy and Structure of Metal Chelate Compounds*, Wiley, New York, 1968;

(b) G.F.Kokoszka and G.Gordon, *Tech. Inorg. Chem.*, 7, 151 (1968);

(c) E.König, *Physical Methods of Advenced Inorganic Chemistry*, Wiley (Interscience), New York, 1968;

(d) H.A.Kuska and M.T.Rogers, in *Radical Ions*, Wiley (Interscience), New York, 1968, p. 579;

(e) B.R.McGarvey, *Inorg. Chem.*, 5, 476 (1966);

(f) A.Abragam and B.Bleaney, *Electron Paramagnetic Resonance of Transition Ions*, Clarendon Press, Oxford, 1970;

(g) B.A.Gordman and J.B.Raynor, *Adv. in Inorg. Chem. Radiochem.*, 13, 135 (1970).

91. D.G.Fortier and A.McAuley, *J. Chem. Soc., Dalton Trans.*, 101 (1991).

92. (a) M.F.C.Ladd and R.A.Palmer, *Structure Determination by X-Ray Crystallograpgy*, 2nd Ed., Plenum Press, New York, 1985;

(b) G.H.Stout and L.H.Jensen, *X-Ray Structure Determination*, The Macmillan Company, New York, 1968.

93. J.G.Mohanty and A.Chakravorty, *Inorg. Chem.*, 15, 2912 (1976).

94. J.G.Mohanty, R.P.Singh and A.Chakravorty, *Inorg. Chem.*, 14, 2178 (1975).

95. A.G.Lappin and M.C.M.Laranjeira, *J. Chem.Soc., Dalton Trans.*, 1861 (1981).

96. J.Korvenranta, H.Saarinen and M.Masakkala, *Inorg. Chem.*, 21, 4297 (1982).

97. C.F.Wells and D.J.Fox, *J. Chem. Soc., Doltan Trans.*, 1498 (1977).

98. J.-C.Brodoritch, R.I.Haines and A.McAuley, *Can. J. Chem.*, 59, 1610 (1981).

99. D.J.Szalda, D.H.Macartney and N.Sutin *Inorg. Chem.*, 23, 3473 (1984).

100. A.McAuley, P.R.Norman and O.Olubuyide, *Inorg. Chem.*, 23, 1939 (1984), and *J, Chem. Soc., Dalton Trans.*, 1501 (1984).

101. K.Wieghardt, W.Schmidt, W.Herrmann and H.J.Kuppers, *Inorg. Chem.*, 22, 2953 (1983).

102. K.Wieghardt, W.Walz, B.Nuber, J.Weiss, A.Ozarowski, H.Stratremeier and D.Reinen, *Inorg. Chem.*, 25, 1650 (1986).

103. A.McAuley, D.H.Macartney and T.Oswald, *J. Chem. Soc., Chem. Commum.*, 274 (1982).

104. F.P.Dwyer and E.C.Gyartas, *Nature* (London), 166, 482 (1950).

105. (a) T.J.Alkins, J.E.Richman and W.F.Oettle, *Org. Syn.*, 58, 86 (1979);

(b) W.Rasshafer, W.Wehner and F.Vötle, *Liebigs Ann. Chem.*, 96, 916 (1976).

106. P.G.Graham and D.C.Weatherburn, *Aust. J. Chem.*, 36, 2349 (1983).

107. J.G.Bailar, H.B.Janassen and A.D.Gott, *J. Am. Chem. Soc.*, 74, 3131 (1952).

108. (a) S.F.Mason and R.D.Peacock, *Inorg. Chim. Acta*, 19, 75 (1976);

(b) A.F.Drake, R.Kuroda and S.F.Mason, *J. Chem. Soc., Dalton Trans.*, 1095 (1979);

(c) M.Nonoyana, *Trans. Metal Chem. (Weinhein)*, 5, 269 (1980).

109. P.G.Graham and D.C.Weatherburn. *Aust. J. Chem.*, 34, 291 (1981).

110. (a) F.L.Urbach, "*Coordination Chemistry of Macrocyclic Compounds*" G.A.Melson Ed., Plenum press, New York, 1979, P. 345-392.

(b) R.Yany and L.J.Zompa, *Inorg. Chem.*, 15, 1499 (1976);

(c) T.N.Margulis and L.J.Zompa, *Inorg. Chim. Acta*, 28, L157 (1978).

111. D.H.Macartney and N.Sutin, *Inorg. Chem.*, 22, 3530 (1983).

112. S.Kirschner, *Coord. Chem. Rev.*, 2, 461 (1967).

113. H.P.Jensen and F.Woldbye, *Coord. Chem. Rev.*, 29, 213 (1979).

114. A.McAuley, O.Olubuyide, L.Spenver and P.R.West, *Inorg. Chem.*, 23, 2594 (1984).

115. M.J.Van der Merwe, J.C.A.Boeyens and R,D.Hancock, *Inorg. Chem.*, 22, 3489 (1983).

116. B.R.Baker, F.Basolo and H.M.Neuman, *J. Phys. Chem.*, 63, 371 (1969).

117. D.H.Macartney and A.McAuley, *Canad. J. Chem.*, 61, 103 (1983).

118. J.F.Endicott, B.Drhan and K.Kumar, *Inorg. Chem.*, 21, 2437 (1982).

119. C.O.Adedinsewo and A.Adegite, *Inorg. Chem.*, 18, 3579 (1979).

120. M.Fairbank and A.McAuley, *Inorg. Chem.*, 26, 2844 (1987).

121. L.Lindoy, *Chemistry of Macrocyclic Ligand Complexes*, Cambridge University Press, Cambridge, Englang, 1989.

122. D.H.Busch, *Adv. Chem. Ser.*, No, 100, 44 (1971).

123. L.Fabbrizzi, *Comments Inorg. Chem.*, 4, 33 (1985).

124. E.Kimura, *Pare. Appl. Chem.*, 58, 1461 (1986).

125. E.K.Barefield, K.A.Foster, G.M.Freeman and K.D.Hodges, *Inorg. Chem.*, 25, 4663 (1986).

126. D.A.Hous and N.F.Curtis, *J. Am. Chem. Soc.*, 86, 1331

(1964).

127. R.H.Prime, D.A.Scotter and P.R.Wooley, *Inorg. Chem. Atca*, 9, 51 (1974).

128. D.G.Fortier and A.McAuley, *Inorg. CHem.* 112, 2640 (1990).

129. D.G. Fortier and A.McAuley, *Inorg. Chem.*, 129, 655 (1989).

130. J.Franz, G.M.Freeman, E.K.Baerfield, W.A.Vlkent G.J.Ehrhardt and R.A.Holmes, *Nucl. Med. Biol.*, 14, 479 (1987).

131. E.K.Barefield, F.Wagner and K.D.Hodges, *Inorg. Chem.*, 15, 1370 (1976).

132. S.M.Hart, J.C.A.Boeyens, J.P.Michael and R.D.Hancock, *J. Chem. Soc., Dalton Trans.*, 1601 (1983).

133. J.Zubieta, K.D.Karlin and J.C.Hayes, in *Copper Coordination Chemistry: Biolchemical and Inorganic Perspectives*, K.D.Karlin and K.Zubieta Eds. Ademine Press, New York, 1983, p. 97-108.

134. S.M.Nelson, P.D.A.McIlroy, C.S.Stevenson, E.Kong, G,Ritter and J.Wiagel, *J. Chem. Soc., Dalton Trans.*, 991 (1988).

135. A.M.Tait and D.H.Busch, *Inorg. Chem.*, 16, 966 (1977).

136. C.Xu and A.McAuley, unpublished results.

137. D.G.Fortier, Ph.D. Dissertation, University of Victoria, 1988.

138. A.McAuley and B.Cameron, unpublished results.

139. G.M.Sheldrick, SHELX76, *Program for Crystal Structure Refinement*, University of Cambridge, Cambridge, U.K., 1976.

140. *International Tables for X-ray Crystallography;* Kynock Press, Birmingham, U.K., 1974, Vol. IV.

141. P.Coppens, L.Lieserowitz, D.Rabinovich, *"Empirical Absorption Correction" (EMPABS)*, modified by G.W.Bushnell, University of Victoria.

142. P.Main, MULTAN, University of York, York, U.K., 1978.

143. M.Ciampolini, M.Micheloni, F.Vizza, F.Zanobini, S.Chimichi and P.Apporto, *J. Chem. Soc., Dalton Trans.*, 505 (1986).

144. M.Micheloni, *J. Coord. Chem.*, 18, 1 (1988).

145. L.Fabbrizzi, M.Micheloni and P.Paoletti, *J. Chem. Soc., Dalton Trans.*, 1581 (1979).

146. V.C.Goedken and D.H.Busch, *Inorg. Chem.*, 10, 2679(1971).

147. R.F.Borch, *Tetrahedron Lett.*, 61 (1968).

148. E.Kimura, T.Koike, H.Nada and Y.Iitaka, *Inorg. Chem.*, 27, 1036 (1988).

149. J.L.Sessler, J.W.Sikert, J.D.Hugdhl and V.Lynch, *Inorg. Chem.*, 28, 1417 (1989).

150. J.R.Dorfman, R.D.Bereman and M.-H.Whangbo, in *Copper Coordination Chemistry: Biolchemical and Inorganic Perspectives*, K.D.Karlin and K.Zubieta Eds. Ademine Press, New York, 1983, p.75-96.

151. L. Cleveland, R.E.Coffamn, P.Coon and L.Davis, *Biochem.*, 14, 1108 (1975).

152. A.A.G.Tomilinson and B.J.Hathaway, *J. Chem. Soc., (A)*, 1685 (1968).

153. A.W.Addison, M.Carpenter, L.K.-M.Lau and M.Wicholas, *Inorg. Chem.*, 17, 1545 (1978).

154. (a) M.F.Cabral, J.De O. Cabral, E.Bouwman and W.L.Driessen, *Inorg. Chem.*, 23, 4181 (1984);

(b) E.Kimura, T.Koike, R.Machida, R.Nagai and M.Kodama, *Inorg. Chem.*, 23, 4181 (1984).

155. K.Miyoshi, H.Tanaka, E.Kimura. S.Tsuboyama, S.Murata, H.Shimizu and K.Ishizu, *Inorg. Chim. Acta*, 78, 23 (1983).

156. (a) G.Reid and M.Schioder, *Chem. Soc. Rev.*, 19, 239 (1990);

(b) D.Reinen, A.Ozarowski, B.Jakob, J.Pebler, H.Stratemeier, K.Wieghardt and I.Tolksdort, *Inorg. Chem.*, 26, 4010 (1987).

157. J.K.Yandell, in *Copper Coordination Chemistry:*

Biochemical and Inorganic Perspectives, K.D.Karlin and K.Zubieta Eds. Ademine Press, New York, 1983, p. 157-166, and references therein.

158. D.B.Rorabacher, M.J.Martin, M.J.Koenigbouer, M.Malik, R.R.Schroder, J.Endicott and L.A.Ochrymowycz, in *Copper Coordination Chemistry: Biochemical and Inorganic Perspectives*, K.D.Karlin and K.Zubieta Eds. Ademine Press, New York, 1983, p. 167-202.

159. D.Kirelson, *J. Chem. Phys.*, 33, 1094 (1960).

160. H.M.McConnell, *J. Chem. Phys.*, 25, 709 (1956).

161. F.G.Herring and R.L.Tapping, *Can. J. Chem.*, 52, 4016 (1974).

162. S.Siddiqui and R.E.Shepherd, *Inorg. Chem.*, 25, 3869 (9186).

163. H.Yokoi and T.Kishi, *Chem. Lett.* 749 (1973).

164. A.W.Addison, in *Copper Coordination Chemistry: Biochemical and Inorganic Perspectives*, K.D.Karlin and K.Zubieta Eds. Ademine Press, New York, 1983, p. 109-128.

165. L.Fabbrizzi, T.A.Kaden, A.Perotti, B.Seghi and L.Siegfried, *Inorg. Chem.*, 25, 321 (1986).

166. K.Coulter and A.McAuley, Unpublished results.

167. K.L.Chellappa, F.P.Bossu and D.W.Margerum, *J. Am. Chem. Soc.*, 99, 2195 (1977).

168. P.A.Tasker and L.Sklar, *Crystl. Mol. Struct.*, 5, 329 (1975).

169. L.Fabbrizzi, C.Mealli and P.Paoletti, *J. Chem. Res. (S).*, 170 (1979).

170. D.C.Olson and J.Vasilevskis, *Inorg. Chem.*, 8, 1611 (1969) and 10, 463 (1971).

171. R.I.Haines and A.McAuely, *Coord. Chem Rev.*, 39, 77 (1981).

172. K.Nag. and A.Chakravorty, *Coord. Chem. Rev.*, 33, (1980).

173. E.Zeigerson, G.Ginsburg, N.Schwartz, Z.Luz and D.Meyerstein, *J. Chem. Soc., Chem. Commum.*, 241 (1988).

174. L.Fabbrizzi, *J. Chem. Soc., Chem. Commum.*, 1063 (1979).

175. A.G.Lappin and A.McAuley, *"The Redox Chemistry of Nickel", Adv. Inorg. Chem.*, 32, 241 (1988).

176. E.S.Gore and D.H.Busch, *Inorg. Chem.*, 12, 1 (1973).

177. R.I.Haines and A.McAuley, *Inorg. Chem.*, 19, 719 (1980).

178. P.Chaudhuri and K.Wieghardt, *Prog. Inorg. Chem.*, 35, 329 (1987).

179. G.Germain, P.Main and M.M.Woolfson, *Acta Crystallogr. Sect. A: Cryst. Phys., Diffr., Theor. Gen. Crystallgr.*, A27, 368 (1971).

180. B.Bosnich, C.K.Poon and M.L.Tobe, *Inorg. Chem.*, 26, 3224 (1987).

181. P.J.Connolly and E.J.Billo, *Inorg. Chem.*, 26, 1102 (1987).

182. L.Fabbrizzi, *J. Chem. Soc., Dalton Trans.*, 1857 (1979).

183. V.J.Thöm, C.C.Fox, J.C.A.Boeyens and D.Hancock, *J. Am. Chem. Soc.*, 106, 5947 (1984).

184. W.N.Setzer, C.A.Ogle, G.S.Wilson, and R.S.Glass, *Inorg. Chem.*, 22, 266 (1983).

185. E.J.Hintsa, J.R.Hartmann and S.R.Cooper, *J. Am. Soc., Dalton Trans.*, 2125 (1983).

186. (a) E.K.Barefield, G.M.Freeman, and D.G.Van Derveer, *Inorg. Chem.*, 25, 552 (1986);

(b) L.Sabatini and L.Fabbrizzi, *Inorg. Chem.*, 18, 438 (1979).

187. (a) R.G.Wilkins, *The Study of Kinetics and Reactions of Transition Metal Complexes*, Allyn an Bacon Inc., Boston, 1974;

(b) D.B.Rorabacher, T.S.Turan, J.A.Defever and W.G.Nickels, *Inorg. Chem.*, 8, 1498 (1969);

(c) J.H.Espensen, J.P.Hunt and R.A.Plane, *J. Am. Chem. Soc.*, 76, 5966 (1954);

(d) Y.Sasaki and A.G.Sykes, *J. Chem. Soc., Dalton Trans.*, 1048 (1975).

188. M.F.Richardson and R.E.Sievers, *J. Am. Chem. Soc.*, 94, 4134 (1972).

189. J.A.Switzer, J.F.Endicott, M.A.Khalifa, F.P.Rotzinger andK.Kumar, *J. Am. Chem. Soc.*, 105, 56 (1983).

190. R.K.Murmann and E.G.Vassian, *Coord. Chem. Rev.*, 105, 56 (1990).

191. (a) D.Dolphin and A.H.Felton *Acc. Chem. Res.*, 7, 26 (1974);

(b) D.Dolphin, T.Nien, R.H.Felton and I.Fujita, *J. Am. Chem. Soc.*, 97, 5288 (1975).

192. G.M.Brown, F.R.Hopf, J.A.Ferguson, T.J.Meyer and D.G.Whitten, *J. Am. Chem. Soc.*, 95, 5939 (1973), and 97, 5385 (1975).

193. M.Millar and R.H.Holm, *J. Am. Chem. Soc.*, 97, 6052 (1975).

194. J.A.Switzer and J.F.Endicott, *J. Am. Chem. Soc.*, 102, 1181 (1980).

195. F.A.Cotton and G.Wilkinson, *Advanced Inorganic Chemistry*, 4th Ed., John Wiley and Sons, New Yorw, 1980, p. 495-497.

196. K.D.Whitburn and G.S.Laurence, *J. Chem. Soc., Dalton Trans.*, 139 (1979).

197. G.W.Roberts, S.C.Cummings and J.A.Cunningham, *Inorg. Chem.*, 15, 2503 (1976).

198. A.McAuley, unpublished results.

199. E.K.Barefield, D.Chueng and D.G.Van Derveer, *J. Chem. Soc., Chem. Commum.*, 302 (1981).

200. J.A.Cunningham and R.E.Seivers, *J. Am. Chem. Soc.*, 95, 7183 (1973).

201. S.I.Subramanian, Ph.D. Dissertation, University of Victoria, 1989.

202. D.H.Busch et al., *Inorg. Chem.*, 26, 440 (1987).

203. D.H.Busch et al., *Inorg. Chem.*, 26, 427 (1987).

204. D.H.Busch. et al. *Inorg. Chem.*, 23, 903 (1984).

205. O.W.Webster, W.Mahler and R.E.Benson, *J. Am. Chem. Soc.*, 84, 2210 (1962).

206. W.D.Phillips and J.C.Rowell, *J. Chem. Phys.*, 33, 626 (1960).

207. O.W.Webster, W.Mahler and R.E.Benson, *J. Org. Chem.*, 25, 1470 (1960).